Investigating multi-modal therapy with radiotherapy, vascular-targeted photodynamic therapy and immunotherapy in pre-clinical models of prostate cancer

Yiannis Philippou

St Cross College

A thesis submitted in fulfilment of the requirements for the degree of Doctor of Philosophy in Oncology



CRUK/MRC Oxford Institute for Radiation Oncology

University of Oxford

Michaelmas Term 2021

Supervisors

Professor Richard J Bryant BMedSci(Hons) MBChB(Hons) FRCSEd(Urol) PhD

Professor Ian Mills M.Biochem, PhD

Examiners

Internal: Professor Amato Giaccia BA PhD, Director MRC Oxford Institute for Radiation Oncology

External: Professor Robert Bristow MD PhD FRCPC, Professor of Cancer Studies, Director of the Manchester Cancer Research Centre (MCRC)

Declaration

I declare that all the data presented in this thesis was conducted by myself unless otherwise stated and does not constitute part of any other thesis submitted elsewhere. The work was carried out while I was a clinical research training fellow and DPhil candidate at the CRUK/MRC Oxford Institute for Radiation Oncology at the University of Oxford under the supervision of Professors Richard J Bryant and Ian Mills (and formerly Professor Ruth Muschel). My DPhil project was funded by a clinical research training fellowship awarded by the CRUK/MRC Oxford Institute for Radiation Oncology and a fellowship award from The Urology Foundation (TUF).

Acknowledgements

Firstly, I would like to thank my primary supervisor Professor Richard Bryant for his continual support and guidance throughout the duration of my DPhil. I am very grateful to him for his mentorship throughout this research project and for allowing me to bring my own ideas to the table. I would also like to thank my co-supervisors Professors Ruth Muschel for her valuable insight into the project who has now retired, as well as Professor Ian Mills for his helpful advice and suggestions.

Furthermore, I am particularly grateful to Dr Hanna Sjoberg, for her help with all *in vivo* experiments and for training me in all relevant *in vivo* techniques to allow me to reach *in vivo* experimental independence. I would also like to thank Said Alyacoubi (who spent a term in the lab completing his MSc in Integrated Immunology at the NDS) for his help with analysis of all nanostring data. I would also like to thank Emma Murphy for her help with some of these experiments.

I would like to acknowledge Sean Smart, Veerle Kersemans, and Danny Allen in the Imaging Core at the Radiobiology Research Institute (RRI) for their help and training in *in vivo* DCE-MRI, and for imaging data analysis. I am also grateful to Uzi Gileadi, Alex Gordon-Weeks and Keaton Jones for help with lentiviral transfection and flow-cytometry experiments. I would also like to thank Professor Boris Vojnovic and Iain Tullis for the design and in house development of the bespoke laser machine that was required for the delivery of vascular-targeted photodynamic therapy. I am grateful to Professor Avigdor Scherz for hosting me in his laboratory at the Weizmann Institute of Science, Israel, in October 2018, where I was able to get training in the VTP technique in pre-clinical models. I am also grateful to Natalia Koudinova, Lilach Agemy and Dina Preise in the Sherz lab for the training they provided in the VTP treatment of pre-clinical models of cancer.

Finally, I am grateful to Cancer Research UK and The Urology Foundation for funding support for this work, and to the Academy of Medical Sciences for the award of a Daniel Turnberg Travel Fellowship, which enabled me to undergo bespoke training in the Scherz laboratory at the Weizmann Institute of Science.

Investigating multi-modal therapy with radiotherapy, vascular-targeted photodynamic therapy and immunotherapy in pre-clinical models of prostate cancer

Yiannis Philippou, St Cross College, DPhil in Oncology, Michaelmas Term 2021

Abstract

Radiotherapy enhances innate and adaptive anti-tumour immunity. It is unclear whether this effect may be harnessed by combining immunotherapy or vascular-targeted photodynamic therapy with radiotherapy fractions used to treat prostate cancer. Firstly, the aim of this study was to investigate the tumour immune microenvironment and tumour vascular responses of pre-clinical prostate cancer models to radiotherapy. Having defined this landscape, the effects of combining fractionated radiotherapy with anti-PD-L1 immune checkpoint blockade or vascular-targeted photodynamic therapy on tumour growth delay was investigated. 3 x 5 Gy caused tumour growth delay in TRAMP-C1 and MyC-CaP. Tumour immune microenvironment changes in TRAMP-C1 at 7 days post-radiotherapy included increased tumour-associated macrophages and dendritic cells and upregulation of PD-1/PD-L1, CD8+ T-cell, dendritic cell, and regulatory T-cell genes. At tumour regrowth post 3 x 5Gy the tumour immune microenvironment flow-cytometry was similar to control tumours, however CD8+, natural killer and dendritic cell gene transcripts were reduced. PD-L1 inhibition plus 3 x 5 Gy in TRAMP-C1 did not enhance tumour growth delay versus monotherapy. Fractionated radiotherapy induced 'vascular normalisation' changes in prostate cancer flank tumour allografts, improving vascular function as demonstrated using dynamic contrast-enhanced magnetic resonance imaging. Fractionated radiotherapy followed by vascular-targeted photodynamic therapy significantly delayed tumour growth in flank prostate cancer allograft pre-clinical models, compared with monotherapy with fractionated radiotherapy or vascular-targeted photodynamic therapy, and improved overall survival. This research suggests that multi-

modal therapies for prostate cancer beyond immunotherapy may be necessary to achieve radiotherapy-induced anti-tumour responses. Combining fractionated radiotherapy with vascular-targeted photodynamic therapy may be a promising multimodal approach in prostate cancer therapy. This research provides proof-of-concept for this multimodality treatment to inform early phase clinical trials.

Contents

Declaration……...2

Acknowledgements……...3

Abstract……4-5

Contents……6-11

List of figures……12-14

List of tables……14-15

List of abbreviations……15-16

Chapter 1. Introduction……..……17-83

1.1 Prostate cancer……..……..17-29

1.1.1 Hallmarks of prostate cancer……..21-25

1.1.1.1 Evading growth suppressors and cell death resistance……...22-23
1.1.1.2 Sustaining proliferative signalling and replicative immortality…….……...23
1.1.1.3 Induction of angiogenesis……23-24
1.1.1.4 Deregulation of cellular energetics……...24
1.1.1.5 Activating invasion and metastasis……..24
1.1.1.6 Tumour promoting inflammation and avoidance of immune destruction……...24-25

1.1.2 Diagnosis and staging of prostate cancer……25-26

1.1.3 Treatment of prostate cancer……..26-28

1.2 Radiotherapy for prostate cancer……..……28-47

1.2.1 Modalities of radiotherapy used in prostate cancer…….30-34

1.2.1.1 External beam radiotherapy……..……. 30-33
1.2.1.2 Brachytherapy……..…….. 33
1.2.1.3 Proton beam therapy……..……..33-34

1.2.2 Radiotherapy and its effects on tumour vasculature……...……35-41

1.2.2.1 Vascular effects of high-dose radiotherapy…….....35-37
1.2.2.2 Vascular effects from low-dose radiotherapy……...37-39
1.2.2.3 Combining radiotherapy and vascular-targeted therapy…….……...……39-41

1.2.3 Effects of radiotherapy on the immune system……..……41-47

1.3 Focal therapy for prostate cancer……48-49

1.3.1 Methods of focal therapy for prostate cancer……..49-53

1.3.2 Palladium-based WST-09 and WST-11 photosensitisers……..54-58

1.3.3 Pre-clinical studies of TOOKAD® (WST-09) and TOOKAD®-soluble (WST-11)-mediated VTP……..…….59-73

1.3.3.1 Effects on tumour vasculature……... 59-66
1.3.3.2 Anti-tumour immunity promoted by WST-09 and WST-11-mediated VTP……..……..67-73

1.3.4 Multimodal therapy using VTP in pre-clinical prostate cancer models……...…….74-75

1.3.5 Clinical trial of evidence of WST-09 and WST-11 mediated VTP in prostate cancer……..……..75-80

1.4 Study aim, hypotheses, and objectives……...…….81-82

Chapter 2. Materials and Methods

2.1 Cell lines……..……..83-84

2.1.1 culture conditions……..……...83-84

2.1.2 Freezing and thawing conditions……..……..84

2.1.3 cell count and viability……..…….84

2.2 TRAMP-C1 lentiviral transfection……..……..84-85

2.3 *In vitro* tumour cell treatments……..85

2.3.1 Treatment with γIFN……..……85

2.3.2 Treatment with ionising radiation……..……..85

2.4 Clonogenic assays to determine cell radiosensitivity……..……...85-86

2.5 Flow-cytometry quantification of *in vitro* MHC Class I and PD-L1 Expression following γIFN and ionising radiation……..……..86-87

2.6 Western blot analysis of *in vitro* TRAMP-C1 PD-L1 expression following γIFN and ionising radiation…….……87-88

2.7 Ethical statement for mouse xenograft studies……..……..89

2.8 Housing and husbandry……..……..89

2.9 Mouse anaesthesia……..……89-90

2.10 Generation of flank xenograft models……..……90

2.11 Treatment of flank PCa xenograft tumours……...…….90-95

2.11.1 Treatment of flank PCa xenograft tumours with radiotherapy…90-91

2.11.2 Treatment of PCa flank xenograft tumours with WST-11 VTP……..91-94

2.11.2.1 Preparation of WST-11……..……...91-92
2.11.2.2 WST-11 VTP treatment protocol……..93-94

2.11.3 Multimodal treatment of flank PCa xenograft tumours……..……95

2.11.3.1 Radiotherapy combined with anti-PD-L1……..……..95
2.10.3.2 Radiotherapy combined with WST-11 VTP……..……..95

2.12 Effects of fractionated 3 x 5 Gy radiotherapy on the TRAMP-C1 and MyC-CaP tumour vasculature……..…….95-96

2.12.1 DCE-MRI of flank xenograft tumours…….…….95-96

2.12.2 DCE-MRI processing and analysis……..96

2.13 Euthanasia of laboratory mice and sample collection……..……96-97

2.14 *Ex vivo* flow-cytometry of prostate cancer flank xenograft tumours..……97-98

2.15 Immune gene expression analysis of prostate cancer flank xenograft tumours……..……...98-99

2.16 Immunofluorescence of tissue sections…….……..99-100

2.17 Digital analysis of tumour vessels…….……..100

2.18 Digital annotation and quantification of tumour vessels and αSMA-positive pericytes……..…….101

2.19 Statistical analysis……..……...101-102

Chapter 3. Characterising the immunogencity and radiosensitivity of murine prostate cancer cell lines *in vitro*

3.1 Introduction……..…….103-105

3.2 Results……..….106-112

3.2.1 Investigating the *in vitro* response of TRAMP-C1 and MyC-CaP cells to ionising radiation……..……106-107

3.2.2 MHC Class I and PD-L1 expression in TRAMP-C1 cells is induced by γIFN treatment……..……..…108-109

3.2.3 MHC Class I and PD-L1 expression in TRAMP-C1 cells

is induced by radiotherapy……..……..…..110-112

3.3 Discussion……...……..113-115

Chapter 4. Impacts of radiotherapy, alone or in combination with immune check point blockade, on the *in vivo* tumour immune microenvironment in murine prostate cancer models

4.1 Introduction……..…….116-118

4.2 Results……..…….118-134

4.2.1 Hypofractionated radiotherapy induces tumour growth delay in TRAMP-C1 and MyC-CaP flank prostate cancer allograft.....118-119

4.2.2 Hypofractionated radiotherapy using 3 x 5 Gy induces immune changes in TRAMP-C1 and MyC-CaP flank prostate cancer tumour allografts……...……..120-130

4.2.3 Concomitant inhibition of PD-L1 does not enhance anti-tumour effects of hypofractionated radiotherapy using 3 x 5 Gy in TRAMP-C1 flank prostate cancer tumour allografts……...131-134

4.3 Discussion…… 134-140

Chapter 5. Treatment of murine prostate cancer allograft models with WST-11 vascular targeted photodynamic therapy

5.1 Introduction……..……141-142

5.2 Results……..……142-144

5.2.1 VTP treatment does not cause any thermal effects on the tumour…….142-143

5.2.2 VTP monotherapy induces tumour growth delay in prostate cancer flank tumour allografts……..….143-144

5.3 Discussion…….145-146

Chapter 6. Combining radiotherapy with vascular targeted photodynamic therapy in murine prostate cancer allograft models

6.1 Introduction……..…….147-149

6.2 Results……..…….150-164

6.2.1 Radiotherapy improved perfusion in prostate cancer flank tumour allografts……..……..150-152
..
6.2.2 Combination therapy with sequential RT and VTP suppressed tumour growth to a greater extent than either treatment alone……152-156

6.2.3 VTP alone or in combination with 3 x 5 Gy RT causes changes in the tumour immune microenvironment.....157-161

6.2.4 Combination therapy of RT with VTP does not result in abscopal anti-tumour effects in a bilateral prostate cancer tumour model compared to VTP monotherapy……..…162-164

6.3 Discussion……..……..165-169

Chapter 7. Discussion

7.1 The prostate cancer research landscape……..……..170-172

7. 2 Combination of RT and anti-PD-L1 does not enhance tumour growth delay in the TRAMP-C1 prostate cancer flank tumour model…172-173

7.3 Hypofractionated RT causes vascular normalisation in pre-clinical models of prostate cancer……..……...174

7.4 Combination therapy using fractionated RT followed by VTP suppressed tumour growth to a greater extent than either treatment alone……174-175

7.5 Conclusion and future work……..…….175-176

Chapter 8. References……..……...…..177-204

Chapter 9. Appendix

9.1 Plasmid transfection of TRAMP-C1 cells……..……...205

9.2 OVA-GFP TRAMP-C1 as a model to study antigen specific T-cell responses…….……..…..205-206

9.3 Radiotherapy induces ‘vascular normalisation’ changes in prostate cancer flank tumour allografts…….…..207-210

9.4 Myeloid immune population gating strategy……..……..211

9.5 Lymphoid immune population gating strategy…….……212

9.6 Antibodies used for all FACS experiments…….……213

9.7 Peer reviewed research outputs from DPhil thesis

Yiannis Philippou*, Hanna Sjoberg, Alastair D. Lamb, Philip Camilleri and Richard J Bryant. **Harnessing the potential of multimodal radiotherapy in prostate cancer.** Nat Rev Urol. 2020 May 1

Yiannis Philippou*, Hanna Sjoberg, Emma Murphy, Said Alyacoubi, Keaton Jones, Alex Gordon-Weeks, Su Phyu, Eileen Parkes, Gillies McKenna, Alastair Lamb, Uzi Gileadi, Vincenzo Cerundolo, David Sheiblin, Stephen Locket, David Wink, Ian Mills, Freddie Hamdy, Ruth Muschel, Richard Bryant. **Impacts of combining anti-PD-L1 immunotherapy and radiotherapy on the tumour immune microenvironment in a murine prostate cancer model.** Br J Cancer. 2020 July 9

Sjoberg HT, **Philippou Y***, Magnussen AL, Tullis IDC, Bridges E, Chatrian A, Lefebvre J, Tam KH, Murphy EA, Rittscher J, Preise D, Agemy L, Yechezkel T, Smart SC, Kinchesh P, Gilchrist S, Allen DP, Scheiblin DA, Lockett SJ, Wink DA, Lamb AD, Mills IG, Harris A, Muschel RJ, Vojnovic B, Scherz A, Hamdy FC, Bryant RJ. **Tumour irradiation combined with vascular-targeted photodynamic therapy enhance antirumour effects in pre-clinical prostate cancer.** Br J Cancer. 2021 June 21.

List of Figures

Figure 1.1. Prostate cancer statistics

Figure 1.2. Human prostate anatomy and epithelial cell reconstitution during progression to prostate cancer

Figure 1.3. The hallmarks of cancer

Figure 1.4. Direct and indirect effects of ionising radiation on DNA

Figure 1.5. Hypofractionation in prostate cancer radiotherapy and the Linear Quadratic model

Figure 1.6. Immunogenic cell death and immunogenic modulation of tumour cells by radiotherapy

Figure 1.7. Mechanism of classical PDT action

Figure 1.8. Patient position and apparatus used to deliver TOOKAD® VTP to patients

Figure 1.9. Chemical structure, pharmacokinetics and biodistribution of WST-11

Figure 1.10. Effects of vascular targeted photodynamic therapy on the tumour vasculature in pre-clinical models

Figure 1.11. H&E analysis and macroscopic appearance of VTP-treated tumours.

Figure 1.12. VTP mechanism of action and effects on the immune system

Figure 1.13. TUNEL staining is enhanced in tumours treated with both VTP and Degaralix

Figure 1.14. Primary Hypothesis

Figure 1.15. Secondary Hypothesis

Figure 2.1. Spectrophotometric determination of protein aggregates and WST-11 concentration

Figure 2.2 SolidWorks model of the VTP optical delivery enclosure

Figure 3.1. Radiosensitivity of TRAMP-C1 and MyC-CaP cells as determined using clonogenic assays

Figure 3.2. FACS analysis of MHC Class I and PD-L1 expression following *in vitro* treatment of TRAMP-C1 and MyC-CaP cells with γIFN

Figure 3.3. Irradiation increases prostate cancer cell surface expression of MHC Class I and PD-L1

Figure 3.4. Temporal pattern of PD-L1 expression in TRAMP-C1 cells following γIFN and 6 Gy ionising radiation

Figure 4.1. Radiotherapy causes tumour growth delay in TRAMP-C1 and MyC-CaP flank tumour allografts

Figure 4.2. Radiotherapy causes early temporal changes in the immune cell composition of TRAMP-C1 flank tumour allografts

Figure 4.3. Heatmap representation of differential gene expression from the 795 gene probe set across different immune cell subsets between 3 x 5 Gy RT treated tumours (n=5) and untreated controls (n=4) at the 7-day timepoint

Figure 4.4. Radiotherapy effects at the ≥400 mm^3 tumour endpoint in TRAMP-C1 tumour allografts

Figure 4.5. Heatmap representation of differential gene expression from the 795 gene probe set across different immune cell subsets between 3 x 5 Gy RT treated tumours and untreated controls at the late time point

Figure 4.6. Radiotherapy effects on MyC-CaP tumour allografts at the 'early' 7-day and ≥400 mm^3 regrowth timepoint.

Figure 4.7. Heatmap representation of differential gene expression from the 795 gene probe set across different immune cell subsets between 3 x 5 Gy RT treated tumours and untreated controls at early (A) and late timepoint (B).

Figure 4.8. Radiotherapy upregulates the PD-1 / PD-L1 axis

Figure 4.9. Tumour growth delay analysis of TRAMP-C1 allograft tumours following treatment with either 3 x 5 Gy RT alone, anti-PD-L1 alone, or combined 3 x 5 Gy and anti-PD-L1

Figure 4.10. FACS analysis at tumour re-growth to ≥400 mm^3

Figure 5.4. Thermal evaluation of flank tumours following laser illumination with and without prior infusion of WST-11

Figure 5.5. VTP causes tumour growth delay in TRAMP-C1 flank tumour allografts

Figure 6.1. 3 x 5 Gy RT improves vascular perfusion of flank TRAMP-C1 prostate cancer tumour allografts as demonstrated using DCE-MRI

Figure 6.2. Representative examples of DCE-MRI images and pimonidazole staining showing pre and post 3 x 5 Gy RT effects on TRAMP-C1 flank tumour perfusion and hypoxia

Figure 6.3. Multimodality therapy with 3 x 5 Gy RT followed at 7 days by VTP causes tumour growth delay in TRAMP-C1 flank tumour allografts presented as individual tumour growth delay kinetics

Figure 6.4. Multimodality therapy with 3 x 5 Gy RT followed at 7 days by VTP causes tumour growth delay in TRAMP-C1 flank tumour allografts presented as grouped tumour growth delay kinetics

Figure 6.5. 3 x 5 Gy RT improves efficacy of subsequent VTP delivered 7 days later

Figure 6.6. FACS analysis of the tumour immune microenvironment of TRAMP-C1 tumour allografts at the 12-day timepoint post initiation of VTP compared to untreated controls and 3 x 5 Gy RT-treated tumours

Figure 6.7. VTP and its combination with 3 x 5 Gy RT immune effects at the ≥400 mm^3 endpoint in TRAMP-C1 tumour allografts

Figure 6.8. Combination therapy with 3 x 5 Gy RT and VTP in a bilateral tumour model does not cause tumour growth delay in the contralateral untreated tumour

Figure 6.9. FACS analysis of contralateral untreated tumours following 3 x 5 Gy RT and VTP, or VTP alone

Figure 9.1. Generation of OVA-GFP TRAMP-C1 cells

Figure 9.2. CD69 expression (an early T-cell activation marker) on OT-1 $CD8^+$ T-cells after co-incubation with OVA-GFP TRAMP-C1 cells or wilt-type (untransfected) TRAMP-C1 controls with 0 ng/mL – 10 ng/mL IFN-γ

Figure 9.3. Fractionated radiotherapy induces vascular normalisation in flank TRAMP-C1 prostate cancer tumour allografts

Figure 9.4. Fractionated RT induces 'vascular normalisation' changes in flank TRAMP-C1 PCa tumour allografts

Figure 9.5. Representative flow cytometry dot plots indicating the gating strategy for identification of myeloid populations

Figure 9.6. Representative flow cytometry dot plots indicating the gating strategy for identification of lymphoid populations

List of Tables

Table 1.1. Genetic changes which can drive primary prostate cancer.

Table 1.2 The Gleason Grade Group risk group scoring system

Table 1.3 EAU risk groups for biochemical recurrence of localised and locally advanced prostate cancer.

Table 1.4 Combination of RT and immunotherapy in prostate cancer pre-clinical models

Table 1.5 Completed and ongoing clinical trials combining radiotherapy and immunotherapy in PCa.

Table 1.6 Summary of VTP anti-tumour effects on multiple pre-clinical models of cancer

Table 1.7 Combination of VTP and immunomodulation in pre-clinical tumour models.

Table 1.8 Clinical trials data on VTP-mediated treatment of prostate cancer

Table 2.1. Tumour cell plating density/well for each dose of ionising radiation

Table 8.1 Antibodies used for flow cytometry analysis

List of Abbreviations

ADT; Androgen deprivation therapy
AE; Adverse event
AIDA; Annotation of Image Data by Assignments
APCs; Antigen presenting cells
AR; Androgen receptor
AS; Active surveillance
ATCC; American Type Culture Collection
Bchl; Bateriochlorophyll
BMDCs; Bone Barrow Derived Cells
BOLD; Blood oxygenation dependent
BSA: Bovine serum albumin
BT; Brachytherapy
CLI; Cherenkov Luminescence imaging
CT; Computed tomography
Cu; Copper
DAMPs; Damage associated molecular patterns
DC; Dendritic cell
DCE-MRI; Dynamic-contrast enhanced MRI
DMEM; Dulbecco's Modified Eagle Medium
DMSO; Dimethyl sulphoxide
DRE; Digital rectal examination
EBRT; External beam radiotherapy
FACS; Fluorescent activated cell sorting
FBS; Fetal bovine serum
FFPE; Formalin-fixed paraffin-embedded
FMO; Fluorescence minus one
FT; Focal therapy
Gd; Gadolinium
GGG; Gleason Grade Group
GFP; green fluorescent protein
Gray; Gy
GS; Gleason score
H&E; Haematoxylin & Eosin
HIF; Hypoxia-inducible factor
HIFU; High-intensity focused ultrasound
HSPs; heat shock proteins
iAUC; initial area under curve
ICB; Immune checkpoint blockade
ICD; Immunogenic cell death
IFN; interferon
IR; Ionising radiation
iRT; immunotherapy and radiotherapy
LDI; light density index
Mn; Manganese

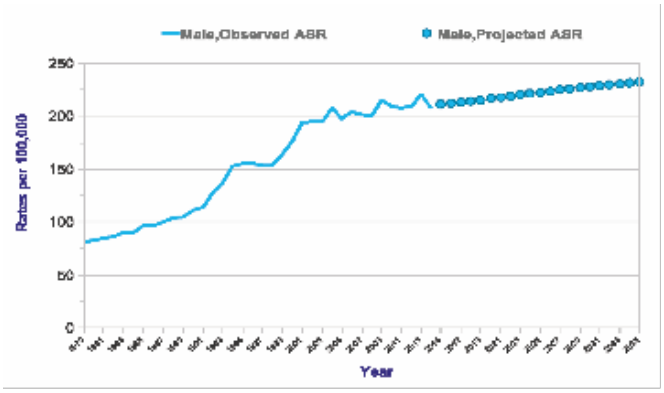
mCRPC; Metastatic castration resistant prostate cancer
MVD; Microvessel density
MDT; Metastasis directed therapy
MDSCs; Myeloid Derived Suppressor Cells
MHCI; Major Histocompatibility Complex - 1
mpMRI; multiparametric magnetic imaging resonance imaging
MSOT; Multispectral optoacoustic tomography
NIR; Near Infra-red
NO; Nitric oxide
OVA; ovalbumin
PBT; Proton beam therapy
PCa; Prostate cancer
PD; Palladium
PDT; Photodynamic therapy
PET: Positron emission topography
PIA; Proliferative inflammatory atrophy
PIN; Proliferative intraepithelial neoplasia
PIL; Procedure Individual License
PPL; Procedure Project Licence
PSA; Prostate specific antigen
RBC; Red blood cell
RCTs; Randomised control trials
RENCA; renal adenocarcinoma cell line
RECIST; Response Evaluation Criteria in Solid Tumours
RIPA; Radioimmunoprecipitation assay
ROS; Reactive oxygen species
RP; Radical prostatectomy
RT; Radiotherapy
SA; Serum albumin
SBRT; Stereotactic body radiotherapy
SOC; Standard of care
$sPO_{2;}$ Oxygen saturation
TAAs; Tumour-associated antigens
TAMs; Tumour-associated macrophages
TBST; Tris-buffered saline 0.1%/Tween 20)
TILs; Tumour infiltrating lymphocytes
TIME; Tumour immune microenvironment
TRAMP; transgenic adenocarcinoma mouse prostate
Treg; $CD4^+$ T-regulatory cells
TRUS; trans-rectal ultrasound guidance
TSG; Tumour suppressor gene
VEGF; Vascular Endothelial Growth Factor
VTP; Vascular-targeted photodynamic therapy
WB; Western blot

Chapter 1. Introduction

1.1 Prostate cancer

Prostate cancer (PCa) is the most commonly diagnosed non-cutaneous malignancy, with approximately 48500 new cases in the UK every year (**figure 1.1A**). It is the second leading cause of male cancer-related death in the UK, contributing to 11700 cancer-related deaths annually (Cancer Research UK, 2015). Increasing age is a primary risk factor for PCa (**figure 1.1B**), whilst race and positive family history, especially at a young age, are additional risk factors.

A



B

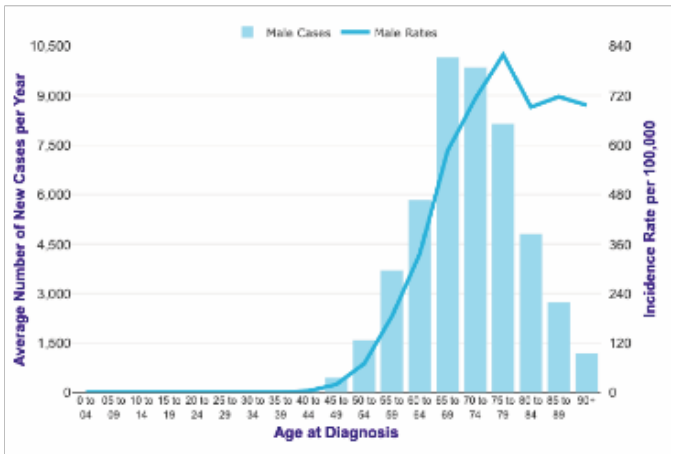


Figure 1.1. Prostate cancer statistics. (A) age standardised observed and projected prostate cancer incidence in the UK. **(B)** prostate cancer incidence according to age. (Image adapted from prostate cancer statistics at cancerresearchuk.org)

The human prostate is a glandular organ situated inferior to the bladder, composed of epithelial acini arranged in a fibromuscular stromal network (**figure 1.2A**). The epithelial acini are highly organised and consist of a layer of terminally differentiated columnar secretory luminal cells, which makes up the majority of the epithelium, and a basal cell layer containing stem, transit amplifying and committed basal cells (**figure 1.2B)** [Packer and Maitland, 2016]. The prostate is an accessory gland of the male reproductive system, and its main function is to contribute to seminal fluid, which makes up to 20-30% of the total volume of fluid in the ejaculate. The prostate contributes important components of the seminal fluid including proteolytic enzymes such as prostate specific antigen (PSA) and prostatic acid phosphatase. PSA functions to liquefy coagulated semen and hence improves the chances of fertilisation. Prostatic secretions also have a protective effect on the urinary tract by preventing bacteria from colonising the urethra.

The aetiology of PCa is multi-factorial, involving a complex interaction between genetic and environmental factors. For example, family history and racial/ethnic background are associated with an increased PCa incidence, suggesting a genetic predisposition. Genome-wide association studies have identified several susceptibility loci contributing to the risk of PCa, partly explaining the familial risk for this disease [Al Olama et al., 2015]. However, only a small subpopulation of men with PCa (9%) have true hereditary disease defined as three or more affected relatives, or at least two relatives who have developed early-onset PCa (age <55 years) [Hemminki, 2012]. Men of African descent show a higher incidence of PCa and generally exhibit a more aggressive disease course [Tan et al., 2016]. A wide variety of exogenous/environmental factors are presumed to be associated with the risk of developing PCa [Leitzmann and Rohrmann, 2012]. Japanese men have a lower PCa risk compared to men from the Western world. However, as Japanese men move from Japan to the USA or Europe, their risk of PCa increases, approaching that of American and European men. This implies a role for environmental or dietary factors [Breslow et al., 1977].

PCa is thought to develop in a stepwise fashion characterised by phenotypic, micro-environmental and molecular changes (**figure 1.2D**). Initial damage to the prostatic tissue may be initiated by an inflammatory insult, which in turn causes proliferative inflammatory atrophy (PIA) characterised by luminal and basal proliferation. It is thought that the hyper-proliferative response in PIA which occurs in association with inflammation can in some cases be a precursor of prostatic intraepithelial neoplasia (PIN), though studies have also shown that PIN can develop *de novo* from normal, non-atrophic glands [Vral et al., 2012]. PIN may eventually progress to PCa, with malignancy characterised by uncontrolled luminal cell proliferation, loss of basal epithelial cells, basement membrane breakdown, immune cell infiltration and the presence of reactive stroma which aids tumour growth [Shen and Abate-Shen, 2010]. Malignancy develops most commonly in the peripheral zone of the organ mimicking the zonal selectivity of PIA and PIN [De Marzo et al., 2007], and multiple independent histological foci of genetically distinct PCa may develop [Lin et al., 2006].

Insights into the genomic complexity of PCa through whole-exome or whole-genome sequencing studies has deepened our recognition of the early and late genetic events which occur in prostate carcinogenesis (**figure 1.2D**) [Taylor et al., 2010]. The spectrum of genes altered by these genetic changes comprises tumour suppressor genes (TSGs), histone modifying genes, the androgen receptor (AR) gene, and genes affecting the DNA damage response such as BRCA1/2 and ATM (**table 1.1**). Such genetic defects cause genomic instability which drive clonal evolution, intra-and inter-tumoural heterogeneity, malignant progression and ultimately therapy resistance [Cahill et al., 1999].

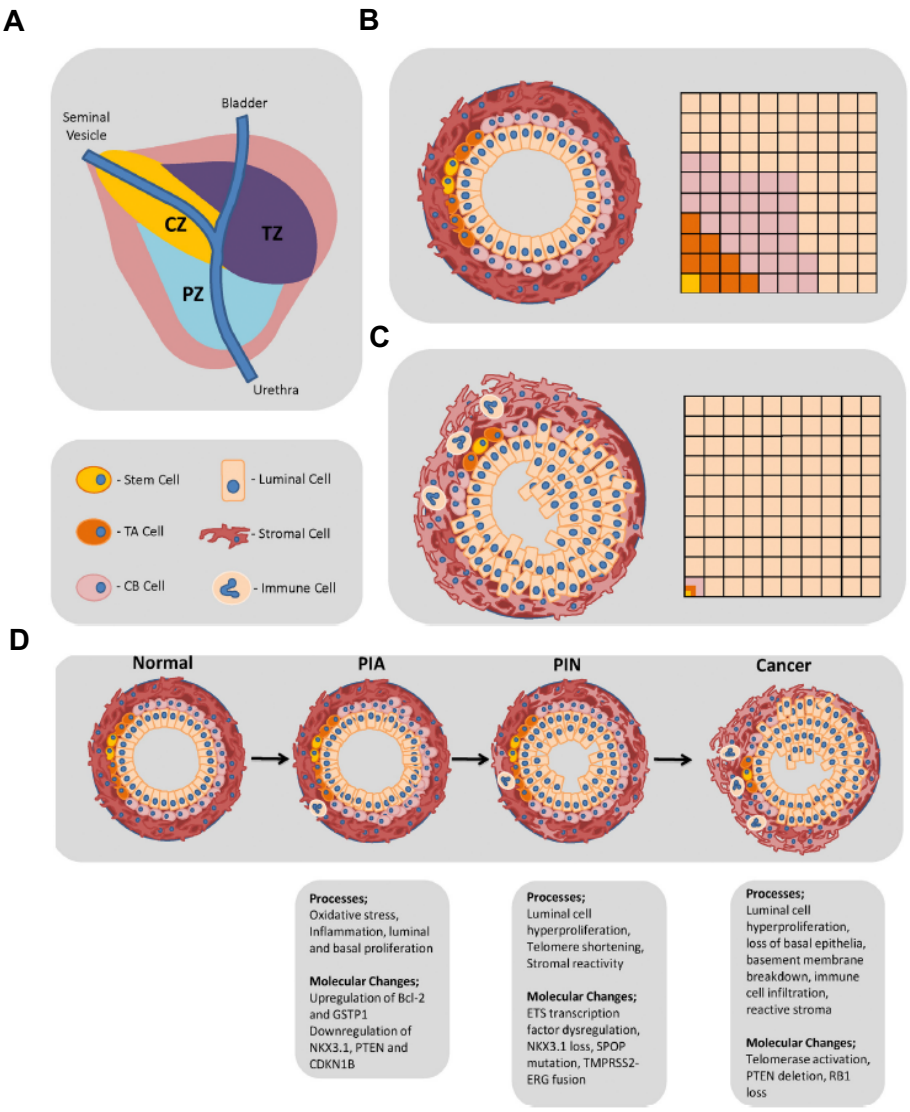


Figure 1.2. Human prostate anatomy and epithelial cell reconstitution during progression to prostate cancer. **(A)** The prostate is located beneath the bladder and is composed of three distinct zones; the central zone (CZ) that contains the ductal tube from the seminal vesicle to where it meets the descending urethra, the peripheral zone (PZ) that is directly below the bladder and surrounds the transitional urethra. Benign prostatic hyperplasia occurs in this region of the prostate. **(B)** Diagrammatic representation of a normal prostatic acinus; the epithelial bilayer of basal and luminal cells surrounded by fibromuscular stroma. The relative content of different epithelial cells in the normal prostate are summarised graphically; luminal 60%, basal 40% and the stem cells constituting ~1% of total epithelia. **(C)** Cellular composition of a cancerous acinus. Prostate cancer is characterised by luminal hyperproliferation, loss of basal layer and breakdown of basement membrane, immune cell infiltration and stromal reactivity skewing the epithelial percentages; the luminal cells make up > 99% of tumours whilst basal cells are estimated to constitute < 0.1% of tumour epithelial cells**. (D)** Phenotypic, micro-environmental and molecular changes incurred through the pre-malignant states of prostate cancer. Image adapted from [Packer and Maitland, 2016]. With permission from Elsevier.

Common prostate cancer genetic changes	
Oncogenic drivers	**Tumour suppressors**
TMPRSS2-ETS fusions A translocation or interstitial deletion event places an ETS factor, most commonly ERG but also ETV1, ETV4 and ETV5, under the control of the TMPRSS2 promoter. The ETS proteins are developmental transcription factors that affect proliferation, migration and transformation of cells These gene fusions are seen in over half of all prostate cancers	**PTEN deletion (10q23)** Heterozygous deletion of the PTEN gene is observed in ~40% of primary tumours. PTEN is the reciprocal phosphatase of PI3K. Reduced removal of PI3K phosphorylations causes unchecked AKT activation that allows for increased cell survival and proliferation. Mutation of the gene is also observed
MYC amplification (8q24) MYC is seen to be upregulated in early prostate tumours and its locus is frequently amplified in advanced cancers. The gene encodes a transcription factor that has well characterised transformative properties due to its role in cell cycle progression	**CDKN1B deletion** CDKN1B is deleted in ~20% of primary tumours. The protein acts as a CDK inhibitor that control the G_1 cell cycle checkpoint, loss of protein allows for easier commitment to the cell cycle and thus promotes increased proliferation. Mutation of the gene also occurs
Telomerase activation The protection of chromosome ends by inappropriate activation of telomerase prevents replicative senescence in highly proliferative cancer cells. Telomerase expression is switched on during PIN and early PCa	**NKX3.1 deletion** NKX3.1 is heterozygously deleted in up to 85% of PCa And is downregulated in PIN. The protein is a homeobox transcription factor that regulates prostate epithelial development
IL-6 expression Inflammation causes upregulation of both IL-6R and oncostatin M, an IL-6 signal transducer, in prostate stem cell population. An increase of systemic IL-6 in PCa patients creates a positive feedback loop favourable towards transformation through enhanced STAT3 activation and associated downstream gene expression	**SPOP mutation** SPOP is mutated in 6-15% of primary cancers. This is a molecular events that is mutually exclusive of TMPRSS2-ERG fusions. SPOP is an adaptor protein for the Cullin3 E3 Ubiquitin Ligase and directs the proteasomal Degradation of oncogenic proteins such as AR, DEK and ERG, and is also involved in the DNA damage response and cellular senescence.
	RB1 loss RB1 loss is late feature in PCa progression occurring in approximately 21% of patients according to the CRPC500 cohort

Table 1.1. Genetic changes which can drive primary prostate cancer.

1.1.1 Hallmarks of prostate cancer

PCa is a complex heterogeneous disease characterised by the acquisition of diverse sets of cancer hallmark capabilities, along with aberrant functioning of AR signalling which is the central driving force behind prostatic tumourigenesis and its transition into metastatic castration resistant disease. The hallmarks of cancer were first described by Douglas Hanahan and Robert A. Weinberg in 2000 [Hanahan and Weinberg, 2000] and updated in 2011 with the addition of further emerging hallmarks [Hanahan and Weinberg, 2011]. These hallmarks (**figure 1.3**) describe the biological capabilities acquired during the multistep development of cancers and constitute an organising principle for rationalising the complexities of neoplastic disease.

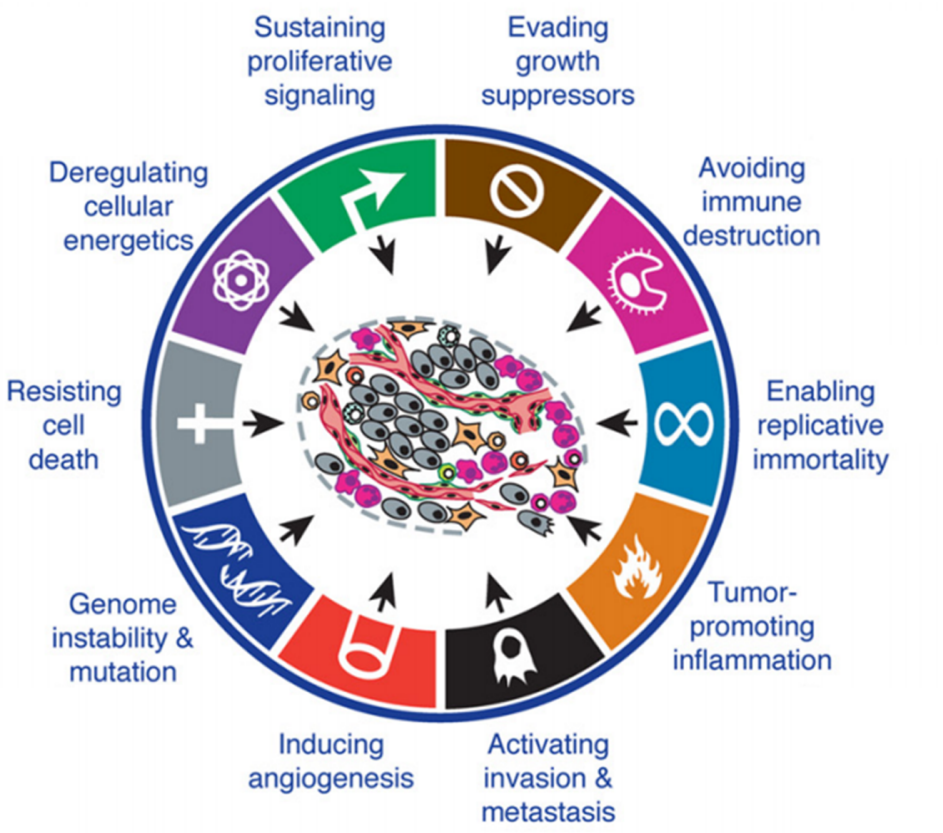


Figure 1.3. The hallmarks of cancer. Image adapted from [Hanahan and Weinberg, 2011]. With permission from Elsevier

1.1.1.1 Evading growth suppressors and cell death resistance

One of the fundamental features of PCa tumourigenesis involves the acquisition of insensitivity to growth inhibitory signals or evasion of growth suppression. This is mainly due to the loss of expression or functional inactivation of TSGs and/or proteins associated with cell cycle regulatory activities. These alterations in the functional behaviour of diverse sets of TSGs are brought about due to deletion, mutation, loss of expression, rearrangement, promoter hypermethylation and haploinsufficiency of multiple chromosomal regions including 1p, 6q, 7p, 7q, 8p, 10q, 13q, 16q, 17p, 17q and 18q, harbouring the sites of many important TSGs [Isaacs and Kainu, 2001; Karan et al., 2003]. Similarly all of the major cell cycle regulators in PCa which respond to anti-proliferative signalling including p14, p16, p21, p27, Rb1 and p53 are deregulated by multiple pathways and are subjected to loss of function [Lee et al., 2008]. PCa cells

acquire cell death resistance mechanisms through the evasion of intrinsic and extrinsic apoptotic pathways, and combined with the evasion of growth suppression these are critical pathophysiological factors for the initiation and progression of PCa to its lethal castration-resistant state [McKenzie and Kyprianou, 2006].

1.1.1.2 Sustaining proliferative signalling and replicative immortality

PCa cells produce their own growth signals to trigger cell growth, proliferation, and survival. Aberrant functioning of the AR is a particular key feature in PCa development and progression [Feldman and Feldman, 2001]. The mechanisms involved in aberrant function of the AR are complex, but include hyperactivation of the AR as a result of genetic mutations involving the receptor, and/or PTEN loss, and hyperactivation of the AR due to overexpression of AR coactivators and downregulation of its co-repressors [Devlin and Mudryj, 2009]. Enhanced AR signalling results in self-sustaining PCa cellular proliferation. Androgen deprivation therapy (ADT) is a key standard of care (SOC) in patients with localised disease treated with radiotherapy (RT), and in patients with metastatic PCa. However, the emergence of an androgen independent phenotype is a typical characteristic of PCa development, and this is responsible for castration-resistant disease which until recently had a mean survival time of only 16-18 months [Katsogiannou et al., 2015]. Telomere dysfunction, and reactivation of the telomerase reverse transcriptase activity causing telomere maintenance, also plays an important role in the limitless replicative potential of PCa cells [Ding et al., 2012].

1.1.1.3 Induction of angiogenesis

Angiogenesis is needed for multiple steps in prostate tumourigenesis, ranging from tumour outgrowth to its metastatic dissemination [Melegh and Oltean, 2019]. Although there are no direct markers to assess angiogenic activity in PCa, microvessel density (MVD) is considered a good surrogate marker of angiogenic activity, and MVD directly correlates with tumour stage, grade and clinical course [Strohmeyer et al., 2000]. Another

surrogate marker for tumour angiogenesis is the level of angiogenic regulators in the tumours such as vascular endothelial growth factor (VEGF). Among the VEGF isoforms, VEGF-A plays an important role in PCa angiogenesis [Wong et al., 2005] and is overexpressed in patients with distant metastasis and poor prognosis [Duque et al., 1999; Green et al., 2007].

1.1.1.4 Deregulation of cellular energetics

Deregulation of cellular energetics refers to the reprogramming of energy metabolism by malignant cells in order to increase the rate of glycolysis during periods of rapid cellular proliferation. Metabolomic analyses have improved understanding of the normal metabolism of prostate cells and the metabolic modifications acquired by PCa cells to accommodate the massive energy requirement for rapid proliferation. These modifications include (a) decrease in zinc uptake, (b) the Warburg effect, (c) *de novo* fatty acid and cholesterol synthesis, and (d) PTEN inactivation [Eidelman et al., 2017].

1.1.1.5 Activating invasion and metastasis

The underlying mechanisms promoting PCa metastasis depend on the orchestration of key complex biological events such as cellular migration, invasion, cell adhesion and epithelial-mesenchymal transition [Clarke et al., 2009]. Although PCa most typically follows a slow progression pattern, metastatic dissemination comprises the principal cause for PCa-associated mortality [Karantanos et al., 2013].

1.1.1.6 Tumour promoting inflammation and avoidance of immune destruction

Studies suggest that inflammation plays a role in multiple stages of PCa development, particularly through the action of inflammatory regulators known as inflammasomes, which cause a cascade of pro-inflammatory cytokines regulating various cellular activities [Karan and Dubey, 2016]. PCa cells play an important role in initiating and amplifying the prostatic inflammatory process through activation of the NF-κB pathway. Downstream

targets of NF-κB include inflammatory cytokines that attract tumour associated macrophages (TAMs) and myeloid-derived suppressor cells (MDSCs) into the tumour immune microenvironment (TIME) [Wong et al., 2009]. These secreted and cellular immunosuppressive factors contribute to the evolution of an immunologically "cold" PCa TIME dominated by immunosuppressive cells [Vitkin et al., 2019].

1.1.2 Diagnosis and staging of prostate cancer

Presently there is no single test for the detection of PCa, and early stage PCa is usually asymptomatic. Diagnosis of PCa initially involves a PSA blood test and digital rectal examination (DRE). If PCa is suspected due to an elevated PSA or an abnormal DRE the patient is nowadays offered a multi-parametric MRI (mpMRI) of the prostate. Diagnosis is then established by trans-rectal ultrasound-guided (TRUS) or transperineal biopsy of the prostate, which involves targeting of any suspicious lesions seen on mpMRI along with systematic biopsy sampling of the prostate gland.

In current day clinical practice PCa is graded using the Gleason scoring (GS) system, which assigns a grade from one to five reflecting the similarity on histological analysis between cells in the cancerous tissue and normal cells in the prostate. Grade 1 indicates high similarity with normal cells while Grade 5 indicates very abnormal cell morphology and growth patterns. Two individual areas that comprise the majority of the cancer are assessed and added together to produce the Gleason sum score, which can vary between two and ten. The GS is then grouped into 5 prognostic Gleason grade groups (GGG) **(table 2**)

Risk Group	Grade Group	Gleason Score
Low	1	Gleason score ≤ 6
Intermediate favourable	2	Gleason score 7 (3+4)
Intermediate unfavourable	3	Gleason score 7 (4+3)
High	4	Gleason score 8
High	5	Gleason score 9-10

Table 1.2. The Gleason Grade Group risk group scoring system

Other investigations which may be undertaken to establish the full clinical extent of PCa include MRI, computerised tomography, bone scintigram or positron emission tomography/computed tomography (PET/CT), and ^{99}Tc bone scans. These imaging modalities facilitate staging of PCa based on the TNM system, which evaluates the primary tumour size and spread to nearby structures such as the bladder or rectum (T), draining lymph nodes (N) and the presence of distant metastasis (M).

1.1.3 Treatment of prostate cancer

Clinical decision making regarding treatment in localised and locally advanced PCa is based on various classification systems, including the use of serum PSA, TNM staging and GGG to stratify PCa patients into low-, intermediate- or high-risk for biochemical recurrence (**table 1.c3**) based on the description by D'Amico and colleagues as well as published guidelines from the European and American Urological Associations [D'Amico *et al.*, 1998; Heidenreich, *et al.*, 2014; Sanda *et al.*, 2018].

Low-risk	Intermediate-risk	High-risk	
PSA < 10ng/mL and Gleason score < 7 (GGG 1) and cT1-2a	PSA 10-20ng/mL or Gleason score = 7 (GGG 2/3) or cT2b	PSA > 20ng/mL or Gleason score > 7 (GGG 4/5) orcT2c	any PSA any Gleason Score or GGG cT3-4 or cN+
Localised			**Locally advanced**

Table 1.3. EAU risk groups for biochemical recurrence of localised and locally advanced prostate cancer. GGG, Gleason Grade Group; PSA, prostate specific antigen

Active surveillance (AS) is an observational follow-up strategy offered to men with newly diagnosed low-risk disease (GGG1) or low-volume intermediate-risk (GGG2) PCa [Tosoian et al., 2016]. AS involves close monitoring of patients in order to avoid unnecessary 'over-treatment' of indolent tumours (as treatment interventions can be associated with significant short- and long-term complications), without compromising disease-specific mortality [Klotz et al., 2015]. AS protocols involve serial PSA monitoring, repeat DRE and mpMRI of the prostate, and repeat prostate biopsies if indicated.

Patients with localised PCa warranting radical treatment can be considered for radical external-beam RT (EBRT) with concomitant ADT, or brachytherapy (BT), or radical prostatectomy (RP) [Heidenreich et al., 2011]. Men with locally advanced PCa might receive RT with concomitant ADT, or increasingly RP with curative intent, based on patient choice and physician recommendations, with competing comorbidity influencing decision making. Metastatic PCa is currently incurable. Patients with hormone-sensitive metastatic PCa receive docetaxel chemotherapy and ADT [Gravis et al., 2013; James et al., 2016; Sweeney et al., 2015]. The choice of first line treatment in men who progress to metastatic castration-resistant PCa (mCRPC) depends on performance status, symptoms, comorbidities and extent of disease but usually includes second generation anti-androgens such as abiraterone and enzalutamide. First-line chemotherapy can also

be considered such as docetaxel or cabazitaxel. Painful bone metastatic lesions are palliated with RT, radionuclides and analgesia [Cornford et al., 2017].

1.2 Radiotherapy for prostate cancer

RT has been an integral cancer treatment for over a century. More than half of all cancer patients undergo RT at some stage during treatment either with curative intent, or in a palliative setting [Delaney et al., 2005]. Since the first introduction of RT in PCa treatment, the clinical benefit of RT has continuously improved both by technical advancements and by increased insight into the biology behind the radiation response. For example, optimised treatment planning and more precise delivery techniques have made it possible to safely increase the tumour-targeted radiation dose while sparing surrounding normal tissues. In addition, research into the cellular effects of ionising radiation (IR) has provided a detailed understanding of the effects of RT on the cell cycle, apoptosis and DNA repair. This has offered insight into optimal dose-scheduling for RT and the benefits of a fractionated treatment schedule, where the dose of radiation is divided into multiple fractions given over several weeks, [Bernier et al., 2004]. This has resulted in the “the five Rs of radiobiology” [Steel et al., 1989]. The 5Rs (Repair. Redistribution, Reoxygenation, Repopulation and Radiosensitivity) of RT represent a conceptual framework that form the rationale behind fractionation of RT [Goedegebuure et al., 2019].

RT can cause tumour cell death through multiple mechanisms (**figure 1.4**). A major direct effect of RT on cancer cells is the generation of lethal DNA double-strand breaks resulting in apoptosis, whilst indirect effects can be mediated by free radicals produced from RT-induced ionisation of cellular free water [Durante and Loeffler, 2010; Lomax et al., 2013]. RT can also be toxic to tumours via inhibition of the proliferative capacity of malignant

cells, induction of senescence, and precipitation of mitotic catastrophe during or after aberrant mitosis [Baskar et al., 2012; Eriksson and Stigbrand, 2010; Vakifahmetoglu et al., 2008]. Other mechanisms of RT-induced tumour cell death involve the generation of immunogenic cell death (ICD) through dispersion of RT-induced immune-stimulating tumour antigens released from dying tumour cells into the tumour microenvironment [Brown et al., 2014; Galluzzi et al., 2017; Golden et al., 2012; Golden and Apetoh, 2015; Janiak et al., 2017; Jeong et al., 2016].

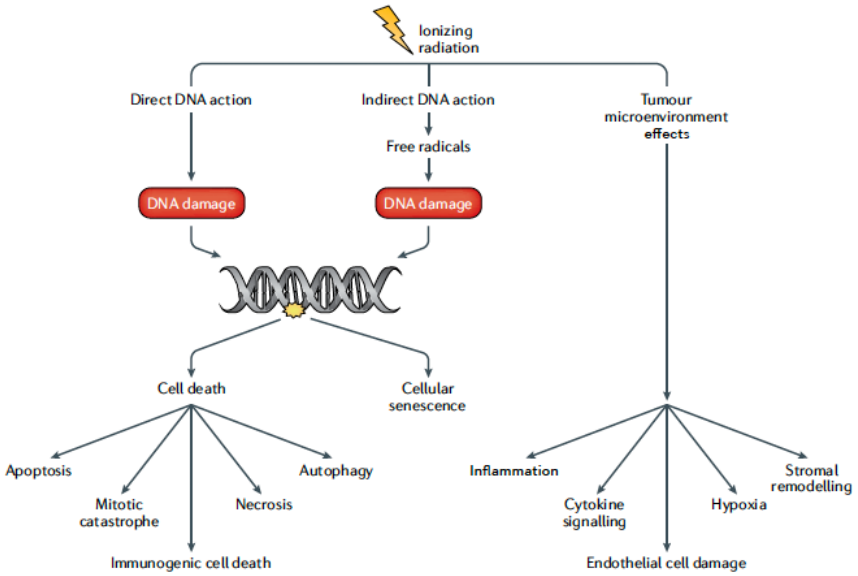


Figure 1.4. Direct and indirect effects of ionising radiation on DNA. Ionising radiation causes direct effects on DNA by inducing ionisation of cellular molecules, which damage DNA by causing single- strand or double- strand breaks. Indirect damage to DNA can be caused via the production of free radicals derived from the ionisation or excitation of the intracellular water component. These DNA damage effects can result in cellular senescence or cell death via apoptosis, mitotic catastrophe, autophagy, necrosis or immunogenic cell death mechanisms. In addition to DNA damage in tumour cells, radiotherapy also has multiple effects on the wider tumour microenvironment, including the induction of inflammation, increased cytokine signalling, endothelial cell damage in blood vessels, hypoxia and stromal remodelling. Image adapted from [Philippou et al., 2020b]. With permission from Springer Nature.

RT is one of the radical treatment options (the other being surgery) offered to patients with localised or locally advanced disease. Approximately 25-35% of patients with localised disease opt to have RT as definitive treatment [Heidenreich *et al.*, 2014; Mottet *et al.*, 2017; Martin G Sanda *et al.*, 2018]. The benefits of RT include the fact that it is non-

invasive and can therefore be used to treat PCa in patients who are older or have greater comorbidity that those who can undergo surgery, and it requires no hospital inpatient stay. Although RT has recognised adverse effects including bowel toxicity and associated sexual dysfunction, it can spare men some of the adverse effects of surgery such as urinary incontinence**.** The use of RT has recently been extended to patients with oligometastatic PCa (generally defined by the presence of three or fewer metastatic sites on imaging). Studies published since 2017 suggest that local RT to the primary PCa tumour is feasible and safe, and confers a survival advantage in the oligometastatic setting. The STAMPEDE trial [Parker et al., 2018] reported an 11% survival advantage following RT to the prostate in the setting of low-volume low-burden oligometastatic PCa. Therefore, RT to the primary tumour in addition to SOC hormone therapy and docetaxel chemotherapy, in the context of oligometastatic PCa, has now become the accepted SOC in light of the results of STAMPEDE.

1.2.1 Modalities of radiotherapy used in prostate cancer

RT for PCa can be administered as EBRT, BT at high or low-dose rates, combined EBRT and BT, or particle therapy, which includes proton beam therapy (PBT) [Zaorsky et al., 2017]. The primary technological advances in RT delivery in the last decade have largely involved changes in dose fraction and increased safety of RT delivery.

1.2.1.1 External beam radiotherapy

EBRT for localised PCa is carried out with conformal-, intensity- or volumetric-modulated RT techniques delivered as a single dose of 1.8-2.0 Gray (Gy) daily fractions for 5 days a week up to a total of 72-78 Gy. These conventional fractionation schemes are based upon the premise that tumours are typically less responsive to fraction size than normal tissues based on the Linear Quadratic model. This model with its alpha/beta value describes the curvature of cell killing both for tumour control and normal tissue toxicity in relationship to

RT dose. The alpha/beta ratio is the dose where the linear as well as the quadratic component cause the same amount of cell killing. The higher the alpha/beta ratio (low beta relative to alpha), the more linear the cell survival curve, whereas the lower the alpha/beta ratio (high beta relative to alpha), the more curved the cell survival curve (**figure 5**).

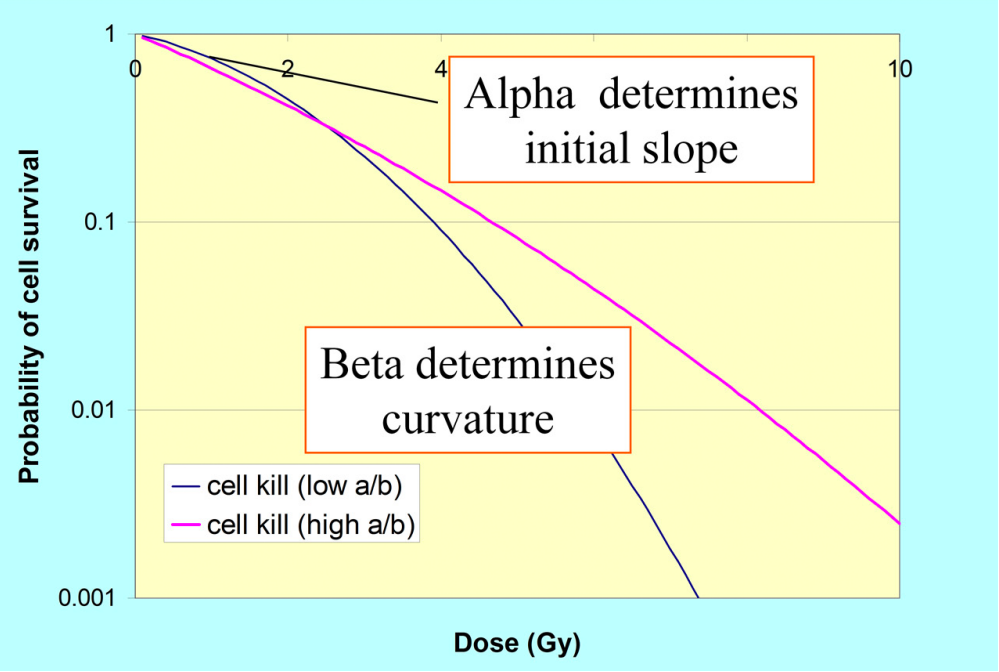


Figure 1.5. Hypofractionation in prostate cancer radiotherapy and the Linear Quadratic model. When the alpha/beta ratio is large (pink line), i.e., when the dose at which the linear and quadratic dose components are equal is large, fractionation leads to a modest effect on tumour cell survival. When the alpha/beta ratio is small (blue line), i.e., in slow growing tumours such as prostate cancer, hypofractionation leads to a large change in tumour cell kill. Image adapted from (https://humanhealth.iaea.org/HHW/RadiationOncology/Treatingpatients/Treatment_planning_and_techniques/Training_Course/03_Altered_fractionation.pdf,last accessed 26/7/2021)

Tissues with a low alpha/beta are relatively resistant to low RT doses compared to tissues with a high alpha/beta ratio. Rapidly proliferating tumours therefore have a high alpha/beta ratio of more than 10 Gy, and slowly proliferating tumours have a low alpha/beta ratio of around 3–5 Gy. Most tumours have a high alpha/beta ratio due to their fast proliferative nature and can be treated with conventionally fractionated RT (using single doses of 1.8 – 2.0 Gy). However a recent study has shown that PCa has an alpha/beta

ratio of 1.4 Gy [Miralbell et al., 2012a] and therefore hypofractionation can be applied with the aim of achieving better tumour control with no added toxicity.

Hypofractionation describes a treatment regimen that delivers high doses of IR using a shorter number of treatments as compared to conventional treatment regimens. There is no internationally recognised dose or number of treatments that constitute hypofractionation, however by definition the dose is greater than 2 Gy per fraction and is typically 2.5-5 Gy per fraction. The Conventional versus Hypofractionated High-dose intensity-modulated RT for PCa (CHHiP) study between 2002-2006 in the UK compared the standard 74 Gy in 37 fractions to moderate hypofractionation using 60 or 57 Gy in 20 or 19 fractions respectively. Results of the trial suggested that after 5 years follow up the hypofractionated doses were safe and caused no more early or late toxicity to healthy tissue than the conventional regime [Dearnaley et al., 2014]. Moreover, 5-year biochemical free survival with 60 Gy in 20 fractions was found to be non-inferior to conventional fractionation using 74 Gy in 37 fractions. Moderate hypofractionation using 60 Gy over 20 fractions is now part of SOC for the management of localised PCa.

Extreme hypofractionation, or ultrafractionation, can be delivered using stereotactic body RT (SBRT). SBRT accurately delivers a high IR dose in one or relatively few treatment fractions, typically between 1-8 fractions in number, again with no specific dose definition but typically with doses equal to or in excess of 6 Gy per fraction. SBRT delivers EBRT with target localisation using image guidance and 5–7 fractions of 6–10 Gy per fraction. Studies investigating outcomes after SBRT for localised PCa are mostly non-randomised phase 2 trials [Kothari et al., 2018]. Data from these trials demonstrate that SBRT is well tolerated and has minimal lasting effects on health-related quality of life [King et al., 2013]. SBRT also enables metastasis-directed therapy (MDT) in the setting of oligometastatic PCa using 3–7 fractions of 6–13 Gy. Although cancer-specific and overall survival outcomes for MDT using SBRT are limited by short follow-up periods, promising early

conclusions are identifiable from the STOMP, POPSTAR and SABR-COMET Phase II trials (Ost *et al.*, 2017, Ost, 2018; Siva *et al.*, 2018, Palma *et al.*, 2018). The use of SBRT is currently reserved for MDT in oligometastatic PCa.

1.2.1.2 Brachytherapy

BT comprises internalised RT using implanted Iodine-125, Palladium-103 or Caesium-131 radioisotope seeds [Dess et al., 2019]. One advantage of BT over EBRT is that it permits extreme dose escalation that exceeds conventional EBRT, and it is delivered with high target conformity [Vanneste et al., 2016]. Low-dose rate (for low- or intermediate-risk PCa permanent seed implantation), or high dose-rate temporary source implantation (for intermediate- or high-risk PCa), may be used to treat localised disease [Vanneste et al., 2016; Zaorsky et al., 2017]. Both low-dose-rate and high-dose-rate BT can be used as a boost combined with ADT and EBRT for patients with intermediate-risk and high-risk PCa. BT generally requires a patient to have a good urinary flow rate, minimal lower urinary tract symptoms, and an optimal prostate gland size [Hoskin et al., 2012, 2014; Morris et al., 2017; Zaorsky et al., 2017].

1.2.1.3 Proton beam therapy

PBT uses heavy particles such as protons and carbon ions to deposit the majority of the radiation dose directly within the tumour, and travel no further through the body, such that this causes maximum radiation-induced DNA damage within malignant cells, whilst sparing adjacent normal tissues from toxicity [Wisenbaugh et al., 2014]. PBT delivers this potential dosimetric benefit by taking advantage of a concept known as the “Bragg peak” whereby maximum dose delivery occurs immediately before particles come to rest, with a high dose being deposited at the target tumour, sparing surrounding healthy tissues [Royce and Efstathiou, 2018]. To date, the use of protons for PCa RT is not preferable to conventional RT [Lancet Oncology, 2014], as robust evidence for improved efficacy of PBT over standard photon-based RT or BT in this setting is absent.

RT has been shown to be more effective with concomitant ADT [Bolla et al., 2002, 2009, 2016; D'Amico et al., 2004], which has made this approach the SOC for intermediate- and high-risk PCa. Patients with intermediate-risk or high-risk localised PCa typically receive neoadjuvant ADT for three or six months respectively. ADT continues during and beyond RT, although the timing and duration of ADT is uncertain given that the available evidence is based on trials using historical rather than contemporary RT techniques [Leal et al., 2015; Payne and Mason, 2011], and moderately hypofractionated doses [Kotecha et al., 2016]. Typically, men with intermediate-risk localised PCa receive six months of adjuvant ADT, and those with high-risk disease receive 24 months of adjuvant ADT. Despite improvement in patient selection, RT delivery techniques and use of ADT systemic therapy, some men develop radiorecurrent PCa. Five-year biochemical progression-free survival after RT ranges from 75-85% for low-risk disease to 30-70% for high-risk and locally advanced disease [Bolla et al., 1997, 2002; Kupelian et al., 2002; Shipley et al., 1999; Zelefsky et al., 2001].

In order to further improve RT efficacy in PCa there is increasing interest in combining RT with other forms of therapy such as vascular targeting strategies or immunotherapy as part of a multimodal treatment approach to maximise therapeutic effectivity through additive or synergistic mechanisms between the different treatment strategies. Such multimodal strategies provide different opportunities and challenges, especially with regard to dose scheduling, temporal administration and timing between the treatments. Addressing these issues requires insight into the interaction between the different treatment modalities, and how they each affect the tumour microenvironment, particularly the tumour vascular bed and tumour infiltrating immune cells.

1.2.2 Radiotherapy and its effects on the tumour vasculature

The relationship between RT and the tumour vasculature became apparent with the recognition that the effects of IR largely depend on the generation of reactive oxygen species (ROS). As the generation of ROS depends on oxygen availability, well-vascularised and perfused tumour tissues are more susceptible to IR. This observation is supported by several studies in patients with head and neck, cervical and colorectal tumours, where it has been shown that radiation damage and treatment response is positively correlated with oxygen availability, while lack of oxygen hampers treatment efficiency [Horsman and Overgaard, 2016; Overgaard, 2007]. Not only does tumour perfusion and oxygenation affect the response to RT, but RT also affects tumour perfusion due to its effect on the tumour vasculature. The mechanisms behind these RT-induced vascular changes are complex and appear to be dependent on the dose and scheduling of RT.

1.2.2.1 Vascular effects of high-dose radiotherapy

High-dose RT (either single dose or fractionated) causes endothelial cell dysfunction, increased permeability, detachment from the basement membrane, and apoptosis [Heckmann et al., 1998; Wang et al., 2007], as well as dose-dependent destruction of the tumour microvasculature [Baker and Krochak, 1989]. SBRT which delivers high doses (typically 8 to 10 Gy) per fraction is thought to cause extensive damage to the tumour vasculature that amplifies tumour cell kill [Bodo et al., 2019; Park et al., 2012; Song et al., 2016]. This can occur within 24 hours [Bussink et al., 2000], possibly due to endothelial cell apoptosis or endothelial-induced vasoconstriction, but more commonly in a delayed manner over 1-3 weeks after IR [Chen et al., 2009; Song et al., 1974]. These RT-induced vascular changes have also been observed in pre-clinical mouse models with multiple lower doses of RT, such as 5 x 6 Gy, whereby the total dose delivered is high [Fenton et al., 2004; Zywietz et al., 1994]. The consequent damaged vasculature and reduction in

perfusion often results in tumour hypoxia. Recent evidence suggests that RT-induced tumour hypoxia induces several parallel pathophysiological cascades which promote angiogenesis and repair of the damaged vasculature, which may ultimately lead to tumour recurrence. This is in addition to the role of tumour hypoxia in causing resistance to RT due to a reduced production of ROS-induced double-strand DNA breaks [Brown and Wilson, 2004].

Hypoxia following high single doses or fractionated doses of RT leads to stabilisation of hypoxia inducible factor (HIF)-1α [Chen et al., 2009; Kane et al., 2016; Kioi et al., 2010; Maeda et al., 2017]. HIF-1 is a transcription factor that regulates many genes involved in the homeostatic responses of cells and tissues to reduced oxygen levels. It is composed of HIF-1α and HIF-1β subunits. HIF-1β, is ubiquitously expressed, whereas HIF-1α is rapidly degraded by oxygen. At low levels of oxygen HIF-1α becomes stabilised, levels increase, and it binds to its partner HIF-1β, before translocating to the nucleus where it induces transcription of genes involved in the cell's response to hypoxia [Jaakkola et al., 2001]. One such response is the induction of pro-angiogenic factors such as VEGF-A and its receptor VEGFR1, which causes rapid and chaotic proliferation of endothelial cells. This results in the sprouting of newly formed blood vessels characterised by irregular branching, an inconsistent diameter, and increased vessel leakiness due to abnormal endothelial cell tight junction formation, which ultimately increases tumour hypoxia [Harris, 2002, Baker and Krochak, 1989].

Accumulating evidence suggests that hypoxia caused by RT-mediated vascular damage and consequent stabilisation of HIF-1α initiates a sequence of events that attracts pro-angiogenic cells, principally from the bone marrow, which promote recovery of the vasculature. HIF-1-mediated transcription of several cytokines and chemokines recruits bone marrow derived cells (BMDCs) following RT-induced hypoxia into the tumour

microenvironment [Stephens, Currie and Peacock, 1978; Ahn and Brown, 2008; Kozin *et al.*, 2010; Lecavalier-Barsoum *et al*., 2019]. These BMDCs are primarily monocytes and express $CD11b^{+}F480^{+}$(macrophages) or $CD11b^{+}/Gr1^{+}$ (MDSCs). One role of these pro-angiogenic BMDCs is to help rescue the RT-damaged tumour vasculature through angiogenesis, and to repair damaged bloods vessels, a process known as "vasculogenesis" [Brown, 2020]. The role of BMDCs in "vasculogenesis" has been shown in several pre-clinical models and is thought to be primarily mediated by CXCL12 and it's receptor CXCR4 or stromal cell derived factor -1, although several other cytokines and chemokines also play a role [Kioi *et al.*, 2010; Liu *et al.*, 2014]. In addition, MDSCs and macrophages, particularly of the anti-inflammatory and pro-angiogenic phenotype (M2), are known to cause an immunosuppressed tumour TIME by down-regulating immune surveillance and the anti-tumour activity of cytotoxic $CD8^{+}$ T-cells, thereby facilitating immune escape and tumour regrowth [Ostrand-Rosenberg and Sinha, 2009]. Several pre-clinical studies have shown increased radiosensitivity of tumours following inhibition of HIF-1 [Kioi et al., 2010; Schwartz et al., 2010], CXCL12-CXCR4 interaction [Chaudary *et al.*, 2017; Lecavalier-Barsoum et al.,2019] or tumour monocyte infiltration by blocking cytokines or their receptors, such as CD11b, CSF-1R or CCL2, known to enhance the influx of these cells into the tumour microenvironment following RT [Ahn et al., 2010; Jones et al., 2018; Kalbasi et al., 2017].

1.2.2.2 Vascular effects from low-dose radiotherapy

RT in low-dose fractions (2-5 Gy) appears to exert a positive effect on the tumour vasculature and tissue perfusion, resulting in increased oxygenation of tumour tissue in multiple pre-clinical models [De Keyzer *et al.*, 2009; Potiron *et al.*, 2013; Kleibeuker *et al.*, 2016] as well as in patients [Banks et al., 2018; Dunst et al., 1999; Hohlweg-Majert et al., 2012; Janssen et al., 2010; SHIBUYA et al., 2011]. Dynamic-contrast enhanced MRI (DCE-MRI) and contrast enhanced ultrasonography have shown that improved perfusion in a xenograft tumour model occurs as early as two weeks following low doses of

fractionated RT. This can translate into reduced intratumoural hypoxia as demonstrated with reduced staining of the tumour hypoxia marker pimonidazole, and increased tumour viability [Kleibeuker et al., 2016]. Other studies have used the injection of intravenous fluorescently-labelled dextrans (which allow real-time mapping of the tumour vasculature) to show improved perfusion in pre-clinical tumour models following low-dose fractionated RT [Potiron, Abderrahmani, *et al.*, 2013]. Increased tumour oxygenation during RT has been linked to different mechanisms such as decreased oxygen consumption and vasodilatation due to RT-induced inflammation or a reduced tumour volume [Crokart et al., 2005]. Moreover, fractionated low-dose RT can promote the growth of new blood vessels, which might also contribute to enhanced perfusion. Low-dose RT can influence angiogenesis by inducing expression of pro-angiogenic growth factors such as VEGF by cancer cells or other cells such as macrophages that reside in the tumour microenvironment. These studies have shown that the RT-induced VEGF expression coincides with increased tumour perfusion (particularly in the tumour core), a reduction in tumour hypoxia, and increased tumour tissue viability [Meng *et al.*, 2010; Solberg *et al.*, 2012; Feng *et al.*, 2015; Kleibeuker *et al.*, 2016]. This enhanced effect of RT on tumour perfusion and reduced hypoxia was often associated with increased tumour growth and metastatic potential [Sofia Vala *et al.*, 2010; Kleibeuker *et al.*, 2016]. These effects can be counteracted with inhibition of VEGF-R signalling using sunitinib, which can augment the antitumour effects of RT [Kleibeuker et al., 2016].

The evidence described above portrays the complex mechanisms involved in the vascular response to RT, and how this is influenced by dose scheduling of RT. Whilst high-dose RT can cause endothelial dysfunction and rapid onset of tumour hypoxia, which contributes to tumour cell death, the consequent hypoxia contributes to RT resistance and also initiates a pathway that promotes the reconstitution of the tumour vasculature, which may lead to tumour recurrence. On the other hand, low-dose RT efficacy may be

strengthened by a pro-angiogenic response, which improves perfusion and tumour oxygenation, but this could at the same time induce unwanted tumour growth.

1.2.2.3 Combining radiotherapy and vascular targeted therapy

Modification of tumour hypoxia and perfusion in order to enhance the clinical benefit of RT has been explored using different approaches. Strategies to restore pre-irradiation tumour oxygenation and thereby improve the response to RT have been attempted using red blood cell (RBC) transfusion, erythropoietin administration, hyperbaric oxygen treatment or the administration of vasodilating drugs. Furthermore, molecular antagonists of HIF-1α, gene therapy strategies against HIF-1α or blockade of HIF-1α-interacting proteins have been tested in both pre-clinical models and the clinic. Although numerous clinical trials have demonstrated that hypoxic radiation resistance can be overcome, hypoxic modification has to date had no impact on clinical practice, with none of these adjuncts yet being incorporated into SOC PCa RT treatment, mainly due to insufficient evidence of clinical and cost effectiveness, as well as associated toxicity [Horsman and Overgaard, 2016].

Another treatment approach that has been combined with RT is anti-angiogenic therapy, which refers to treatment strategies that aim to inhibit angiogenesis. These treatments mostly involve targeted inhibition of the VEGF family and their cognate receptors. It was initially anticipated that anti-angiogenic drugs could hamper the effect of RT due to decreased perfusion and oxygenation. However, multiple pre-clinical studies observed an enhanced effect of the combinatorial approach [Kozin et al., 2001; Lee et al., 2000; Mauceri et al., 1998; Winkler et al., 2004]. These findings have also been confirmed in patients in a clinical trial setting [Crane et al., 2006; Czito et al., 2007]. Thus far, the results from larger and more recent clinical trials are less conclusive, reporting variable efficacy as well as increasing toxicity [Kleibeuker et al., 2015], therefore the use of anti-

angiogenic agents alongside RT is not currently a SOC option as the efficacy of this combination is variable. It remains unclear how best to combine these therapeutic modalities to achieve maximum response and minimal toxicity in patients [Kanthou and Tozer, 2018].

While such clinical observations warrant further investigation regarding therapy optimisation, the potential positive interaction between RT and anti-angiogenic therapy has been attributed to several distinct mechanisms such as ‘vascular normalisation’. Vascular normalisation refers to the paradoxical observation that anti-angiogenic drugs enhance the effect of therapies such as RT that rely on a functional vasculature. The tumour vasculature is typically dysfunctional due to its abnormal and chaotic structure as a result of the continuous imbalance between pro- and anti-angiogenic signalling. Anti-angiogenic therapy is able to restore this balance, thereby improving vessel function and perfusion [Jain, 2001, 2005]. Vascular normalisation is characterised by several features including attenuation of vessel hyperpermeability, increased pericyte (i.e. peri-vascular supporting cell) coverage, restoration of a normal basement membrane, and a resultant reduction in tumour hypoxia and interstitial fluid pressure [Goel et al., 2011]. In addition, anti-angiogenic therapy promotes vascular normalisation by “pruning” immature blood vessels, resulting in a tumour vascular network composed of larger, mature, pericyte-covered vessels. This in turn can improve the efficacy of RT along with delivery of exogenously administered therapeutics such as chemotherapy, and the more efficient homing of anti-tumour effector immune cells into the tumour microenvironment.

It has been observed that anti-angiogenic therapy is not only beneficial when given before RT, but can achieve similar effects when given concurrently with RT, or even after RT [Kleibeuker et al., 2016]. This suggests that other mechanisms in addition to vascular normalisation may drive the additive or synergistic effects of combination therapy. Interestingly with low doses (i.e. up to 5 Gy) of fractionated RT, reduced doses of anti-

angiogenic therapy were required to achieve tumour control, whilst the administration of anti-angiogenic therapy alone at similar doses had no effect on tumour growth rate [Kleibeuker et al., 2016; Wachsberger et al., 2007]. The mechanisms behind this RT-induced increase in vascular sensitivity to anti-angiogenic therapy are unknown. Whether this is purely the effect of RT-induced angiogenesis as shown in previous studies, or whether low-dose fractionated RT schedules may in fact also normalise the tumour vasculature through similar mechanisms such as “pruning” of immature blood vessels whilst leaving larger more mature vessels intact allowing better delivery of vascular-targeting agents, is yet to be determined. Irrespective of this, this observation of an improved treatment response provides rationale for combining low-dose fractionated RT with vascular-targeting agents as a plausible multimodal strategy in the treatment of PCa.

1.2.3 Effects of radiotherapy on the immune system

Cancer immunotherapy aims to overcome the weak immunogenicity of tumour-associated antigens (TAAs) in order to stimulate an immune response against cancer cells whilst minimising autoimmunity [Makkouk and Weiner, 2015]. RT has been regarded as being immunosuppressive [Ko and Formenti, 2018], in partly due to its toxic effects on local lymphocytes and local recruitment of immunosuppressive cells such as TAMs and MDSCs [Barker et al., 2015]. However, evidence now suggests that RT can also be immunostimulatory [Finkelstein et al., 2015]. Evidence that the host immune system may contribute to anti-tumour RT efficacy came from a preclinical study which demonstrated that effects of RT were compromised in immunodeficient and $CD8^+$ T-cell depleted mice [Slone et al., 1979]. Additional evidence for a role of the immune system during RT comes from pre-clinical research [Demaria *et al.*, 2004; Rodríguez-Ruiz *et al.*, 2018] and case study reports [Abuodeh et al., 2016] that reported regression of metastatic tumour deposits distant from the irradiated site. This so called “abscopal effect” is thought to

occur due to a systemic anti-tumour effect initiated by RT. In recent years, several mechanisms have been proposed to explain how RT affects the anti-tumour immune response (**figure 1.6**).

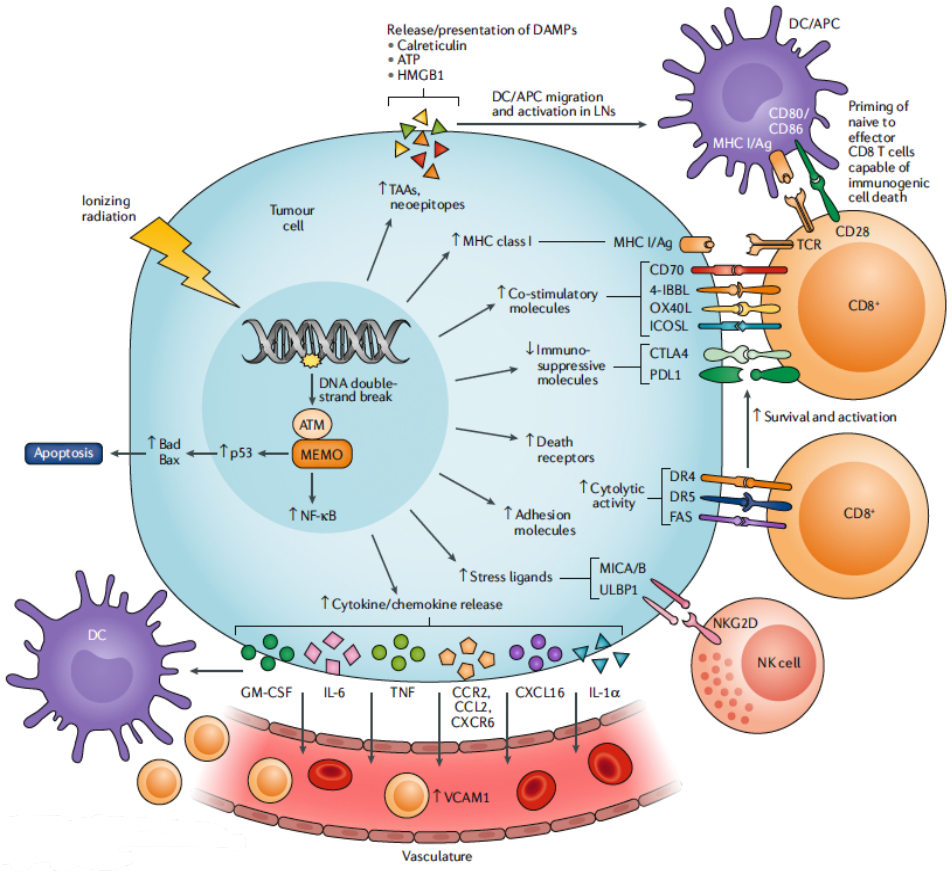


Figure 1.6 Immunogenic cell death and immunogenic modulation of tumour cells by radiotherapy. Radiotherapy induces several cellular events that can activate the immune system, including expression of tumour-associated antigens, increased expression of MHC class I molecules, co-stimulatory molecules death receptors, adhesion molecules, stress ligands, cytokines and chemokines. Unlike normal cell death, immunogenic cell death makes cancer cells "visible" to the immune system by the release of damage-associated molecular patterns, such as calreticulin, high mobility group box 1 and adenosine triphosphate which act as "danger signals" along with the release of neoantigens or TAAs. DAMPs bind to pattern recognition receptors such as Toll-like receptors on antigen presenting cells including dendritic cells. This leads to DC activation which subsequently cross-present antigens and migrate to the tumour-draining lymph nodes where they prime naïve T-cells and B cells to initiate a systemic immune response. Recent studies have identified the cGAS-STING pathway, activated upon recognition of double-stranded DNA breaks via cytosolic DNA sensors as also a key regulator of radiotherapy-induced immunogenic cell death. The expression of NF-κB target genes in tumour mediated by radiotherapy-induced DNA damage is an important mechanism by which radiotherapy causes immunogenic modulation of tumour cells. Image adapted from [Philippou et al., 2020b]. With permission from Springer Nature.

Pre-clinical research in immunocompetent mouse models has investigated multi-modality therapy using immunotherapy and RT (iRT) in order to elucidate the optimal RT dose, delivery, timing, and sequence of delivery of multi-modality therapies, for efficient immune priming. Most of these pre-clinical experiments have been in tumour models other than PCa, with a paucity of iRT multi-modal therapy approaches being investigated in pre-clinical PCa models (**table 1.4**). To date the available evidence from pre-clinical models suggests that the optimal timing of delivery of the adjunct immunomodulating treatment with RT is specific to the tumour type and immunotherapy agent [Dovedi et al., 2014; Harris et al., 2008; Wang et al., 2018; Young et al., 2016]. The immunoregulatory response to RT also appears to be dose and schedule dependent, as is the case for the vascular response to RT. For example, in pre-clinical models tumour cell surface expression of MHC class I (MHCI) and presentation of TAAs, necessary for the induction of ICD, as measured by the eight peptide Ovalbumin (OVA) epitope SIINFEKL in OVA-transfected cell lines, depends on the dose of RT. High doses of RT (greater than 10 Gy) are required to induce expression of MHCI and SIINFEKL epitope presentation, and this occurs in a dose-dependent manner [Reits et al., 2006; Sharabi et al., 2015b]. In addition, a high single dose of 30 Gy was necessary to cause an increase in $CD8^+$ TILs in CT26 and MC38 colon tumours, but this did not occur with a fractionated dose of 3 x 10 Gy. In support of this, high RT doses (12, 5 x 3, 20 Gy) but not low doses (6, 5 x 2 Gy) were needed to cause an effective anti-tumour immune response which sensitised tumours to immune checkpoint blockade (ICB) using anti-PD-L1 in pre-clinical models of pancreatic ductal adenocarcinoma [Azad et al., 2017]. There is no clear current consensus regarding optimal RT scheduling and its effect on establishing an effective anti-tumour immune response [Goedegebuure et al., 2019]. For example, a single 15 Gy fraction was more effective than 3 x 5 Gy in terms of generating anti-tumour immune responses in mice with melanoma tumours [Lugade et al., 2005]. Other studies have shown no difference between single or fractionated doses, as long as the total dose is significant [Azad et al.,

2017], whilst there is also evidence that fractionated dosing schedules are more effective [Dewan et al., 2009; Schaue et al., 2012]. In a mouse model of breast cancer an enhanced anti-tumour effect at the primary tumour site, or an abscopal effect where an anti-tumour effect was seen at a distant site away from the primary tumour, was only seen when an anti-CTLA-4 antibody was combined with fractionated RT (3 x 8 Gy or 5 x 6 Gy), and not when combined with a single 20 Gy fraction [Dewan et al., 2009].

The overall effect of RT on the immune response is not only dependent on dose scheduling, but is also determined by the tumour type and the associated TIME. This is particularly relevant to PCa which is a malignancy characterised by a low mutational burden accompanied by low infiltration of effective immune cell types and high infiltration of MDSCs and M2 TAMs, resulting in a predominantly immunosuppressive TIME in the primary tumour [Chi et al., 2014; Idorn et al., 2014; Lopez-Bujanda and Drake, 2017]. This has also been documented in mouse models of PCa where RT has been shown to enhance the infiltration of myeloid cells, particularly MDSCs and TAMs [Xu et al., 2013]. It is therefore important to explore to what extent the pre-treatment immunogenic profile of the tumour tissue can predict the response to RT. This is also relevant given the observation that RT can induce an immunosuppressive TIME by inducing the expression of chemokines and cytokines that attract immunosuppressive cell populations such as $CD4^+$ T-regulatory cells (Tregs), MDSCs and M2 TAMs. In support of this, multiple studies have shown that inhibition of cytokines such as CSF-1 or CCL2, which attract monocytes into the TIME, in combination with RT may enhance the RT-induced anti-tumour effect and sensitise tumours to ICB [Jones et al., 2018; Kalbasi et al., 2017].

The immunostimulatory effects of RT have led to several studies combining RT and ICB in patients with high-risk localised and mCRPC (**table 1.5).** Ipilimumab blocks the inhibitory signal CTLA-4, thereby activating T-cells [Egen et al., 2002]. Nivolumab and Pembrolizumab (PD-1 and PD-L1 inhibitors respectively) can target the PD-1 and/or PD-

L1 axis, thereby enhancing the priming and effector phases of the anti-tumour T-cell response. Evidence suggests that PD-1 and its ligand PD-L1 are expressed by PCa infiltrating lymphocytes (TILs) and PCa cells respectively, as evaluated by IHC of tissue microarrays from surgically resected PCa cases following RP. In addition, these same studies have shown expression of PD-1 and PD-L1 to be prognostic for biochemical recurrence following primary treatment with RP [Gevensleben *et al.*, 2016, Ness *et al*., 2017].. Recently, the KEYNOTE-199 phase II clinical trial of immunotherapy using the anti-PD-1 antibody Pembrolizumab in men with mCRPC following prior endocrine therapy and docetaxel reported a 5% treatment response according to Response Evaluation Criteria in Solid Tumours (RECIST) reporting [Antonarakis et al., 2020]. Despite this overall modest response in the entire patient cohort, this trial provides evidence that ICB can be successful in a subset of patients (so-called “extreme responders”) with aggressive disease refractory to chemotherapy and second-generation ADT. Overall, iRT strategies are currently showing only a modest benefit of this combination treatment approach in patients with PCa. Further research is needed, particularly in pre-clinical mouse models of PCa, to investigate the effect on the PCa TIME of low-dose fractions of RT used in the clinic. Such approaches will help determine the optimal RT dose, timing and sequence of iRT delivery for optimal immune priming, and also identify potential resistance mechanisms to iRT and how these could be overcome.

Study	Tumour model	Treatment protocol & experimental set up	Summary of results
[Harris et al., 2008]	Autochthonous TRAMP PCa model (spontaneous development of orthotopic PCa tumour). A variant of the TRAMP model was used in which the model tumour antigen influenza HA is co-expressed with the SV-40 large T-antigen that drives tumourigenesis in the TRAMP model	**Radiation protocol** three doses of 10 Gy given on day 1, 5 and 10. **Immunotherapy protocol:** Recombinant Vaccine against HA	RT and vaccine alone did not mediate an active anti-cancer immune response as measured by the proliferation and effector cytokine production (TNF-α and γIFN) of $CD4^+$ T-cells following adoptive cell transfer. Anti-tumour immune responses occurred when vaccine and RT were combined but these responses only occurred when the vaccine was administered 3-5 weeks post-RT. These responses were undetectable when the vaccine was administered at the time of RT
[Xu et al., 2013]	**Mouse species:** C57BL/6 **Cell line:** RM-1 or MyC-CaP **Xenograft location:** subcutaneous in the thigh	**Radiation protocol** 3 Gy daily for 5 days **Immunotherapy protocol:** CSF-1R inhibitors given by oral gavage beginning on the same day of irradiation	Local RT of the flank tumour enhances MDSCs and TAMs infiltration into tumours driven by an increased expression of CSF1 through the tyrosine kinase ABL1. Combination of RT with CSF-1R inhibitors suppressed tumour growth more effectively than RT alone with associated decrease in intratumoural MDSCs and TAMs populations
[Dudzinski et al., 2019a]	**Mouse species:** FVB mice **Cell line:** MyC-CaP **Xenograft location:** subcutaneous in the flank and hindlimb	**Radiation protocol**: 20 Gy in two 10 Gy fractions given on days 7 and 8 **Immunotherapy protocol:** anti-mouse PD-1 or PD-L1 antibody, 0.2 mg intraperitoneally given on days 0, 2, 4, and 7	iRT delayed tumour growth and increased survival of mice in this treatment arm. Abscopal effects where the unirradiated tumour graft responded similarly to the irradiated graft in the same mouse was only seen with iRT. Flow cytometry identified $CD8^+$ immune populations as key in mediating this improved local and abscopal anti-tumour effect in the iRT treated mice.

Table 1.4. Combination of RT and immunotherapy in prostate cancer pre-clinical models.
Gy, Gray; HA, haemagglutinin; iRT, immunotherapy and radiotherapy; MDSCs, myeloid derived suppressor cells; PCa, prostate cancer; RT, radiotherapy; TAMs, tumour associated macrophages; TRAMP, Transgenic Adenocarcinoma of the Mouse

Study	Design	No. of patients	Treatment	Measurements	Outcomes
[Finkelstein et al., 2012]	Non-randomised, open-label pilot study in men with high-risk localised PCa	5	28 months of ADT + 45 Gy EBRT in 25 fractions over 5 weeks+ DC injections after fractions 5, 15 and 25	Interval biopsies and blood tests to assess immune reaction	Some response seen to suggest priming of $CD8^+$ T-cells to test tumour antigens
[Slovin et al., 2013]	Non-randomised open-label phase I/II trial in men with mCRPC with disease progression after discontinuation of ADT who had received ≤ 1 previous course of chemotherapy	50	Comparison of ipilimumab 10 mg/kg monotherapy (n=16) with ipilimumab in combination with EBRT (n=24)	PSA decline and tumour response	Eight patients had a PSA decline of > 50%; one patient had a complete PSA response; six patients had stable disease
[Kwon et al., 2014]	Multicentre, randomised double-blind phase III trial in men with mCRPC who had progressed after docetaxel	799	Patients were randomised to receive bone-directed RT (8 Gy in one fraction) followed by either ipilimumab 10mg/kg or placebo every 3 weeks for up to four doses	Overall survival	Median 11.2 months with ipilimumab and 10.0 months with placebo (HR 0.85, 95% CI 0.72-1.00; p = 0.053)
NCT03543189 (in progress)	Open-label single-group assignment	34	After ADT, participants will receive nivolumab, high-dose-rate BT and EBRT, followed by a 2-year follow-up period	Safety and relapse free survival	Trial in progress; estimated completion 2021

Table 1.5. Completed and ongoing clinical trials combining radiotherapy and immunotherapy in PCa. ADT, androgen deprivation therapy; BT; brachytherapy; DC, dendritic cells; EBRT, external beam radiotherapy; Gy; Gray; mCRPC, metastatic castration resistant prostate cancer; PCa, prostate cancer; PSA; prostate specific antigen; RT, radiotherapy

1.3 Focal Therapy for prostate cancer

Focal therapy (FT) refers to various minimally invasive surgical techniques, which are applied to the prostate gland via the perineum or transrectally, in order to destroy cancerous cells using a range of energy sources. These treatments allow focal ablation of the tumour in an organ-sparing fashion, with the potential for reduced treatment-related toxicity and side effects compared to whole gland therapies such as RT or RP. The prostate gland is readily accessible, and many urologists are familiar with performing image-guided procedures via the perineum or urethra or transrectally. mpMRI and targeted biopsy localisation of PCa have paved the way for FT techniques to ablate PCa tumours in a targeted fashion, thereby preserving the prostate gland and sparing the neurovascular bundles and adjacent structures such as the urethra and rectum, thus minimising treatment-associated toxicity such as sexual dysfunction and bowel and urinary side effects. However, very few large scale multicentre randomised controlled trials (RCTs) have been performed to rigorously evaluate FT techniques against SOC whole gland treatments for localised PCa. To date prospective cohort observational studies have suggested that FT in well-selected patients can achieve short-term local disease control, with minimal adverse side-effects [Ahmed et al., 2015; Azzouzi et al., 2015a, 2017b; Faure Walker et al., 2018; Guillaumier et al., 2018; Jung et al., 2018; Mendez et al., 2015; Ramsay et al., 2015; Shah et al., 2019; Tay et al., 2017; Valerio et al., 2017b]. These reports have made FT an attractive potential alternative to whole-gland therapy for PCa, although these FT options are not currently SOC, and guidelines recommend their current use only in the context of a clinical trial setting. To date the only large scale RCT to have been completed to evaluate a FT approach against a SOC option is a trial of vascular targeted photodynamic therapy (VTP), compared against AS for low-risk low-volume PCa [Azzouzi et al., 2017]. This study demonstrated that VTP is safe with minimal associated sexual or urinary side effects. However, no RCTs of other FT techniques have been performed, nor have robust studies yet evaluated FT in the

context of clinically significant PCa, nor have studies yet incorporated FT in a multi-modality therapy approach.

1.3.1 Methods of focal therapy for prostate cancer

A variety of minimally invasive surgically performed FT technologies exist for PCa. These include cryotherapy, high-intensity focused ultrasound (HIFU), and VTP. Cryotherapy is ablation of malignant tissue using localised application of extremely cold temperatures, and this achieves tissue destruction by direct cell damage from the freeze–thaw cycle, progressing to coagulative necrosis within a few days after treatment and cancer cell apoptosis. The procedure involves transperineal placement of needle probes using a template grid under TRUS guidance. Pressurised argon gas is used to achieve cooling, and helium is used for warming, to produce freeze-thaw cycles. Real-time ultrasound permits visualisation of the “ice-ball” (the visible formation of an area of frozen tissue within the prostate). A target temperature of –40°C is desired to achieve maximal tumour eradication [Gage, 1998]. The main side-effects reported for cryotherapy include erectile dysfunction, urinary incontinence, urethral sloughing, rectal injury and rectourethral fistula formation [Jung et al., 2018].

HIFU uses high-energy ultrasound waves (0.8–3.5 MHz) focused to a specific point within the target organ in order to ablate tissue. Cellular damage occurs by two mechanisms; firstly, conversion of mechanical energy into heat causes irreversible cell death from coagulative necrosis, and alternating cycles of compression and rarefraction of sound waves causes inertial cavitation; secondly at the time of rarefaction, gas can be drawn out of solution to form bubbles, which then collapse rapidly, causing acoustic shockwaves which induce mechanical stress. The procedure involves placement of an ultrasound probe transrectally. To minimise the thermal effects on the rectal wall, the rectum is irrigated with degassed, cooled water, which also eliminates acoustic interference

between the transducer and the rectal mucosa. The major adverse effects of HIFU include acute urinary retention, erectile dysfunction, urethral stricture, rectourethral fistula and pelvic pain. Further disadvantages of HIFU include difficulty in achieving complete ablation of the prostate, especially in glands larger than 40 cc, and difficulty targeting cancers in the anterior zone of the prostate [Marberger et al., 2008].

Classical photodynamic therapy (PDT) is based on uptake of a photosensitiser molecule which is excited by light of a specific wavelength, which in turn induces a reaction with oxygen, generating species including free radicals and singlet and triplet oxygen in target tissues, causing cell death [Moore *et al.*, 2005, Dos Santos *et al.*, 2019] (**figure 1.7**).

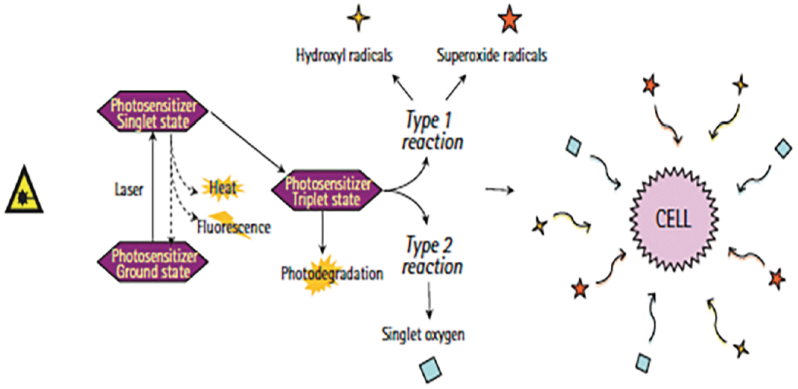


Figure 1.7. Mechanism of classical PDT action. Three elements need to be present for a photodynamic effect to occur: photosensitiser, light and oxygen. The photosensitiser is administered in a stable form or ground state. Once excited by light the photosensitiser transits from its ground state to its singlet excited and triplet excited states. In the triplet state the photosensitiser can react directly with biomolecules like proteins, lipids or nucleic acids via a type I photochemical reaction, resulting in the formation of hydroxyl or superoxide radicals capable of initiating radical chain reactions. The photosensitiser in its triplet state can also react with molecular oxygen $^3O_2$ via a type II photochemical reaction to form singlet oxygen ($^1O_2$). This singlet oxygen in turn reacts with proteins, lipids, and nucleic acids in cells causing functional and structural damage, which leads to cell death. Image adapted from [Moore et al., 2005]. With permission from Wiley

VTP is a specialised novel submodality of PDT, which targets the tumour vessels rather than cancer cells *per se* [Eggener and Coleman, 2008]. It has been suggested that the abnormal structure and function of tumour blood vessels compared to their physiological counterparts may make the tumour vasculature more sensitive to ROS-induced damage induced by VTP [Kawczyk-Krupka et al., 2015]. During VTP treatment the TOOKAD® Soluble (WST-11, STEBA Biotech S.A., Luxembourg City, Luxembourg) photosensitiser is administered intravenously and preferentially accumulates in tumour vessels. Intravenously administered WST-11 is focally activated by low-power near-infrared (NIR) laser light of a specific wavelength (753 nm) in the presence of oxygen. The photosensitiser absorbs light and transfers energy to oxygen molecules, resulting in the rapid generation of ROS and nitrogenous species, which causes tumour micro-vessel thrombosis followed by localised vascular collapse [Ashur et al., 2009; Madar-Balakirski et al., 2010a] and tumour necrosis as early as 7 days post-treatment [Azzouzi et al., 2013]. Treatment planning involves MRI to define the target cancer volume and the safety margin required for protection of the urethra and rectal wall. A software called TOOGUIDE® uses the MRI data to optimise parameters of treatment such as the number and placement of optical fibres within the prostate gland, and the length of the light diffusing off each optical fibre [Betrouni et al., 2011]. The surgical FT procedure is performed under general anaesthesia in aseptic conditions, with the patient placed in the lithotomy position (**figure 1.8A**) using a BT 'stepper' (**figure 1.8B**) and an attached transperineal prostate template **(figure 1.8C**). The procedure involves transperineal placement of transparent hollow fibre insertion catheters **(figure 1.8D**) through the template grid using the TRUS scan system in accordance with the treatment guidance provided by the TOOGUIDE® software. Optical laser fibres are inserted through the hollow fibre insertion catheters ensuring a safety margin of 5 mm to protect the urethra rectal wall, urinary sphincter and prostatic capsule **(figure 1.8E**). Once all the optical fibres are in position the light of the room is dimmed and the patient is entirely protected from light exposure, and infusion of TOOKAD® WST-11 is initiated. Activation of TOOKAD® WST-11

is achieved by continuous illumination of the prostate gland through these optical fibres with a 753-nm laser light at a power of 150 mW/cm^2 and light energy of 200 J/cm^2 delivered by a multichannel diode laser (**figure 1.8F**). The illumination starts immediately after the end of the injection after 22 min and 25 sec to coincide with the peak serum concentration of TOOKAD® WST-11. The procedure lasts around 2 hours, and the patient is kept under dimmed light for at least 6 hours, before often being discharged home the same day.

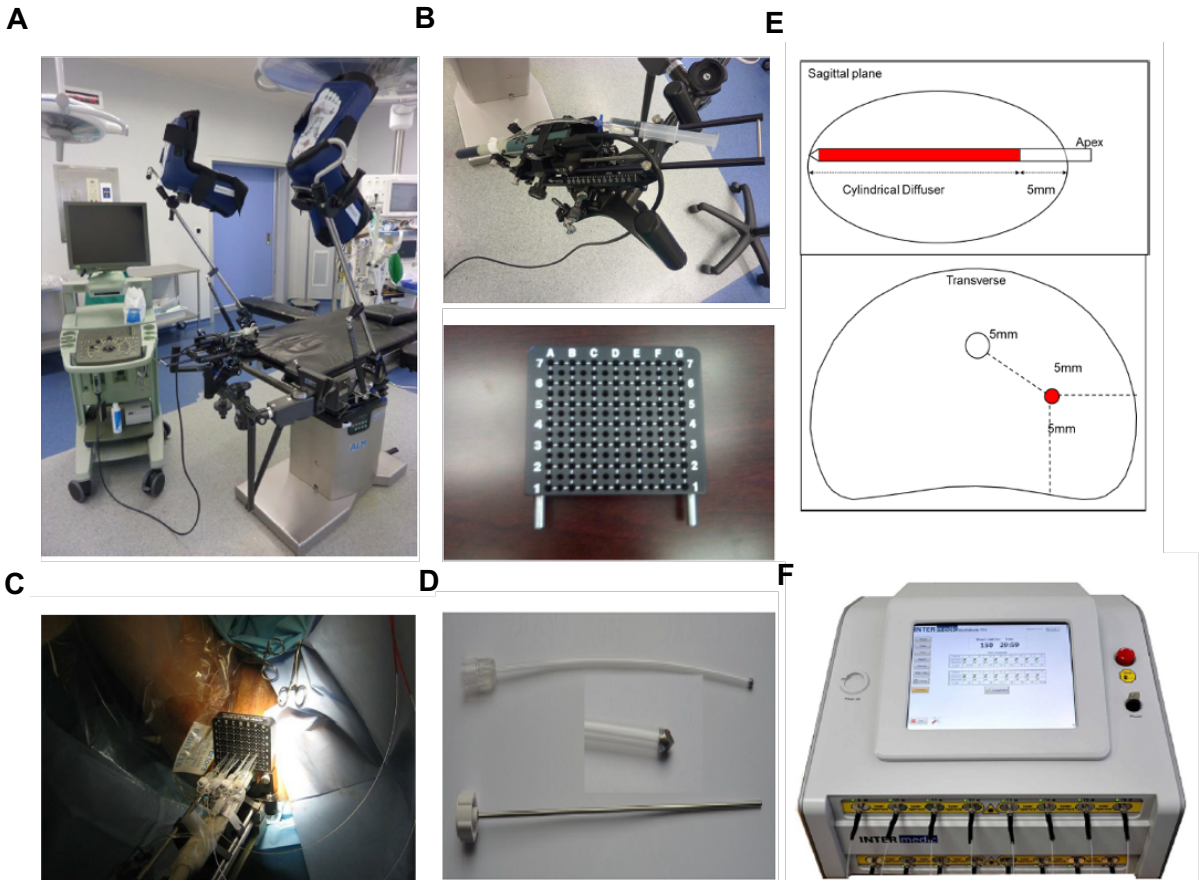


Figure 1.8. Patient position and apparatus used to deliver TOOKAD® VTP to patients. **(A)** Installation of the operating table, the ultrasound device with brachystepper and VTP preoperative view in a patient. **(B)** TRUS probe attached to a standard brachytherapy stepper. **(C)** a transperineal prostate template enables accurate position of **(D)** fibre insertion catheters. **(E)** safety margin for the optical fibre positions. **(F)** laser generator. Images adapted from [Azzouzi et al., 2015b]. With permission from SpringerLink.

VTP is the only FT technique to have been investigated in a phase III RCT. In this multicentre RCT, VTP was found to be safe and well-tolerated, and significantly reduced the number of men found to have a higher grade PCa at subsequent biopsy compared to men on AS for low-risk low-volume PCa, leading to fewer men requiring radical therapy [Azzouzi et al., 2017]. Further trials such as PART (Partial prostate Ablation versus Radical prosTatectomy) are now underway to evaluate cancer control and quality of life (especially urinary and erectile function) in patients with a dominant focus of intermediate-risk PCa treated with VTP compared against radical whole-gland therapy. The CHRONOS trial (Comparative Health Research Outcomes of NOvel Surgery in prostate cancer) ***(NCT04049747***) is randomising men to either partial ablation (using HIFU or cryotherapy) or whole gland therapy. In both the PART and CHRONOS trials the FT technologies are being evaluated against whole gland therapy using RP or RT (EBRT 74-78 Gy in 2 Gy fractions or BT) combined with ADT. In addition, the phase II IP2-ATLANTA trial (***NCT03763253***) will explore sequential multi-modal treatment using systemic therapy, local physical cytoreduction and MDT in men with oligometastatic hormone sensitive PCa versus systemic therapy alone which comprises of ADT +/- docetaxel or any other systemic SOC treatment such as second-generation ADT. Local physical cytoreduction will be performed with either minimally invasive ablative therapies using HIFU and cryotherapy or RP with or without pelvic lymph node dissection (PLND) or local hypofractionated (60 Gy in 20 fractions) or standard dose (74-78 Gy in 2 Gy fractions) RT with or without simultaneous nodal irradiation. Men in both intervention arms will be eligible for MDT in the form of SBRT or surgery. The results of these trials will be key in defining the role of FT in localised PCa, and in particular will inform patients and clinicians of the 'trade-off' between health-related quality of life and long-term oncological outcomes and its role as a cytoreductive treatment approach as part of a multimodal therapy for advanced and oligometastatic PCa.

1.3.2 Palladium-based WST-09 and WST-11 photosensitisers

Weizmann-Steba 09 and 011 (WST-09/11) are second generation photosensitisers derived from bacteriochlorophyll (Bchl), which are photosynthetic pigments that occur in phototrophic bacteria. The spectra, photophysics and photochemistry of native Bchl make them very efficient sensitisers. Specifically, Bchl have a high extinction coefficient at wavelengths in the NIR spectrum (650-850 nm) where light can penetrate deep into tissues. Due to their intense absorption of light in these spectral regions, Bchl photosensitisers can generate ROS at a high yield [Mazor et al., 2004]. Several second generation photosensitisers have been generated by *A. Sherz and colleagues* at the Weizmann Institute of Science, where the central Bchl magnesium atom is replaced by other metal atoms such as palladium (Pd), Copper (Cu), Zinc (Zn) or Manganese (Mn) (Scherz A et al., 2011). These agents have been further developed as VTP photosensitisers for clinical application in collaboration with Steba-Biotech (Paris, France) [Mazor et al., 2004]. An example is WST-09 where the central Mg atom was replaced by Pd to form Pd-bacteriophorbide. This heavy atom was previously shown to markedly increase the oxidation potential of Bchl, and simultaneously enhances the inter-system crossing rate of the molecule to its triplet state [Noy et al., 1998]. WST-09 is a hydrophobic compound with low solubility in aqueous solution. Its pre-clinical and clinical application requires use of amphiphilic vehicles such as Cremaphor® [Sheer et al., 1999]. In order to avoid use of such agents, which are pharmacologically active, a soluble derivative of WST-09 has been developed by the same group with the aim of improving the pharmacokinetic profile of the photosensitiser after intravenous administration. This was achieved by modifying WST-09 with taurine, resulting in the taurinated dianionic salt WST-11 or TOOKAD® Soluble [Sherz et al., 2011].

WST-11 (**figure 1.9A**) is isolated as a black-purple crystalline powder. It has a molecular weight of 916 g/mol and is soluble in aqueous solution. It is characterised by the following properties [Mazor *et al.*, 2004; Sherz et al., 2011]; (a) four main absorption peaks (750, 530, 385 and 330 nm), the strongest absorbance of light being 750 nm which is in the NIR of the electromagnetic spectrum (**figure 1.9B**); (b) cytotoxicity in the dark is very low and thus tissue damage can be controlled by the light dose (mW/cm^2) and length of exposure; (c) When dissolved in serum, WST-11 undergoes disaggregation to monomers by adsorbing mostly to serum albumin (SA) through non-covalent bonds. The binding of free WST-11 to SA affects its pharmacokinetics, clearance rate, biodistribution and phototoxicity.

Albumin is the most abundant protein in blood plasma. Its levels are tightly regulated, and it is important in homeostasis [Frei, 2011]. One of the many roles of albumin is to transport drugs to target organs or receptors. Albumin is taken up by endocytosis into the lysosomal compartment of cells where it is degraded. In endothelia the gp60 protein albondin binds albumin and acts as a 'shuttle', enabling endocytosis of albumin-bound molecules by cells [Schnitzer and Oh, 1994]. *In vitro* experiments demonstrated that the pre-incubation of WST-11 with SA reduced its cellular uptake by H5V endothelial cells, and this consequently reduced the phototoxicity of WST-11 following H5V endothelial cell illumination. These findings suggest that binding of WST-11 to SA reduces cellular uptake of the photosensitiser due to a reduction in free pigment concentration, and therefore WST-11 uptake by endothelial cells becomes albondin dependent. This effect was SA dose-dependent, and was not seen when pre-incubation was performed with γ–globulins, these being abundant proteins found in plasma. The clinical significance of this is that SA-bound WST-11 remains confined within the vasculature and does not extravasate into interstitial spaces, therefore it exerts its photocytotoxicity intravascularly, as is required for a vascular-targeted therapy.

The adsorption of WST-11 to SA also affects its biodistribution following intravenous injection (**figure 1.9C**). *In vivo* biodistribution experiments have shown that following a bolus WST-11 intravenous injection the photosensitiser does not extravasate from the circulation for the above reasons, and it reaches a high concentration within the blood stream and target organs, quickly followed by rapid clearance. The highest levels of WST-11 following injection are found in the blood at 2 minutes. The clearance of WST-11 from the blood is rapid with a $t_{1/2}$ of 1.65 minutes (**figure 1.9D**). Approximately 90% of the injected pigment is cleared within 5 minutes, reaching almost background levels 30 minutes after injection. WST-11 reaches maximal concentration in the liver, kidney, lung and spleen 5 minutes after injection. Clearance of WST-11 is completed in all of these tissues by 60 minutes, and in the lungs by four hours. The concentration of WST-11 remains low in the kidney after 2 and 5 minutes, providing further evidence of WST-11 adsorbing to SA and thus being excluded from the glomerular filtrate.

WST-11 is cleared by the liver, and the fast rate of WST-11 clearance from target tissues may be related to its properties of water solubility, negative charge due to the taurine side group, and its moderate affinity to SA [Mazor et al., 2004]. The adsorption to SA allows its rapid transport to the liver where the conjugation of taurine to different hepatic molecules in the course of detoxification increases WST-11 polarity and aqueous solubility, resulting in dissociation of the SA-WST-11 covalent bond, facilitating hepatic clearance [Biopharmaceutics et al., 1984]. Rapid hepatic clearance is also facilitated by the moderate affinity of WST-11 to SA. A higher affinity would pose a problem because of the significant half-life of SA (19 days in humans), which would otherwise extend the lifetime and bioavailability of WST-11 in the circulation, subjecting the patient to prolonged skin toxicity [Mazor et al., 2004; Mccurdy et al., 2004].

The properties exhibited by WST-11 make it an ideal photosensitiser for VTP. Firstly, the spectra, photophysics and photochemistry of this Bchl-derived photosensitiser allow the effective generation of ROS in deep-lying tumour tissues, with minimal skin photo-toxicity. Secondly, the adsorption of WST-11 to SA prevents its extravasation from the circulation and allows rapid transfer of WST-11 to the vasculature of target tumour tissue at high concentration, followed by rapid hepatic clearance. The rapid clearance of WST-11 from the circulation leaves only a short window of time for illumination whilst pigment levels in the blood are photodynamically effective. Therefore, pre-clinical and human VTP protocols administer the drug as an infusion with illumination of target tissue commencing once the desired drug concentration has reached the required intravascular concentration (**figure 1.9D**).

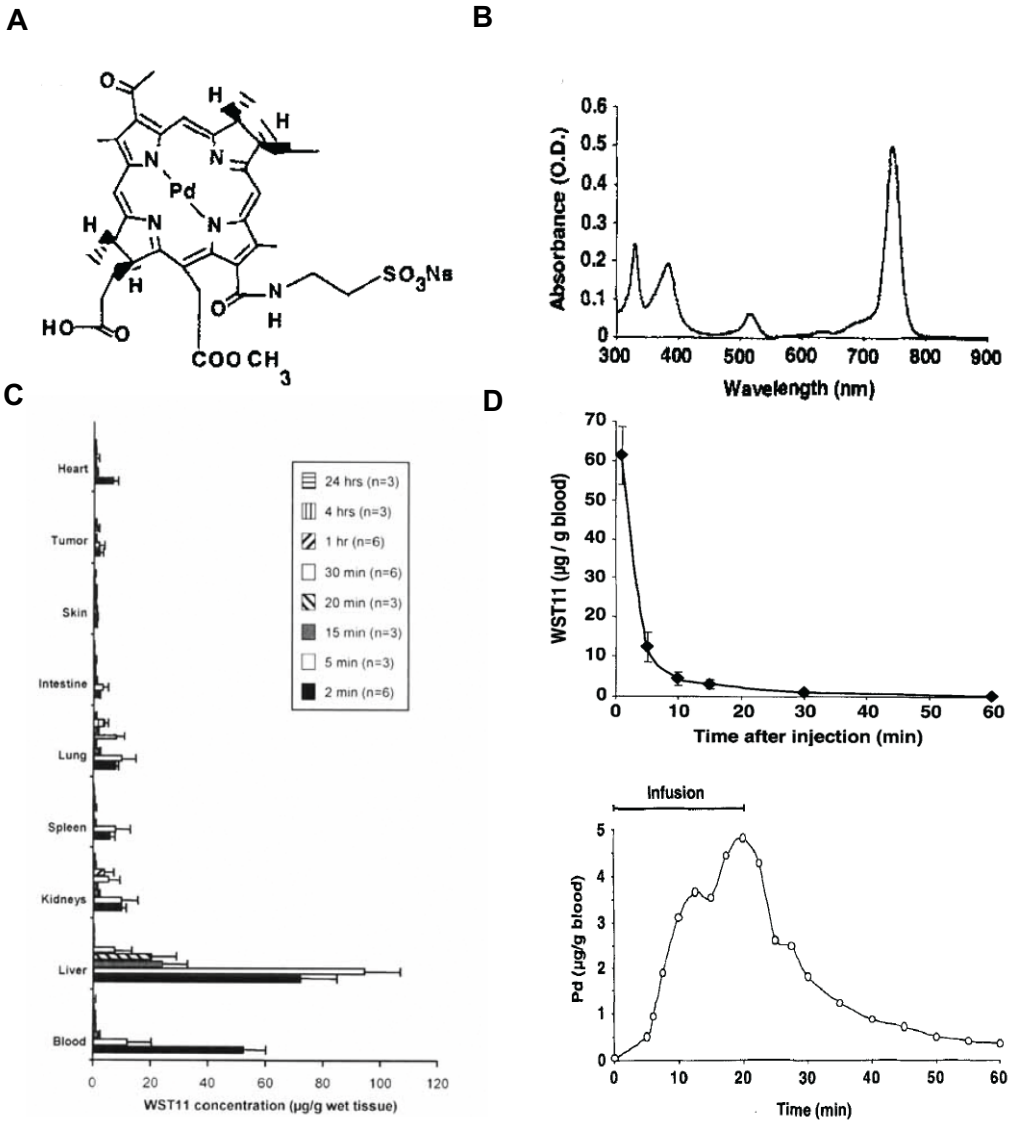


Figure 1.9. Chemical structure, pharmacokinetics and biodistribution of WST-11. (A) The chemical structure and **(B)** absorption spectrum of WST-11. **(C)** Biodistribution of WST-11 in mice bearing melanoma xenografts. Mice were euthanised at different times after intravenous injection of 6mg/Kg WST-11 and WST-11 content in the respective tissues was determined by inductively coupled plasma mass spectrometry and presented as micrograms WST-11 per gram wet tissue. The values for each timepoint represent the mean ± SEM of three to six animals.**(D)** Blood levels of WST-11 during and after bolus and infusion for 20 minutes. Images adapted from [Mazor et al., 2004]. With permission from Wiley.

1.3.3 Pre-clinical studies of TOOKAD® (WST-09) and TOOKAD®-soluble (WST-11)-mediated VTP

WST-09 and WST-11-mediated VTP have been extensively studied in pre-clinical tumour models. This evidence supports a direct cytotoxic endothelial effect of VTP, causing rapid vascular shutdown and resultant ischaemic death of tumour tissue, accompanied by a prompt inflammatory reaction. Further pre-clinical evidence from immunocompetent tumour models suggests that VTP stimulates tumour-specific immune responses capable of eliminating locally treated tumour masses and distant untreated metastatic sites, establishing long-lasting protective immunity against tumour recurrence [Preise et al., 2009].

1.3.3.1 Effects on tumour vasculature

The details of the haemodynamic tumour vasculature response, and changes in intravascular oxygenation following WST-09 or WST-11-mediated VTP, were examined in murine MADP106 earlobe, M2R melanoma, and renal adenocarcinoma (RENCA) tumour models [Madar-Balakirski *et al.*, 2010; Gross *et al.*, 2003; Neuschmelting *et al.*, 2018]. In these studies, several imaging techniques such as fluorescent intravital microscopy, dynamic light scattering imaging, angiography, blood oxygenation level-dependent (BOLD) MRI, and multispectral optoacoustic tomography (MSOT) have been used to track RBC flow and changes in intratumoural oxygen saturation (sPO_2) as an imaging correlate of tumour hypoxia, allowing real time characterisation of the emerging treatment effects of VTP in time and space. In the MADP106 earlobe tumour model, VTP initially caused a focal transient blood vessel vasodilation and increase in blood flow, followed by abrupt vasospasm, thrombosis, vessel permeabilisation, and a sharp reduction in blood flow rates. Complete and irreversible blood stasis due to luminal occlusion occurred after 63.2 (± 1.5 SEM) seconds. The primary target of VTP were larger calibre tumour feeding arteries and draining veins, as opposed to smaller

calibre intra-tumoral vessels (**figure 1.10A**) [Madar-Balakirski et al., 2010a]. The observed initial transient vasodilation and increased blood flow is believed to occur due to an abrupt rise in oxygen consumption due to photogeneration of superoxide and hydroxyl ROS, resulting in a sharp reduction in haemoglobin saturation levels [Gross et al., 2003]. In efforts to restore local normoxia, endothelial cells release nitric oxide (NO), which is a potent vasodilator, and this is believed to cause the VTP-induced burst in arterial blood flow. Moreover, the released NO is thought to interact with the photogenerated superoxide and hydroxyl radicals, and consequently contributes towards rapid vascular occlusion [Beckman et al., 1990] and subsequent tumour ablation. These changes in blood flow, coupled with the photo-consumption of oxygen, resulted in a reduction in intratumoural sPO_2, which was identified in solid melanoma and RENCA tumours *in vivo* using imaging techniques such as BOLD contrast MRI and MSOT (**figure 1.10B-D**) [Gross *et al.*, 2003, Neuschmelting *et al.*, 2018].

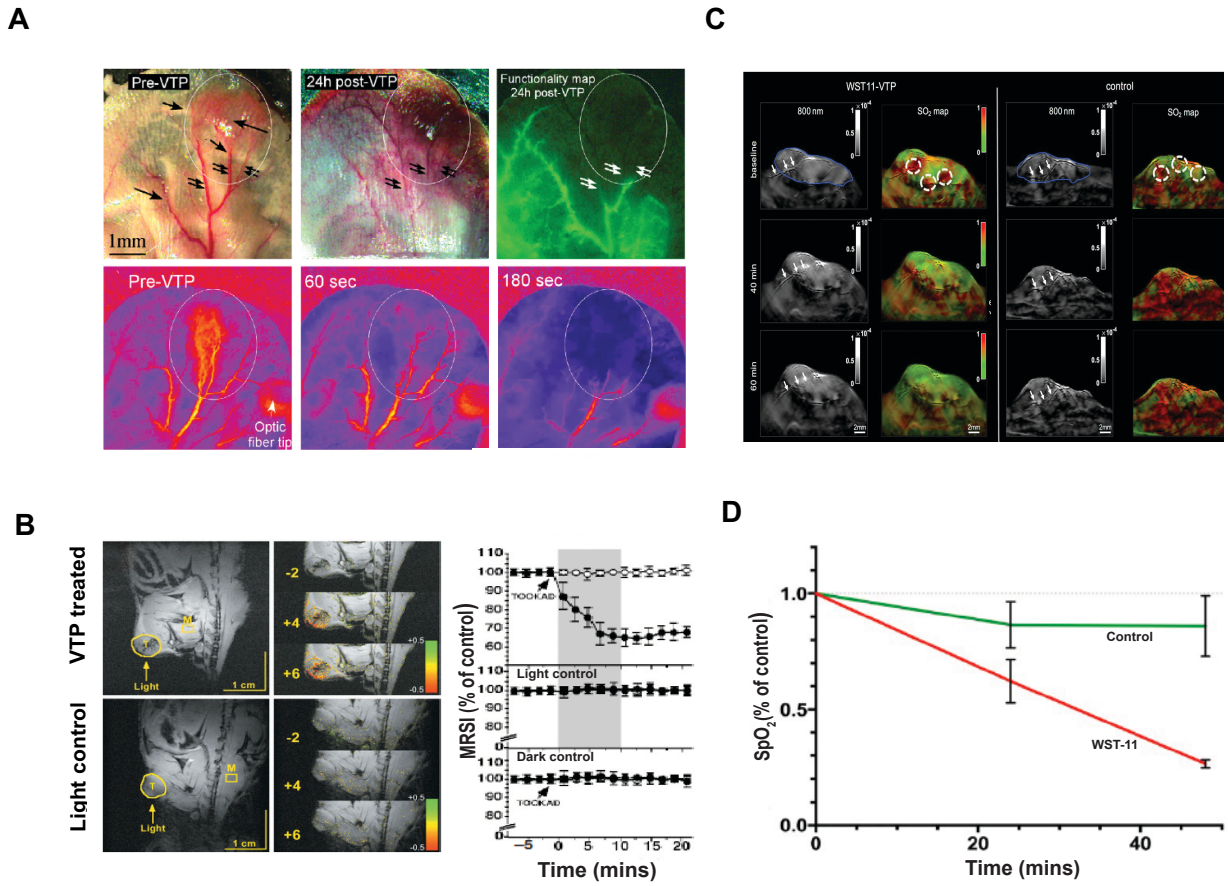


Figure 1.10. Effects of vascular targeted photodynamic therapy on the tumour vasculature in pre-clinical models. (A) Selective occlusion of tumour vasculature (t) following VTP. Dynamic light scattering images of the mouse MADP106 earlobe tumour, before, 60 sec and 180 sec after Tookad-VTP demonstrates selective reduction in tumour perfusion. **(B)** Magnetic resonance spectroscopic imaging (BOLD-contrast MRI) and graphical representation of spectroscopic signal intensity relative to control of VTP-treated melanoma flank xenografts tissue at the indicated time points (-2, +4, and +6), relative to the onset of irradiation. BOLD contrast MRI relies on the paramagnetic properties of deoxyhaemoglobin and can detect spatial and temporal changes in blood oxygenation, flow and volume. A reduction in T2-weighted magnetic resonance signal intensity (MRSI) was seen upon illumination of the TOOKAD-treated mouse. This is confined to the illuminated tumour (t) and not neighbouring muscle tissue (M), whereas no changes in signal intensity are seen in the absence of TOOKAD (light-control). **(C)** multispectral optoacoustic tomography of VTP- treated sham-treated RENCA tumours showing destruction of large tumour feeding vessels and reduced oxygen saturation in the perivascular tumour (dotted white circles) over the course of 60 minutes following treatment. **(D)** Graphic representation of the temporal reduction in oxygen saturation following VTP-treated and sham-treated tumours. Images adapted from [Gross et al., 2003; Neuschmelting et al., 2018]. With permission from IVYSPRING international publisher and www.plosone.org.

Histological assessment of VTP-treated tumour tissue showed that the first sign of vascular damage was characterised by a reduction in CD31-positive endothelial cells, and this occurred as early as one hour post treatment (**figure 1.11A**) [Neuschmelting et al., 2018]. Progression to vessel thrombosis with associated with multifocal areas of haemorrhage, which occurred at 3 hours (**figure 1.11B**). This was followed by tumour necrosis and inflammation caused by the influx of lymphocytes, particularly neutrophils, within 24-48 hours post-treatment (**figure 1.11C**). By ten days after VTP tumours had undergone complete necrosis and liquefaction and were surrounded by newly formed granulation tissue (**figure 1.11D**). Macroscopically the earliest findings were tissue oedema which was maximal at 48 hours, followed by tumour debulking and flattening and the formation of a superficial crust (eschar) 3-12 days after VTP treatment (**figure 1.11E**) [Koudinova et al., 2003; Plaks et al., 2004; Preise et al., 2003; Vilensky et al., 2005]. Control experiments demonstrated that infusion of the photosensitiser alone (dark control) or illumination of the tumour alone without photosensitiser (light control) had no macroscopic or microscopic effects on the tumour which continued to grow at the same rate as untreated controls (**figure 1.11F**) [Koudinova et al., 2003; Preise et al., 2003; Vilensky et al., 2005].

The effects of WST-09-mediated VTP have been examined in the normal canine prostate gland. Haematoxylin and Eosin (H&E) assessment of the prostate one-week post VTP was characterised by marked haemorrhage and homogeneous necrotic debris in the centre of the treated tissue. VTP-induced lesions were well delineated from the adjacent untreated normal tissue, and no histological evidence of damage from possible light scatter was found in neighbouring structures such as bladder, colon and urethra [Huang et al., 2007]. Safety and efficiency data for the more advanced soluble WST-11 photosensitiser obtained from healthy dog experiments largely resembled those for WST-09. A strong fluence-dependence of necrosis was observed

on H&E analysis, with prompt clearance of the photosensitiser, mild transient urinary complications, and no derangement of systemic parameters during or after treatment [Chevalier *et al.*, 2011, Chevalier et al., 2013].

Application of WST-09 or WST-11-mediated VTP in xenograft mouse models of cancer have demonstrated the effective anti-tumour effects of VTP-induced ischaemic injury in terms of local tumour control. Treatment protocols have typically consisted of a single treatment session whereby the photosensitiser was injected intravenously, followed by immediate illumination of the tumour using either a Xenon light source (650-800 nm) or a diode laser emitting light at 750-770 nm (**table 1.6**).

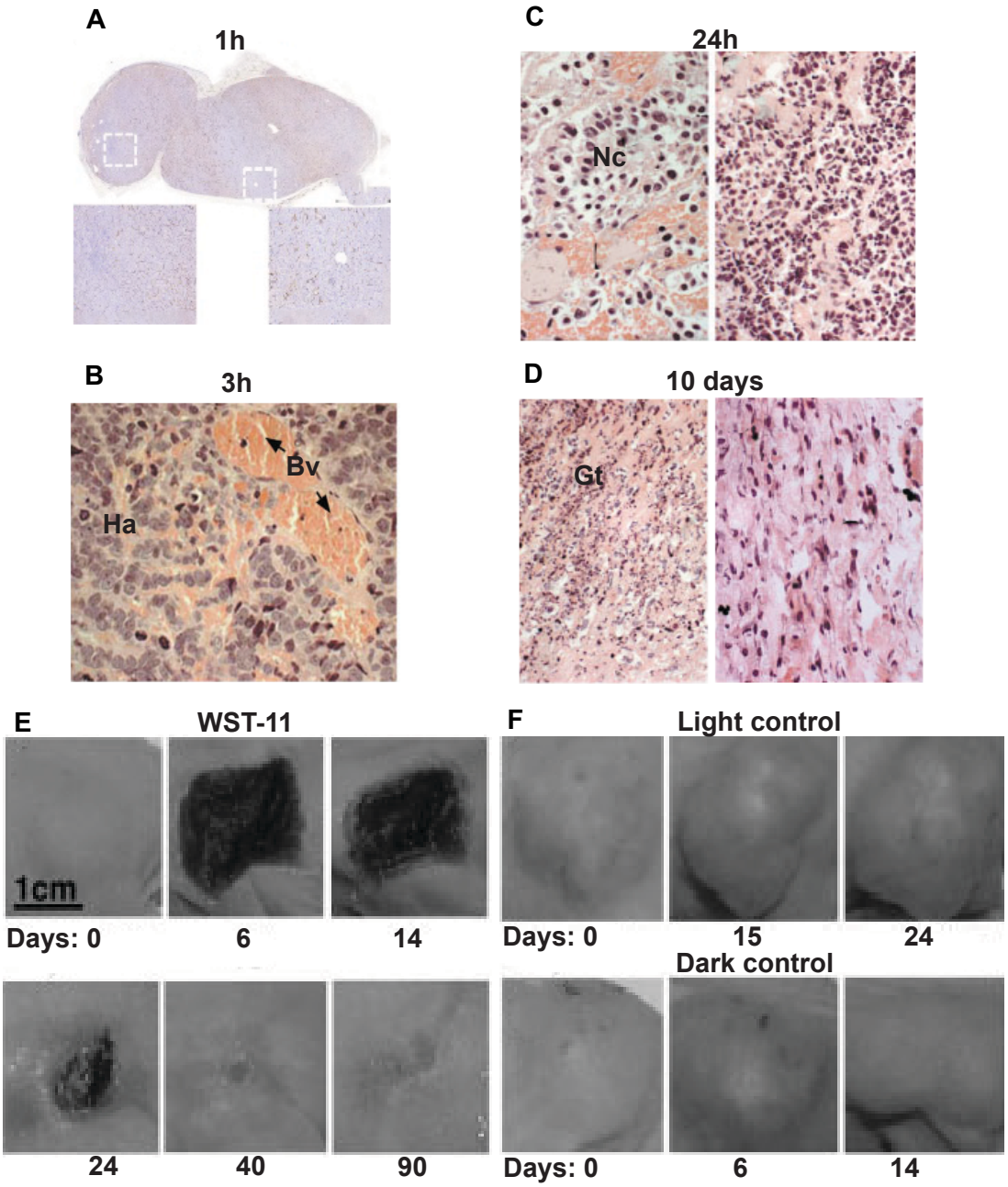


Figure 1.11. H&E analysis and macroscopic appearance of VTP-treated tumours.
(A) Vascular damage is seen as early as one hour after VTP with the loss of CD31 staining. **(B)** By 3 hours tissue haemorrhage (Ha) is seen as red blood vessels extravasate from damaged blood vessels (Bv) into the interstitial space and this is associated with **(C)** tumour necrosis (Nc) at 24 hours post treatment. **(D)** By day 10 tumours are composed of newly formed granulation tissue (Gt). **(E)** VTP-mediated necrosis is seen as early as 6 days with the development of a superficial eschar and complete regression of the tumour. The eschar is present for 15-29 days followed by healing with minimal scarring. **(F)** The tumours continued to grow in light and dark controls. Images adapted from [Koudinova et al., 2003; Neuschmelting et al., 2018]. With permission from IVYSPRING international publisher and Wiley.

Reference	Tumour model	Treatment protocol	Summary of results
[Schreiber et al., 2002]	**Mouse species**: male nude CD1 **Cell line**: C6 rat glioma **Xenograft location**: subcutaneous in distal dorsal foot of hindleg	**WST-09 dose**: 5 mg/Kg **Duration of illumination**: 30 mins **Light dose**: 150-200 mW/cm^2 (270-360 J/cm^2) **Method of light delivery**: transcutaneous **Size of tumour at treatment**: NR	Subcutaneous tumours were cured in 64% of mice after a 5-week follow up post VTP
[Koudinova et al., 2003]	**Mouse species**: CD1 **Cell line**: SPCC **Xenograft location**: subcutaneous, intratibial & orthotopic	**WST-09 dose**: 4mg/Kg **Duration of illumination**: 30 minutes **Light dose**: 150 mW/cm^2 **Method of light delivery**: Transcutaneous for subcutaneous and intratibial tumours; direct into tumours using a laser delivering fibre in orthotopic tumours	Subcutaneous tumours exhibited complete regression within 28-40 days with a long-term (90-day post VTP) cure rate of 69% Intratibial & orthotopic tumours responded with complete regression in 40% of treated mice at 70-90 days post VTP as documented histologically
[Preise *et al.*, 2003]	**Mouse species**: CD1 **Cell line**: human HT29 colorectal adenocarcinoma **Xenograft location**: subcutaneous	**WST-09 dose**: 10 mg/Kg **Duration of illumination**: NR **Light dose**: 150 mW/cm^2 (90 J/cm^2) **Method of light delivery**: transcutaneous **Size of tumour at treatment**: 100 mm^3	14/17 (82.4%) mice showed complete response as measured by tumour volume and degree of necrosis on H&E analysis
[Plaks et al., 2004]	**Mouse species**: CD1 male nude mice **Cell line**: human WISH-PC14 human prostate cancer adenocarcinoma **Xenograft location**: subcutaneous	**WST-09 dose**: 10mg/Kg **Duration of illumination**: 10 minutes **Light dose**: 108 J/cm^2 **Method of light delivery**: transcutaneous **Size of tumour at treatment**: diameter of 7-12mm	14/19 (74%) treated tumours exhibited complete necrosis at 48-72 hours. 9/14 tumours had no tumours palpable after 30- day follow-up Tumour response as evaluated by measurement of serum PSA showed a 50% decrease in PSA at 7 hours post-VTP, which

			continued to decline, reaching undetectable levels by 1-week post treatment
[Vilensky et al., 2005]	**Mouse species**: CD1 **Cell line**: CTVT **Xenograft location**: subcutaneous	**WST-09 dose**: 10 mg/Kg **Duration of illumination**: NR **Light dose**: 150 mW/cm^2 (90 J/cm^2) **Method of light delivery**: transcutaneous **Size of tumour at treatment**: Volume of >50 mm^3	13/15 mice (86.7%) were cured of tumour by 25-35 days post treatment. Tumour was still undetected in 10 of these mice 90 days after treatment. Light and dark control tumours continued to grow
[Mazor et al., 2004]	**Mouse species**: male CD1 nude **Cell line**: m2R melanoma **Xenograft location**: subcutaneous	**WST-11 dose**: 6 or 9 mg/Kg **Duration of illumination**: 5 minutes **Light dose**: 30, 39 or 45 J/cm^2 **Method of light delivery**: transcutaneous **Size of tumour at treatment**: NR	A WST-11 dose of 6 mg/Kg at a light dose of 45 J/cm^2 resulted in a 6/10 cure rate. Increasing the dose to 9 mg/Kg at a light dose of 30 J/cm^2 increased the cure rate to 7/10 mice at 90 days after treatment At lower light doses of 39 and 30 J/cm^2 the cure rates decline to 2/8 and 6/14 mice respectively
[Fleshker et al., 2008]	**Mouse species**: Female BALB/c mice **Cell line**: mouse CT26 colon carcinoma expressing the luciferase gene (CT26-luc) **Xenograft location**: subcutaneous	**WST-11 dose**: 9 mg/Kg **Duration of illumination**: 5 minutes **Light dose**: 100 mW/cm^2 (30 J/cm^2) **Method of light delivery**: transcutaneous **Size of tumour at treatment**: Diameter of 8 mm	WST-11 VTP abolished luciferin bioluminescence in 75% of treated tumours and this was maintained up to a follow up of 90 days 25% of tumours recurred signified by a return of luciferase signal. A second VTP treatment in these mice increased the success rate of treated from 75% to over 90%

Table 1.6. Summary of VTP anti-tumour effects on multiple pre-clinical models of cancer. CTVT, canine-transmissible venereal tumour; NR, not reported; PSA, prostate-specific antigen; SPCC, human small cell carcinoma of prostate; VTP, vascular targeted photodynamic therapy

1.3.3.2 Anti-tumour immunity promoted by WST-09 and WST-11-mediated VTP

The rapid vascular shutdown and consequent ischaemic death of tumour tissue, accompanied by a VTP-induced inflammatory reaction, provides a milieu for efficient stimulation of the host immune system. Evidence that an immune-mediated VTP response can translate into improved local tumour control comes from studies of tumour response to VTP in immunocompetent and immunodeficient mouse strains. In some murine tumour models a functional host immune system is necessary for effective eradication of VTP-treated tumours. Specifically, the response to VTP in murine CT26 colon adenocarcinoma xenografts differed significantly between immunocompetent wildtype BALB/c mice and BALB/nude and NOD/scid mice with defects in adaptive immunity. High cure rates (above 70%) were seen in immunocompetent mice, whereas BALB/c and NOD/scid mice responded poorly (18.7 and 11% respectively). This suggests an essential role for the host adaptive immune system in effective VTP treatment [Preise *et al.*, 2009]. Importantly, no differences were found in the acute response to VTP between immunocompetent and immunodeficient mouse strains, implying that the initial tissue necrosis caused by rapid vascular shutdown is independent of an immune-mediated mechanism. Rather, the anti-tumour immune response post-VTP may play a role in eliminating tumour tissue that may have survived the acute initial tissue insult due to a heterogeneous tumour vascular network conferring an inherent regional susceptibility to VTP, or by halting the emergence of new tumours from tumour progenitors or cancer stem cells that escape the acute pathophysiological cascade of events caused by VTP.

Further evidence in support of VTP-generated anti-tumour immunity comes from the observation of variable efficacy against tumours with different immunogencities [Preise, 2008]. Tumour immunogenicity is the ability of a tumour to induce an immune response that can slow its rate of growth. Non-immunogenic tumours are characterised by fast

growth *in vivo*, and these often develop widespread metastases, in contrast to immunogenic tumours, which often have a slower rate of growth and remain localised at the site of tumour cell grafting. Certain properties of tumour cells such as their cell surface expression of MHCI molecules are thought to contribute to their inherent immunogenicity. CT26 colon, RENCA renal and transgenic adenocarcinoma of the mouse prostate (TRAMP)-C1 prostate tumours are reported to be immunogenic, whereas 4T1 breast tumours are weakly or non-immunogenic [Agrawal et al., 2004; Wysocki et al., 2006]. Immunogenic CT26 and RENCA tumours responded better to VTP in terms of local tumour control (71% and 66% respectively) than non-immunogenic 4T1 tumours (31%).

In addition to the effect of the immune system on local tumour eradication by VTP, mice were found to resist repeated tumour challenges post-VTP treatment. Moreover, adoptively transferred $CD8^+$ and $CD4^+$ T-cells isolated from surviving mice 3 months post-VTP were able to protect naïve recipients from subsequent challenge with viable cancer cells from the same tumour type. In support of these findings, lymphocytes from spleens of cured mice were able to produce γIFN when co-cultured *in vitro* with photodynamically-treated tumour cells of the same stain. This suggests that VTP treatment can effectively prime naïve T-cells into tumour antigen-specific T-cells capable of cytotoxic activity and immunological memory [Preise *et al.*, 2009].

Several mechanisms have been proposed by which VTP-mediated tumour vascular occlusion and tumour necrosis may enhance tumour immunogenicity. Some insight is provided by the extensive published literature outlining the immunological effects of PDT [Reginato, 2014], however VTP has not been as thoroughly studied in this respect. When drawing any potential conclusions about the immunological mechanisms of VTP from PDT it is important to bear in mind that PDT targets tumour cells directly, whilst

VTP impairs the function of blood vessels through photosensitised vascular occlusion, and therefore the anti-tumour immunological mechanisms of PDT and VTP may be similar in some respects but differ in others.

One of the initial events at the treatment site following PDT-induced tissue damage is the generation of damage-associated molecular patterns (DAMPs). Several studies have shown that PDT, similarly to RT, results in the release of DAMPs, particularly heat shock proteins (HSP), calreticulin, adenosine triphosphate and high mobility group protein 1. An increase in expression of HSP72 in CT26 subcutaneous tumour xenografts treated with VTP was demonstrated in tumour cell lysates by western blot (WB) [Preise et al., 2011], suggesting that VTP-induced release of HSP from necrotic cells serves as a danger signal, stimulating effective tumour recognition by immune cells. In support of this finding is the nature and kinetics of the acute inflammatory response initiated by VTP in the murine CT26 adenocarcinoma tumour model. A rapid and massive neutrophil infiltration was observed within a few hours of treatment, likely mediated by the release of DAMPs. This was followed within 48 hours by T-cell infiltration as demonstrated by immunostaining for the pan T-cell marker $CD3^{+}$. The effect of dendritic cell (DC) depletion on the generation of a VTP anti-tumour immune response was tested in CT26 xenograft tumours. DC depletion resulted in common tumour recurrence post-VTP, supporting a role for DCs in successful VTP treatment [Preise *et al.*, 2009]. This data suggests that the tissue damaging effects of VTP due to acute vascular occlusion results in release of DAMPs, coupled with exposure of several tumour antigens, which overcomes immunological tolerance and generates effective anti-tumour immune responses.

Another postulated mechanism whereby PDT may enhance tumour immunogenicity is the creation of new T-cell epitopes by oxidative modification of proteins caused by

ROS. It has been shown that cellular stress involving oxidative conditions enhances the binding of immunogenic peptides to HSPs such as HSP70. HSP70 acts as a chaperone, forming highly stable HSP70-peptide complexes which transport peptides to sites were antigen presenting cells (APCs) can take up these antigens and prime $CD8^+$ T-lymphocytes [Callahan et al., 2002]. It has also been shown that free-peptides, or SA-bound peptides introduced into the cytosol, become ligands of MHCI molecules at a far lower efficiency than peptides chaperoned by HSPs [Binder et al., 2001]. This suggests that under oxidative stress there is an increase in the quantity of peptides chaperoned by HSPs, which enhances overall antigen delivery to APCs and presentation of these antigens on MHCI molecules. Moreover, during VTP-mediated oxidative stress, ROS can attack polyunsaturated fatty acids of membrane phospholipids and lipoproteins, causing lipid hydroperoxides which decompose to form highly reactive aldehydes [Gross et al., 2003; Koudinova et al., 2003; Preise et al., 2003]. These electrophilic reactive aldehydes react with proteins causing a lipoxidation process resulting in post-translational oxidative modification of these proteins. Studies have demonstrated significant improvement of B- and T-cell-mediated immune responses towards such modified antigens [Kurien et al., 2006; Wang et al., 2008; Wuttge et al., 1999; Yla-Herttuala et al., 1994].

Despite the accumulating evidence that WST-mediated VTP can generate potent local and systemic anti-tumour immune responses in some pre-clinical cancer models, the resulting hypoxic microenvironment can also play a role in shaping recruitment of pro-angiogenic and immunosuppressive cells. Hypoxia demands immune cells to maintain their viability in conditions of low oxygen tension in order to preserve their functionality for executing effector tasks. As discussed in the previous section, the hypoxic response is mainly ascribed to HIF, and induction of HIF following photosensitisation has been documented following PDT [Mitra *et al.*, 2006]. A recent study interrogated the

transcriptome of VTP-treated human LNCaP-AR xenograft tumours using Gene Set Enrichment Analysis, and this identified enrichments of gene sets related to hypoxia, HIF-1α, and VEGFR pathways at three to six hours post-VTP treatment, providing further evidence of a HIF-1α mediate response to VTP-induced hypoxia [Kim et al., 2018].

The observation that tumour cells, under the transcriptional regulation of HIF-1α, release chemokines and growth factors such as CCL2, CCL3, CCL5, CCL7, CCL8, CCL9 and CXCL12, CSF-1, GM-CSF and TGF-β is of particular relevance to the potential role of VTP-induced hypoxia in shaping an immunosuppressive TIME, as these promote TAM and MDSC infiltration [Chouaib et al., 2017]. Studies in mouse models of CT26 colon cancer and TRAMP-C1 and MyC-CaP PCa have shown that myeloid cells characterised by CD11b expression are recruited into the TIME in response to VTP [Fleshker et al., 2008; Lebdai et al., 2019]. Flow-cytometry (FACS) and H&E analysis of VTP-treated tumours at different timepoints found that $CD11b^+$ tumour infiltration occurred at around 10 days post treatment, and predominantly comprised MDSCs and M2 TAMs. In addition, upregulation of CSF1R was seen on H&E analysis of MyC-CaP tumour sections. CSF-1 plays a critical role in the differentiation, proliferation, and migration of myeloid cells to the tumour via signalling through the CSF1 CSF1R. This evidence supporting the immunomodulating role of VTP has led to studies combining VTP with ICB and other immunomodulating agents such as anti-CSF-1R antibodies in murine models of urothelial, renal cell, and PCa to investigate whether combination therapy can improve rejection of established local tumours and prevent metastases [Corradi et al., 2019; Lebdai et al., 2019; O'Shaughnessy et al., 2018] (**table 1.7**).

Reference	Tumour model	Treatment protocol	Summary of results
[O'Shaughnessy et al., 2018]	**Mouse species**: Balb/c **Cell line**: RENCA tumour cells **Xenograft location**: upper pole of kidney	**WST-11-VTP**: 9 mg/Kg IV bolus of WST-11 followed by a 10 min laser illumination (753 nm/150 mW/cm^2) **Antibody administration:** 250 mg anti–PD-1 + 100 mg anti–PD-L1 in 0.2 mL PBS intraperitoneally twice weekly for 3 weeks starting 6 days after tumour implantation	Combination treatment, but neither treatment alone, resulted in regression of primary tumours, prevented growth of lung metastases, and prolonged survival. Treatment effect was associated with increased $CD8^+$:Treg and $CD4^+$:Treg ratios in primary renal tumours and increased T-cell infiltration in sites of lung metastasis. PD-L1 expression was induced following VTP treatment of human renal cell carcinoma xenografts
[Corradi et al., 2019]	**Mouse species**: C57BL/6 **Cell line**: MB-49 – luciferase transfected **Xenograft location**: flank	**WST-11-VTP**: 9 mg/Kg IV bolus of WST-11 followed by a 10 min laser illumination (755 nm/150 mW/cm^2) **Antibody administration:** 100 μg anti-CTLA-4 was administered intraperitoneally for a total of 4 doses (1,4,7 and 10 days after WST-11 VTP treatment)	In the combination treatment group, tumour bioluminescence signal was reduced compared to the untreated control, VTP or anti-CTLA-4 monotherapy treatment groups. This translated into improved overall survival of the mice in the combination group as measured by spontaneous death of the mouse or a tumour volume of 2000 mm^3. Mice in the combination group had fewer lung metastatic lesions and did not develop new tumours following rechallenge experiments
[Lebdai et al., 2019]	**Mouse species**: FVB/6 or C57BL/6 **Cell line**: MyC-CaP or TRAMP-C2 **Xenograft location**: hindlimb	**WST-11 mediated VTP treatment protocol:** IV infusion of WST11 (9 mg/kg) followed immediately by 10 min laser illumination (755 nm, 150 mW/cm) **Antibody administration**: 250 mg anti-CSF1R was administered intraperitoneally on days 1,4,7,10,13.	Combination of VTP and CSF1R blockade enhanced VTP treatment efficacy as measured by tumour growth delay experiments. Combination treatment led to a reduction in the relative proportion of the TAM and MDSC tumour infiltrate. Moreover, this was associated with a significant increase in the tumour $CD8^+$ T-cell infiltrate and cytotoxic potential of these cells as measured by granzyme B expression

Table 1.7. Combination of VTP and immunomodulation in pre-clinical tumour models.
MDSC; myeloid derived suppressor cell; PBS, phosphate buffered saline; PSA, prostate-specific antigen; TAM; tumour macrophage; Treg, T-regulatory cells; VTP, vascular targeted photodynamic therapy

Overall, these pre-clinical studies have demonstrated that VTP is capable of activating both the innate and adaptive immune systems, and through HIF-driven mechanisms can also promote infiltration of monocytic cells such as TAMs and MDSCs, creating a predominantly immunosuppressed TIME that facilitates immune escape (**figure 1.12**).

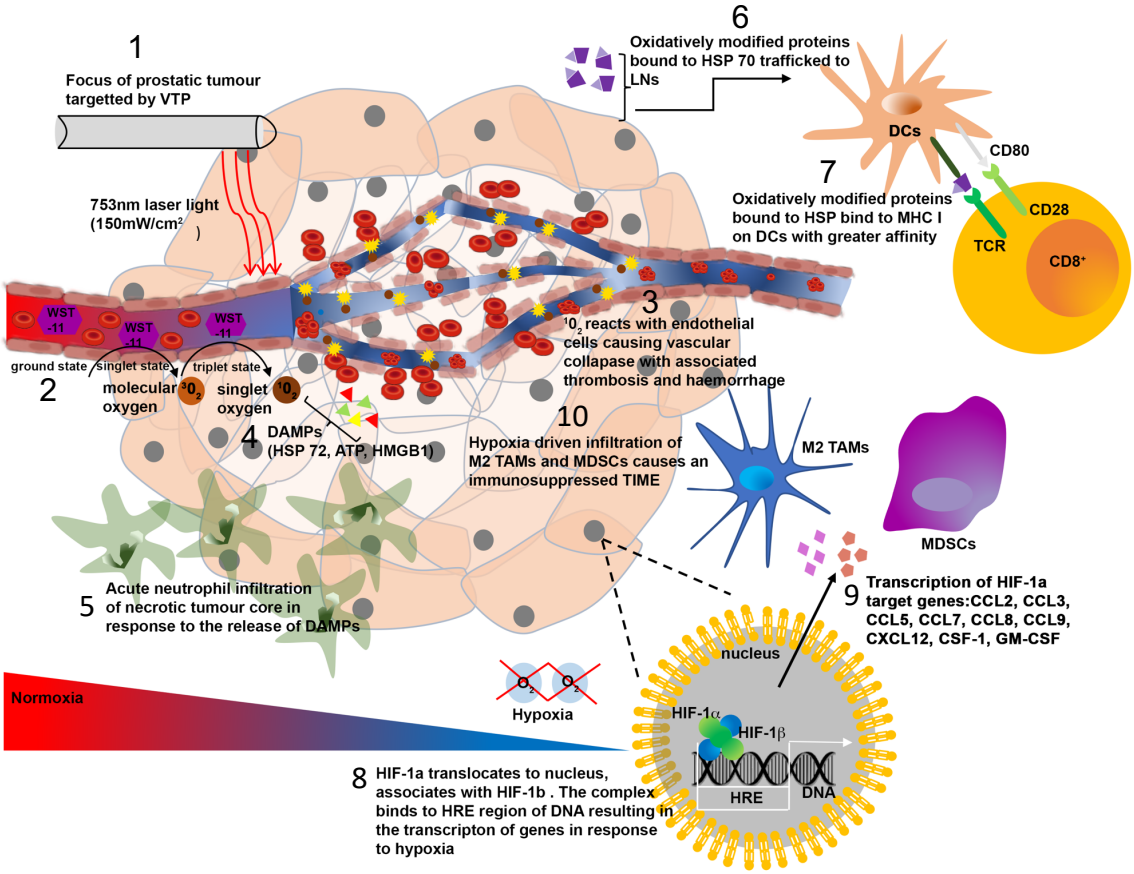


Figure 1.12. VTP mechanism of action and effects on the immune system. (1) Focus of PCa treated with VTP using a 753 nm laser light at 150 mW/cm^2. **(2)** Intravenously injected WST-11 is focally activated by the laser light and transits from its ground state to its single state and then triplet state where it reacts with molecular oxygen to form singlet oxygen. **(3)** Singlet oxygen then reacts with endothelial cells causing vascular collapse with associated thrombosis and haemorrhage. **(4)** This results in the release of DAMPs, which cause an **(5)** acute neutrophil infiltration into the necrotic core. **(6)** DAMPs and oxidatively modified proteins bound to HSP-70 are trafficked to tumour draining lymph nodes and **(7)** presented on MHC class I to naïve CD8$^+$-T-cells causing priming of an effector anti-tumour immune response. **(8)** The associated vascular damage and tumour hypoxia causes HIF-mediated transcription of **(9)** several genes involved in the cell's response to hypoxia. **(10)** This results in the infiltration of TAMs and MDSCs causing an immunosuppressed tumour immune microenvironment

1.3.4 Multimodal therapy using VTP in pre-clinical prostate cancer models

VTP has been combined with other treatment modalities such as bombesin antagonist-based RT and ADT, to test the hypothesis that sequential treatment of PCa with these VTP treatment combinations enhances treatment effectiveness and local tumour control beyond that seen from monotherapy [Kim et al., 2017, 2018]. Bombesin antagonist-based RT involves administration of ^{90}YDOTA-AR, a bombesin-antagonist peptide conjugated with the beta radiation-releasing radioisotope ^{90}Y. Bombesin receptors are overexpressed in a variety of human tumours. In particular, the gastrin-releasing peptide receptor has been identified on PCa and breast cancers [Abiraj et al., 2011]. However, treatment efficacy of radiolabelled peptides is limited due to the relatively low uptake in target cell populations coupled with their prompt urinary excretion. In this study, the sequential treatment of PCa with ^{90}YDOTA-AR followed by WST-11-mediated VTP was tested to investigate whether VTP-mediated destruction of tumour feeding arteries and draining veins would improve the retention of the accumulated ^{90}YDOTA-AR in PCa xenografts and improve treatment efficacy as measured by tumour growth rate. Experiments showed that combination therapy resulted in longer retention of ^{90}YDOTA-AR in PC-3 and VCaP xenograft tumours as measured by Cherenkov Luminescence Imaging (CLI) at all time points tested (24-144 hours). Increased CLI intensity in the ^{90}YDOTA-AR and VTP treated mice translated into a significantly longer tumour growth delay compared to mice in the control or the monotherapy groups.

Gene set enrichment analyses have shown that AR signalling gene sets are upregulated in VTP-treated tumours compared to control mice [Kim et al., 2018]. Experiments using human LNCaP AR-expressing mouse xenograft tumours treated with VTP in combination with a single dose of ADT (using Degaralix given three days

before WST-11 mediated VTP) demonstrated that combination treatment significantly inhibited tumour growth compared to monotherapy. Tumours displayed more extensive TUNEL staining 7 days post-treatment, suggesting that increased cell death underlies the prolonged tumour growth delay seen after combination treatment [Kim et al., 2018].

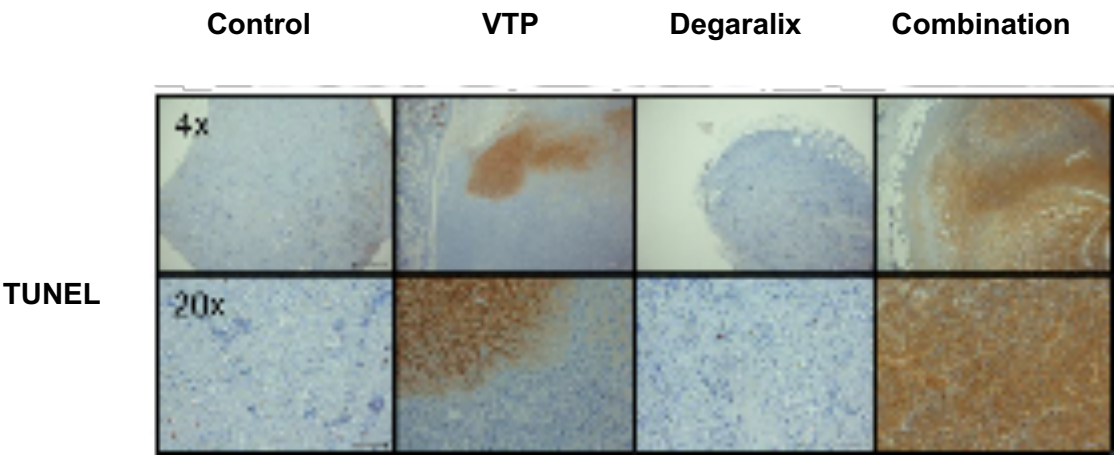


Figure 1.13. TUNEL staining is enhanced in tumours treated with both VTP and Degaralix. Images adapted from [Kim et al., 2018]. With permission from HHS Public Access.

1.3.5 Clinical trial evidence of WST-09 and WST-11 mediated VTP in prostate cancer

VTP has been investigated in a clinical trial setting as a treatment option for low-risk low-volume PCa, or as salvage therapy after failed EBRT for localised PCa (**table 1.8).** Initial trials tested WST-09-mediated VTP, whilst more recent trials using the water-soluble derivative WST-11. These trials collectively established that VTP is a feasible, well-tolerated, safe and effective minimally invasive surgical procedure for total ablation therapy in radiorecurrent PCa as well as in hemiablation of the affected lobe for localised low-risk low-volume PCa. These trials also allowed standardisation of the procedure, which is an essential step in the evaluation of any new health technology. In these studies, the degree of prostate devascularisation on contrast-enhanced MRI, and negative biopsy rates following treatment, were used as surrogate markers of

treatment effectiveness. Negative biopsy rates at 6 months post-VTP were found to be reduced compared to untreated men with low-risk low-volume PCa receiving repeat biopsy as part of an AS protocol [Azzouzi et al., 2015a]. Extra-prostatic treatment effects (i.e., devascularisation outside of the prostate) were seen on MRI in some patients who underwent VTP for low-risk low-volume PCa. Despite this, VTP proved to be safe and well tolerated. The majority of treatment related adverse events (AEs) were mild or moderate and often self-resolving without further treatment. The most common AEs were dysuria, haematuria, erectile dysfunction, perineal pain, haematuria, urinary retention and micturition urgency. IPSS urinary bother scores often increased soon after treatment but returned to baseline or even showed improvement by 6 months, suggesting a VTP-related reduction in urinary symptoms. Erectile function, measured using IIEF-5 questionnaires, also deteriorated transiently after treatment but returned to baseline levels by 6 months. In some patients mild self-resolving aberrations in liver function tests were observed, and a small but important number of patients reported serious AEs including rectourethral fistulae in two patients [Trachtenberg et al., 2008], two cases of large extraprostatic necrosis and two cases of prostatitis. All other serious AEs were single occurrences of pelvic pain, prostatic urethral stricture and worsening epididymorchitis [Azzouzi et al., 2013; Moore et al., 2015]. Trials also explored the optimum treatment parameters for prostatic hemiablation for unilateral PCa by testing several WST-11 and light doses [Azzouzi et al., 2013; Moore et al., 2015]. The results pointed towards 4 mg/Kg of body weight as the optimum dose of WST-11 activated by 753 nm light at a dose of 200 J/cm^2. In addition, these trials showed that the light dose per volume of prostate is an important determinant of the effect of the treatment as determined by contrast-enhanced MRI at 7 days, and at the 6-month biopsy result. Specifically, the light density index (LDI), defined as the ratio between total light-emitting length of inserted VTP fibres (cm) and the baseline volume by planimetry (cm^3) of targeted prostate volume showed a direct correlation with the extent of prostatic

ablation achieved. A pooled analysis of 117 patients from 3 phase II clinical trials (PCM201:NCT00707356; PCM202:NCT00946881; PCM203:NCT00975429) who received the recommended dose/light combination revealed that 68.4% of treated patients had a negative biopsy result at 6 months follow up. For these patients the intraprostatic necrosis percentage on MRI was 76.5% at day 7. When these analyses were confined to men who had been treated with LDI≥1, the 6 month negative biopsy rate improved to 77.6% and the necrosis percentage to 86.3% at day 7 [Azzouzi et al., 2015a]. Treatment planning algorithms for VTP ensure a LDI≥1 by increasing the number of fibres, or the length of fibre, inserted into the prostate according to the volume of prostatic tumour that needs treating as determined by pre-treatment MRI.

Reference	Patient & Study characteristics	Treatment protocol	Summary of main oncological outcomes
Trachtenberg *et al.*, 2007	**Study**: Phase I/II prospective trial of whole gland prostatic ablation using VTP **Eligibility**: Men with recurrent localised PCa after failed EBRT; n = 24	**TOOKAD® treatment:** 1. Escalating doses of WST-09 (0.1-2 mg/Kg) at a fixed laser dose of 100 $J/cm^{2.}$ 2. Escalating light doses of 230 J/cm^2 & 360 J/cm^2 at a fixed WST-09 dose of 2 mg/Kg.	In the drug escalation arm 3/6 patients developed prostatic devascularisation as seen on MRI. One response was seen at 1 mg/kg WST-09 and two responses at 2 mg/kg In the light dose escalation arm an increasing volume of prostatic devascularisation was seen on MRI with 2/3 patients in the first light escalation cohort (230 J/cm^2) responding and all six responding at the highest light dose (360 J/cm^2) with hypovascularised lesions encompassing up to 70% of the peripheral zone
Trachtenberg *et al.*, 2008	**Study**: Phase II prospective trial of whole gland prostatic ablation using WST-09 mediated VTP **Eligibility**: Men with recurrent localised PCa after failed EBRT; n = 28	**TOOKAD® treatment:** Single, 20 min, IV administration of 2 mg/Kg escalating light doses (30 min duration) to determine which light fluence would cover 90% of the gland volume (D_{90})	Treatment was shown to be efficient starting at a threshold dose of 23 J/cm^2. 8/13 patients receiving a D_{90} of 23 J/cm^2 had a negative biopsy result at six months post treatment and MRI evidence of marked prostatic devascularisation suggesting a 60% success rate in this small cohort of patients
Taneja et al., 2016	**Study**: prospective multicentre phase I/II, nonrandomised, open-label, single IV, escalating drug dose and light energy dosage clinical trial of WST-11 mediated VTP (PMC 202) **Eligibility:** Men with unilateral, low volume, GS 3+3 PCa; n = 30	**TOOKAD® Soluble treatment:** single, 10 min, IV administration, doses of either 2, 4 or 6 mg/kg. 753-nm laser light (20 min duration) at escalating fixed energy doses of 200 J/cm^2 (167 mW/cm^2) and 300 J/cm (250 mW/cm^2).The number and length of optic fibres varied to achieve a LDI of <1 or >1	At the optimal WST-11 and light dose of 4 mg/Kg and 200 J/cm^2 respectively with a LDI $\geq$ 1, the median non-perfused prostate tissue was 74.3% ± 15.3 and the negative biopsy rate at six months was 73.3% (11/15 patients). When the LD<1, prostatic non perfused tissue was 38.5% ± 28.6. The negative biopsy rate dropped to 33.6% (2/6 patients) At 2mg/Kg WST-11 and light dose of 200J/cm^2 with a LDI $\geq$ 1 the median non-perfused tissue was 70.4% ± 12.4. The negative biopsy rate was 100% (2/2 patients)
Azzouzi *et al.*, 2013	**Study**: Multicentre, phase II, open-label, single IV dose, 6-month, nonrandomised	**TOOKAD® Soluble treatment:** Single, 10 min, IV administration of either 4 or 6 mg/Kg. 753 nm laser light	83% (38/46) patients treated with hemiablation using the optimal dose of 4 mg/Kg and 200 J/cm^2 had negative biopsies at six-month follow-up. The mean prostatic necrosis percentage seven days after VTP was 88%.

	clinical trial (PCM 203) **Eligibility:** Men with Gleason 3+3 or low volume Gleason 3+4 disease who fit criteria for AS; n = 86	(20–25-minute duration) at escalating energy doses of 200 J/cm^2 or 300 J/cm^2. Hemi or whole gland ablation was performed depending on the location(s) of the tumours. The number and length of optic fibres varied to achieve a LDI of <1 or >1	Further exploratory analysis of patients who received an LDI≥1 showed that the efficacy of VTP improved compared to those who received the same drug and light dose with an LDI<1. 6 mg/Kg WST-11 did not result in larger volumes of effect than 4 mg/Kg
Moore *et al.*, 2015	**Study**: Multi-centre, phase II, open-label, single IV dose, 6-month clinical trial **Eligibility:** Men with Gleason 3+3 or low volume GS 3+4 disease who fit criteria for AS; n = 42 (PCM 201)	**TOOKAD® Soluble treatment:** Single, 10 min, IV administration, doses of 2 to 6 mg/kg, 753 nm laser light at fixed power 150 mW/cm^2 and energy 200 J/cm^2	With all doses combined, 53% of patients had a negative biopsy at six months (20/37). Patients who received the optimal dose of 4 mg, 54% had a negative six-month biopsy (15/28). When patients received the optimal WST-11 dose of 4 mg/Kg and an LDI>1, 83% (10/12) of patients had a negative biopsy
Azzouzi *et al.*, 2017) & Gill *et al.*, 2018	**Study:** Multi-centre, phase III, randomised controlled trial of WST-11 mediated VTP versus AS **Eligibility:** Men with low-risk PCa who fit criteria for AS. Patients with GS pattern 4 or 5 or tumour core length >5 mm were excluded	**TOOKAD® Soluble treatment:** Single, 10 min, IV administration, dose of 4 mg/kg, 753 nm laser light at fixed power 150 mW/cm^2 and energy 200 J/cm^2 for 22 min 15 seconds	The proportion of patients who experienced progression from low to moderate or high-risk PCa or developed metastatic disease or died from PCa at month 24 was 28% (58/206) in the VTP arm compared to 58% (120/207) in the AS group (adjusted risk ratio 0.34, 95% CI 0.24-0.46; p<0.001). The negative biopsy rate following VTP was 49% (101/206) compared to 14% (28/207) in the AS arm At 4 year follow up conversion to radical therapy due to histological upgrading, increasing PSA, volume of tumour or patient choice was lower in the VTP arm (24%) compared to AS (53%). The negative biopsy rate was 50% in the VTP arm versus 14% in the AS cohort. Higher-grade cancer (GGG>1) was found in 10% after VTP versus 34% in the AS cohort. In field positive biopsy rate after VTP was 25%

Table 1.8. Clinical trials data on VTP-mediated treatment of prostate cancer.
AS, active surveillance; EBRT, External beam radiotherapy; GGG, gleason grade group; GS, gleason score; PCa, prostate cancer; LDI, light density index; VTP, vascular-targeted photodynamic therapy

Histopathological data obtained from 56 patients at six months following VTP showed the characteristics of post therapy tissue remodelling. VTP-treated areas were characterised by sharply demarcated areas of fibrosis with dense hyalinised collagen deposition often associated with coagulative-type necrosis and chronic inflammation. A few atrophic benign glands were seen among the fibrotic tissue surrounded by multinuclear macrophages. When persistent cancer was present, tumour foci were mostly found outside the scar tissue and showed no cytonuclear or architectural modification in comparison with the cancer tissue prior to therapy. This clinical study provided long-term H&E data that WST-11 mediated VTP can effectively destroy PCa in the targeted area complementing the MRI findings of prostatic devascularisation 7 days after treatment [Eymerit-Morin et al., 2013].

At present, the lack of long-term oncological outcomes, existing shortcomings in mpMRI targeted biopsy alone in detecting clinically significant PCa without systematic biopsy [Sathianathen et al., 2020], and uncertainties about the clinical efficacy of VTP for intermediate- or high-risk tumours has led to organisations such as BAUS, EAU and AUA to recommend against VTP as part of the SOC of treatment at this time [van der Poel et al., 2018; Sanda et al., 2018].

The effects of RT or VTP on the tumour microenvironment provide a clear rationale to combine RT, VTP and/or immunotherapy as part of a multi-modality therapy approach to PCa. RT is an established treatment option, whilst VTP is an option within the context of a clinical trial, for patients with PCa, and therefore any potential benefits of multi-modality therapy seen in preclinical models can be tested in the context of an RCT in patients. However, prior to first-in-man use, evaluation of multi-modality therapy in pre-clinical models of PCa is necessary to determine safety along with the optimal temporal administration of these therapies, along with an increased understanding of the potential mechanisms of treatment benefit if this exists.

1.4 Study aim, hypotheses and objectives

The aim of this study is to investigate whether multi-modality therapy using optimally combined sequential delivery of RT and a minimally invasive surgical intervention (WST-11 VTP) and/or immunomodulation in the form of ICB results in an additive or synergistic anti-tumour effect in a pre-clinical mouse model of PCa.

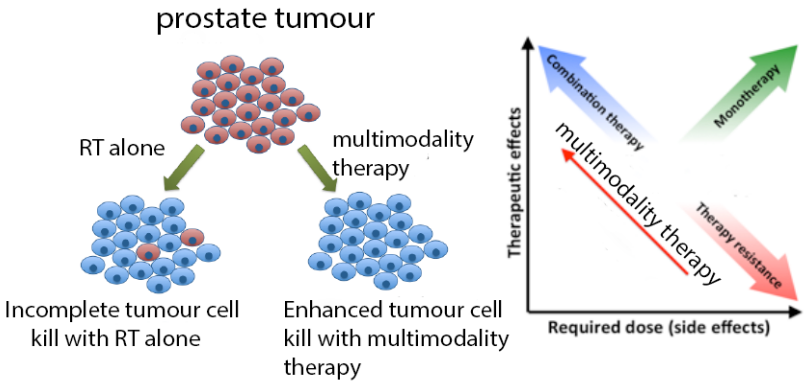


Figure 1.14. Primary Hypothesis. Multimodality treatment of prostate cancer improves local tumour control, enabling reduced radiotherapy doses and reduced toxicity and side effects. Figure adapted with permission from Richard Bryant's CRUK Clinician Scientist application 2016.

A further aim of this study is to explore in a bilateral tumour model whether combination treatment of primary tumours using WST-11 VTP and RT in oligo-metastatic disease causes immune-mediated metastasis reduction.

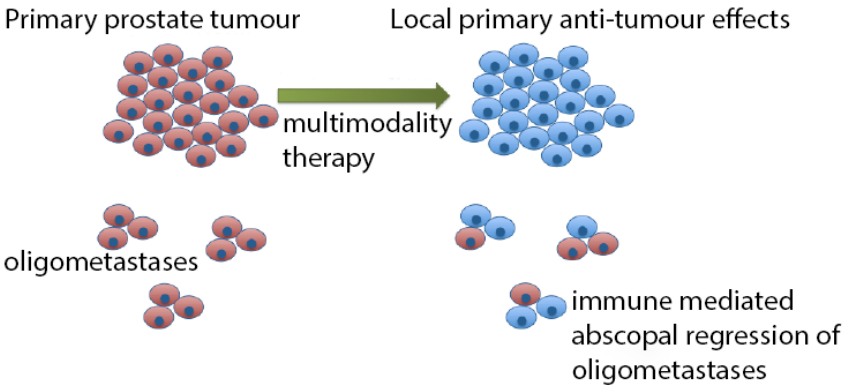


Figure 1.15. Secondary Hypothesis. Treatment of primary tumours with WST-11 VTP and RT in oligo-metastatic disease causes immune-mediated abscopal metastasis burden reduction. Figure adapted with permission from Richard Bryant's CRUK Clinician Scientist application 2016.

To test the above hypotheses the study will address the following objectives:

- Determine the immunogenicity of TRAMP-C1 and MyC-CaP murine PCa cells by measuring cell surface expression of MHCI and PD-L1 in response to type II interferon (γIFN) treatment and IR *in vitro.*
- Establish two immunocompetent PCa xenograft mouse models using the TRAMP-C1 and MyC-CaP murine PCa cell lines.
- Investigate tumour response to RT by measuring tumour growth delay following conventional fractionation (2 Gy dose per fraction) or with hypofractionated doses (5-10 Gy dose per fraction).
- Analyse the tumour vessel response to hypofractionated doses of RT in both pre-clinical PCa models for optimal combination with TOOKAD-soluble® VTP.
- Determine the local tumour immunological response to hypofractionated doses of RT in both pre-clinical models at early and late timepoints and identify potential targets for immunomodulation.
- Adapt and optimise the platform designed to treat xenograft mouse flank tumours with TOOKAD-soluble® VTP in Oxford by establishing a safe and effective VTP-treatment protocol of PCa flank xenograft tumours.
- Analyse the local tumour immunological response following treatment with TOOKAD-soluble® VTP at early and late timepoints.
- Investigate potential benefit from combined RT and immunomodulation in PCa flank xenograft tumours.
- Investigate potential benefit from combined RT and WST-11 VTP in PCa flank xenograft tumours. Experiments will investigate different temporal administration (i.e., RT first followed by VTP, or VTP followed by RT) and will also test different doses of WST-11 VTP.

Chapter 2. Materials and Methods

2.1 Cell lines

TRAMP-C1 (ATCC® CRL-2730™) and MyC-CaP (ATCC® CRL-3255™) cells were purchased from American Type Culture Collection (ATCC®) in 2016. TRAMP-C1 cells were derived from the TRAMP model in C57BL/6 mice harbouring a construct comprising the minimal rat probasin promoter driving prostate-specific epithelial expression of SV40 large T antigen [Foster et al., 1997a; Greenberg et al., 1995]. MyC-CaP cells were derived from a *c-myc* transgenic mouse with PCa [Watson et al., 2005]. Both TRAMP-C1 and MyC-CaP cells express the AR [Ellis et al., 2012; Foster et al., 1997a; Greenberg et al., 1995], however TRAMP-C1 are androgen-independent whilst MyC-CaP cells are androgen-sensitive. TRAMP-C1 and MyC-CaP cells are tumourigenic when grafted into syngeneic C57BL/6 and FVB mice respectively, to establish immunocompetent subcutaneous PCa tumour models.

2.1.1 Culture conditions

Cells were cultured in optical growth conditions according to the supplier's protocol. TRAMP-C1 cells were cultured in Dulbecco's modified Eagle's medium (DMEM) with 4 mM L-glutamine, 1.5 g/L sodium bicarbonate, 4.5 g/L glucose, 0.005 mg/ml bovine insulin, 10 nM dehydroisoandrosterone, 5% Nu-Serum IV, 5% fetal bovine serum (FBS). MyC-CaP cells were cultured in DMEM with 10% FBS, 1% penicillin and 100 µg/ml streptomycin. Both culture solutions were supplemented with 1% Penicillin-Streptomycin (5000 U/mL) solution (Gibco™). Cells were maintained mycoplasma free (LookOut® Mycoplasma PCR Detection Kit, Sigma) at 37ºC and 5% CO_2. At 90% confluency, cells

were passaged and split by no more than a 1:10 ratio. Cells of 10 passages or less were used for all *in vitro* and *in vivo* experiments.

2.1.2 Freezing and thawing conditions

TRAMP-C1 and MyC-CaP were placed in long-term storage in cryovials by suspending 1-2 x 10^6 cells in 10% dimethyl sulfoxide (DMSO) (Sigma) premixed with FBS in a total volume of 1000 μL. Cryovials were placed at -80°C overnight and stored in liquid nitrogen thereafter. Defrosting of cells was done by gently thawing at 37°C and immediate removal of DMSO by re-suspending in PBS and centrifugation at 240 x g for five minutes. After the DMSO was removed, cells were re-suspended in their respective cell culture medium in tissue culture flasks and maintained in the conditions outlined above.

2.1.3 Cell count and viability

Cells count and viability was performed using a TC20^{TM} automated cell counter (Bio-Rad). In brief, 10 μL of cells suspended in PBS or media were mixed with 10 μL 0.4% Tryphan Blue solution (BioLegend). 10 μL of the mixed solution was then placed on a counting slide which was then inserted into the cell counter for quantification of total live cell count.

2.2 TRAMP-C1 lentiviral transfection

TRAMP-C1 cells were transfected with lentivirus harbouring an OVA-Green Fluorescent Protein (OVA-GFP) construct. Lentiviral vectors were a kind donation from the Cerundolo Lab (Weatherall Institute of Molecular Medicine, University of Oxford). In brief, 1 x 10^5 TRAMP-C1 cells were mixed with lentiviral particles in the presence of 8 μl/mL polybrene in a 1.5 mL Eppendorf tube in 0.5 mL DMEM medium. Cells together with lentiviral

particles were centrifuged at 3500 rpm using a Thermo Scientific™ Medifuge™ Small Benchtop Centrifuge at 4ºC for 30 minutes. Cells were then seeded in a 12-well plate in 0.5 mL medium and placed at 4ºC for two hours. Cells were transferred to 37ºC, and 5% CO_2 and the medium was changed on day two. On day three, cells were washed with PBS for six times to remove all lentivirus particles. Cells were then detached using Accutase solution and resuspended in PBS in Falcon™ round bottom test tubes. Selection for OVA-GFP TRAMP-C1 cells was performed by GFP cell sorting with the Aria II FACS cell sorter.

2.3 *In vitro* tumour cell treatments

2.3.1 Treatment with γIFN

TRAMP-C1 and MyC-CaP cells were treated with 1.0-10 ng/mL mouse recombinant murine γIFN (Invitrogen). When not in use γIFN was stored at -80°C.

2.3.2 Treatment with ionising radiation

Cells were irradiated in tissue culture flasks or six-well plates using a Caesium irradiator at a dose rate of 1.46 Gy/min. Flasks or plates containing control untreated cells were sham irradiated.

2.4 Clonogenic assays to determine cell radiosensitivity

Clonogenic assays were performed to determine intrinsic cellular radiosensitivity of TRAMP-C1 and MyC-CaP cells and determine the α/β ratio for each cell line. Single cells were plated at different densities in six-well plates, depending on the IR dose (**table 2.1**). Cells were irradiated using a Caesium irradiator as described above and incubated for 10 days. After 10 days the media was removed and the cells washed with PBS. Cells were then stained with crystal violet (Sigma-Aldrich) to facilitate colony counting. Colonies were counted to determine plating efficiency, and the fractions of cells surviving after application of a single dose of 2, 4, 6, 8 and 10 Gy IR was determined. These experiments were conducted in duplicate and repeated three times to determine a mean survival fraction at each dose of IR for each cell line.

Ionising radiation dose (Gy)	TRAMP-C1 (cells/well)	MyC-CaP (cells/well)
0	100	200
2	200	400
4	400	600
6	800	800
8	1600	1000
10	3200	2000

Table 2.1. Tumour cell plating density/well for each dose of ionising radiation.

2.5 Flow-cytometry quantification of *in vitro* MHC Class I and PD-L1 expression following γIFN and ionising radiation

40,000 TRAMP-C1 or MyC-CaP cells were plated in duplicate in six-well plates and treated with 0, 0.1, 1.0 or 10 ng/mL γIFN for FACS quantification of MHCI (H-2K^b) and PD-L1 expression and changes induced after 72 hours of γIFN treatment. To test whether IR induces MHCI and PD-L1 expression, TRAMP-C1 cells were treated with 2, 6 and 10 Gy RT using a Caesium irradiator in the presence or absence of 1.0 ng/mL γIFN. After 72 hours incubation, the media was removed, cells were washed with PBS and detached to form a single cell suspension using Accutase solution (BioLegend). Cells were then washed with PBS and counted and diluted to 10^6 cells/mL of FACS buffer (PBS with 2% FBS). 1x10^6 cells in 100 μL FACS buffer were stained with Pe-Cy7 H-2Kb (MHC-I, eBioscience, AF6–88.5.53), APC anti-mouse H-2K^b bound to SIINFEKL (BioLegend 25-D1.16), BV421- CD274 (B7-H1, PD-L1, Biolegend, 10F.9G2) and LIVE/DEAD™ Fixable Green Dead Cell Stain Kit (ThermoFisher Scientific, L23101) antibodies or Propidium Iodide. A time course experiment was performed to determine the temporal pattern of PD-L1 expression in TRAMP-C1 cells following 1.0 ng/mL γIFN or 6 Gy IR . For all *in vitro* FACS experiments appropriate isotype and unstained controls were performed. FACS data (20,000-50,000 live events) were acquired using NxT Attune (Thermo Fischer Scientific) and analysed by FlowJo.v10 software. At least three separate independent experiments were performed.

2.6 Western blot analysis of *in vitro* TRAMP-C1 PD-L1 expression following γIFN and ionising radiation

For WB experiments, TRAMP-C1 cells were cultured in six-well plates and treated with 6Gy IR and/or 1.0 ng/mL γIFN. After 72 hours incubation the media was removed, cells were washed with ice-cold PBS and placed on ice. To collect whole tumour cell extracts, adherent cells were scraped off the six-well plate using a cold plastic cell scraper in radioimmunoprecipitation assay (RIPA) lysis buffer (Thermo Scientific) containing protease (Sigma-Aldrich) and phosphatase inhibitors (Roche). At this stage samples were collected in 1.5 mL Eppendorf tube, frozen on dry ice and then placed at -80ºC for long-term storage or for immediate use centrifuged at 12,000 x g for 15 minutes at 4ºC. The supernatant was then carefully moved to a new Eppendorf tube and subjected to sonication at 20 KHz for 20 seconds per sample. Protein concentration measurement was performed using the Pierce™ Rapid Gold BCA Protein Assay Kit (Thermo Scientific). In brief, diluted bovine serum albumin (BSA) standards (0-2000 μg/mL) were prepared according to the manufacturer's recommendations and 10 μL of each BSA standard was placed in duplicate in a 96-well plate. The test protein sample was first diluted 1:10 and 10 μL of the diluted protein sample was placed in duplicate in the same 96-well plate. 200 μL of the Pierce Rapid Gold BCA Working Reagent was added to each well containing test and standard protein sample. The plate was shielded from light and placed on a plate shaker for 30 seconds. Absorbance was measured at 595 nm using the POLARstar® Omega and analysed using the Magellan™ software. Known dilutions of the BSA standards were used to plot a standard curve of absorbance against protein concentration to allow calculation of the test protein concentration.

Proteins were then reduced at 95°C with 4x Laemmli Sample Buffer (Bio-Rad) containing 2-Mercaptoethanol (1:3 dilution). Lysates (~30 μg protein/well) were resolved on 4-15%

“Criterion™ TGX™ Precast Midi” polyacrylamide gels (Bio-Rad) at 120 V for 1.5 hours in 1X Tris/Glycine BioRad running buffer (Bio-Rad). The proteins were then transferred to PVDF membranes using a Trans-Blot Turbo transfer system (Bio-Rad) at 2.5 A constant; up to 25 V for 7 minutes. Membranes were blocked for one hour at room temperature in 5% (w/v) milk in Tris-buffered saline (50 mM Tris-Cl, pH 7.5 and 150 mM NaCl) containing 0.1% Tween 20 (TBST). Anti-PD-L1 (1:400, AF1019, R&D systems) and vinculin (1:1000, sc-25336, Santa Cruz Biotechnology) primary antibodies in 5% milk TBST were used to blot the membranes at 4°C overnight. Membranes were washed for five minutes for three times in TBST prior to one hour incubation with 1:5000 HRP conjugated secondary antibodies (anti-Goat, Sigma-Aldrich and anti-Rabbit IgG, GeneTex respectively). Membranes were exposed to the enhanced chemiluminescence detection reagent (Amersham, GE Healthcare) followed by detection of the protein signals with the ChemiDoc System (Bio-Rad) and densitometries were quantified by ImageJ.

2.7 Ethical statement for mouse xenograft studies

All pre-clinical *in vivo* experiments were performed under appropriate Home Office Procedure Project Licence (PPL) legislation (PPL: 30/2306) by fully competent Procedure Individual Licence (PIL) holders. All experiments were approved by the ethical committees of the University of Oxford and conducted under the Home Office Animals (Scientific Procedures) Act 1986 (UK) requirements. Animal experiments were undertaken in accordance with the Animal Research: Reporting of *in vivo* Experiments (ARRIVE) guidelines of the National Centre for the Replacement, Refinement and Reduction of Animals in Research (NC3Rs) [Kilkenny et al., 2010].

2.8 Housing and husbandry

Naïve male 6-8 week old immunocompetent C57BL/6 and FVB mice (Mus Musculus, Charles River laboratories), 18.0-25.0 grams in weight were housed at the Radiation Research Institute, Churchill Hospital, Oxford UK, a pathogen-free facility with 12-hour light cycles. Mice were housed in groups of six to limit fighting in individually ventilated cages on woodchip bedding, with access to water and food *ad libitum*, at 22ºC (range 21-24ºC) and 50% humidity (range 35-75%), with environmental enrichment and bedding material, and monitored for body weight changes twice weekly. Following any intervention, mice were monitored three times weekly.

2.9 Mouse anaesthesia

Anaesthesia was induced and maintained using isoflurane (typically 4% and 1–2%) in room air supplemented with oxygen (80%/20% v/v; flow rate 1 L/min). Inhalable isoflurane anaesthesia was chosen to aid rapid recovery following procedures, and because of its quick elimination through the lungs and relative technical ease of administration. Anaesthesia depth was based on respiration rate monitored using a pneumatic cushion, and isoflurane levels were adjusted to maintain a respiration rate of 40–60 breaths per minute. Induction and recovery from anaesthesia was performed in a heated unit with a base temperature of around 37℃.

2.10 Generation of flank xenograft models

TRAMP-C1 and MyC-CaP cells at 70%-80% confluency were trypsinised, washed twice with PBS, and harvested by centrifugation at 300 x g for 5 minutes, and a single-cell suspension was prepared in serum-free PBS. Cells were counted using an automated cell counter as described above. TRAMP-C1 (2×10^6) or MyC-CaP (1×10^6) cells in PBS and 1:1 high concentration phenol red-free Matrigel® (Corning,UK) were injected into the right lower flank of 7-9 week old C57BL/6 or FVB mice respectively under isofluorane inhalational anaesthesia. In the case of bilateral tumour generation, cells were injected in the right and left lower flank on the same session under the same anaesthetic. Tumour size was assessed three times weekly using callipers (tumour volume = $L*W*H*[\pi/6]$).

2.11 Treatment of flank PCa xenograft tumours

2.11.1 Treatment of flank PCa xenograft tumours with radiotherapy

When tumours reached 100-120 mm^3, mice were assigned treatment on a 'first come, first allocated' basis using a randomly generated treatment list (GraphPad Prism 10, USA) in one of the following treatment groups: (a) control; (b) 1 x 5 Gy; (c) 3 x 5 Gy; (d) 5 x 2 Gy; (d) 5 x 5 Gy; (e) 3 x 10 Gy. RT was delivered using a Gulmay 320 irradiator (300 kV, 10 mA, 2.25 Gy/minute). The animals were maintained under anaesthesia throughout RT treatment and their body was protected by lead shielding except for the flank tumour to be irradiated. Where a mouse received a fractionated treatment regimen (i.e., 3 x 5 Gy, 5 x 2 Gy, 5 x 5 Gy or 3 x 10 Gy), RT fractions were given on consecutive days.

2.11.2 Treatment of PCa flank xenograft tumours with WST-11 VTP

2.11.2.1 Preparation of WST-11

Clinical grade TOOKAD®-soluble 200 mg (WST-11) (STEBA Biotech, Luxembourg) was a kind gift from Professor Avigdor Sherz at the Weizmann Institute of Science, Rehovot, Israel. The powdered form of the drug was reconstituted in 200 mL of sterile 5% dextrose solution to a final concentration of 1 mg/mL under light protected conditions. Source of light was provided by a filtered lamp emitting only yellow light of wavelength 560-590 nm which does not activate the drug. 1 mL aliquots of drug were placed in 1.5 mL Eppendorf tubes and covered with aluminium foil to prevent contact with light. Aliquots were then stored at -20°C for future use.

Flank tumours were treated with WST-11 VTP at a volume of 100-120 mm^3. On the day of treatment, an aliquot of WST-11 was thawed and filtered through a 0.2 μm disc syringe filter (Thermoscientific) in light protected conditions. 100 μL of the filtered drug sample was used for spectrophotometric analysis. Spectrophotometric analysis was done to determine the presence of protein aggregates caused by potential oxidation of drug whilst in cold storage. The presence of aggregates would render the drug unusable and was determined by the presence of an absorbance peak at 650 nm. Absorbance of the drug at its maximal absorbance peak of 753 nm was also determined to calculate the exact dose of WST-11 prior to treatment using the following equation: $\frac{Absorbance\ (at\ 753nm) x\ 1000\ x\ 916}{Ex100}$, where 916 is the molecular weight of WST-11, 1000 is the dilution factor, and E is 10^5. 5% dextrose was used as the control solution for the 'blank' measurement (figure 2.1). The drug was protected from light at all times, including when being transported to the animal facility. The volume of drug to be infused was determined according to the weight of the mouse (as measured the morning of treatment) and the dose to be used (7 or 9 mg/kg) (**table 2.2**).

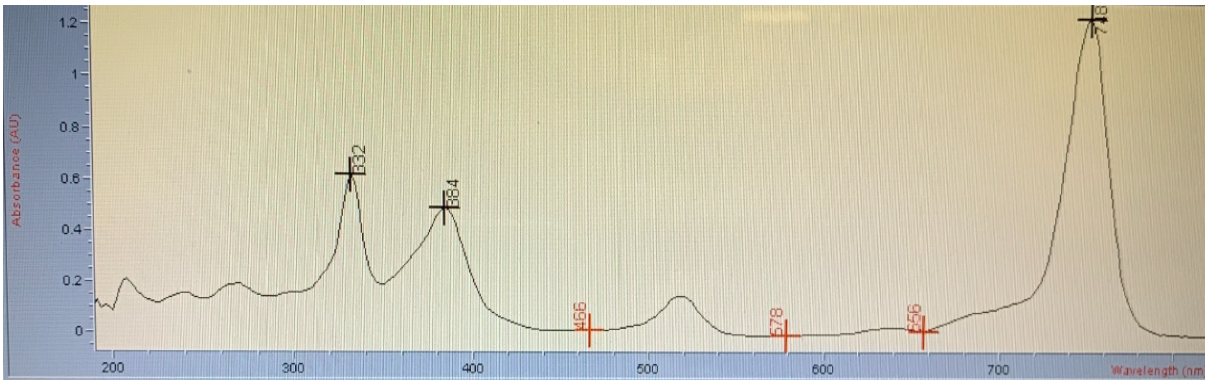


Figure 2.1. Spectrophotometric determination of protein aggregates and WST-11 concentration. Oxidation of WST-11 during prolonged storage would be evident with a peak at 650 nm. This trace shows the absence of a peak at 650 nm suggesting the drug has not been oxidised and can therefore be used. Absorbance of the drug at its maximal absorbance peak of 753 nm was also determined to calculate the exact dose of TOOKAD®-soluble prior to treatment using the following equation: $\frac{Absorbance\ (at\ 753nm) x\ 1000\ x\ 916}{Ex100}$, where 916 is the molecular weight of WST-11, 1000 is the dilution factor, and E is 10^5. 5% dextrose was used as the control solution for the 'blank' measurement.

Date of treatment	Animal ID	Absorbance	Concentration of drug (mg/mL)	mouse weight	Dose of drug	drug dose/mouse	volume of drug (ul)	volume of tubing dead space	total volume of drug (ul)	infusion rate (ul/min)
10/28/2019	1RR	1.2393	0.945999	30.5	7mg/Kg	0.2135	225.6873422	12	237.6873422	47.53746843
	2O	1.2393	0.945999	28.2	9mg/Kg	0.2538	268.28781	12	280.28781	56.05756201
	8R	1.2393	0.945999	25.3	7mg/Kg	0.1764	186.4695417	12	198.4695417	39.69390834
10/31/2019	1RL	1.36	1.038896667	28.1	7mg/Kg	0.1967	189.3354809	12	201.3354809	40.26709617
	8RR	1.36	1.038896667	29	7mg/Kg	0.203	195.3996066	12	207.3996066	41.47992131
	10	1.36	1.038896667	26.4	9mg/Kg	0.2376	228.7041701	12	240.7041701	48.14083401
	7RL	1.36	1.038896667	30.7	9mg/Kg	0.2763	265.9552281	12	277.9552281	55.59104561
11/4/2019	2LL	1.231	0.939663333	28.3	9mg/Kg	0.2547	271.0545266	12	283.0545266	56.61090532
	2L	1.231	0.939663333	27	7mg/Kg	0.189	201.1358678	12	213.1358678	42.62717356
	6RL	1.231	0.939663333	28.3	9mg/Kg	0.2547	271.0545266	12	283.0545266	56.61090532
11/6/2019	1LL	1.1838	0.903634	28.1	9mg/Kg	0.2529	279.8699473	12	291.8699473	58.37398947
	3O	1.1838	0.903634	22.2	7mg/Kg	0.1554	171.9722808	12	183.9722808	36.79445616
11/11/2019	1L	1.15	0.877833333	29.3	7mg/Kg	0.2051	233.6434403	12	245.6434403	49.12868806
	4RR	1.15	0.877833333	28.8	7mg/Kg	0.2016	229.6563509	12	241.6563509	48.33127017
	7RR	1.15	0.877833333	29.3	7mg/Kg	0.2051	233.6434403	12	245.6434403	49.12868806
11/11/2019	2RR	1.2887	0.983707667	27.1	9mg/Kg	0.2439	247.9395132	12	259.9395132	51.98790264
11/13/2019	6O	1.3565	1.035461667	29.8	7mg/Kg	0.2086	201.4560333	12	213.4560333	42.69120666
	6LL	1.3565	1.035461667	30.4	9mg/Kg	0.2736	264.2299651	12	276.2299651	55.24599301
11/15/2019	3LL	1.2506	0.954624667	32.3	9mg/Kg	0.2907	304.517587	12	316.517587	63.3035174
11/22/2019	5RL	1.15008	0.8778944	29.1	9mg/Kg	0.2619	298.3274526	12	310.3274526	62.06549052
12/2/2019	6R	1.3799	1.053323667	29.4	7mg/Kg	0.2058	195.3815399	12	207.3815399	41.47630798
	7R	1.3799	1.053323667	27.9	9mg/Kg	0.2511	238.3882637	12	250.3882637	50.07765274
	7L	1.3799	1.053323667	24.9	7mg/Kg	0.1743	165.4762022	12	177.4762022	35.49524043
	9RL	1.3799	1.053323667	28.3	9mg/Kg	0.2547	241.8060166	12	253.8060166	50.76120331
12/4/2019	9L	1.332	1.01676	27.8	7mg/Kg	0.1946	191.3922656	12	203.3922656	40.67845313
	5RR	1.332	1.01676	24.5	7mg/Kg	0.1715	168.6730399	12	180.6730399	36.13460797

Table 2.2. Total volume of drug and infusion rate used for treatment based on spectrophotometric absorbance of WST-11. After determining the concentration of the drug using the absorbance, which was always around 1 mg/mL as 200 mg of lyophilised WST were diluted in 200 μl of 5% dextran, the volume of drug per mouse was determined based on the weight of the mouse and dose of drug (i.e. 7 or 9 mg/kg). 12 μl of drug was added to the final drug volume to account for dead space in the 15 cm tubing used to deliver the drug in the tail vein with the volume held per cm of tubing being 0.8 μL. The infusion rate per minute was calculated by dividing the drug volume by 5.

2.11.2.2 WST-11 VTP treatment protocol

A bespoke optical excitation system was constructed by collaborators (Boris Vojnovic and Ian Tullis) contained an animal heating pad, inhalational anaesthesia tubing and physiological monitoring apparatus. Animal imaging, illumination and fibre-coupled

excitation and guide beam illumination optics were housed in the enclosure lid. WST-11 VTP excitation was provided by a 755 nm thermoelectrically cooled semiconductor laser diode (LDX Optronix, Missouri, USA, type USA LDX-3210-750), and its output power was controlled by bespoke hardware controlled by a software system and a graphical user interface, which also controlled optical exposure time. A low power (<1 mW) excitation guide beam was provided, generated by a single 590 nm LED (type SMB1N-590-02, Roithner LaserTechnik GmbH, Austria), the output of which was combined with the laser output using a dichromatic reflector (DMLP638R, Thorlabs, UK) prior to launching into the output fibre. A multimode fibre (type M53L02 Ø600µm,0.50 NA, Thorlabs, UK) carried both the guide beam and excitation light to the enclosure where it was homogenised and collimated to a slightly diverging beam diameter of 8 mm nominal, delivering a typical excitation intensity of 120 mW/cm^2. A simple mechanical system and turning prism allowed the excitation and guide beam to be positioned over the area of interest. In addition, the enclosure was fitted with diffuse LEDs operating at 590 nm (Roithner LaserTechnik GmbH, Austria type SMB1N-590-02). The animal in the enclosure could be viewed at all times with the aid of a miniature high dynamic range monochrome camera mounted in the enclosure lid. The wavelength of the guide beam and the illumination (590 nm) was chosen as it was in the nadir of the WST-11 VTP spectral absorption. Similarly, WST-11 injections were performed under yellow light generated by an array of T1¾ 590 nm LEDs (type HLMP-EL3G-VX0DD, Broadcom, USA). Under the same light conditions described above, mice with 120 mm^3 tumours received VTP treatment in the morning under isofluorane inhalational anaesthesia with physiological monitoring. Anaesthetised mice received an intravenous infusion of 7 or 9 mg/kg WST-11 via the tail vein followed immediately by 10 minutes laser excitation of the subcutaneous flank tumour at 100-120 mW/cm^2 using a collimating lens. The optical irradiation light field was arranged to cover the entire subcutaneous flank tumour area plus a 1 mm rim. Mice were returned to the home cage following recovery from anaesthesia and under-went post-procedure health monitoring and tumour measurements using digital callipers.

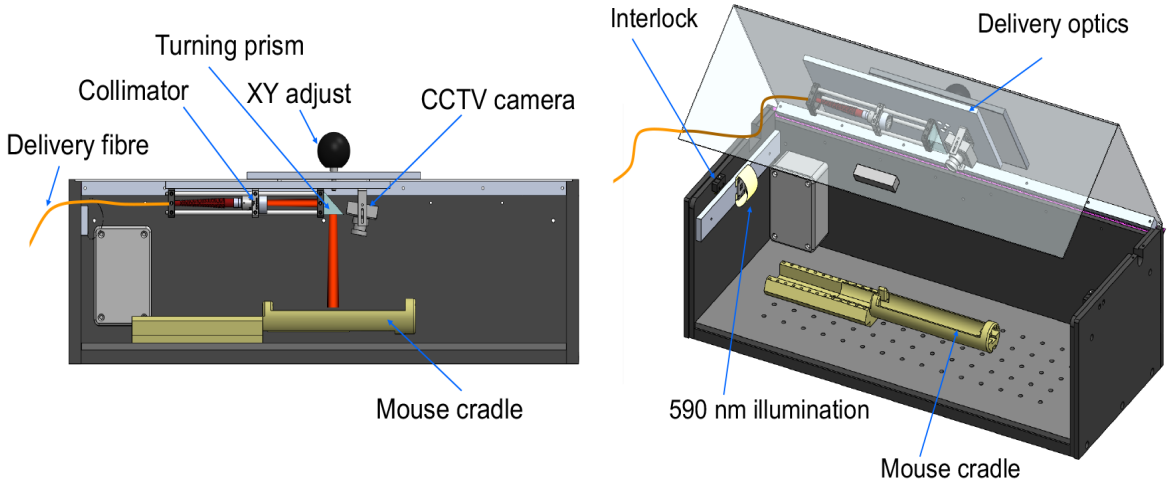


Figure 2.2 SolidWorks model of the VTP optical delivery enclosure. (**A**) Anterior view of VTP optical delivery enclosure. Homogenised excitation light delivery is via a multimode fibre coupled to a collimator delivering a slightly diverging light beam, with spot size adjusted by changing collimator to prism distance. A turning prism directs light onto the tumour surface. A high dynamic range camera allows the beam and mouse to be viewed within a bespoke cradle. Anaesthesia system not shown. (**B**) View of the open enclosure to reveal the animal illumination, laser interlock switch and adjustable cradle. The whole optical delivery system can be moved laterally to ensure correct illumination. The light source (not shown) is a thermoelectrically cooled broad area laser diode (LDX3210-750) driven by an in-house developed regulated current amplifier, with delivery time and energy shown on a graphical user interface.

2.11.3 Multimodal treatment of flank PCa xenograft tumours

2.11.3.1 Radiotherapy combined with anti-PD-L1

3 x 5 Gy RT was delivered in 5 Gy fractions given over three consecutive days as described above. 10mg/kg anti-PD-L1 (BioXCell, clone 10F.9G2) or isotype control (BioXCell, clone 2A) was administered by intra-peritoneal (IP) injection on days 1 (i.e. with first 5 Gy RT fraction), 4, 7 and 10 relative to commencement of RT at 100 mm^3 tumour size.

2.11.3.2 Radiotherapy combined with WST-11 VTP

3 x 5 Gy RT was delivered in 5 Gy fractions given over three consecutive days as described above, with tumours being 100-120 mm^3 at the start of the experiment. On day

7 after the first 5 Gy fraction, mice receiving the combination therapy were treated with WST-11 VTP.

2.12 Effects of fractionated 3 x 5 Gy radiotherapy on the TRAMP-C1 and MyC-CaP tumour vasculature

2.12.1 DCE-MRI of flank xenograft tumours

Inhalational anaesthesia was induced and maintained with isofluorane (1–4% in air) in order to maintain a respiration rate of 40–60 breaths per minute, and the temperature was maintained at 35°C using a homeothermic temperature maintenance system as previously described [Gilchrist et al., 2016; Kersemans et al., 2015; Kleibeuker et al., 2016]. DCE-MRI was performed with 7.0 T scanners (Varian, VNMRS console) using 25 mm inner diameter birdcage coils (Rapid Biomedical, Germany) as previously described [Kleibeuker et al., 2016]. Respiratory-gated 3D gradient-echo scans (echo time=0.6 ms;repetition time=1.15 ms; nominal 5°flip angle) with an isotropic resolution of~420 μm and a respiratory rate-dependent frame acquisition time of~8–10 seconds were obtained [Kleibeuker et al., 2016]. Fifty frames were acquired with a 25 μl bolus infusion of Gadolinium (Gd) solution (Omniscan GE HEALTHCARE) administered using a syringe pump (PHD2000, Harvard Apparatus) over 5 seconds commencing at the beginning of frame 11. Radiofrequency field inhomogeneities were accounted for using a respiratory-gated implementation of the Actual Flip Angle technique, and baseline T1 was measured using a variable flip angle sequence as reported previously [Kleibeuker et al., 2016]. To measure respective tumour hypoxia at the seven day endpoint after RT, mice were injected intraperitoneally with 60 mg/Kg of pimonidazole solution prepared by resuspending the Hydroxyprobe^{TM} (pimonidazole hydrochloride) at a concentration of 30

mg/mL in 0.9% sterile saline. The injected pimonidazole solution was allowed to circulate *in vivo* for 90 minutes before the mice were euthanised.

2.12.2 DCE-MRI processing and analysis

To analyse tumour perfusion, manual segmentation was initially performed from the average image of the DCE sequence using ITK-SNAP medical image segmentation software [Yushkevich et al., 2019]. The MR signal was then converted to Gd concentration, as previously described [Schabel and Parker, 2008]. The initial area under the Gd curve (iAUC) was measured by integrating the first 90 s after injection and used as an indicator of perfusion.

2.13 Euthanasia of laboratory mice and sample collection

Mice were killed by a schedule one procedure at pre-defined humane endpoint in the morning using pentobarbitone injection overdose followed by cervical dislocation according to institutional guidelines. For growth delay experiments the humane endpoint was defined as tumour volume not exceeding 500 mm^3. In the case of bilateral tumour experiments, the human endpoint was defined as maximal combined tumour volume not exceeding 1000 mm^3. Mice were culled by terminal anaesthesia after the repeat DCE-MRI on day seven after the initiation of RT. For immunological analysis of the TIME following treatments, mice were culled at pre-defined endpoints, typically on day four, seven, twelve or when tumours reached 400 mm^3 in volume. Upon sacrifice, blood was collected using a cardiac puncture technique, and incubated with citrate-dextrose solution (SIGMA) and centrifuged at 2000 RPM for 10 minutes to separate the plasma. Plasma was stored at -80°C. The flank tumour was dissected, with half of the tissue being used for FACS analysis of tumour infiltrating immune cells, and half placed in 4% parafolmaldehyde

(SIGMA). For immunohistochemistry of the tumour vasculature following RT, mice were sacrificed with terminal anaesthesia following the second DCE-MRI on day seven after the initiation of RT. The flank tumour was dissected, and embedded in OCT compound (Cellpath^{TM}), snap frozen on dry ice and stored at -80ºC.

2.14 *Ex vivo* flow-cytometry of prostate cancer flank xenograft tumours

TRAMP-C1 tumours were mechanically dissociated using a scalpel into small 2-3 mm pieces and enzymatically digested in a 5 mL digestion cocktail containing 400 µl of 5 g/ml collagenase IV (Worthington), 5 U/mL DNAse I (195 U/µL) (Invitrogen) in Hanks Balanced Salt Solution (Gibco^{TM}) for 30 minutes at 37°C in a bacterial shaker at 180 RPM. The digested tissue was filtered through a 70 µm nylon cell strainer (Falcon) and RBC were removed using 1X RBC lysis buffer (BioLegend). Cell number was determined using an automated cell counter as described above. 1x10^6 cells in 100 µl FACS buffer were transferred to FACS tubes for antibody staining. Cells were incubated for 5 minutes at room temperature with 2 µL purified anti-mouse CD16/CD32 Fc block (BioLegend) before addition of cell surface antibodies at a dilution of 1:100 or 1:200 for 30 minutes at room temperature (**table 2.2**). For intracellular antibody staining, cells were permeabilised using a Foxp3/Transcription Factor Staining Buffer Set (Invitrogen) according to the manufacturer's protocol followed by a 20-minute incubation with intracellular antibodies (**table 2.2**). Appropriate isotype and Fluorescence Minus One (FMO) staining controls were also performed for appropriate gating of different cell populations (**Appendix 9.4 & 9.5**). Cells were washed twice with PBS before analysis. FACS data (total of 50,000-100,000 live events) was acquired using NxT Attune (Thermo Fischer Scientific) and analysed using Flowjo v10 software.

Panel	Antibodies
Tumour infiltrating myeloid cells	PE-Cy7 CD11b (eBioscience – M1/70), PerCP/Cy5.5 CD206 (BioLegend – C068C2), BV510 Gr-1 (BioLegend – RB6-8C5), BV421 F4/80 (BioLegend – BM8), APC Ly6G (BioLegend – 1A8), APC-Cy7 Ly6C, (BioLegend – HK1.4), BV605 CD11c (BioLegend – N418), BV711 I-A/I-E (BioLegend – M5/114.15.2), PE iNOS2 (Invitrogen – CXNFT), LIVE/DEAD™ Fixable Green Dead Cell Stain Kit (ThermoFisher Scientific - L23101)
Tumour infiltrating lymphoid cells	PE CD45 (invitrogen – 30-F11), APC-Cy7 CD3 (BioLegend – 17A2), APC CD4 (BioLegend – RM4-5), PECy7 CD8 (BioLegend – 53-6.7), PerCP/Cy5.5 NK1.1 (BioLegend - PK136), LIVE/DEAD™ Fixable Green Dead Cell Stain Kit (ThermoFisher Scientific - L23101)
$CD8^+/CD4^+$ T-cell PD1	PE CD45 (Invitrogen – 30-F11), CD8a BioLegend – 53-6.7), APC CD4 (BioLegend – RM4-5), BV421 PD1 (BioLegend – 29F.1A12), LIVE/DEAD™ Fixable Green Dead Cell Stain Kit (ThermoFisher Scientific - L23101)
$CD4^+$ regulatory T-cells	APC-Cy7 CD45 (BioLegend – 30-F11), APC CD4 (BioLegend – RM4-5), BV421 CD25 (BioLegend 29F.1A12), PE Anti-Mo FoxP3 (invitrogen – NRRF–30), LIVE/DEAD™ Fixable Green Dead Cell Stain Kit (ThermoFisher Scientific - L23101)

Table 2.2 Antibodies and markers used in flow cytometry to discriminate different immune cell subtypes

2.15 Immune gene expression analysis of prostate cancer flank xenograft tumours

The NanoString platform and the nCounter PanCancer Immune Profiling Panel (NanoString Technologies, Inc., Seattle, Washington, USA) was used to analyse gene expression profiles of PCa xenograft tumours following treatment. The nCounter gene expression assay (Nanostring Technologies, Seattle, WA) was performed as previously described [Geiss et al., 2008; Kulkarni, 2011]. RNA was isolated and purified from x2-4 10 mm thick formalin-fixed paraffin-embedded (FFPE) tissue samples using the RNeasy FFPE Kit (Qiagen) according to the manufacturer's specifications. RNA was eluted from columns in DEPC treated water and assessed for concentration and purity using the NanoDrop 2000 instrument (Thermo Fisher Scientific). All RNA samples used in the study exhibited optical density $(OD)_{260/280}$ ratios of 1.7-2.3 and $OD_{260/230}$ of 1.8-2.3 as per the manufacturer's recommendation. Gene expression code sets (designed and produced by NanoString Technologies, Seattle, WA), hybridisation buffer and 50 ng total RNA per

sample were hybridized in a T100^{TM} thermal cycler (Bio-Rad) for 18 hours at 65ºC (total sample volume = 13 μl) followed by scanning and data collection using the nCounter SPRINT Profiler (NanoString Technologies, Inc., Seattle, Washington, USA). Downstream normalisation using control 'house-keeping genes' and gene quantification was performed using the nSolver analysis software 4.0 (Nanostring Technologies).

2.16 Immunofluorescence of tissue sections

Freshly excised TRAMP-C1 tumours were placed into a cryomold filled with optimal cutting temperature compound and quickly frozen in a cold bath containing isopropanol and dry ice. In total, four 10 μm frozen tissue sections were cut and placed onto superfrost microscope slides (FisherBrand), and fixed with 4% dilution electron microscopy grade paraformaldehyde (Electron Micro-scopy Sciences) in PBS for 30 minutes at room temperature in a Coplin jar. Tissue section slides were then washed with PBS in a Coplin jar prior to a combined blocking and permeabilisation step using 3%BSA in 0.3% triton/PBS for 90 minutes at room temperature. Tissue sections were then encircled with a hydrophobic PAP marking pen, and 200 μl of primary antibody (1:200 anti-αSMA antibody,eBioscience, clone 1A4, efluor 570; 1:200 anti-CD31 antibody,Biolegend, clone MEC13.3, Alexa Fluor 488) diluted in blocking solution was added for incubation in a humidified chamber at 4°C overnight, with this and all subsequent steps under light protection. After removal of primary antibody, a 300 nM DAPI nuclear counterstain in PBS was applied for 30 minutes incubation prior to washes in PBS, and mounting with coverslips sealed with Wirosil dental silicone. αSMA and CD31 sample images were acquired with a Plan Apo 20 × 0.75 NA objective on a Nikon Ti Widefield Microscope equipped with a Lumencor SpectraX LED light source and an Andor Neo Zyla Camera.

2.17 Digital analysis of tumour vessels

Tumour CD31-positive blood vessel quantification was performed with classical image processing methods. Following image pre-processing, image segmentation was performed to identify tissue areas and CD31-positive blood vessels in an automated fashion. The vessel segmentation was analysed using the Euclidian distance transformation to obtain the local thickness of all segmented objects in the images. The combined binary masks indicating the presence of tissue and CD31-positive blood vessel masks were used to compute the vessel density and the distance from any tissue pixel to the closest vessel.

2.18 Digital annotation and quantification of tumour vessels and αSMA-positive pericytes

α-SMA is often used to identify pericytes [Skalli et al., 1989] as these are relatively poorly defined heterogeneous perivascular cell types, without highly specific markers available for their identification [Yamazaki and Mukouyama, 2018]. Computer-assisted image annotation was used to identify αSMA-positive pericytes by overlapping the image channels corresponding to αSMA (red) and CD31 (green), and selecting αSMA-positive cells adjacent to, or overlapping, CD31-positive blood vessels. To assist annotation, αSMA-positive cells with a distance of more than 10 pixels, or 3.2 μm, from CD31-positive blood vessels were suppressed. Annotation was performed using the Annotation of Image Data by Assignments (AIDA) web application platform (https://github.com/alanaberdeen/AIDA) developed in-house for the annotation of large microscopy images. Relevant regions of interest in the tumour were selected, and the annotators then marked αSMA-positive cells and CD31-positive blood vessels in these

regions. Areas in the αSMA channel selected by at least three of four independent observers were accepted as αSMA-positive pericytes. In order to investigate the extent of αSMA-positive pericyte coverage of CD31-positive blood vessels, the fraction of blood vessels in each region with a spatially adjacent αSMA-positive cell was computed. Control untreated samples were compared against fractionated RT treated samples

2.19 Statistical analysis

Statistical analysis was performed using GraphPad Prism 8 (GraphPad Software, USA). For *in vitro* experiments the one-way or two-way ANOVA test, with Dunnett's or Tukey's *post hoc* adjustment for multiple comparisons, was performed. For *in vivo* tumour growth delay experiments, one-way ANOVA was performed using Tukey's test for multiple comparisons following Brown-Forsythe's test for equality of the means. Tumour growth delay was defined as an increase in days for a tumour treated at 100-120 mm^3 to reach end-point size of 400 mm^3 compared against control untreated tumours, a single mouse being considered an experimental unit. Power calculations for *in vivo* experiments investigating tumour growth delay following combined RT with anti-PD-L1 or WST-11 VTP assumed that if RT-treated tumours take 28 days to grow from treatment at 100-120 mm^3 to 500 mm^3, to observe that combined treatment takes 42 days to grow between these sizes requires n=6 mice per group to show this difference (80% power, 5% type 1 error rate). T-tests were performed for FACS data. All results are mean +/- standard error of the mean, $p<0.05$ being statistically significant.

Chapter 3. Characterising the immunogencity and radiosensitivity of murine prostate cancer cell lines *in vitro*

3.1 Introduction

The development of mouse models which recapitulate human PCa has been limited due to several factors including the absence of models of metastatic disease, presence of atypical histologic features (e.g. neuroendocrine or sarcomatoid phenotypes), lack of models with the genomic instability seen in human PCa, or use of driver genes rarely altered genetically in human PCa [Ittmann et al., 2013]. Despite these limitations, mouse models of PCa have proved valuable in understanding the biology of PCa initiation and progression, and for testing new treatment modalities. Syngeneic PCa mouse models, also known as 'allograft mouse tumour models', are critical for testing novel therapies in the presence of a functional immune system, prior to 'first in man' early phase clinical trials. This is particularly relevant in studies assessing multi-modality therapy in PCa, and the effects of such treatment strategies on the TIME.

Unlike dogs and a few strains of rat, normal wild-type mice do not develop spontaneous PCa [Senapati et al., 2012]. However, genetically engineered mouse models (GEMs) have been generated that develop PCa [Mimeault and Batra, 2011]. Due to the spontaneous (i.e. without the effects of a carcinogen) and autochthonous (i.e. within the prostate gland) development of PCa in the presence of an intact immune system, these models mimic the natural progression of human PCa in many ways, and have been instrumental in increasing the understanding of the genetic basis of PCa initiation and progression. Furthermore, cell lines established from these models have been used in

xenograft models in PCa therapeutic studies. Examples of the most investigated murine PCa cell lines used in many studies are the TRAMP-C1/C2/C3 and MyC-CaP cell lines. TRAMP-C1/C2/C3 were established from 32 week old heterogeneous prostate tumours obtained from the TRAMP model in C57BL/6 mice harbouring a construct comprising the minimal rat probasin promoter driving prostate-specific epithelial expression of SV40 large T antigen [Foster *et al.*, 1997]. Interestingly, these cells lines do not express the SV40 antigen but instead are positive for cytokeratin, E-cadherin and the AR (Foster *et al.*, 1997). TRAMP-C1 and TRAMP-C2 cells are tumourigenic when injected subcutaneously in syngeneic C57BL/6 mice. The MyC-CaP cell line was established from a 16-month-old Hi-Myc transgenic mouse [Watson et al., 2005]. MyC-CaP cells express the *c-Myc* proto-oncogene, which is overexpressed in many human PCa cases, and its activation is thought to occur in the early stages of PCa progression [Koh et al., 2010]. MyC-CaP cells have been demonstrated to express *c-Myc* at an equivalent level to that seen in human PCa tumours, and overexpress the AR, due to genomic AR amplification as detected by Fluorescence In situ Hybridisation analysis [Watson et al., 2005]. MyC-CaP cells are tumourigenic when injected subcutaneously in syngeneic male FVB mice in the presence of androgens. Surgical or medical castration results in initial regression of established MyC-CaP tumours, but these tumours eventually recur in an androgen-independent manner, therefore this cell line is especially useful in understanding the development of castration-resistant PCa.

In this chapter the *in vitro* radiosensitivity and immunogenicity of TRAMP-C1 and MyC-CaP murine PCa cell lines was characterised. This work was necessary to inform subsequent *in vivo* experiments testing multi-modality therapy for PCa using RT, VTP and immunotherapy in the form of ICB as it allowed determination of the inherent radiosensitivity of these cell lines to IR, in order to guide selection of RT treatment fractions for *in vivo* experiments. Characterisation of cancer cell immunogencity, which is a fundamental determinant of the ICB response, would help determine which cell line may

be most suitable for multimodality therapy incorporating ICB. Theoretically, tumours of low/no immunogenicity may not respond to therapeutic strategies designed to enhance the immune response. Determinants of cancer cell immunogenicity include multiple factors related to the tumour cell itself, such as the expression of neoantigens and antigen processing capability, and factors related to the tumour microenvironment, such as the functioning of professional APCs such as DCs [Blankenstein et al., 2012]. *In vitro* cancer cell immunogenicity can be measured in several ways, including cell surface expression of MHCI and PD-L1 [Grenga et al., 2014]. Reduced neoantigen presentation due to downregulation of MHCI is a recognised mechanism whereby cancer cells escape immunosurveillance, thus contributing to failure of ICB therapy [Zaretsky et al., 2016]. In addition, upregulation of tumour cell membrane-bound expression of PD-L1, in response to γIFN produced by cytotoxic T-cells recruited to the tumour microenvironment, is another well-characterised immune escape mechanism. Based on these observations, an additional aim of Chapter 3 was to analyse the expression of MHCI and PD-L1 in TRAMP-C1 and MyC-CaP cells in response to IFNγ and IR, to determine which cell line may be most appropriate for multimodality therapy incorporating RT and immunotherapy (iRT) in the form of treatment with an anti-PD-L1 antibody.

3.2 Results

3.2.1 Investigating the *in vitro* response of TRAMP-C1 and MyC-CaP cells to ionising radiation

To assess the *in vitro* radiosensitivity of TRAMP-C1 and MyC-CaP cell lines to IR, these cells were exposed to a single IR dose of 0, 2, 4, 6, 8 and 10 Gy, and their survival curves were determined using colony-forming assays. As expected, an increasing dose of IR was

associated with increased cell death in both cell lines, with both cell lines showing a similar radiosensitivity profile (**figure 3.1A**). This is demonstrated by the initial slope of the cell survival curve (alpha or α), which represents the intrinsic radiosensitivity of the cell and was calculated using the Linear-Quadratic formula as 0.351±0.041 for TRAMP-C1 and 0.358±0.066 for MyC-CaP cells (**figure 3.1A**). The alpha/beta ratio was calculated as 26.2 and 19.7 for the TRAMP-C1 and MyC-CaP cell line respectively.

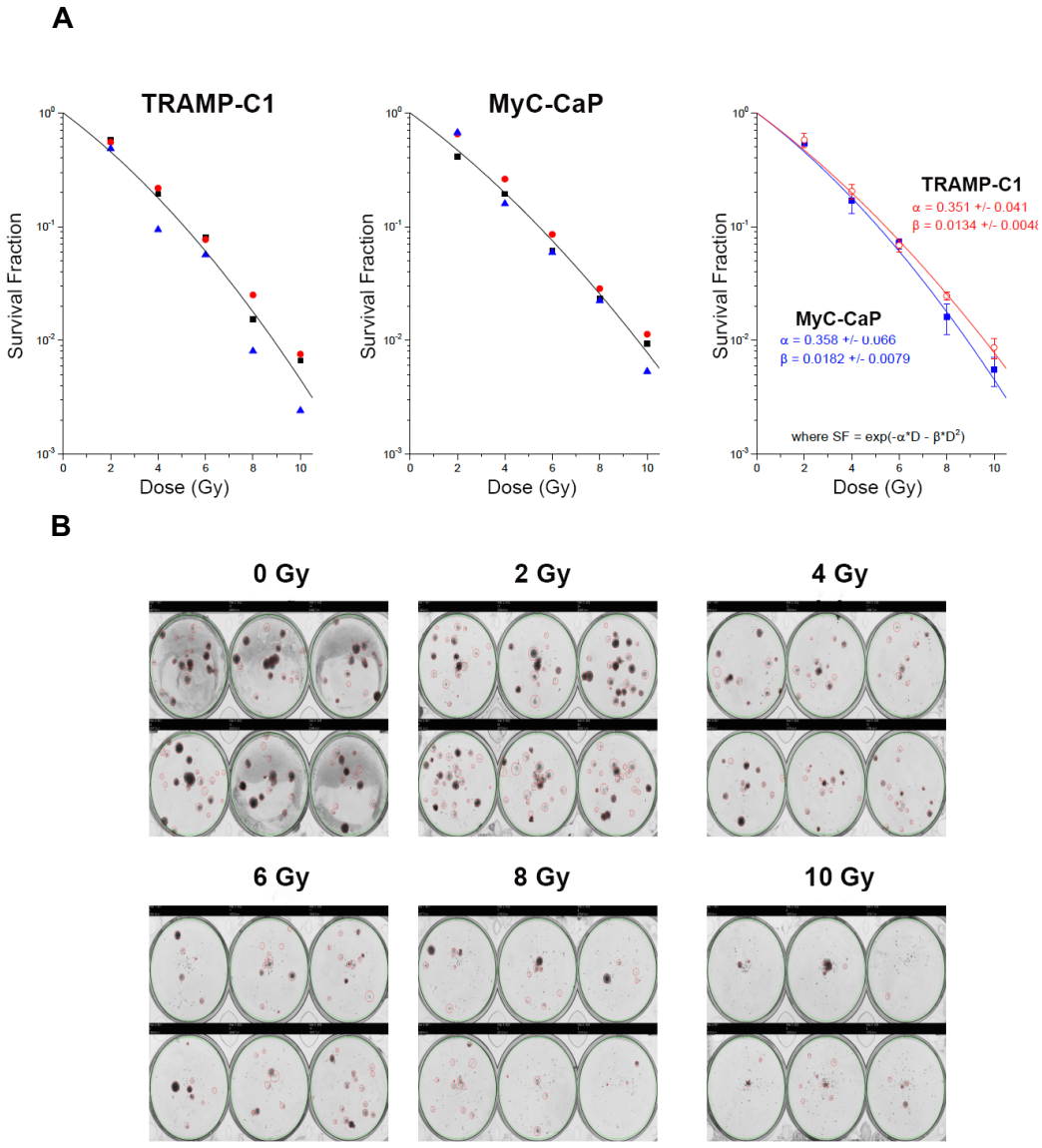


Figure 3.1. Radiosensitivity of TRAMP-C1 and MyC-CaP cells as determined using clonogenic assays. (A) Cells were irradiated with 0, 2, 4, 6, 8 and 10 Gy IR, and the survival was determined by the counting of surviving colonies, with data noramalised to plating efficiency. TRAMP-C1 and MyC-CaP cells were observed to have similar intrinsic radiosensitivity to IR. **(B)** Representative image of TRAMP-C1 colony formation at different doses of IR stained with crystal violet (n = 3 independent experiments).

3.2.2 MHC Class I and PD-L1 expression in TRAMP-C1 cells is induced by γIFN treatment

In order to select PCa cells for iRT experiments in a syngeneic immunocompetent *in vivo* model, TRAMP-C1 and MyC-CaP cells were treated with γIFN, and effects on tumour cell surface expression of MHCI and PD-L1 were analysed with FACS. *In vitro* treatment of TRAMP-C1 with γIFN increased MHCI expression in a dose-dependent manner at 72 hours. This effect was not observed in MyC-CaP cells, where baseline MHCI expression remained low despite treatment with increasing γIFN doses (**figure 3.2A & B**). Increased PD-L1 expression was observed in TRAMP-C1 and MyC-CaP 72 hours following treatment with 10 ng/mL γIFN, with PD-L1 upregulation following γIFN being greater in TRAMP-C1 versus MyC-CaP (**figure 3.2C & D**). PD-L1 expression in TRAMP-C1 following 1 ng/mL γIFN peaked at 48 hours and returned to baseline 120 hours post-treatment (**figure 3.4A**).

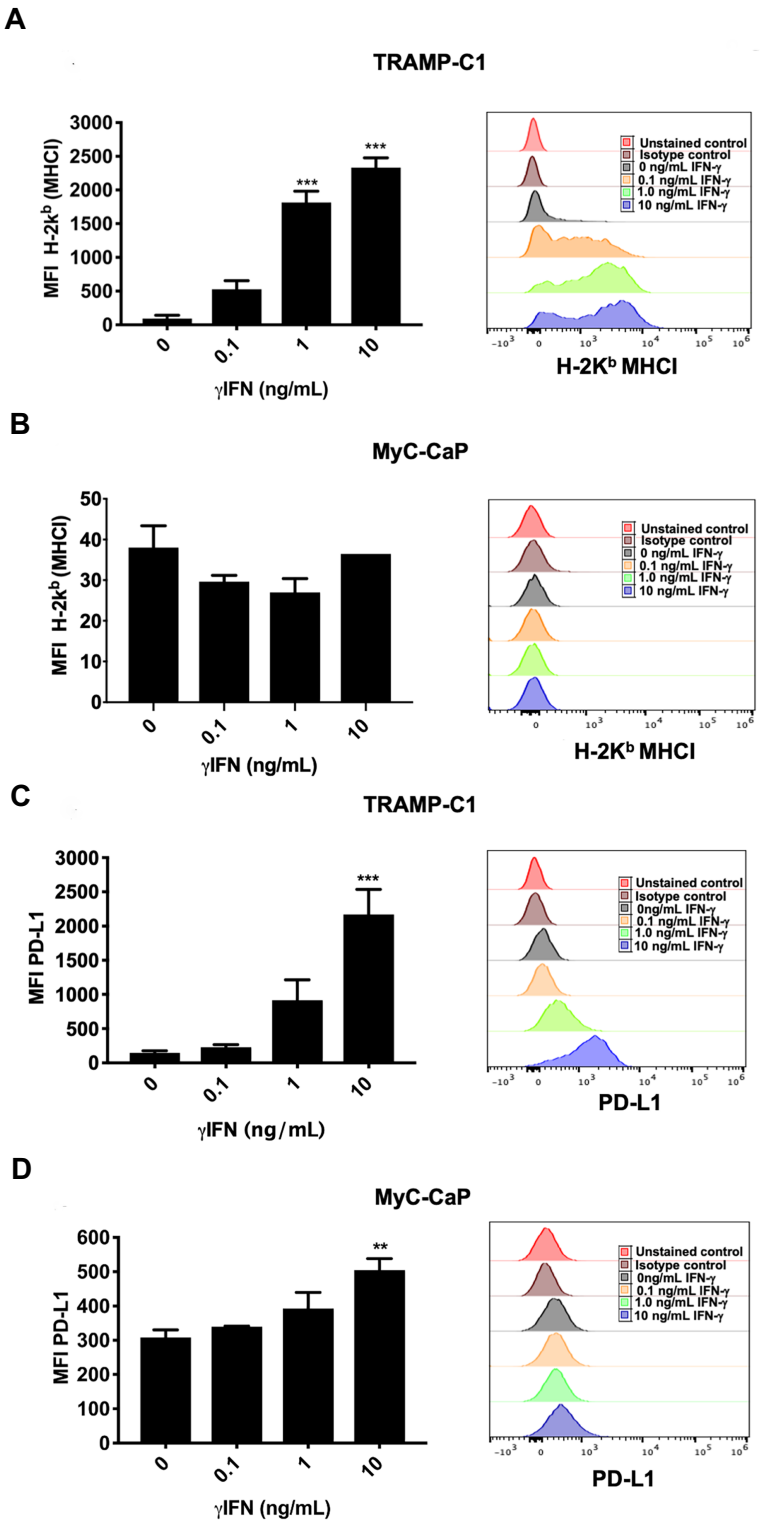


Figure 3.2. FACS analysis of MHC Class I and PD-L1 expression following *in vitro* treatment of TRAMP-C1 and MyC-CaP cells with γIFN. Increased expression of MHCI was observed in FACS analysis of **(A)** TRAMP-C1 following 1 ng/mL and 10 ng/mL γIFN, but not in **(B)** MyC-CaP cells at 72 hours. Increased expression of PD-L1 following *in vitro* treatment with 10 ng/mL γIFN was seen in both cell lines at 72 hours, with PD-L1 upregulation in response to γIFN being greater in **(C)** TRAMP-C1 than in **(D)** MyC-CaP cells. Data are presented as mean fluorescent intensity (MFI) ± SEM, and analysed using ordinary one-way ANOVA with Dunnett's *post hoc* adjustment for multiple comparisons (n = 3 independent experiments). $^{**}p < 0.01$; $^{***}p < 0.001$.

3.2.3 MHC Class I and PD-L1 expression in TRAMP-C1 cells is induced by radiotherapy

To assess the suitability of TRAMP-C1 cells for iRT experiments combining anti-PD-L1 and RT, MHCI and PD-L1 expression were investigated *in vitro* following RT. MHCI expression was increased in TRAMP-C1 at 72 hours following 6 Gy RT in the presence of 1 ng/mL γIFN, whereas expression of the control transferrin receptor protein remained unchanged (**figure 3.3A**). A non-significant increase in MHCI expression was seen following 6 Gy in the absence of γIFN (**figure 3.3B**). PD-L1 expression was increased 72 hours following 6 Gy and 10 Gy in the presence or absence of γIFN (**figure 3.2C & D**). Maximal increased PD-L1 expression in TRAMP-C1 post-6 Gy was observed at 24 hours **(figure 3.4B**).

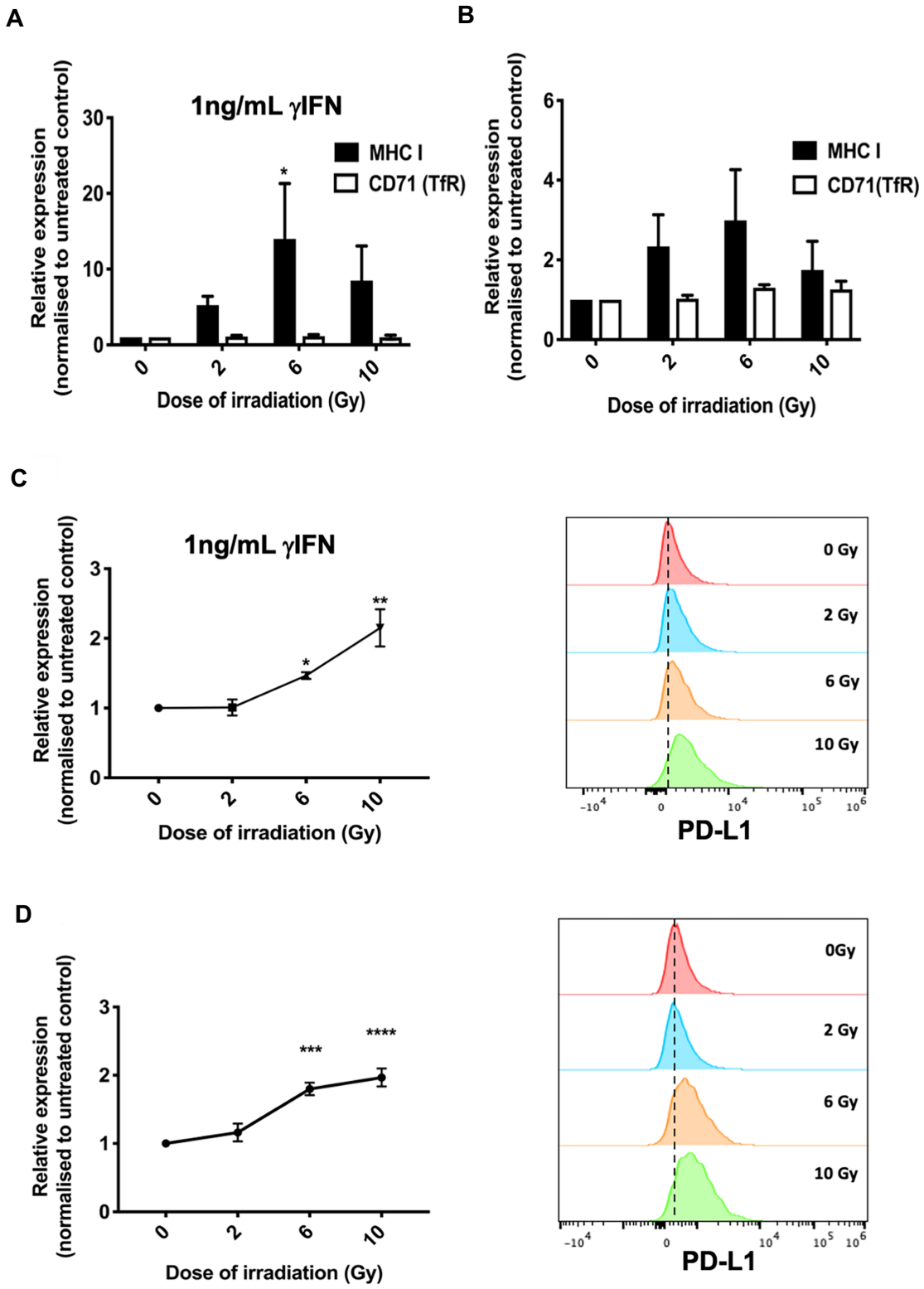


Figure 3.3. Irradiation increases prostate cancer cell surface expression of MHC Class I and PD-L1. *In vitro* FACS analysis of MHCI and control transferrin receptor expression following treatment of TRAMP-C1 cells with 6 Gy RT in the **(A)** presence or **(B)** absence of 1 ng/mL γIFN. FACS analysis of PD-L1 expression following RT in the (**C**) presence or **(D)** absence of concomitant γIFN treatment. Data are presented as relative expression normalised to untreated control and analysed using ordinary two-way ANOVA with Tukey's *post hoc* adjustment for multiple comparisons (n = 3 independent experiments). *** $p < 0.001$, ****$p < 0.0001$.

Increased PD-L1 expression at 72 hours following treatment of TRAMP-C1 with 6 Gy RT with or without 1 ng/mL γIFN was confirmed on WB analysis, validating previous FACS findings (**figure 3.3C**).

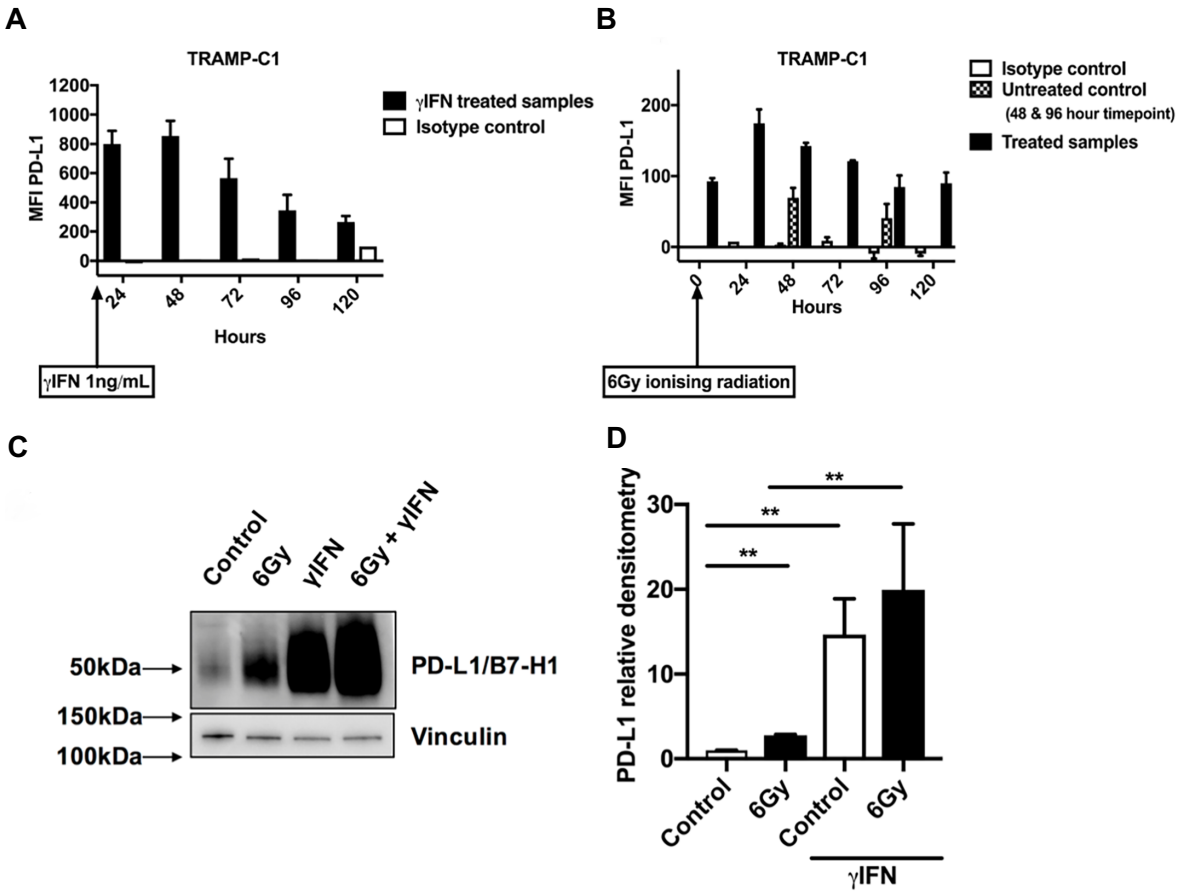


Figure 3.4 Temporal pattern of PD-L1 expression in TRAMP-C1 cells following γIFN and 6 Gy ionising radiation. PD-L1 expression was observed to be maximal at 48 hours following treatment with **(A)** γIFN and (**B**) 6 Gy. (**C** & **D**) Western blot analysis confirmed the increased PD-L1 expression observed using FACS analysis following γIFN and 6Gy IR *$p < 0.05$; **$p < 0.01$. *Experiment 3.4 C & D performed in collaboration with Su Phyu, post-doctoral fellow in Eileen Parke's lab.*

3.3 Discussion

Pre-clinical studies demonstrate that tumour cell MHCI expression is a surrogate marker of intrinsic cancer cell immunogenicity, and is positively associated with the presence of increased numbers of cytotoxic T-cells in the TIME, and an increased response of tumour models to immunotherapy, along with an inverse relationship to tumour growth rate [Lechner et al., 2013; Yu et al., 2018]. In this chapter the baseline *in vitro* cell surface expression of MHCI and PD-L1 in TRAMP-C1 and MyC-CaP cells was investigated, along with the response to γIFN, as a measure of *de novo* cancer cell immunogenicity. Baseline levels of MHCI were observed to be higher in TRAMP-C1 compared to MyC-CaP cells, and MHCI expression increased in a dose dependent manner in TRAMP-C1 but not MyC-CaP cells following γIFN. Similarly, treatment with γIFN resulted in increased PD-L1 expression in TRAMP-C1 cells at 72 hours. Although this effect was also observed in the MyC-CaP cell line, the level of increased PD-L1 expression was lower than in TRAMP-C1 cells. Taken together these results suggest that TRAMP-C1 cells have a greater potential to induce anti-tumour immunogenicity than MyC-CaP cells, given the higher MHCI and PD-L1 expression at baseline and following γIFN.

RT in combination with ADT is a SOC treatment option for localised and locally advanced PCa, and it has recently been investigated in clinical trials treating the primary tumour in low-burden oligometastatic disease [Parker et al., 2018]. RT may cause immune-mediated anti-tumour responses [Grassberger et al., 2019] through increased tumour peptide availability, tumour cell expression of MHCI, enhanced neoantigen generation and presentation, and sensitisation to tumour specific cytotoxic lymphocytes [Gaipl et al., 2014; Reits et al., 2006; Rudqvist et al., 2018; Vanpouille-Box et al., 2015; Wan et al., 2012], and type I and type II IFN production [Ganss et al., 2002; Lugade et al., 2005]. These effects sensitise irradiated tissues to tumour-specific cytotoxic lymphocytes,

inducing immunological anti-tumour responses. Increased cell surface MHCI expression following RT may be due to direct effects on the pool of poly-ubiquitinated proteins targeted for proteosomal degradation, resulting in more peptides for MHCI antigen presentation, and enhanced MHCI expression [Neefjes et al., 1993]. The observation that RT increased MHCI expression in TRAMP-C1 cells *in vitro* in a dose dependent manner in both the presence and absence of γIFN is consistent with previous reports in the literature [Garnett et al., 2004; Reits et al., 2006; Santin et al., 1997]. The effects of γIFN and RT on TRAMP-C1 surface expression of PD-L1 were demonstrated using FACS and validated with WB analysis. These observations suggest that TRAMP-C1 is relatively immunogenic, and may be a suitable pre-clinical model to investigate iRT.

The radiation response of TRAMP-C1 and MyC-CaP cells *in vitro* was evaluated using clonogenic assays, ahead of an *in vivo* assessment of radiation response as determined by tumour-growth delay experiments following RT. TRAMP-C1 and MyC-CaP cell survival curves generated from these experiments demonstrated that MyC-CaP cells had a non-significant trend towards increased radiosensitivity, and this was more evident at higher doses of IR. This is also represented by the lower alpha/beta ratio exhibited by MyC-CaP compared to TRAMP-C1 cells. The Linear Quadratic Model, with its alpha/beta value, describes the curvature of cell killing for tumour control and normal tissue complication in relationship to RT dose. The higher the alpha/beta ratio, the more linear the cell survival curve, whereas the cell survival curve will appear more curved with lower alpha/beta ratios. The alpha/beta ratio was calculated as 26.2 and 19.7 for TRAMP-C1 and MyC-CaP cells respectively. The lower alpha/beta ratio exhibited by MyC-CaP cell line is evident by the greater curvature of the cell survival curve.

The alpha/beta ratio of these murine PCa cell lines is significantly higher than reported for the commonly used human PCa cell lines such as LNCaP, DU-145 and PC-3, where the alpha/beta ratios in several studies have been estimated to be about 3-4 Gy [Carlson et

al., 2004]. These reported alpha/beta ratios for human PCa cell lines are higher than the alpha/beta ratio of human PCa tumours, which is reported to be around 1.4 Gy [Miralbell et al., 2012b]. This suggests that even though the radiation sensitivity parameters (alpha and beta) can be measured *in vitro,* artificial cell line cultures may not always be representative of clinical radiobiological calculations. The alpha/beta ratios for the TRAMP-C1 and MyC-CaP cells used in this study were observed to be higher than those quoted in the literature for human PCa cell lines, perhaps because of the higher proliferation rate of murine PCa cells compared to human PCa cells. Tissues with rapidly proliferating cells have a high alpha/beta ratio, and will respond better to high radiation dose fractions, compared to tissues with more slowly proliferating cells, which have lower alpha/beta ratios and therefore respond better to low radiation dose fractions [Hegemann et al., 2014]. The doubling time of TRAMP-C1 and MyC-CaP cells is 25 and 18 hours respectively, which is considerably faster than more slowly proliferating human PCa cell lines such as LNCaP (34 hours) or VCaP (54 hours) (https://www.lgcstandards-atcc.org/en.aspx, 16/12/2020). These observations highlight a limitation of this study, whereby the radiobiological characteristics of the murine PCa cells are not characteristic of human PCa cell lines or human PCa. The information gained from the clonogenic assays also informs regarding which RT schedule should be used for *in vivo* experiments. In the context of multi-modality therapy, a sublethal dose of RT should be selected in order to investigate additive or synergistic effects of adding ICB and/or a focal ablation treatment (such as VTP) to the RT treatment regime. The survival curves suggest that fraction sizes of 5-8 Gy will likely have a sublethal effect on the *in vivo* tumour response to RT.

In summary, these *in vitro* experiments demonstrate that TRAMP-C1 cells are likely to be more immunogenic that MyC-CaP cells, and therefore TRAMP-C1 cells were taken forwards for *in vivo* experiments.

Chapter 4. Impacts of radiotherapy, alone or in combination with immune check point blockade, on the *in vivo* tumour immune microenvironment in murine prostate cancer models

4.1 Introduction

RT combined with ADT is a SOC therapy for high-risk localised and locally advanced PCa [Mottet et al., 2017; Payne and Mason, 2011]. Technological advances in RT delivery have improved treatment efficacy, however patients with high-risk PCa have a 32–70% 5-year biochemical recurrence rate [Cooper and Sanfilippo, 2015], and RT can reduce the quality of life of long-term survivors due to the side effects of treatment such as haematuria from radiation cystitis, proctitis, and erectile dysfunction [Gaither et al., 2017; Lardas et al., 2017b; Matta et al., 2019a]. Improved RT efficacy in terms of increased cure rates, and reduced treatment toxicity through the use of reduced RT doses, might be achieved by combining immunomodulation with RT. RT to the primary tumour in the context of low-burden metastatic PCa may also provide benefit [Parker et al., 2018] through RT-induced anti-tumour immune responses (the so-called 'abscopal effect'), which may be enhanced through the use of an iRT approach. Whilst iRT may improve tumour control, pre-clinical studies in PCa models investigating RT combined with adjuncts frequently describe the use of doses considerably higher than those used in clinical practice, such as 10, 20, or 25 Gy fractions [Chen et al., 2009; Dudzinski et al., 2019b; Harris et al., 2008; Kachikwu et al., 2011; Oh et al., 2004; Tsai et al., 2006, 2007b]. Standard clinical RT has typically delivered 2 Gy fractions over 6 weeks to a dose of 74–78 Gy. More recently, alternative RT schedules use moderate hypofractionation with 62 Gy in 20 fractions over 4 weeks, and ultrahypofractionation with 36.25 Gy in 5

fractions over 1–2 weeks, and these schedules have been demonstrated to result in effective PCa tumour control without an appreciable increase in acute toxicity [Brand et al., 2019]. Although these studies suggest the potential for a change in clinical practice, with an increased dose per fraction, and reduced overall numbers of fractions, these doses per fraction are lower than those used in most published pre-clinical iRT PCa experiments.

Anti-tumour RT effects include the generation of DNA breaks which result in apoptosis [Liauw et al., 2013], immunological effects [Demaria et al., 2004; Postow et al., 2012; Sharabi et al., 2015a], and anti-tumour immune responses [Apetoh et al., 2007; Deng et al., 2014; Reits et al., 2006]. Despite the observation of pro-inflammatory tumour effects following RT, the immunosuppressive TIME of pre-clinical models includes abundant TAMs and MDSCs. These myeloid-derived cells may impede RT-induced anti-tumour responses, and may promote tumour progression through growth factors, cytokines, chemokines and ROS, increasing the survival and growth of cancer cells [Azad et al., 2017; Jones et al., 2018; Kalbasi et al., 2017]. Although RT is a potential immunostimulatory anti-PCa therapy, with opportunities for combination with immunotherapy as an iRT approach, it may be difficult to harness immune-mediated anti-tumour responses in PCa due to the moderate mutational burden of this malignancy [Alexandrov et al., 2013; Lawrence et al., 2013; Vitkin et al., 2019]. Indeed, this may be one potential reason for the disappointing immunotherapy clinical trial results observed to date in studies of this malignancy. However, the first FDA-approved immunotherapy, albeit without concomitant RT, for a solid-organ cancer was Sipuleucel-T in PCa [Handy and Antonarakis, 2018; Kantoff et al., 2010], and immunomodulation may be effective if appropriately combined with RT. Moreover, the recent KEYNOTE-199 study demonstrates that anti-PD1 may induce a favourable response in treatment-refractory metastatic castration-resistant PCa [Philippou et al., 2020a]. A clinical study combining anti-CTLA4 with an 8 Gy fraction to PCa bony metastases demonstrated a non-significant

improvement in overall survival [Kwon et al., 2014; Slovin et al., 2013], and a trial investigating the efficacy of anti-PD-1 and RT in high-risk and oligometastatic PCa is underway (NCT03543189). In this chapter, the hypothesis was tested that RT fractions used in the clinic may induce PCa TIME effects. Flank tumour allografts in immunocompetent mice were treated with RT, and effects of RT were investigated using tumour growth delay, FACS and nanoString immune gene expression changes. Following these experiments, the effects of iRT with concomitant anti-PD-L1 were investigated in order to test the hypothesis that iRT increases anti-tumour effects.

4.2 Results

4.2.1 Hypofractionated radiotherapy induces tumour growth delay in TRAMP-C1 and MyC-CaP flank prostate cancer allografts

Flank TRAMP-C1 and MyC-CaP 100 mm^3 tumour allografts were treated with daily 2 Gy, 5 Gy and 10 Gy RT fractions. The various RT doses and schedules consisted of a single 5 Gy fraction, 3 x 5 Gy, 5 x 2 Gy, 5 x 5 Gy and 3 x 10 Gy, given over consecutive days (**figure 4.1A**). Treatment of TRAMP-C1 with 3 x 5 Gy and 5 x 5 Gy resulted in significant tumour growth delay compared with untreated control tumours, however all tumours eventually recurred (**figure 4.1B**). TRAMP-C1 tumour growth was well controlled with 3 x 10 Gy, however, this caused skin toxicity in most mice compared with lower doses. No significant tumour growth delay was seen with 5 x 2 Gy. Similarly to TRAMP-C1, treatment of MyC-CaP tumours with 3 x 5 Gy caused significant tumour growth delay compared with untreated control tumours, however all tumours eventually recurred (**figure 4.1C**).

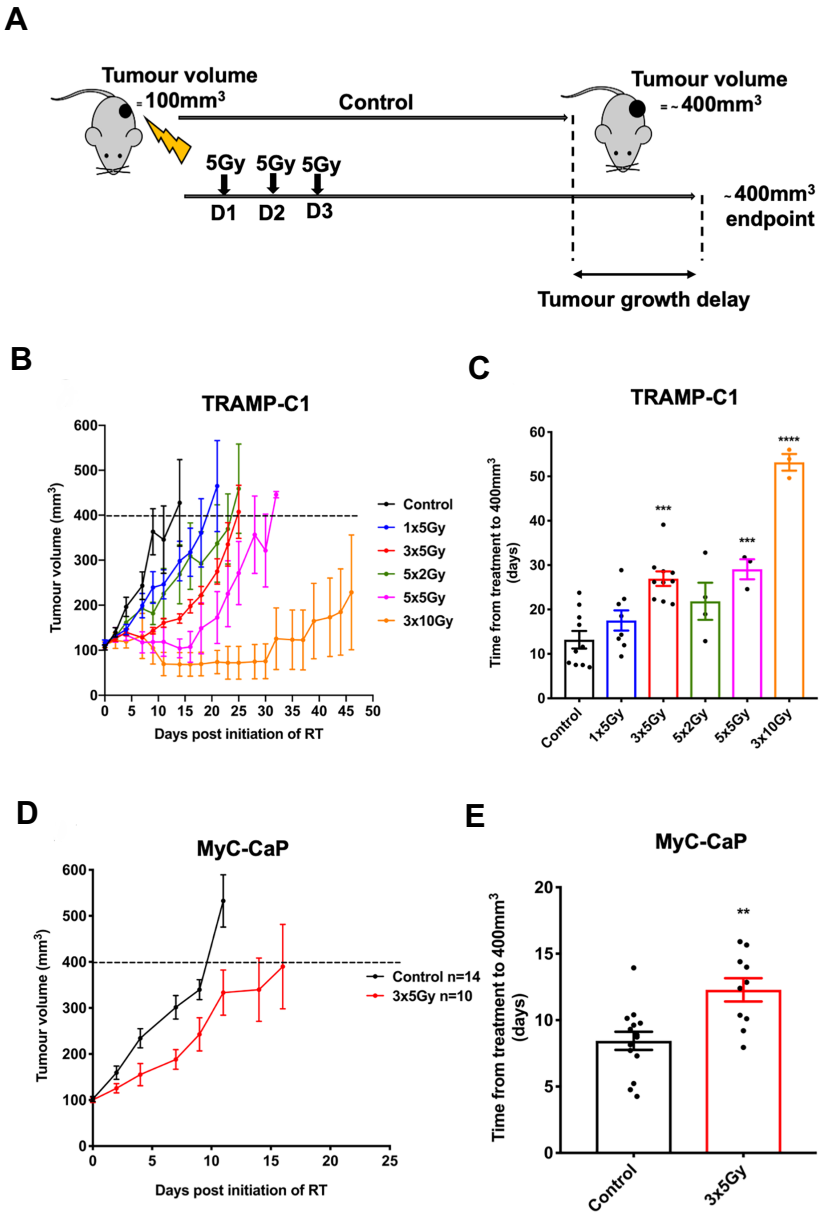
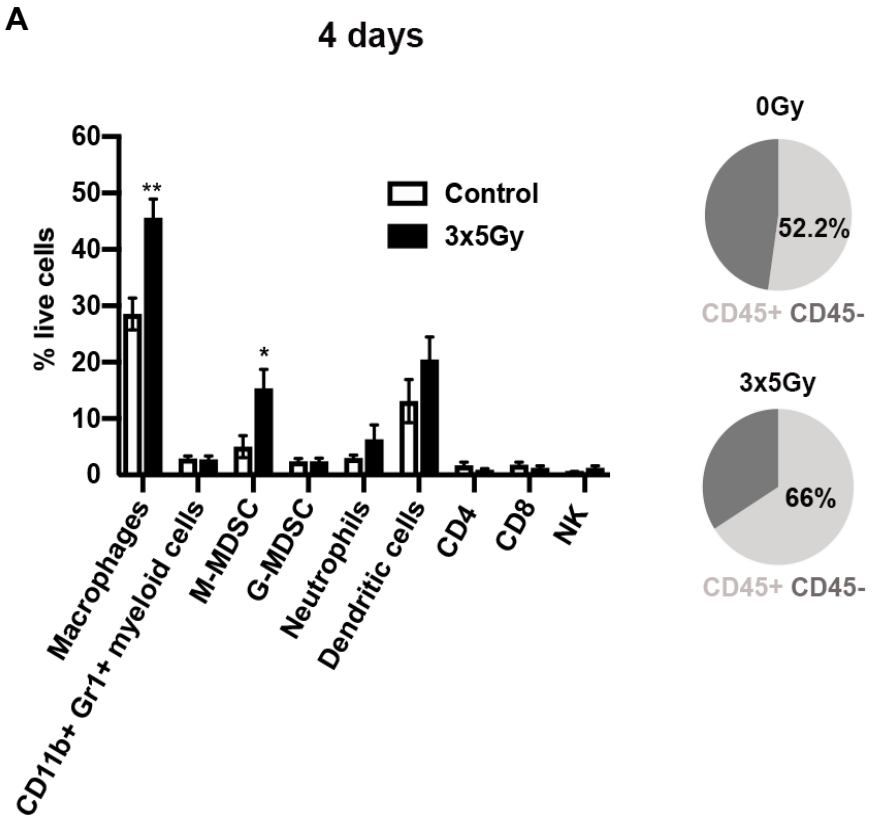
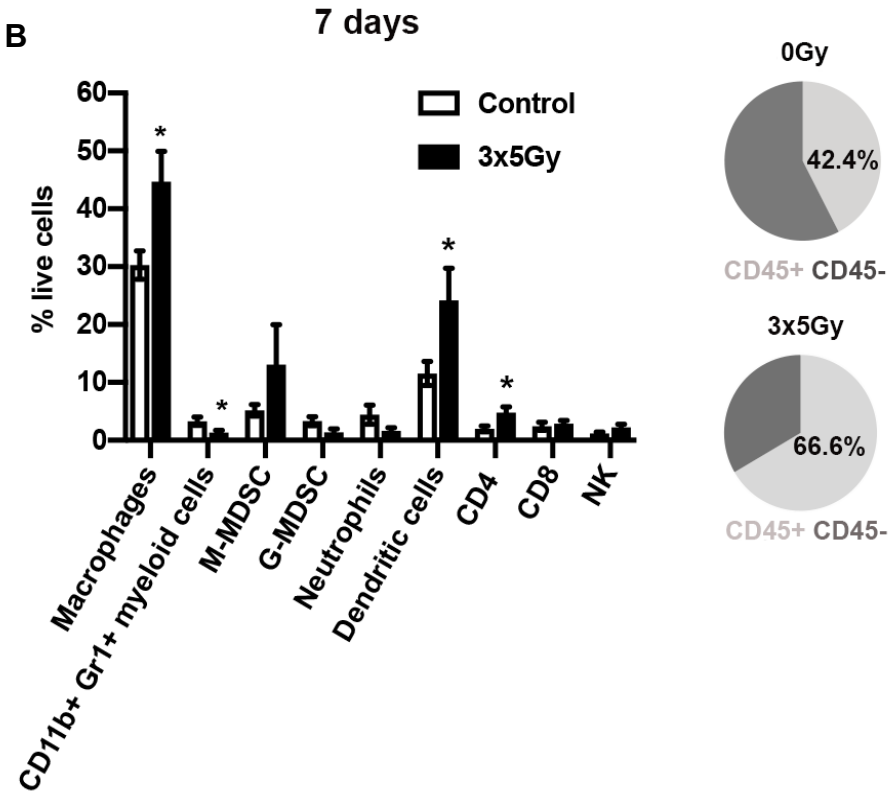


Figure 4.1. Radiotherapy causes tumour growth delay in TRAMP-C1 and MyC-CaP flank tumour allografts. **(A)** Outline schematic of treatment of subcutaneous flank TRAMP-C1 and MyC-CaP tumour allografts with various RT doses and schedules. **(B)** Growth kinetics of TRAMP-C1 tumours following the indicated treatments (n=10 untreated control; n=8, 1 x 5Gy; n=10, 3 x 5Gy; n=4, 5 x 2Gy; n=3, 5 x 5Gy; n=5, 3 x 10 Gy). **(C)** Results shown are pooled data from four experiments, with untreated control tumours included in each experiment. Median (range) body weight at treatment = 22.2 g (19.0–26.3 g). **(D)** Growth kinetics of MyC-CaP tumours following the indicated treatments (n = 14 untreated control; n = 10 3 × 5 Gy RT). Median (range) body weight at treatment = 27g (25.3-30.4 g). Data are presented as mean tumour volume as mean tumour volume ± SEM. Tumour growth delay to 400mm^3 analysis of TRAMP-C1 (**C**) and MyC-CaP (**E**) allograft tumours treated with a range of RT doses and schedules. Data are presented as mean tumour volume ± SEM and analysed using ordinary one-way ANOVA with Tukey's *post hoc* analysis *$p < 0.05$ **$p < 0.01$ *** $p < 0.001$****$p < 0.0001$. *Experiment performed in collaboration with Hanna J Sjoberg, post-doctoral fellow in Richard Bryant's lab.*

4.2.2 Hypofractionated radiotherapy using 3 x 5 Gy induces immune changes in TRAMP-C1 and MyC-CaP flank prostate cancer tumour allografts

FACS analysis of the TIME of TRAMP-C1 tumours at 4 and 7-days post initiation of 3 x 5 Gy RT demonstrated an increased proportion of cells expressing the $CD45^+$ general leukocyte marker compared to control untreated tumours. The $CD45^+$ immune cells were predominantly myeloid cells, and a significantly increased proportion of $CD11b^+F480^+$ TAMs as early as 4 days and $CD11b^+CD11c^+MHCII^+$ DCs at 7 days were observed in RT-treated tumours compared to control untreated tumours. A significantly reduced proportion of $CD11b^+Gr1^+$ MDSCs was observed in 3 x 5 Gy RT-treated tumours compared to untreated controls at 7 days (**figure 4.2A & 4.2C**). iNOS and CD206 expression (markers of M1 and M2 polarisation respectively) was analysed to define the activation status of TAMs within the TIME following 3 x 5 Gy RT. Most of the TAMs were M2-polarised in both 3 x 5 Gy RT-treated tumours and untreated control tumours, however following 3 x 5 Gy there was a non-significant increase in iNOS-expressing TAMs (**figures 4.2D**). An increase in $CD45^+CD3^+CD4^+$ T-cells, and a non-significant increase in $CD45^+CD3^-NK1.1^+$ NK cells, was seen in 3 x 5 Gy RT-treated tumours compared to untreated control tumours at 7 days but not at 4 days following RT (**figure 4.2A & 4.2C**). The proportion of $CD45^+CD3^+CD8^+$ T-cells and $CD45^+CD4^+CD25^+FoxP3^+$ regulatory T-cell (Treg) cells remained unchanged in 3 x 5 Gy RT-treated tumours compared to untreated control tumours (**figure 4.2E**).


A
4 days
% live cells
60
50
40
30
20
10
0
**
*
Control
3x5Gy
Macrophages
CD11b+ Gr1+ myeloid cells
M-MDSC
G-MDSC
Neutrophils
Dendritic cells
CD4
CD8
NK
0Gy
52.2%
CD45+ CD45-
3x5Gy
66%
CD45+ CD45-


B
7 days
% live cells
60
50
40
30
20
10
0
*
*
*
*
Control
3x5Gy
Macrophages
CD11b+ Gr1+ myeloid cells
M-MDSC
G-MDSC
Neutrophils
Dendritic cells
CD4
CD8
NK
0Gy
42.4%
CD45+ CD45-
3x5Gy
66.6%
CD45+ CD45-

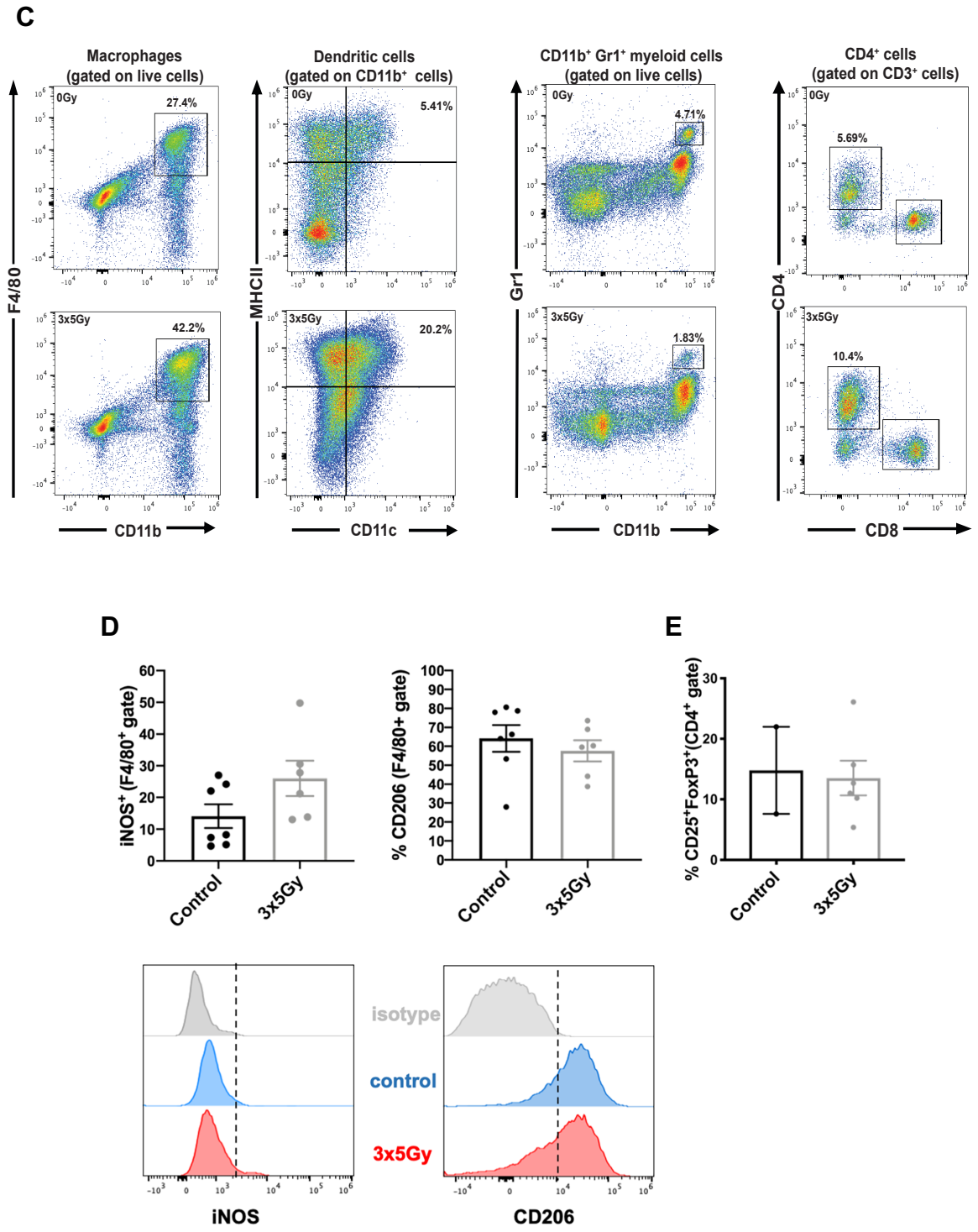


Figure 4.2. Radiotherapy causes early temporal changes in the immune cell composition of TRAMP-C1 flank tumour allografts. FACS analysis of the tumour immune microenvironment of TRAMP-C1 tumour allografts at the 4-day timepoint post initiation of 3 x 5 Gy RT compared to untreated controls (**A**) and at the 7-day timepoint (**B**) with (**C**) representative dot plots shown. Pie charts represent the proportion of CD45$^+$ leucocytes within the total population of live cells. **(D)** The proportion of M1 iNOS expressing macrophages is significantly increased at the 7-day time point following 3 x 5 Gy compared to untreated controls with representative histogram plots. (**E**) The proportion of CD25$^+$ and FoxP3$^+$ expressing CD4$^+$ T-cells remains unchanged following 3 x 5 Gy RT. FACS data are presented as mean percentage of total live cells ± SEM and analysed by the unpaired t-test (n = at least 4 independent tumour samples analysed). *p<0.05.

NanoString analysis of TRAMP-C1 tumours at 7-days post-RT (performed with Said Alyacoubi in the Bryant lab) revealed increased expression of $CD8^+$ T-cell, DC, and Treg-specific function genes (**figure 4.3**). Taken together, the TIME FACS and nanoString data suggests that 7-days following RT a mixed immunological tumour response may have been generated. For example, the increased $CD11b^+F480^+$ TAMs seen on FACS may be pro-tumorigenic, whereas the increased DC number/function may be anti-tumorigenic.

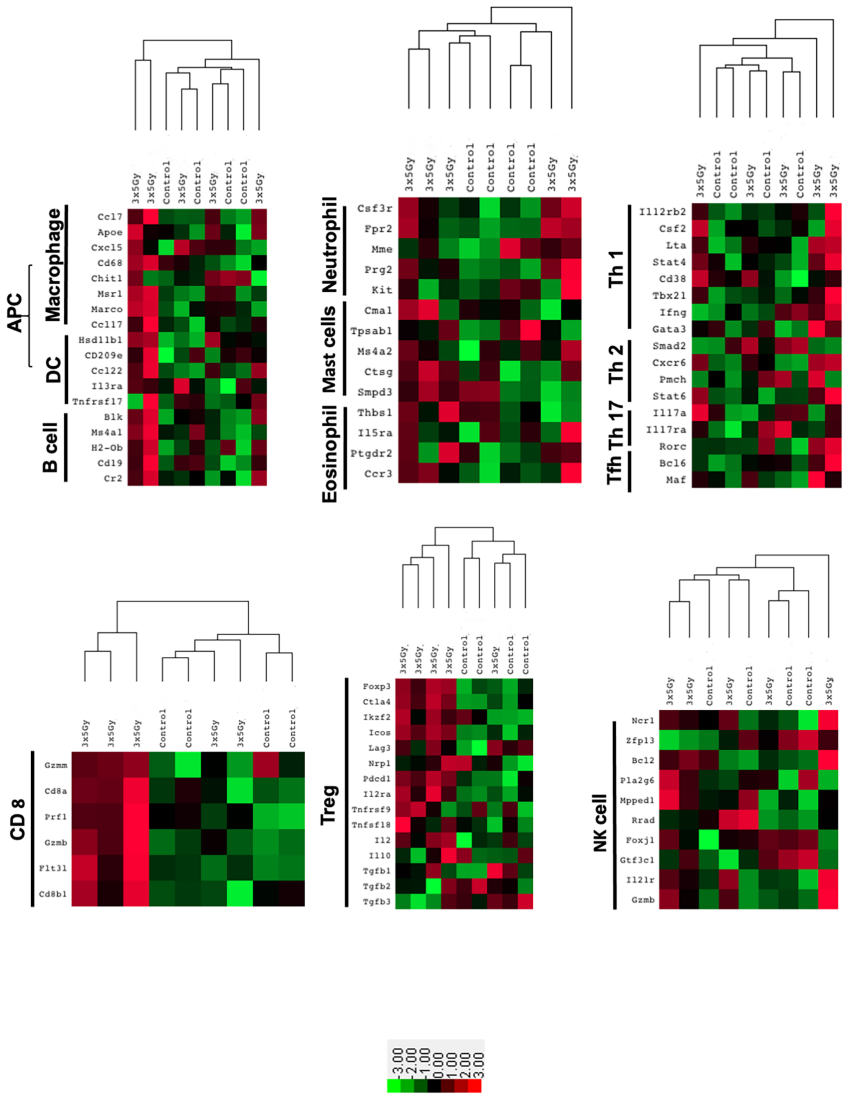


Figure 4.3 Heatmap representation of differential gene expression from the 795 gene probe set across different immune cell subsets between 3 x 5 Gy RT treated tumours (n=5) and untreated controls (n=4) at the 7-day timepoint. Red indicates gene upregulation and green indicates gene down-regulation. n = at least 4 independent tumour samples analysed. *Experiment performed in collaboration with Said Alyacoubi. NDS Masters Student in Richard Bryant's lab.*

In contrast to data at the 7-day time-point, at tumour regrowth to ≥400 mm^3 following 3 x 5 Gy RT the TIME on FACS analysis was similar to untreated control tumours of similar volume. There were no significant differences in the proportion of immune cell subtypes in 3 x 5 Gy RT-treated tumours versus untreated controls at the tumour regrowth to ≥400 mm^3 end-point, although there was a non-significant increase in the proportion of $CD11b^+Gr1^+$ myeloid cells (p=0.072), $CD11b^+Ly6C^-Ly6G^+$ (p=0.057) cells, and $CD11b^+Ly6G^+$ neutrophils (p=0.070) in radio-recurrent tumours versus controls (**figure 4.4A**). PD-1 expression in $CD45^+CD8^+$ T-cells was upregulated in 3 x 5 Gy-treated TRAMP-C1 tumours at regrowth to ≥400 mm^3 compared to untreated control tumours (p=0.02) (**figure 4.4B**). Corresponding nanoString analysis at ≥400 mm^3 tumour regrowth demonstrated that $CD8^+$ T-cell, helper T-cell, and DC gene expression was reduced in radio-recurrent tumours versus controls (**figure 4.5A**), even though the proportion of these immune populations on FACS were similar between these groups at end-point. Significantly altered nanoString immune genes at the 7-day timepoint are listed for TRAMP-C1 in **figure 4.5B**. In summary, this orthogonal analysis of TRAMP-C1 tumours following 3 x 5 Gy demonstrated that the TIME comprised both pro-tumourigenic and anti-tumourigenic immune cells at the 'early' 7-day timepoint. FACS analysis demonstrated a DC and CD4+ helper T-cell immune response which can be regarded as anti-tumourigenic, along with an increase in the proportion of $CD11b^+F480^+$ TAMs which suggests a parallel pro-tumourigenic response. NanoString gene expression analysis demonstrated increased expression of $CD8^+$ T-cell and DC-specific function genes that may be considered anti-tumourigenic, and an increased expression in Treg-specific function genes that may be considered pro-tumourigenic. At the tumour regrowth stage to ≥400 mm^3 a similar orthogonal analysis using FACS and nanoString suggested that radiorecurrent tumours (following treatment with a sublethal 3 x 5 Gy dose of RT) might have developed a more immunosuppressive TIME. FACS analysis demonstrated a non-significant trend towards an increased proportion of $CD11b^+Gr1^+$ myeloid cells (which are

known to be immunosuppressive), and increased PD-1 expression in $CD45^+CD8^+$ T-cells at the ≥400 mm^3 tumour regrowth end-point.

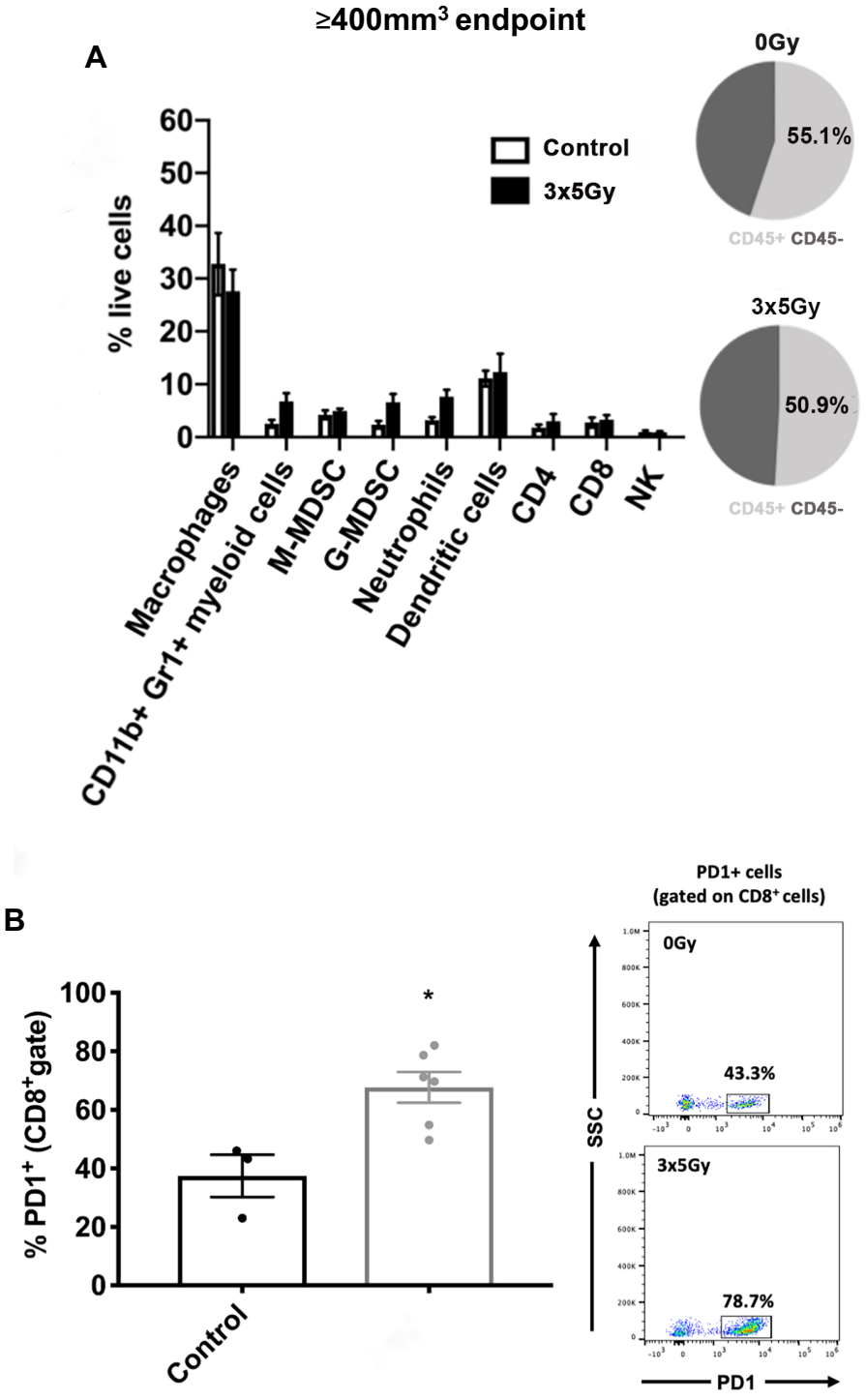
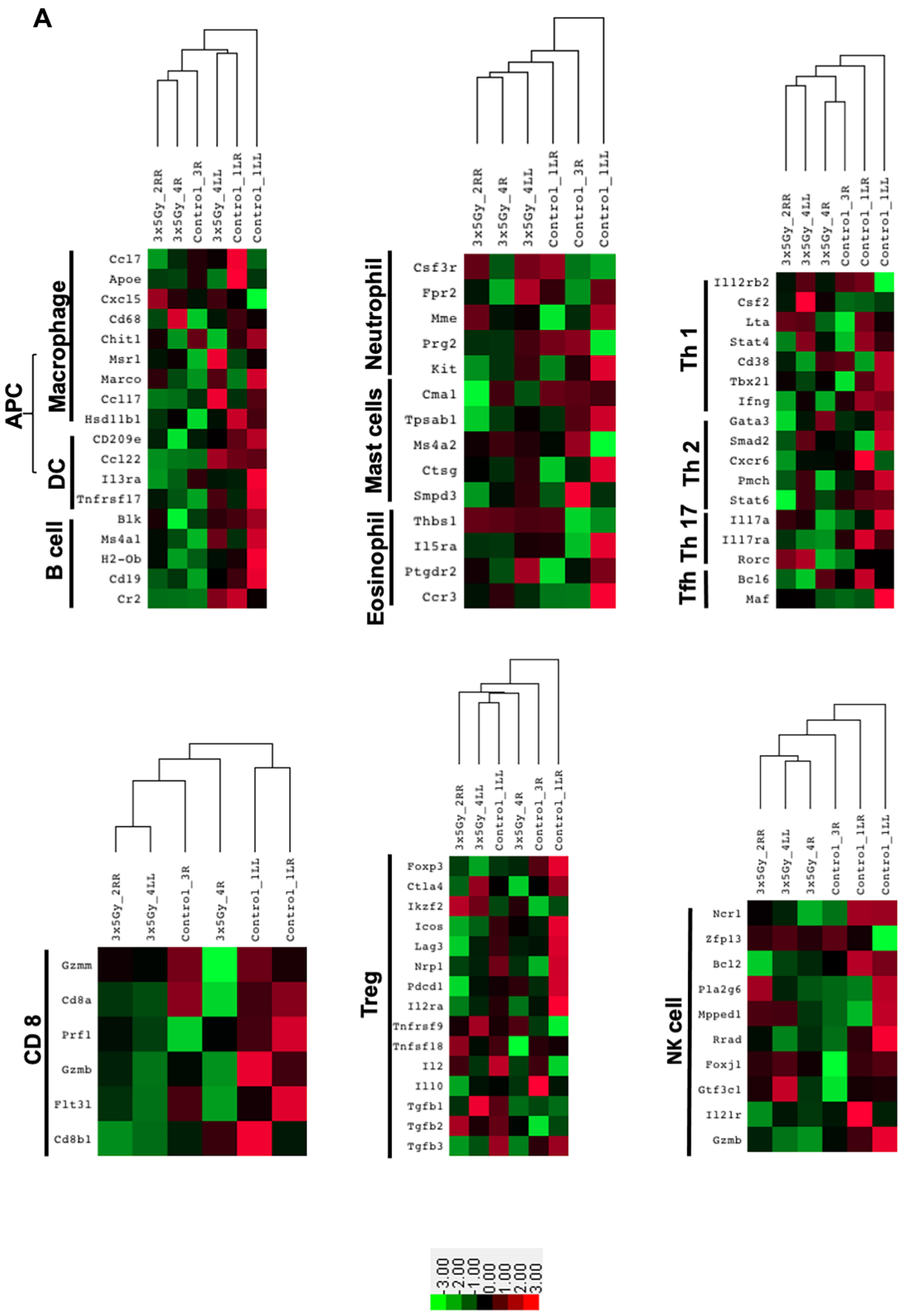
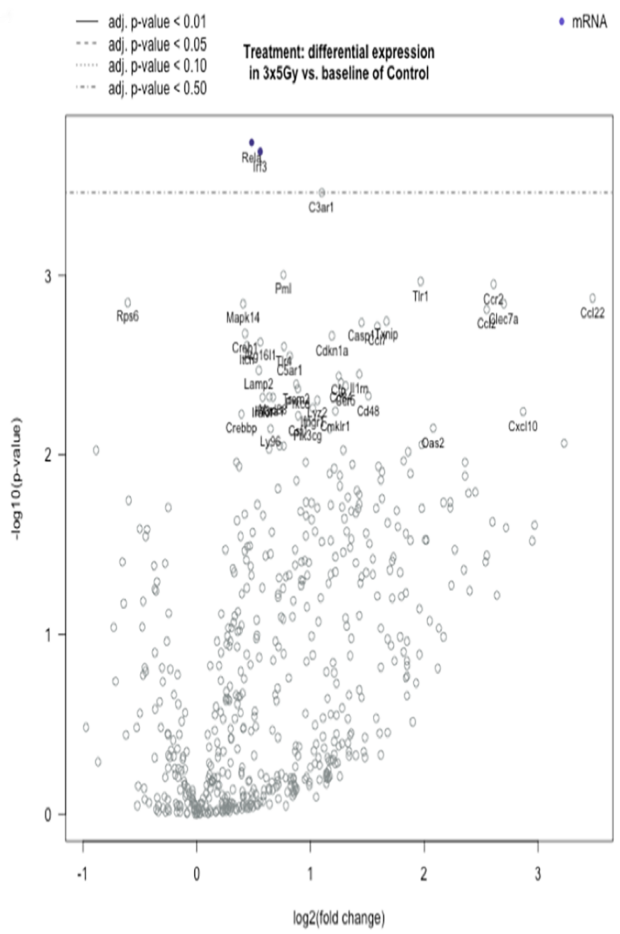


Figure 4.4. Radiotherapy effects at the ≥400 mm^3 tumour endpoint in TRAMP-C1 tumour allografts. (A) The immune cell composition of RT-treated tumours and untreated control tumours is similar. **(B)** Quantification of PD-1 expression on gated $CD45^+$ $CD8^+$ T-cells following treatment of TRAMP-C1 allograft tumours with 3 x 5 Gy RT compared to untreated controls. *p<0.05.

NanoString analysis demonstrated that CD8^{+} T-cell, helper T-cell, and DC gene expression was reduced in radio-recurrent tumours versus controls **(figure 4.5 A&B**)



B



Gene	*p*-value
C3ar1	0.000218
Rela	0.00022
Irf3	0.00101
Cdkn1a	0.00159
Itch	0.00226
Rps6	0.00234
Trem2	0.00239
Clec7a	0.00242
C5ar1	0.00275
Tnfsf13	0.00291
Pml	0.00295
Tlr1	0.00392
Ccr2	0.00402
Bmi1	0.00473
Ccl2	0.00486
Mapk14	0.00489
Tlr4	0.00547
Ccl7	0.00548
Atm	0.00555
Psmd7	0.00573

Figure 4.5. Heatmap representation of differential gene expression from the 795 gene probe set across different immune cell subsets between 3 x 5 Gy RT treated tumours and untreated controls at the late time point. (A) Red indicates gene upregulation and green indicates gene down-regulation. **(B)** Volcano plots demonstrating significantly altered nanoString immune genes at the 'early' 7-day time point following 3 x 5 Gy RT treatment of TRAMP-C1 flank tumour allografts with corresponding table listing these genes and associated *p*-value. *Experiment performed in collaboration with Said Alyacoubi, NDS Masters Student in Richard Bryant's lab.*

An orthogonal immune cell analysis was performed in MyC-CaP flank PCa allografts 7-days post-RT and at the ≥400 mm^3 tumour regrowth end-point following 3 x 5 Gy RT. FACS analysis revealed that the immune cell infiltrate was generally lower in MyC-CaP tumours compared to TRAMP-C1 tumours. Analysis of the TIME in MyC-CaP at 7-days post-RT demonstrated no change in the relative proportion of $CD45^+$ cells compared to control untreated tumours. At 7 days post-RT a significant reduction in the proportion of

$CD45^+CD3^+CD4^+$ T-cells, and a non-significant reduction in the proportion of $CD45^+CD3^+CD8^+$ T-cells (p=0.08), was seen in 3 x 5 Gy RT-treated versus untreated tumours (**figure 4.6A&D**). No significant difference in myeloid cell proportion (including TAMs, neutrophils and DCs) was observed in 3 x 5 Gy RT-treated versus control tumours, although a non-significant increase in M-MDSC infiltration (p=0.075) was seen in 3 x 5 Gy RT-treated tumours (**figure 4.6A**). At the ≥400 mm^3 tumour regrowth end-point in MyC-CaP, TIME FACS analysis demonstrated no significant differences in the proportion of myeloid immune cell subtypes in 3 x 5 Gy RT-treated versus control tumours (**figure 4.6B**). Analysis of the lymphoid immune cell subtypes in MyC-CaP demonstrated an increased tumour infiltrate of $CD45^+CD4^+CD25^+FoxP3^+$ Treg cells (**figure 4.6C&D**), and a non-significant reduction in the proportion of $CD45^+CD3^+CD8^+$ T-cells, in 3 x 5 Gy RT-treated tumours versus untreated controls (**figure 4.6B**). Overall, the FACS data suggests that at the 'early' 7-day timepoint following 3 x 5 Gy RT the TIME have an immunosuppressive phenotype, with a significant reduction in the relative proportion of CD4+ T-helper cells, a non-significant reduction in the proportion of CD8+ T-cells and a significantly increased proportion of Tregs.

NanoString analysis of MyC-CaP tumours at 7-days and at ≥400 mm^3 tumour regrowth endpoint following 3 x 5 Gy RT revealed similar observations to those seen in TRAMP-C1 tumours, although the numbers of MyC-CaP tumours analysed in these experiments were fewer than for TRAMP-C1, therefore a direct comparison of results should be interpreted with caution. Similar to TRAMP-C1 tumours, heatmap clustering of genes suggested an increased expression of $CD8^+$ T-cell, DC, and Treg function genes in 3 x 5 Gy RT-treated tumours compared to control untreated tumours (**figure 4.7A**), pointing towards 'early' anti-tumour immunogenic effects post-RT in MyC-CaP, as had been observed in TRAMP-C1. NanoString analysis at ≥400 mm^3 tumour regrowth endpoint in MyC-CaP demonstrated reduced DC gene expression in radio-recurrent tumours versus control untreated tumours (**figure 4.7B**).

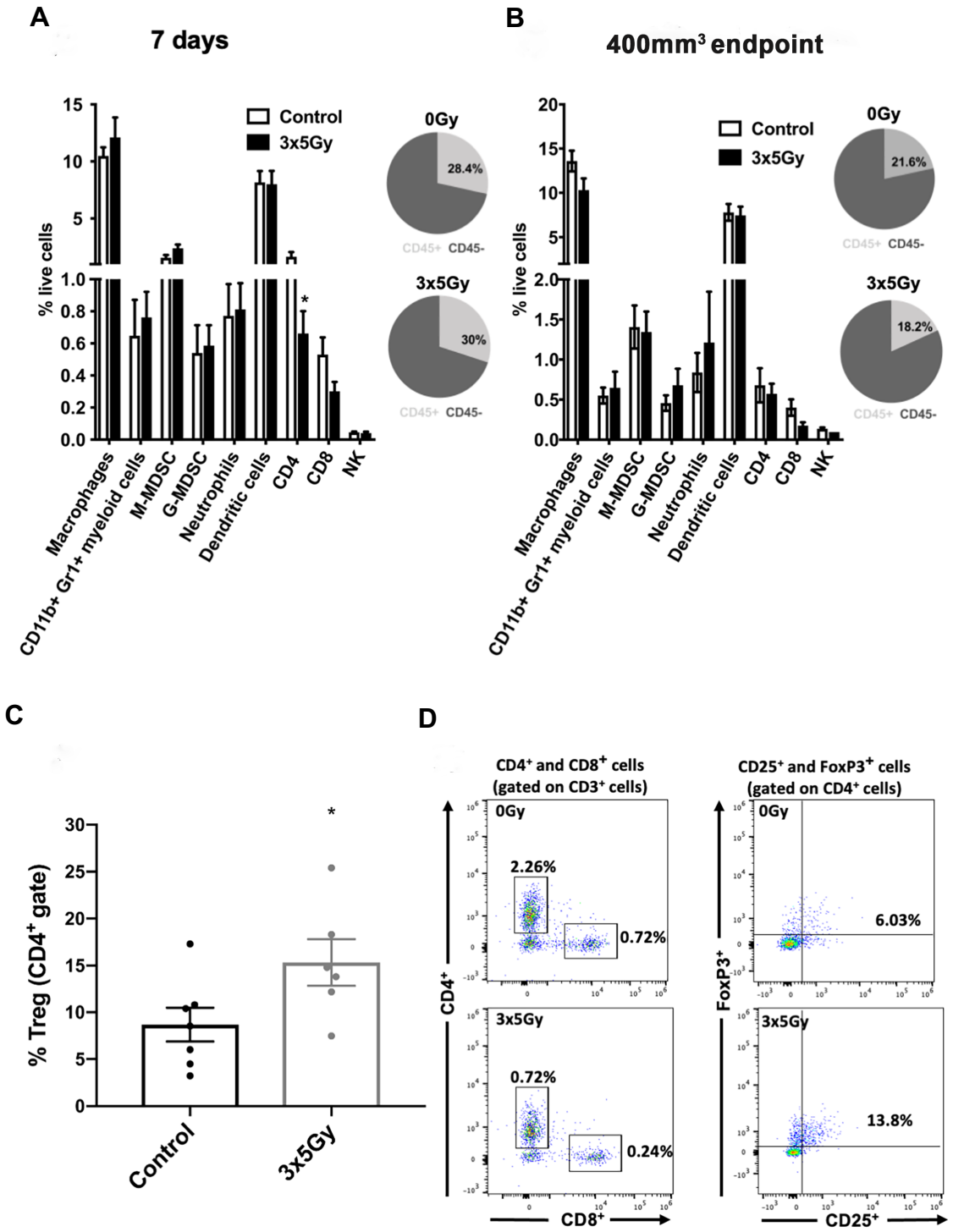


Figure 4.6. Radiotherapy effects on MyC-CaP tumour allografts at the 'early' 7-day and ≥400 mm^3 regrowth timepoint. FACS analysis of the tumour immune microenvironment of MyC-CaP tumour allografts at the **(A)** 7-day timepoint post initiation of 3 x 5 Gy RT compared to untreated controls and at **(B)** regrowth to ≥400 mm^3 with **(D)** representative dot plots of significant differences shown. Pie charts represent the proportion of CD45$^+$ leucocytes within the total population of live cells. **(C&D)** The proportion of CD25+ and FoxP3+ expressing CD4+ T-cells increases following 3 x 5 Gy RT. FACS data are presented as mean percentage of total live cells ± SEM and analysed by the unpaired t-test (n= at least 5 independent tumour samples analysed). *p<0.05.

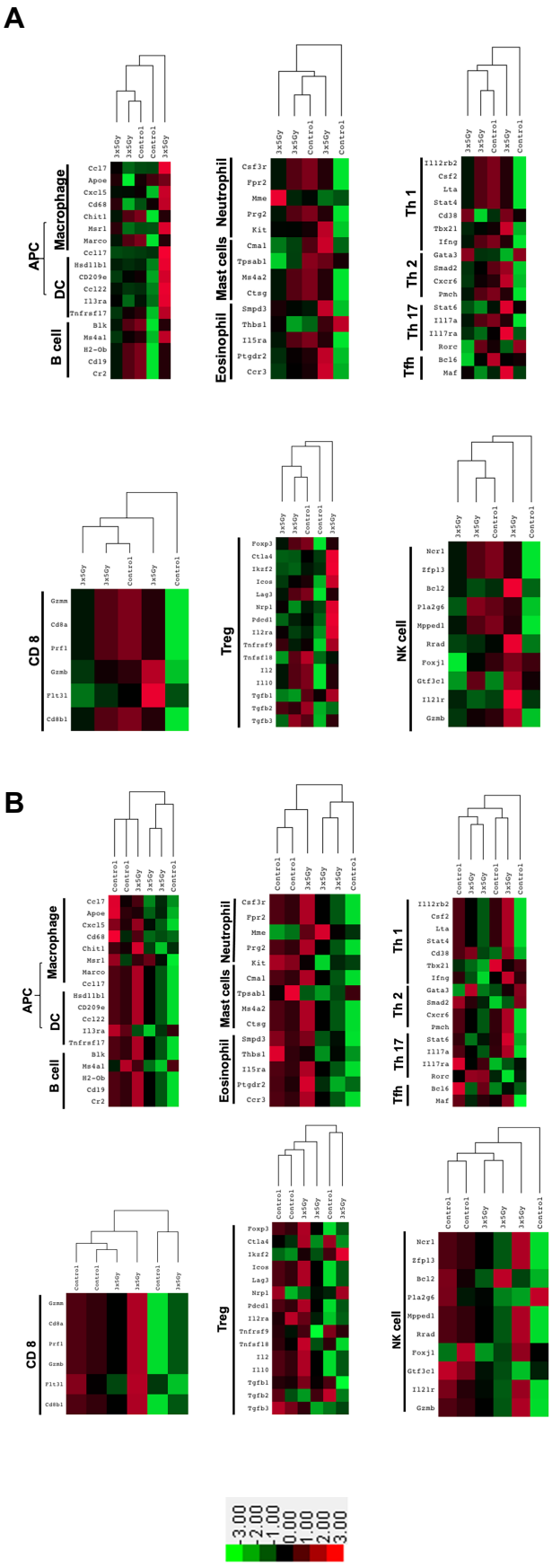


Figure 4.7 Heatmap representation of differential gene expression from the 795 gene probe set across different immune cell subsets between 3 x 5 Gy RT treated tumours and untreated controls at (A) early and (B) late timepoint. Red indicates gene upregulation and green indicates gene down-regulation. n = 3 control tumours and n=3 3 x 5 Gy RT treated tumours.

4.2.3 Concomitant inhibition of PD-L1 does not enhance anti-tumour effects of hypofractionated radiotherapy using 3 x 5 Gy in TRAMP-C1 flank prostate cancer tumour allografts

FACS analysis of the $CD45^-$ non-immune cell population within the TRAMP-C1 TIME at 4-days following initiation of 3 x 5 Gy revealed increased PD-L1 expression (**figure 4.8A**), and nanoString analysis at 7-days demonstrated increased PD-1 expression and a non-significant increase in PD-L1 expression (**figure 4.8B**). To test the hypothesis that anti-PD-L1 enhances anti-PCa effects of RT, flank TRAMP-C1 tumours were treated with 3 x 5 Gy plus anti-PD-L1, and compared against 3 x 5 Gy alone, anti-PD-L1 alone, or untreated tumours (**figure 4.8C**). Inhibition of PD-L1, rather than combined inhibition of PD-L1 and PD-1, was chosen as iRT with 3 x 5 Gy due to concerns that combined anti-PD-L1 and anti-PD-1 might cause excessive toxicity *in vivo*, and given that only one agent is usually administered in the clinic. Anti-PD-L1 or isotype control was given at days 0, 3, 6, and 9 relative to the first 5 Gy fraction as informed by similar experiments performed by collaborators at the Oxford Institute of Radiation Oncology [Azad et al., 2017]. Commencement of anti-PD-L1 with the first 5 Gy fraction was chosen to ensure that therapeutic levels of anti-PD-L1 coincided with RT-induced upregulation of PD-L1 in TRAMP-C1 tumours, and four doses were administered as this had not been reported to have welfare implications in previous studies [Azad et al., 2017].

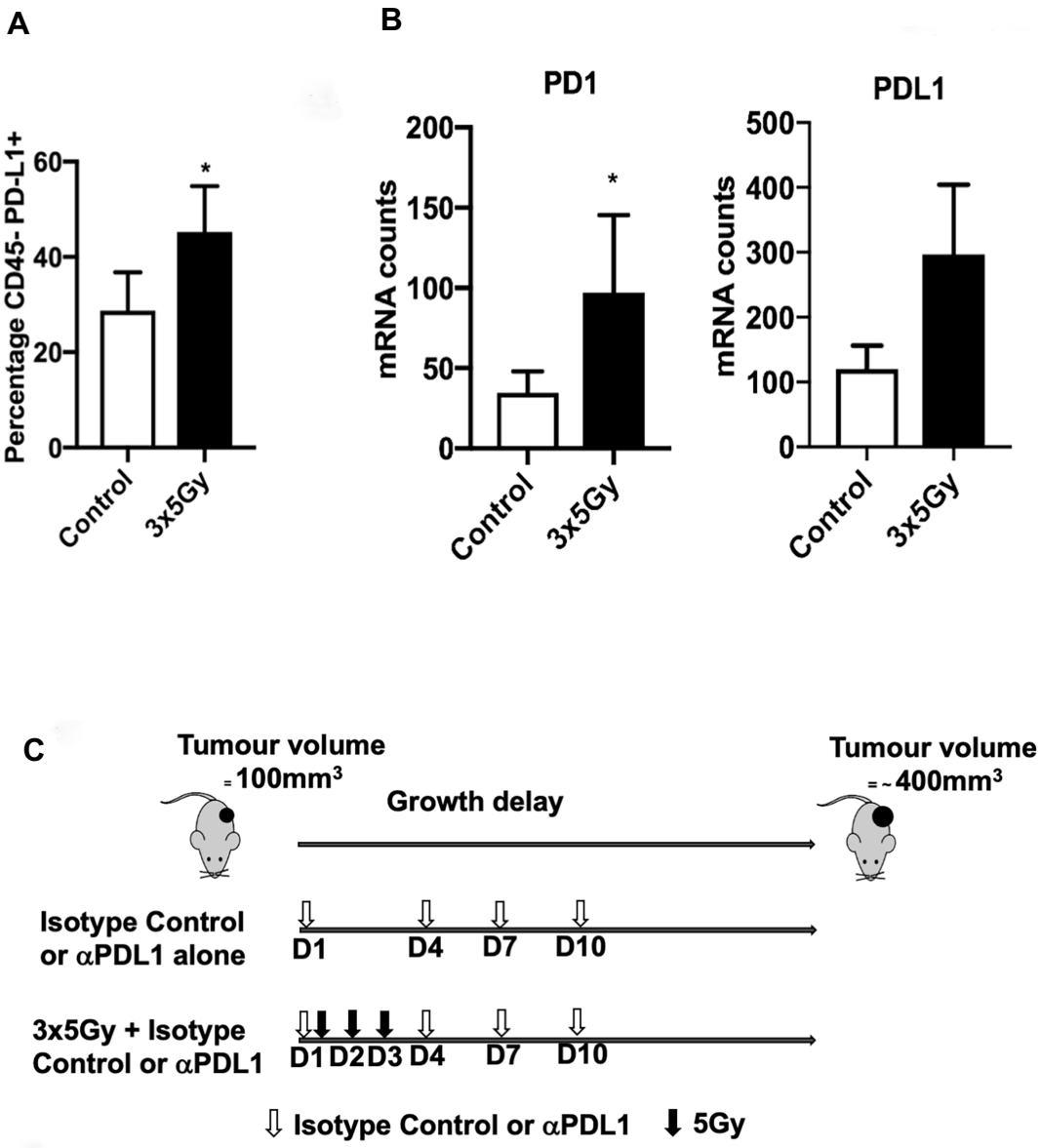


Figure 4.8 Radiotherapy upregulates the PD-1 / PD-L1 axis. (A) FACS quantification of PD-L1 expression in the CD45− non-immune cell population within the tumour immune microenvironment at the 4-day time-point post-initiation of 3 x 5 Gy RT compared to untreated control tumours. **(B)** NanoString immune gene expression analysis of PD-1 and PD-L1 expression at the 7-day time-point post-initiation of 3 x 5 Gy RT compared to untreated control tumours. Data are presented as mean ± SEM and analysed using the unpaired t-test. **(C)** Outline schematic of treatment of subcutaneous flank TRAMP-C1 tumour allografts with 3 x 5 Gy RT, anti-PD-L1, or a combination of 3 x 5 Gy RT and anti-PD-L1.

Inhibition of PD-L1 in combination with 3 x 5 Gy did not significantly enhance tumour growth delay compared to 3 x 5 Gy alone in these conditions (**figure 4.9 A-C**). FACS analysis of the TIME at the ≥400 mm^3 tumour regrowth timepoint showed a non-significant increase in the $CD8^+$ T-cell infiltrate in tumours receiving anti-PD-L1 alone or RT plus anti-PD-L1 (**figure 4.10**).

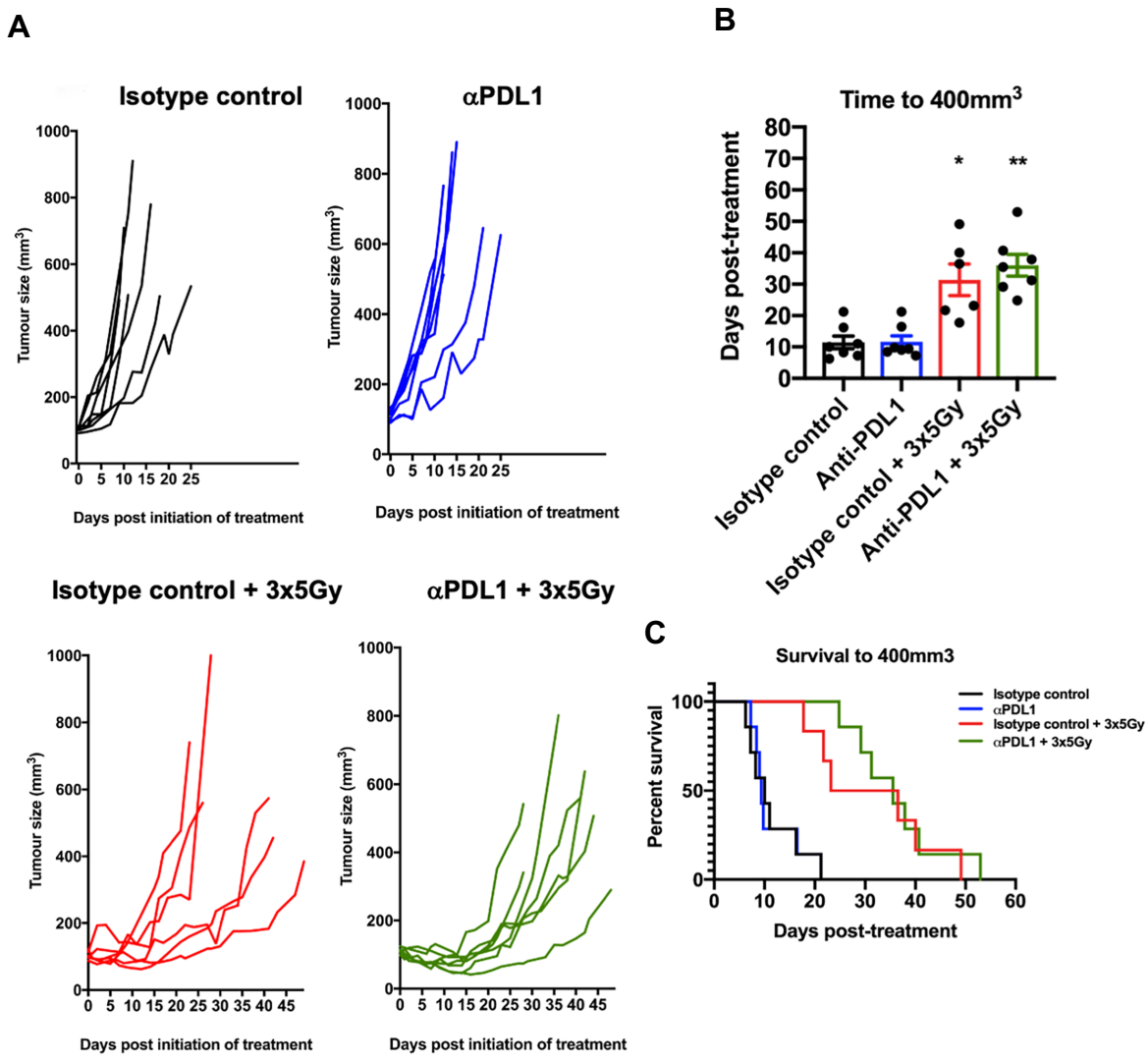


Figure 4.9 Tumour growth delay analysis of TRAMP-C1 allograft tumours following treatment with either 3 x 5 Gy RT alone, anti-PD-L1 alone, or combined 3 x 5 Gy and anti-PD-L1. The number of mice per group were: isotype control alone n = 7, isotype control plus RT n = 6, anti-PD-L1 alone n = 7, anti-PD-L1 plus RT n = 7. Median (range) body weight at treatment = 21.8 g (19.6–25.5 g). **(A)** Data in all four treatment groups are presented as individual tumour growth kinetics, **(B)** grouped tumour growth kinetics, mean ± SEM growth delay to ≥400 mm^3, and **(C)** survival to ≥400 mm^3 using Kaplan-Meier curves. Data were analysed using ordinary one-way ANOVA with Tukey's *post hoc* adjustment for multiple comparisons. *p<0.05; **p<0.01.

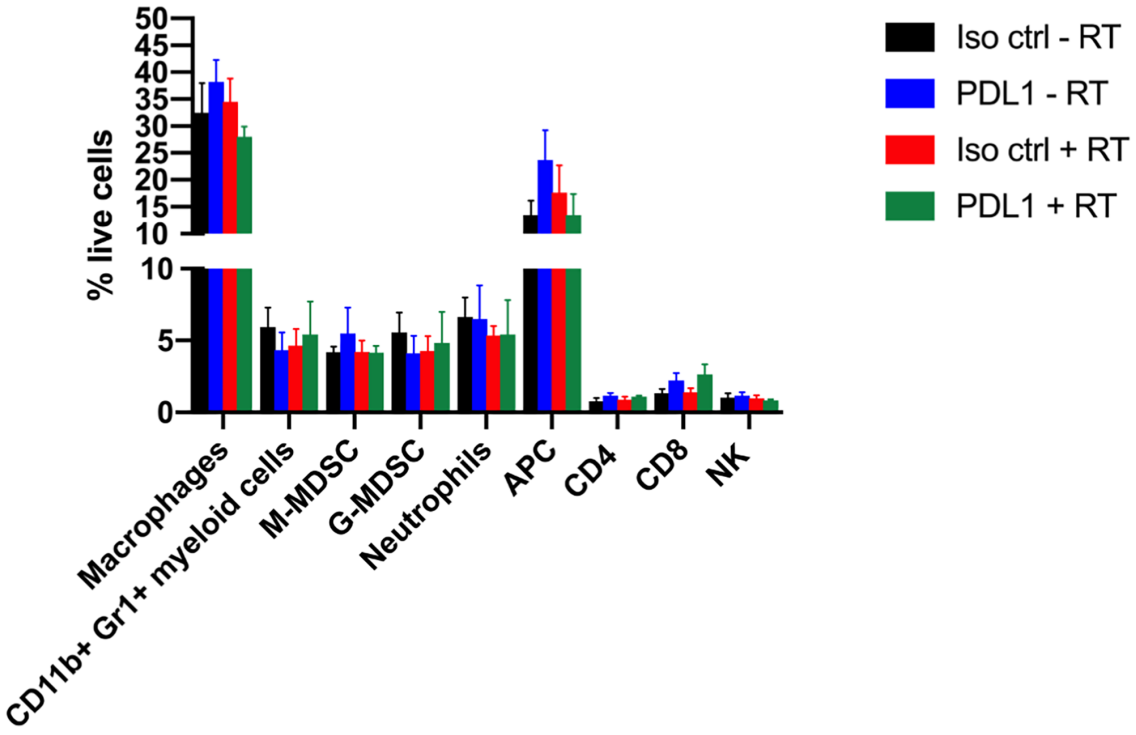


Figure 4.10 FACS analysis at tumour re-growth to ≥400mm^3 FACS analysis showed no significant differences in the TIME of RT + PDL1 treated tumours compared to RT alone, PDL1 alone and untreated controls.

4.3 Discussion

RT has previously been regarded as a largely immunosuppressive treatment, and thus may potentially be inappropriate for combination with immunomodulation [Finkelstein et al., 2015]. However, RT may also be an immunostimulatory anti-PCa therapy [Finkelstein et al., 2015], and the relationship between RT and immune reactivity is complex. Data on the use of RT and immunotherapy are accumulating and suggest opportunities to use RT to 'prime' the immune system and thereby enhance the anti-tumour effects of immunotherapy [Ganss et al., 2002]. FACS analysis of the TRAMP-C1 TIME following 5 Gy RT fractions suggests an 'early' predominantly immunostimulatory TIME 7-days post-initiation of RT, with increased numbers of DCs and $CD4^+$ T-helper cells, and a reduction in the proportion of $CD11b^+Gr1^+$ myeloid cells (which are regarded as being

immunosuppressive MDSCs). Corresponding NanoString analysis of TRAMP-C1 allografts at this 'early' 7-day time-point also suggests generation of anti-tumour immunogenic effects, with increased expression of genes associated with $CD8^+$ T-cell and DC function. The lack of any observed increase in infiltration of cytotoxic $CD8^+$ T-cells in the TIME as analysed using FACS may be due to the use of 5 Gy RT fractions, and higher fraction sizes doses may be necessary to achieve this effect. Despite 3 x 5 Gy RT resulting in a significant tumour growth delay and predominantly immunostimulatory effects, this RT dose was sub-lethal and failed to generate a sufficiently effective anti-tumour response to cure animals of these tumours. In contrast, and in support of the potential immunosuppressive effects of RT, 'early' time-point FACS of the TIME in MyC-CaP demonstrated significantly reduced $CD4^+$ helper T-cells, increased $CD4^+$ Treg cells, and a trend towards a reduction in the proportion of the $CD8^+$ T-cell population.

Pre-clinical models of PCa, such as TRAMP-C2 allografts, have demonstrated barriers to generating an anti-tumour immune response, including poor numbers of $CD8^+$ T-cells infiltrating the TIME, and high intra-tumoral proportions of immunosuppressive myeloid cells such as TAMs and MDSCs [Ager et al., 2017]. Consistent with these reports, experiments in this chapter describe poor infiltration of $CD8^+$ T-cells in TRAMP-C1 flank tumour allografts, with TAMs and MDSCs comprising the majority of $CD45^+$ cells. Whilst RT doses used in the literature are higher than the 3 x 5 Gy used in the experiments described herein, the observation of an increase in $CD11b^+F480^+$ TAMs 7-days following 3 x 5 Gy is consistent with observations by others in TRAMP-C1 [Tsai et al., 2007]. TAMs are myeloid cells present in many solid-organ tumours including PCa, and they demonstrate functional plasticity and differentiate into various phenotypes during inflammatory responses. TAMs are described as having an M1 phenotype with predominantly anti-tumorigenic effects, or M2 with predominantly pro-tumorigenic effects such as angiogenesis and immunosuppression. Analysis of TAM activation status using iNOS and CD206 suggests M2 TAMs are predominantly present in the TRAMP-C1 TIME.

In TRAMP-C1 allografts, treatment with 3 x 5 Gy recruited both M1 and M2 TAMs into the PCa TIME, and it may be speculated that blockade of this recruitment may enhance the anti-tumour RT response. The observed trend towards an increased proportion of MDSCs at the 'late' ≥400 mm^3 tumour regrowth time-point following 3 x 5 Gy RT may result in immunosuppression and $CD8^+$ T-cell exhaustion, above and beyond that induced by a RT-induced influx of TAMs. The observation that PD-1 expression is increased in $CD8^+$ T-cells at ≥400 mm^3 tumour regrowth following 3 x 5 Gy RT suggests the presence of T-cell exhaustion in TRAMP-C1, and reduced $CD8^+$ T-cell, helper T-cell, and DC gene expression on nanoString analysis in radio-recurrent compared with control untreated tumours suggests establishment of an immunosuppressed TIME at eventual tumour re-growth. Further experiments to target this effect are warranted.

Differentially expressed genes in TRAMP-C1 at the 'early' 7-day time-point post-RT included upregulation of chemokine genes such as CCL2 and its receptor CCR2, CCL17, CCL22, CXCR3 and CCL7. Chemokines and their receptors are expressed by cancer cells and play roles in tumour progression and therapeutic outcomes. Several chemokines and their receptors, in particular CCL2 and CCR2, are implicated in PCa progression, metastasis and chemoresistance [Natsagdorj et al., 2019; Zhang et al., 2010], and may be expressed by tumour cells or TAMs recruited to the TIME. Tumour-derived CCL2 mediates RT resistance in pre-clinical pancreatic ductal adenocarcinoma through recruitment of TAMs and MDSCs, supporting cancer cell proliferation and neovascularisation post-RT [Kalbasi et al., 2017]. Approaches to mitigate immunosuppressive TIME effects of RT-induced TAMs by blocking CCL2-CCR2, or depleting these cells using concomitant anti-CSF with RT, may be necessary in PCa to derive benefit from iRT [Jones et al., 2018].

Analysis of TRAMP-C1 tumours demonstrated that the PD-1/PD-L1 axis is upregulated in the TIME following 3 x 5 Gy. The hypothesis that iRT through PD-L1 inhibition with

concomitant 3 x 5 Gy RT may enhance tumour growth delay compared to RT alone was therefore tested in the described experiments. There are several possible explanations for the absence of a demonstrable increase in tumour growth delay through iRT in these conditions in this model. The 3 x 5 Gy RT dose may be insufficient to generate $CD8^+$ T-cell dependent anti-tumour responses that can be further harnessed through anti-PD-L1. Moreover, combined anti-PD-1 and anti-PD-L1 with RT may be necessary to harness a response through enhanced blockade of the PD-1/PD-L1 axis, however this combination was not tested in these experiments due to concerns about possible *in vivo* toxicity, and given that combined anti-PD-1 and anti-PD-L1 is not standard in the clinic. The tumour growth delay and survival curve analysis suggests a possible initial enhanced response to anti-PD-L1 with RT compared to RT alone, however this effect was not maintained, with no observed difference once the anti-PD-L1 was no longer administered. It may be the case that administration of anti-PD-L1 for a longer time period than the x4 doses delivered over 12 days in this model, and as previously described [Azad et al., 2017], is necessary for an enhanced effect. It is possible that the anti-PD-L1 needs to be continued for several weeks post-RT, however, we did not pursue this approach due to concerns that prolonged anti-PD-L1 may be poorly tolerated *in vivo* and lead to significant toxicity. It is also possible that the experiment was under-powered given the variable response of TRAMP-C1 tumours to 3 x 5 Gy RT, with three of the combined treatment animals demonstrating enhanced response, whilst a further three did not, leading to no significant difference overall. Future experiments using a longer time course of concomitant anti-PD-L1, and using combined anti-PD-1 and anti-PD-L1 and RT, subject to acceptable toxicity *in vivo*, may help to answer these questions.

Previous experiments in autochthonous TRAMP models developing spontaneous PCa suggest that neither RT (administered as 3 x 10 Gy, with a 5-day interval between doses) nor immunotherapy alone (in the form of a tumour vaccine) can prime an anti-tumour immune response in animals with evolving tumours, but that iRT could result in anti-

tumour T cell activation, although this effect was dependent on the relative timing of RT and immunotherapy [Harris et al., 2008]. Anti-tumour immune responses occurred when immunotherapy was administered 3-5 weeks post-RT, but these responses were undetectable when immunotherapy was administered at either earlier (peri-RT) or later time-points. It is possible that there is a relatively narrow therapeutic temporal window of opportunity for immunotherapy post-RT to be effective in highly aggressive immunosuppressive tumour models such as the autochthonous TRAMP model and the TRAMP-C1 flank allograft tumour model used in these experiments, albeit these studies used different RT doses and fractionation. The TIME results from the experiments described in this thesis suggest that despite RT, the $CD8^+$ T-cells that play important roles in the anti-tumour effects of ablative RT [Filatenkov et al., 2015] remain at low levels following 3 x 5 Gy RT, despite iRT with anti-PD-L1. This observation suggests that therapeutic strategies combining RT with T-cell-based therapies such as ICB may not be clinically effective without first finding strategies to enhance T-cell immunosurveillance. Monocytes in particular play important roles in the immune evasion/tolerance of PCa [Wu et al., 2019], and it may be that immunotherapy directed at inhibiting TAMs or MDSCs recruitment to the TIME in combination with RT are needed to improve disease control in PCa.

These experiments have several limitations. Flank tumour allografts were used, rather than orthotopic tumours, or *de novo* PCa arising within transgenic mice, which might better recapitulate the TIME of spontaneously arising PCa. Standard implanted tumour models may not be ideal for iRT studies as they may fail to properly model the physiological setting in which tolerogenic tumours arise over extended time periods. However, the flank allograft tumour approach within immunocompetent syngeneic mice was necessary to deliver iRT with follow-up and measurement of tumour growth. It is possible that the length of time between subcutaneous injection of TRAMP-C1 cells and formation of 100 mm^3 tumours, which was found to be 6-8 weeks in the conditions tested,

led to changes in the immunogenicity of these tumours, perhaps with development of immune tolerance in the animals, such that iRT was less effective. A variation in the efficacy of immunomodulation, dependent upon the timing of initiation of treatment following tumour implantation, and consistent with a decay of the initial immune response following tumour implantation, has recently been reported [Crittenden et al., 2018]. However, failure of delayed immunomodulation may be due to accumulation of a greater tumour burden or acquisition of an immunosuppressed TIME. RT may need to be continued for a greater number of fractions than 3 x 5 Gy in order to enhance the effects of anti-PD-L1. This warrants further analysis, provided animals tolerate a higher number of RT fractions over several weeks, and given that RT is administered under general anaesthetic. An additional limitation of these experiments is the absence of concomitant ADT, given that this is administered with 2 Gy RT fractions as SOC in patients. However, adding ADT would have introduced a third variable (in addition to RT and anti-PD-L1), and the TRAMP-C1 model is androgen independent. Moreover, recent clinical trials such as PACE (Prostate Advances in Comparative Evidence) [Brand et al., 2019] are investigating hypofractionated RT without ADT versus conventional RT plus ADT. It may be the case that ADT plus RT leads to enhanced anti-tumour responses through addition of anti-PD-L1, and this possibility warrants investigation in future studies.

The possibility for an iRT approach to be beneficial in patients with PCa is an important idea to test given that the 5-year biochemical relapse rate for high-risk patients is 32-70% [Cooper and Sanfilippo, 2015]. If iRT was successful then this may permit a reduction in the necessary RT dose for effective treatment, and could have clinical benefit for patients, as RT reduces quality of life due to side effects [Gaither et al., 2017; Lardas et al., 2017a; Matta et al., 2019b]. Immunotherapy is an attractive option combined with RT given recent clinical trial results where RT to the primary tumour in oligometastatic disease was observed to be associated with clinical benefit [Parker et al., 2018], suggesting possible RT-induced immunological responses which may be enhanced with iRT. However, for iRT

to be successfully used in the clinic, studies need to be performed in pre-clinical models, and in early phase first-in-man clinical trials, in order to determine the optimal timing, sequence of delivery, and type of immunomodulation to be used in iRT.

In conclusion, 3 x 5 Gy hypofractionated RT resulted in a tumour growth delay in MyC-CaP and TRAMP-C1 PCa models. 3 x 5 Gy resulted in an initial increase in TAMs and DCs, and up-regulation of PD-1/PD-L1, in the TRAMP-C1 TIME, however anti-PD-L1 combined with RT in the conditions tested did not increase tumour growth delay. These results suggest that adjuncts beyond immunomodulation, such as perhaps combination with PCa focal ablation therapies or other cancer cell-targeting treatments, which warrants evaluation in future studies, are necessary to improve the anti-tumour response from RT fraction sizes used in the clinic.

Chapter 5. Treatment of murine prostate cancer allograft models with WST-11 vascular targeted photodynamic therapy

5.1 Introduction

VTP is novel form of minimally invasive focal ablation precision surgery, which is achieved by rapid free radical-mediated destruction of the tumour vasculature, leading to focal necrosis of target tissues [Koudinova et al., 2003; Madar-Balakirski et al., 2010a; Preise et al., 2009]. VTP has been demonstrated to be effective in the focal ablation of low-risk PCa in a phase 3 RCT [Azzouzi et al., 2013c, 2015b, 2017a], and has been investigated in observational cohort studies as a salvage therapy option for patients with radio-recurrent PCa [Trachtenberg et al., 2007, 2008]. VTP involves intravenous administration of the soluble photosensitising agent WST-11, which conjugates to albumin, and is focally activated upon illumination with near infra-red light in the presence of oxygen. VTP requires the presence of functional tumour vasculature in order for the WST-11 photosensitiser to be efficiently delivered to the target tumour tissue prior to focal activation upon illumination.

The first “in house” *in vivo* treatments of murine PCa models with VTP at the Oxford Institute of Radiation Oncology (OIRO) were performed as collaborative studies between the Nuffield Department of Surgical Sciences, OIRO, the Department of Oncology, and the Weizmann Institute of Science, Israel. The *in vivo* aspect of the protocol was carefully optimised in order to deliver safe VTP treatment of pre-clinical flank allograft tumours, which specifically required mouse anaesthesia, tail vein cannulation, infusion of drug, transcutaneous delivery of near infra-red laser treatment, followed by mouse recovery and post-procedure analgesia. Training was undertaken in the Weizmann Institute of Science

(for myself and my supervisor Professor Bryant) prior to transfer of this technique to the University of Oxford, along with preparation of an “in house” bespoke VTP treatment platform and protocol in Oxford. Optimisation of the VTP treatment protocol required several iterations to ensure optimal treatment conditions, with particular emphasis on correct delivery of the WST-11 drug and laser activation, and maintenance of optimal physiological conditions for the treated mice, with measurements of their core temperature, and respiratory and heart rates, during anaesthesia. Safe recovery of the mice from anaesthesia, delivery of analgesia, and post-procedure monitoring were vital to ensure animal wellbeing post VTP. Initial pilot experiments were conducted in close collaboration with the Veterinary Medicine Department at the University of Oxford, with use of daily monitoring of treated mice using bespoke animal welfare monitoring checklists. During these initial experiments it became apparent that it was important to a) maintain core temperature as close to 37^{o}C as possible during the prolonged anaesthetic required for VTP treatment, and b) treat tumours with a minimum volume of 90 mm^3 (and ideally 100-120 mm^3), and with a depth of at least 5 mm, to prevent laser-mediated damage to the underlying thigh muscle, thus maintaining animal welfare during experiments.

5.2 Results

5.2.1 VTP treatment does not cause any thermal effects on the tumour

Light (i.e. laser alone, without prior infusion of WST-11), and dark (i.e. WST-11 infusion alone, without laser illumination), control experiments were performed by the Scherz laboratory as outlined in the introduction (**figure 1.10),** and therefore according to the principles of the 3Rs these control experiments were not repeated in Oxford. However, a

control experiment was performed using our bespoke apparatus to investigate whether a 10 minute application of the laser light on a flank tumour allograft, with or without prior infusion of WST-11, leads to a significant temperature rise within the tumour, which could cause tumour cell death and result in tumour growth delay. The temperature of the tumour was measured using a thermal camera prior to, and immediately after, application of laser light for 10 minutes, with or without prior infusion of WST-11 (**figure 5.4**). In both instances the temperature rose by approximately 1.5^{o}C. This rise in temperature is insignificant, and should not result in tumour cell death, thus excluding any possible thermal effects of the VTP treatment on tumour growth delay seen following VTP treatment of flank tumour allografts.

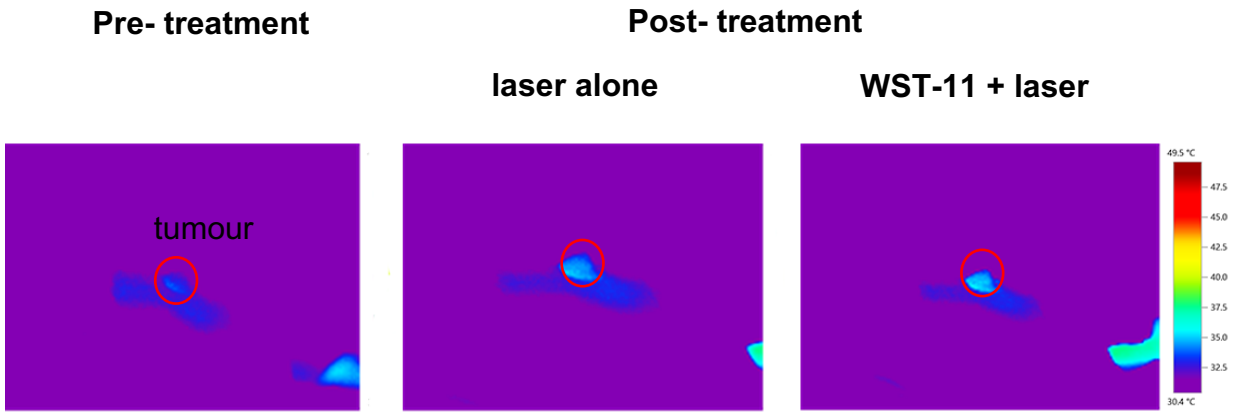


Figure 5.4. Thermal evaluation of flank tumours following laser illumination with and without prior infusion of WST-11. Flank tumour temperature does not significantly rise following exposure of flank tumour allografts to laser treatment with or without prior WST-11 infusion. *Experiment performed in collaboration with Sean Smart.*

5.2.2 VTP monotherapy induces tumour growth delay in prostate cancer flank tumour allografts

Flank TRAMP-C1 tumour allografts were treated using the 'in house' bespoke VTP platform when they reached 100-120 mm^3 volume. VTP treatment was performed with 9 mg/kg WST-11 at 120 mW/cm^2 for 600 seconds (**Figure 5.5**). Treatment of TRAMP-C1 tumour allografts with 9 mg/kg WST-11 resulted in tumour growth delay to a final tumour size of 400 mm^3 compared with untreated control tumours (**Figures 5.5A, 5.5B, 5.5C** and **5.5D**), with no significant welfare implications, however all tumours eventually recurred.

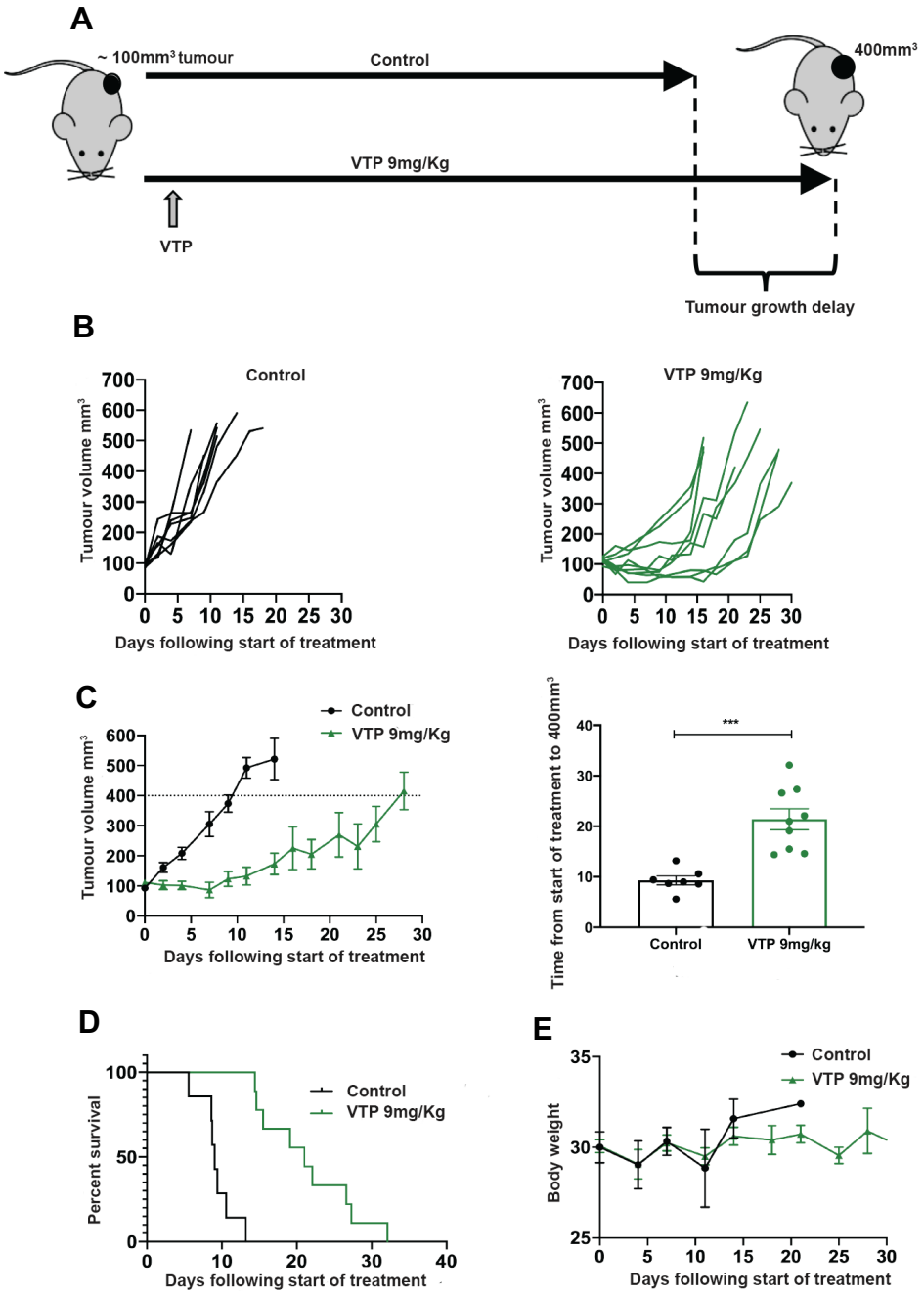


Figure 5.5. VTP causes tumour growth delay in TRAMP-C1 flank tumour allografts. (**A**) Outline schematic of treatment of subcutaneous flank TRAMP-C1 tumour allografts with VTP. (**B**) Growth kinetics of TRAMP-C1 tumours following the indicated treatments (n = 7 untreated control; n = 10 VTP 9 mg/kg WST-11, 120 mW/cm^2, 600 seconds). (**C**) Tumour growth delay to ≥400 mm^3 analysis of TRAMP-C1 allograft tumours treated with VTP 9 mg/kg WST-11, 120 mW/cm^2, 600 seconds. Data are presented as mean tumour volume ± SEM and analysed using ordinary one-way ANOVA with Tukey's post hoc adjustment for multiple comparisons. *p < 0.05; **p < 0.01; *** p < 0.001, ****p < 0.0001. **(D)** Treatment of TRAMP-C1 tumour allografts with 9 mg/kg WST-11, 120 mW/cm^2, for 600 seconds resulted in enhanced survival to a tumour size of 400 mm^3 compared with untreated control tumours. **(E)** Median (range) body weight at start of experiment: untreated control = 21.2 g (20.2–23.5 g); VTP 9 mg/kg = 20.9 g (18.5–23.8 g).

5.3 Discussion

This chapter describes the application of WST-11-based VTP treatment to a murine PCa xenograft model, using bespoke equipment constructed 'in house' in order to deliver VTP treatment in a small animal facility. The treatment protocol underwent iterations over several months prior to its finalisation, to ensure safety and effectiveness. The successful delivery of the VTP protocol is based upon the photochemical properties of the photosensitiser and its damage to the tumour vasculature, coupled with ensuring the optical treatment conditions for the mice, correct handling of the WST-11 drug, and careful post-procedure monitoring of the mice along with delivery of adequate analgesia post-procedure. Thermal monitoring of the tumours during treatment did not reveal any changes in temperature that could result in anti-tumour effects, consistent with previous reports stating that the anti-tumour activity of WST-11 VTP is secondary to photodynamic induction of local hypoxia and necrosis [Koudinova et al., 2003]. WST-11-mediated VTP was demonstrated to be safe when applied to xenograft PCa flank tumours, with minimal effects on animal welfare. WST-11 VTP results in an acute inflammatory response, together with a rapid reduction in size of the tumour mass. Transcutaneous VTP treatment results in the development of an eschar by 72 hours, which extends deep into the tumour core. These changes were consistent with observations made by our collaborators at the Weizmann Institute of Science in other animal tumour models [Preise et al., 2003; Vilensky et al., 2005]. The surrounding non-illuminated tissues remained intact. Delivery of transcutaneous WST-11 VTP treatment to a TRAMP-C1 flank tumour xenograft model resulted in a mean tumour delay to 400 mm^3 of 22 days, compared to 9 days in untreated controls. These observations are consistent with results from our collaborators, who have reported tumour growth delay (and in some cases complete tumour cure) following WST-11 VTP treatment in various different flank tumour xenograft models [Koudinova et al., 2003; Plaks et al., 2004; Preise et al., 2009; Vilensky et al.,

2005]. Taken together, these results suggest that VTP treatment can be delivered safely, and can cause a significant tumour growth delay, with minimal implications on animal wellbeing, in a similar manner to RT. Safe and effective establishment of a bespoke VTP treatment platform thus provided an opportunity to combine this treatment modality with RT, in order to investigate any potential additive or synergistic anti-tumour effects, which could further enhance tumour growth delay.

Chapter 6. Combining radiotherapy with vascular targeted photodynamic therapy in murine prostate cancer allograft models

6.1 Introduction

The tumour vasculature is typically abnormal, and is characterised by blood vessel immaturity, increased permeability, increased interstitial pressure, reduced peri-vascular supporting cell number and function, aberrant vessel branching, and inefficient blood flow. These properties can impair therapeutic drug delivery and reduce the efficacy of treatment [Azzi et al., 2013; Hanahan and Weinberg, 2011a]. RT can alter several aspects of the tumour microenvironment, including the transient restoration of tumour blood vessel function, resulting in improved perfusion and increased oxygenation of tumour tissue, particularly when RT is delivered in low-dose fractions of 2-5 Gy [Yoshimura et al., 2013]. The restoration of blood vessel function following low-dose fractionated RT involves several mechanisms such as 'pruning' of abnormal vessels, reduced vessel tortuosity, improved perivascular supporting cell coverage and function, restoration of the perivascular basement membrane, and generation of a pressure gradient between the intravascular and interstitial compartment, leading to a more normal vessel function, which ultimately improves perfusion [Barker et al., 2015]. The mechanisms involved in the vascular response to RT are complex. However, evidence from several pre-clinical studies suggests that RT in low-dose fractions (2-5 Gy) appears to exert positive effects on the tumour vasculature, improving tissue perfusion and resulting in increased oxygenation of tumour tissue [De Keyzer *et al.*, 2009; Potiron *et al.*, 2013; Kleibeuker *et al.*, 2016]. The enhanced effect of RT on tumour perfusion has several implications. On the one hand, it may promote tumour growth and increased metastatic potential. Conversely, improved tumour perfusion may have several anti-

tumour effects, such as improved drug delivery and enhanced anti-tumour immune responses. Given that effective VTP treatment requires delivery of the WST-11 photosensitiser drug to target tissues via the tumour vasculature, it would be of particular interest to investigate the effects of low-dose fractionated RT on the tumour vasculature of pre-clinical PCa models ahead of further experiments combining RT and VTP. Transient vascular changes post-RT may influence the anti-tumour effects of VTP. First, it would make sense to assume the effectiveness of VTP depends on the photosensitiser reaching the tumour through its vascular network. However, it has been shown that immature blood vessels characterised by endothelial cell dysfunction resulting in increased vascular permeability, together with the absence of contractile smooth muscle elements, makes them preferentially susceptible to VTP [Madar-Balakirski et al., 2010b; Nogueira et al., 2020]. Madar-Balakirsi *et al* demonstrated that the unusual fragility of the tumour vasculature makes them selectively susceptible to VTP-induced collapse. The same study showed that adjacent healthy tissue with normal vasculature remained functional with intact vessels, despite exposure to the same ablative process. The observation that immature blood vessels are more susceptible to VTP has also been made with other vascular targeted therapies, such as anti-VEGFR therapy. It is therefore possible that any post-RT vascular effects may make VTP less effective. Therefore, understanding the effects of low-dose fractionated RT on the vasculature of pre-clinical PCa allograft tumour models will be key in understanding any potential mechanisms of synergy of a combined RT and VTP treatment approach for PCa.

Whilst VTP has been investigated in small observation cohort studies of patients with radio-recurrent PCa, to date the application of VTP shortly after RT (i.e. before the tumour has recurred) has not been investigated. It may be possible, and indeed it is attractive, to combine fractionated RT with VTP in treating PCa. This may obviate the need for neo-adjuvant and/or concomitant ADT, as well as reduce the dose of conventional fractionated RT administered. The conception of an organ-sparing strategy in PCa management,

which is directed towards a focal lesion or takes a hemi- gland approach in order to deliver effective tumour control and/or cure with reduced toxicity compared to whole gland treatment, is becoming an increasing focus of PCa research, as it may lead to improved quality of life compared against current standard-of-care whole gland therapy [Ahmed et al., 2009; Valerio et al., 2014, 2017a].

The experiments descried herein aimed to investigate the effects of a low dose fractionated RT regime on the vasculature of PCa flank allograft tumours. RT and VTP were then combined in a multi-modality therapy approach to PCa treatment in a pre-clinical model, in order to investigate the hypothesis that sequential combination treatment may enhance tumour growth delay compared to RT or VTP monotherapy. If sequential combined RT and VTP was to enhance tumour control versus monotherapy, this pre-clinical data could potentially inform future early phase first-in-man clinical trials. Given that the treatment parameters for VTP in terms of WST-11 photosensitiser dose and activation have been established for optimal targeted tumour ablation, along with the fact that fractionated RT for PCa is well established, it could be feasible, based on pre-clinical data, to combine these treatments in an early phase clinical trials in due course, if this approach was safe and effective in pre-clinical models. The hypothesis that sequential delivery of RT followed 7 days later by VTP improves tumour control, compared to monotherapy with RT or VTP alone, was specifically tested in the TRAMP-C1 flank PCa tumour allograft model.

6.2 Results

6.2.1 Radiotherapy improved perfusion in prostate cancer flank tumour allografts

In order to investigate whether fractionated RT influences perfusion in TRAMP-C1 flank tumour allografts at 7 days following the first fraction of RT, dynamic contrast enhanced magnetic resonance imaging (DCE-MRI) analysis was performed (**Figure 6.1A**). This revealed that fractionated RT resulted in enhanced perfusion, as measured by the iAUC at 90 seconds after Gadolinum (Gd) injection, 7 days after initiation of fractionated RT in TRAMP-C1 flank tumour allografts (**Figure 6.1B**). Gd contrast-induced enhancement of the fraction of voxels assessed by DCE- MRI was indicative of an improvement of tumour perfusion post-fractionated RT, and this enhanced perfusion occurred predominantly in the core (the central 1/5th of the tumour segmentation by volume) of the tumour (**Figure 6.1B & 6.1C**). In order to investigate whether this fractionated RT-induced enhanced perfusion effect could be seen using the same imaging modality in a second tumour model, this experiment was repeated using MyC-CaP tumours in FVB mice. A similar effect on tumour perfusion at 7 days post-fractionated RT was seen in MyC-CaP tumours (**Figure 6.1D & 6.1E**). Where paired pre- and post fractionated RT treatment DCE-MRI iAUC90 image maps demonstrated enhanced perfusion in TRAMP-C1 flank tumour allografts, corresponding tissue samples demonstrated decreased hypoxia as demonstrated by pimonidazole staining (**Figure 6.2B**).

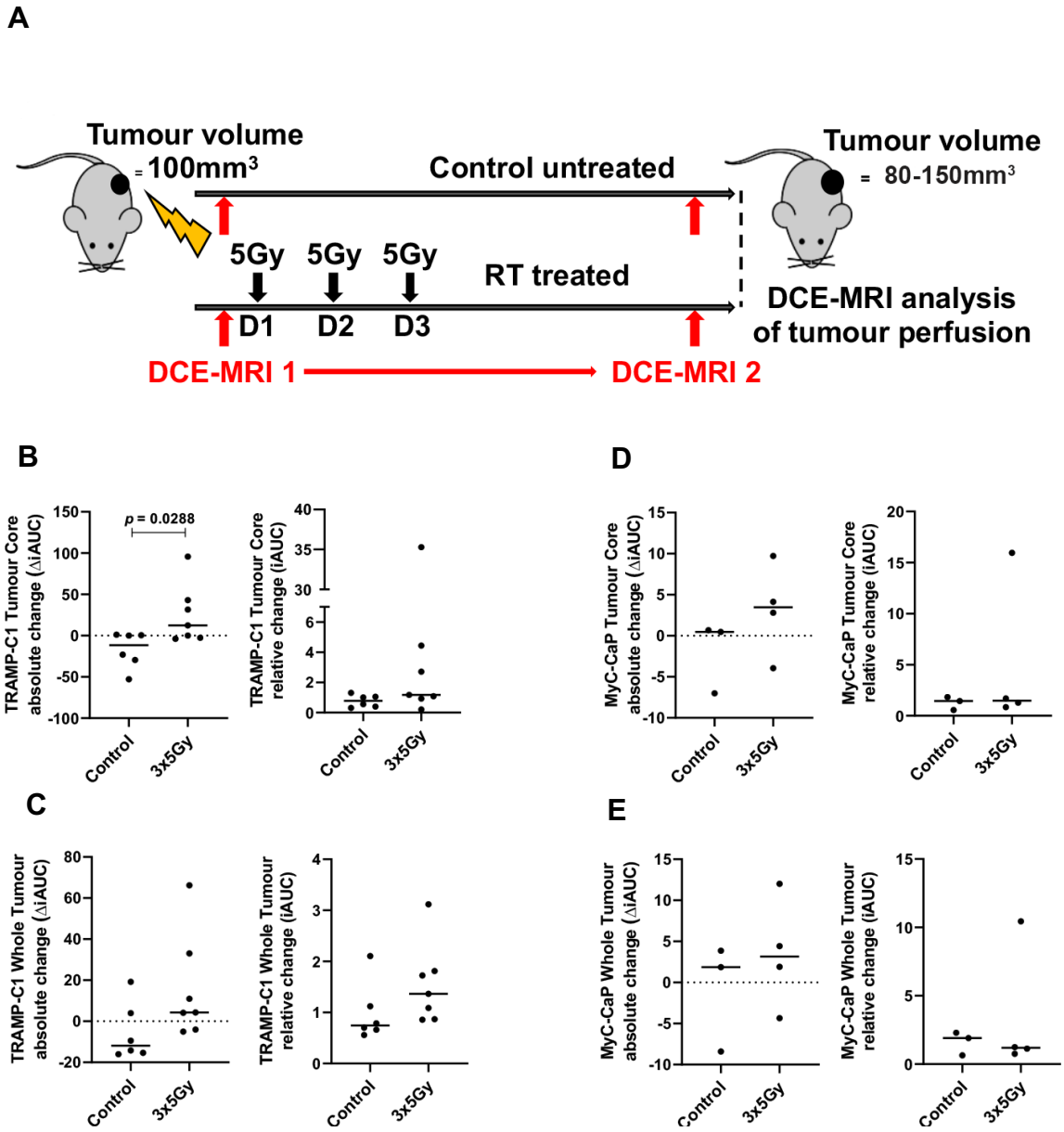


Figure 6.1. 3 x 5 Gy RT improves vascular perfusion of flank TRAMP-C1 prostate cancer tumour allografts as demonstrated using DCE-MRI. (**A**) Outline schematic of sequential DCE-MRI imaging of flank TRAMP-C1 tumour allografts immediately pre- and 7 days post treatment. (**B**) Analysis of changes in the iAUC in paired image samples pre- and post-treatment revealed a significant increase in contrast uptake in the central core of TRAMP-C1 tumours, (**C**) and a trend towards an increase in contrast uptake in the entire TRAMP-C1 tumour, following treatment versus control tumours. Analysis of paired image samples pre- and post treatment in MyC-CaP tumours revealed a similar trend towards increase in contrast uptake in both the (**D**) central core and the (**E**) entire tumour. Data are presented on a scatter plot with a line representing the median and analysed using a two-tailed unpaired t-test (n = 6 untreated control tumours; n = 7 3 x 5 Gy treated tumours). Median (range) body weight at start of experiment: untreated control tumours = 22.2 g (21.0–24.7 g); 3 x 5 Gy treated tumours = 21.5 g (20.0–25.6 g). *Experiments performed in collaboration with Hanna J Sjoberg, Veerle Kersemans, Danny Allen, Sean Smart and Paul Kinchesh.*

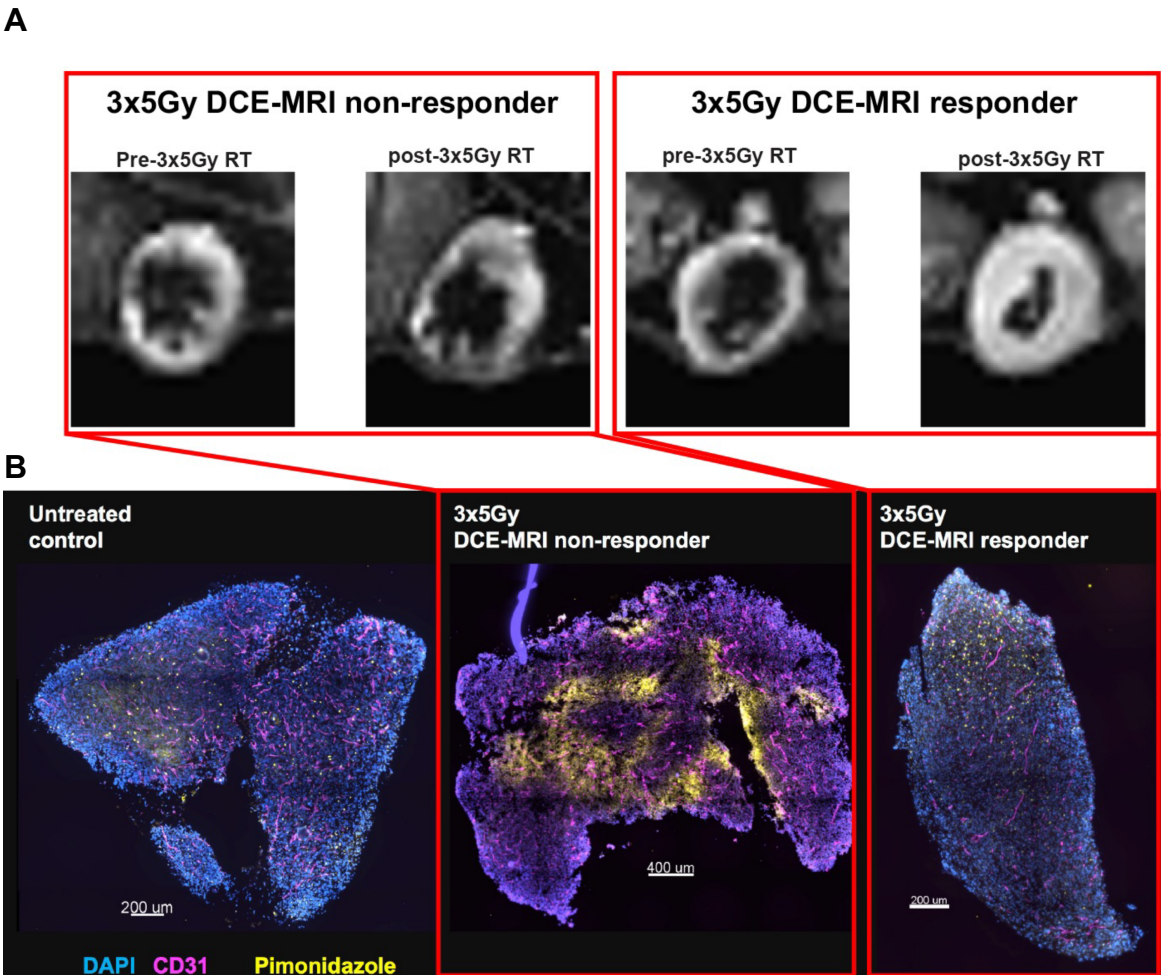


Figure 6.2. Representative examples of DCE-MRI images and pimonidazole staining showing pre and post 3 x 5 Gy RT effects on TRAMP-C1 flank tumour perfusion and hypoxia. (A) In the 3 x 5 Gy RT responder, improved perfusion can be visualised by the greater extent of Gadolinum contrast extending towards the tumour core. (**B**) Hypoxia, measured by pimonidazole staining corresponds to less well perfused tumour areas as seen on DCE-MRI. *Experiments performed in collaboration with Hanna J Sjoberg, Danny Allen and Anette Magnusson.*

6.2.2 Combination therapy with sequential RT and VTP suppressed tumour growth to a greater extent than either treatment alone

To test the hypothesis that the improved tumour perfusion induced by 3 x 5 Gy RT might improve the effects of VTP on tumour growth control, the effects of sequential treatment of TRAMP-C1 flank allograft tumours with 3 x 5 Gy RT followed by VTP were studied in syngeneic immunocompetent C57BL/6 mice (**figure 6.3**). In order to administer the VTP

at the time of the observed fractionated RT-induced increased vascular perfusion, VTP was administered seven days following initiation of fractionated RT (**figure 6.3A**). Whilst pilot studies with VTP as monotherapy had established that 7 mg/kg WST-11 had a lesser effect than 9 mg/kg in terms of inducing an anti-tumour effect as demonstrated by tumour growth delay experiments, the sequential effects of 3 x 5 Gy RT and VTP using both the 7 mg/kg and 9 mg/kg WST-11 dose were tested, in order to ascertain whether any particular combination might be most effective in enhancing a resultant tumour growth delay. The tumour growth delay effects of 3 x 5 Gy RT followed sequentially at 7 days by either 7 mg/kg or 9 mg/kg WST-11 VTP were therefore explored. The sequential combination of 3 x 5 Gy RT followed at 7 days by 9 mg/kg WST-11 VTP delayed tumour growth significantly compared to 9 mg/kg WST-11 VTP alone, and led to a trend towards enhanced tumour growth delay compared to 3 x 5 Gy RT alone (**figures 6.3B &6.4**). The sequential combination of 3 x 5 Gy RT and 7 mg/kg WST-11 VTP significantly increased tumour growth delay compared to either 7 mg/kg WST-11 VTP alone or 3 x 5 Gy RT alone (**figures 6.3B &6.4**). In a survival analysis, sequential combination of 3 x 5 Gy RT and 9 mg/kg WST-11 VTP significantly enhanced survival to a tumour volume of 400 mm^3 compared to 9 mg/kg WST-11 VTP alone, or 3 x 5 Gy RT alone. Similarly, the sequential combination of 3 x 5 Gy RT and 7 mg/kg WST-11 VTP significantly enhanced survival to a tumour volume of 400 mm^3 compared to 7 mg/kg WST-11 VTP alone, or 3 x 5 Gy RT alone. Sequential combination of 3 x 5 Gy RT and 7 mg/kg WST-11 led to the longest survival to 400 mm^3, with one animal being cured. 7 mg/kg WST-11 appeared to have greater efficacy than 9 mg/kg WST-11 when combined with prior 3x5 Gy RT (**figure 6.4C**).

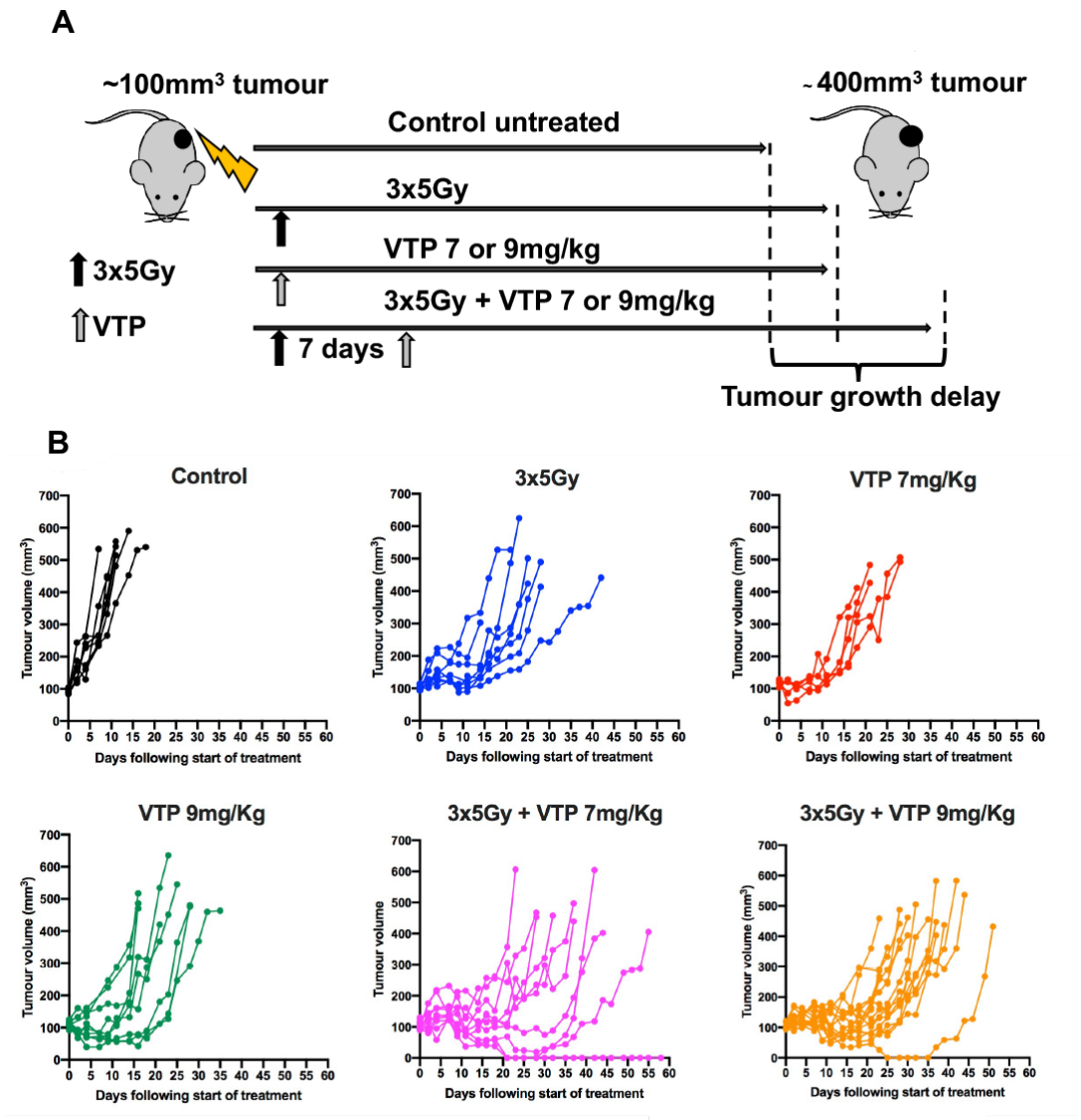


Figure 6.3. Multimodality therapy with 3 x 5Gy RT followed at 7 days by VTP causes tumour growth delay in TRAMP-C1 flank tumour allografts presented as individual tumour growth delay kinetics. (**A**) Outline schematic of treatment of tumours with 3 x 5 Gy RT, VTP (7 or 9 mg/kg WST-11), or a sequential combination of 3 x 5 Gy RT followed at 7 days by VTP (7 or 9 mg/kg WST-11). (**B**) Individual tumour kinetics of TRAMP-C1 flank tumours treated as described above. Numbers per group: control n = 7, 3 x 5 Gy RT n = 8, VTP 7 mg/kg n = 5, VTP 9 mg/kg n = 9, 3 x 5 Gy and VTP 7 mg/kg n = 10, 3 x 5 Gy and VTP 9 mg/kg n = 15. Median (range) body weight at treatment: control = 21.1 g (20.8 – 22.1 g), 3 x 5 Gy = 21.1 g (19.8 – 24.3 g), VTP 7 mg/kg = 21.6 g (20.8– 23.8 g), VTP 9 mg/kg = 20.9 g (18.5 – 23.8 g), 3 x 5 Gy and VTP 7 mg/kg = 21.9 g (18.9 – 24.3 g), 3 x 5 Gy and VTP 9 mg/kg = 21.3 g (19.6 – 23.8 g. *Experiments performed in collaboration with Hanna J Sjoberg.*

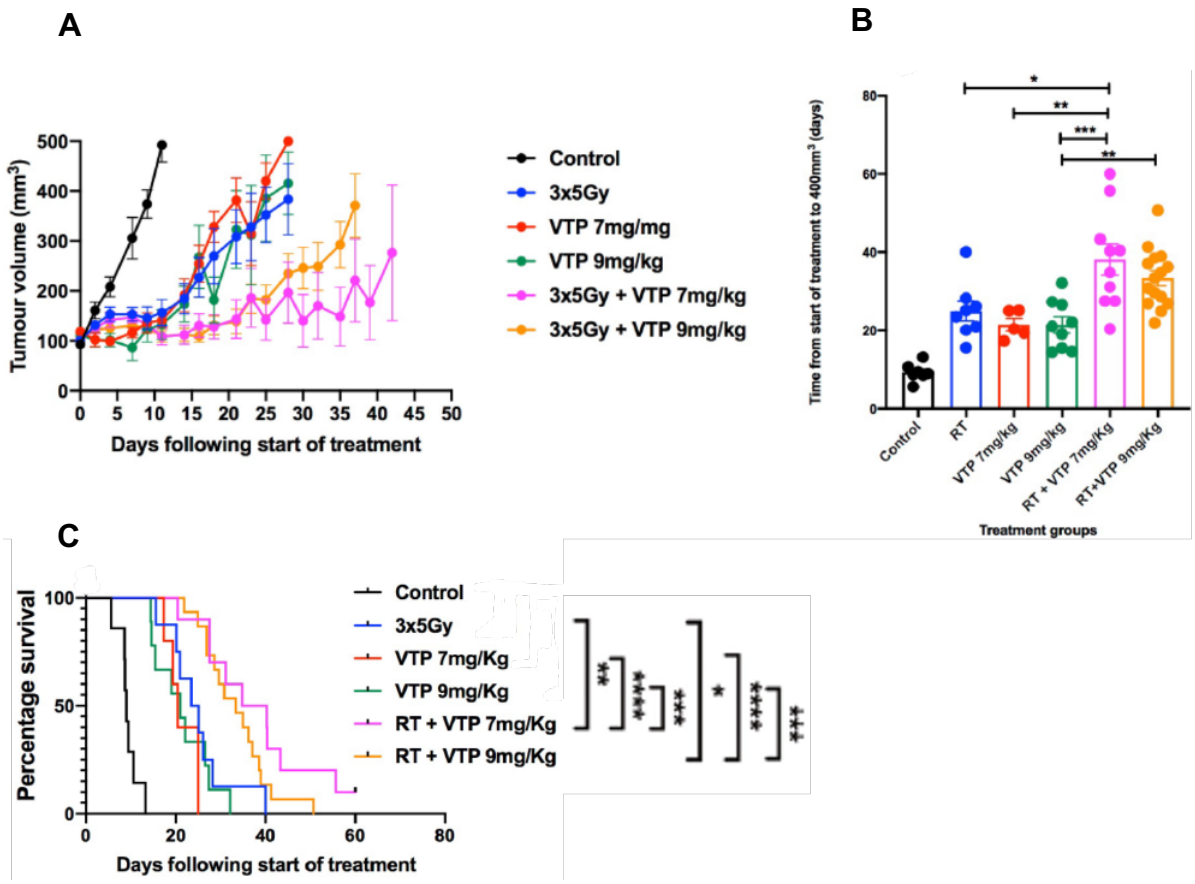


Figure 6.4 Multimodality therapy with 3 x 5 Gy RT followed at 7 days by VTP causes tumour growth delay in TRAMP-C1 flank tumour allografts (**A**) grouped tumour growth kinetics, (**B**) mean ± SEM growth delay to ≥400 mm^3 and (**C**) survival to ≥400 mm3 using Kaplan-Meier curves. Data were analysed using ordinary one-way ANOVA with Tukey's *post hoc* adjustment for multiple comparisons (**C**), and Log-Rank (Mantel-Cox) test. * p<0.05; ** p<0.01; *** p<0.001; **** p<0.0001. *Experiments performed in collaboration with Hanna J Sjoberg.*

Further analysis of this data demonstrated that the TRAMP-C1 tumour growth delay effects of the VTP component of treatment were enhanced following 3 x 5 Gy RT, compared against VTP alone. When analysing the time for tumour regrowth at the time of VTP delivery to ≥400 mm3 end-point, a trend was observed towards enhanced delay in tumour growth for VTP following 3 x 5 Gy RT, compared to VTP alone for 9 mg/kg (**figure 6.5A**) and 7 mg/kg (**figure 6.5B**) WST-11. A combined analysis of 7-9 mg/kg WST-11 VTP alone versus combined sequential 3 x 5 Gy RT and 7-9 mg/kg WST-11 (**figure 6.5C**), including all animals in this experiment, showed a significant enhancement in tumour growth delay following VTP delivered 7 days post-3 x 5 Gy RT, compared to VTP alone.

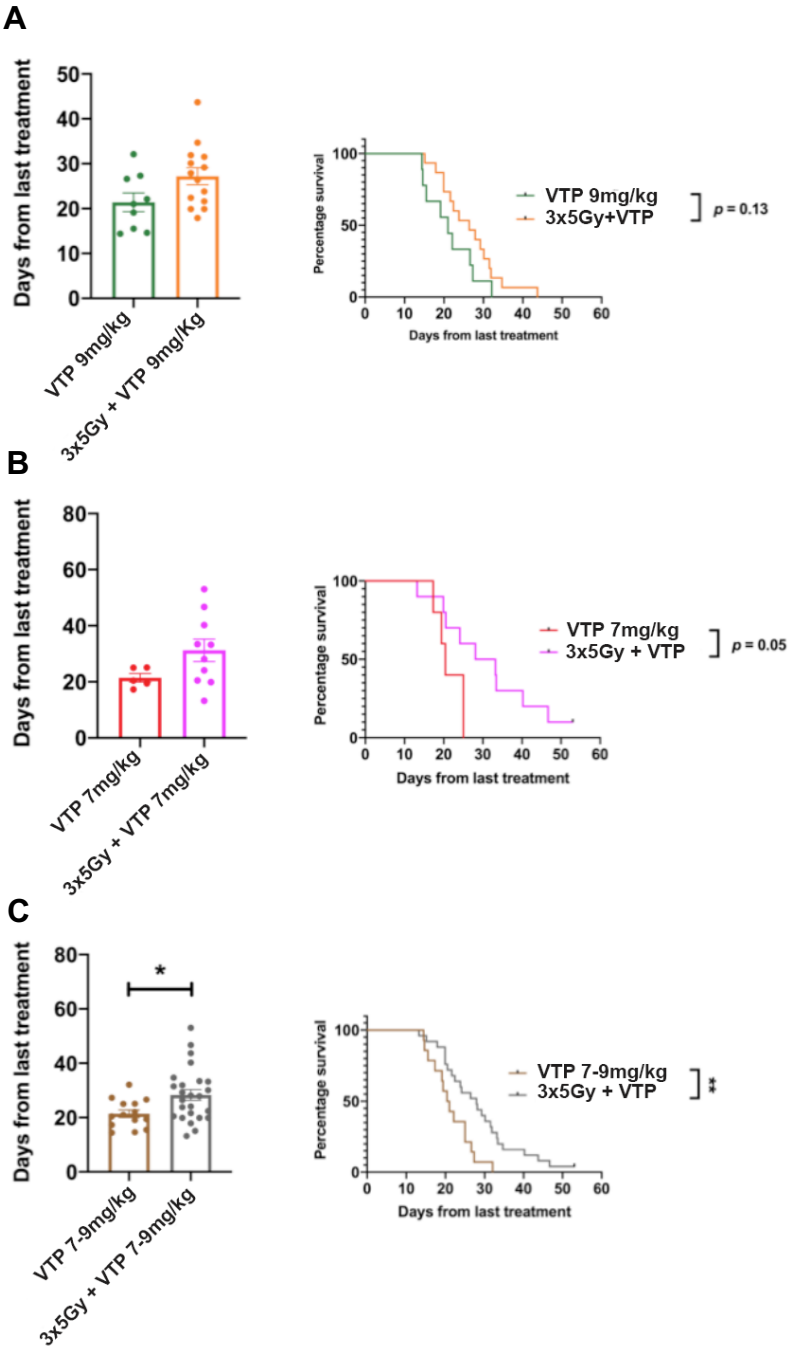


Figure 6.5. 3 x 5 Gy RT improves efficacy of subsequent VTP delivered 7 days later. (**A-B**) Analysis of time for tumour regrowth from 150mm^3 at VTP delivery to the 400mm^3 endpoint revealed a trend towards enhanced tumour growth delay for VTP post 3x5Gy RT compared toVTP alone for 9mg/kg and 7mg/kg WST-11. (**C**) Combined analysis of mice treated with 7-9mg/Kg WST-11 VTP alone versus combined sequential 3x5Gy RT and 7-9mg/Kg WST-11 revealed a significantly enhanced tumour growth delay following administration of VTP if delivered 7 days post 3x5Gy RT, compared with VTP alone. Data were analysed using a two-tailed unpaired t test for the bar char and long-rank (Mantel-Cox) test for the Kaplan-Meier curves |*p<0.05; **p<0.01.

6.2.3 VTP alone or in combination with 3 x 5 Gy RT causes changes in the tumour immune microenvironment

To investigate the effects of 3 x 5 Gy RT followed by VTP on the TIME, FACS analysis of tumours was performed as previously described at the tumour endpoint of 400 mm^3, or at 12 days following VTP treatment (i.e. on day 19 post initiation of treatment). Day 12 was chosen following several pilot experiments at different earlier timepoints such as day 4 and 7 post VTP. Due to the initial tumour necrosis caused by VTP, FACS analysis at these early timepoints revealed high numbers of dead cells, and a paucity of an immune infiltrate, precluding accurate FACS analysis.

FACS analysis at 4 and 7 days respectively revealed primarily dead cells and an absence of any immune infiltrate (data not shown). FACS analysis at the 'early' day 12 timepoint demonstrated that following VTP alone, there was a reduction in cells expressing the general leucocyte marker $CD45^+$ compared to the other treatments (**figure 6.6**). This is likely due to tumour necrosis immediately after VTP due to tumour vascular occlusion preventing the infiltration of immune cells or destruction of the existing immune infiltrate. Interestingly, in the combination arm of 3 x 5 Gy RT and VTP, this reduction in immune infiltrate was not demonstrated, even though in both arms of the experiment FACS analysis was performed 12 days after VTP. The observed reduction in the $CD45^+$ immune infiltrate following VTP alone appeared to be due to a reduction in the proportion of $CD11b^+F4/80^+$ TAMs and M-MDSCs (**figure 6.6A**). In the 3 x 5 Gy RT and VTP combination arm this reduction in the proportion of $CD11b^+F4/80^+$ TAMs was not demonstrated, however there was a non-significant trend towards a reduction in the proportion of M-MDSCs. At the 12 day timepoint, combined 3 x 5 Gy RT and VTP treatment resulted in an increased proportion of $CD45^+CD3^+CD4^+$ expressing T-cells, compared to no treatment or 3 x 5 Gy RT alone. This was also the case when compared

to VTP alone, although this observation did not reach statistical significance. In addition, combination treatment with 3 x 5 Gy RT and VTP resulted in an increased proportion of $CD11b^{+}CD11c^{+}MHCII^{+}$ DCs, which was significant when compared to VTP alone. A trend towards significance was demonstrated when compared to untreated control and 3 x 5 Gy RT alone. Combination treatment also resulted in a non-significant trend in the proportion of $CD45^{+}CD3^{+}CD8^{+}$ cytotoxic T-cells. This data is preliminary and requires validation in greater number of samples, however it suggests that there may be anti-tumour immunogenic effects following VTP alone or in combination with prior RT, with a decreased proportion of immunosuppressive cells such as TAMs and MDSCs, and an increased proportion of APCs such as DCs, together with increased proportion of both CD4+ T-helper calls and CD8+ cytotoxic T-cells.

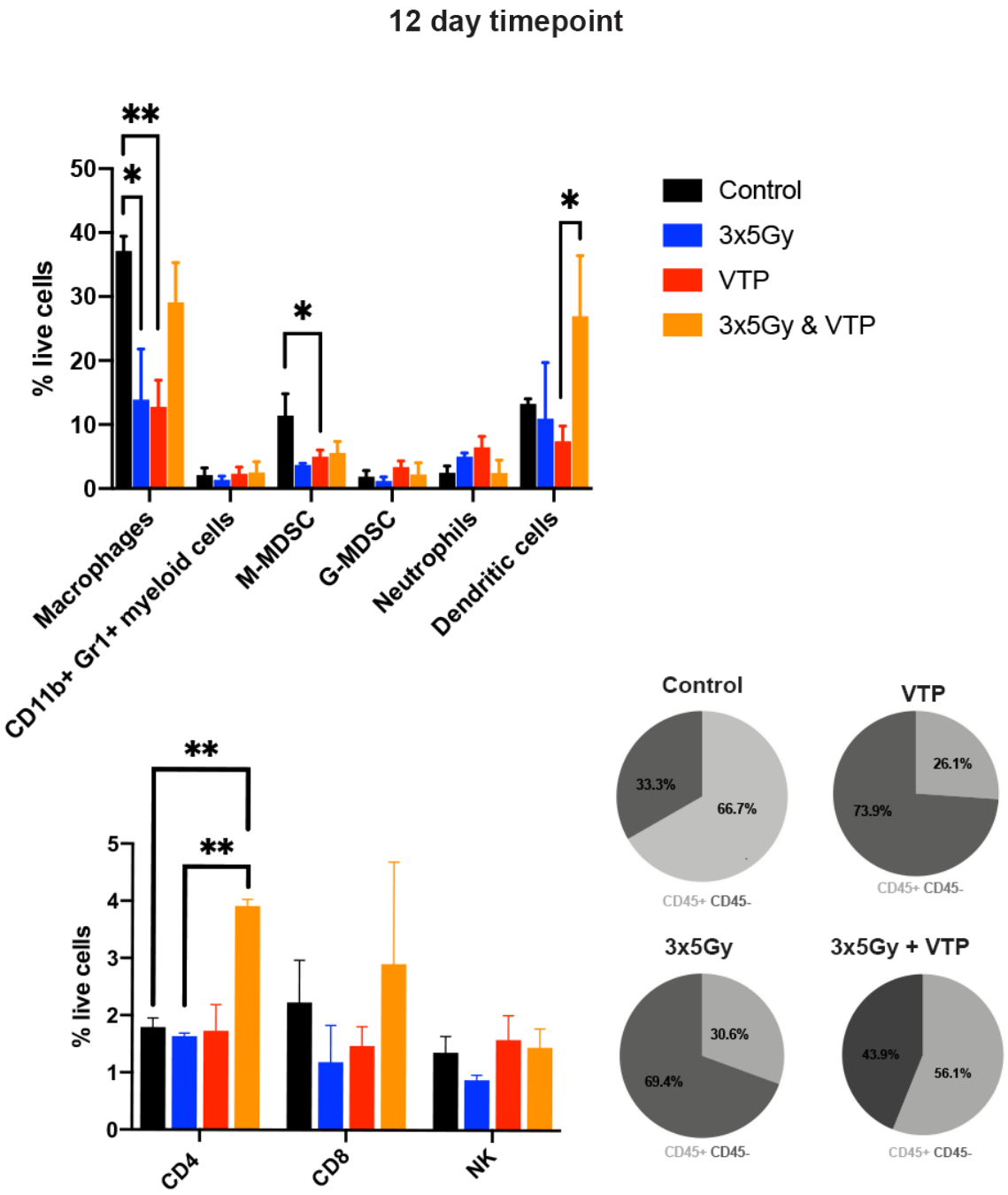


Figure 6.6. FACS analysis of the tumour immune microenvironment of TRAMP-C1 tumour allografts at the 12-day timepoint post initiation of VTP compared to untreated controls and 3 x 5 Gy RT-treated tumours. Pie charts represent the proportion of $CD45^+$ leucocytes within the total population of live cells. The reduced proportion of $CD45^+$ cells is attributed to a reduction in macrophages and M-MDSCs following VTP. VTP combined with 3 x 5 Gy RT causes an increased proportion in DCs and $CD4^+$ T-cells. FACS data are presented as mean percentage of total live cells ± SEM and analysed by the unpaired t-test (n = at least 2 independent tumour samples analysed). *p<0.05; **p<0.01.

FACS analysis at the 'late' tumour endpoint of tumour growth to 400 mm^3 showed normalisation of the tumour microenvironment, with a similar proportion of $CD45^+$ expressing cells between control, VTP, 3 x 5 Gy RT, and sequential combined 3 x 5 Gy RT and VTP treatment arms. The reduction in the proportion of $CD11b^+F4/80^+$ TAMs following VTP was also observed at this timepoint, and was noted following 3 x 5 Gy RT and VTP combination treatment. An increased proportion of $CD45^+Ly6G^+$ neutrophils was noted after VTP compared to control untreated tumours. This may be due to the increased tumour necrosis caused by VTP, attracting phagocytotic neutrophils to clear necrotic cells. A reduction in the proportion of $CD45^+CD3^+CD8^+$ T-cells was demonstrated at this 'late' timepoint following VTP.

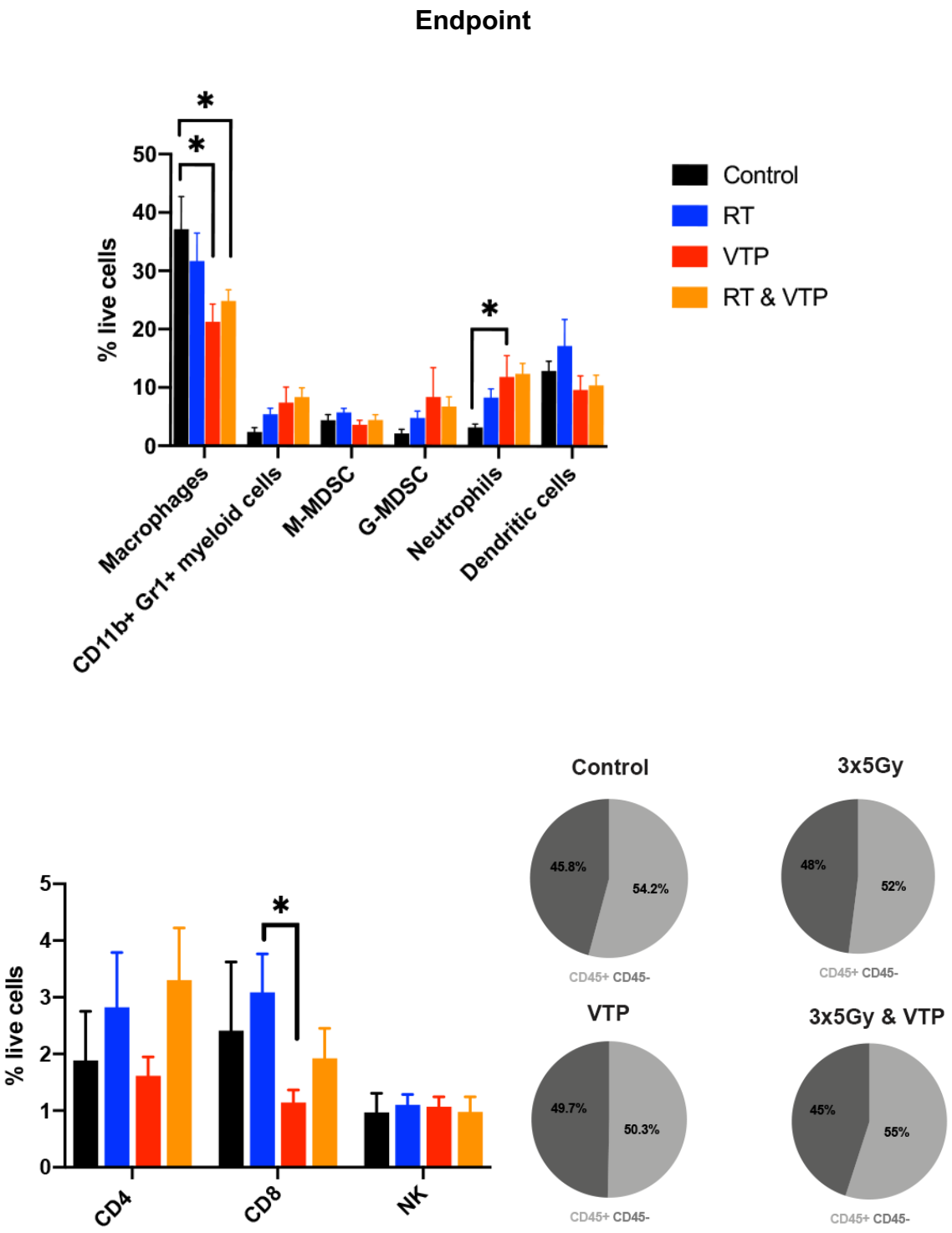


Figure 6.7. VTP and its combination with 3 x 5 Gy RT immune effects at the ≥400 mm^3 endpoint in TRAMP-C1 tumour allografts. FACS analysis at this timepoint shows persistent reduction in the proportion of macrophages in VTP treated tumours. VTP treated tumours exhibit a greater proportion of neutrophils at this 'late' time point in addition to a reduction in the proportion of CD8$^+$ infiltrating cytotoxic T-cells. FACS data are presented as mean percentage of total live cells ± SEM and analysed by the unpaired t-test (n = at least 4 independent tumour samples analysed). *p<0.05.

6.2.4 Combination therapy of RT with VTP does not result in abscopal anti-tumour effects in a bilateral prostate cancer tumour model compared to VTP monotherapy

To investigate whether the anti-tumour immune changes observed following VTP, and following the combination of VTP with prior 3 x 5 Gy RT, are capable of inducing an abscopal anti-tumour immune response, a bilateral TRAMP-C1 flank tumour model was developed in syngeneic C57BL/6 mice. The first tumour to reach 100 mm^3 was treated with 9 mg/kg VTP alone, or 3 x 5 Gy RT followed by 9 mg/kg VTP, as described in previous experiments (**figure 6.8A**). The volume of the contralateral untreated tumour was measured in both treatment arms. The endpoint was reached when the combined tumour volume reached just below 1000 mm^3 in order to comply with the *in vivo* experimental regulations. At that point FACS analysis was performed on the contralateral untreated tumour. No difference was observed in tumour growth delay of the contralateral untreated tumour between the two treatment arms, as demonstrated by tumour volume growth charts over time, rate of growth by measuring the K constant, and survival curves (**figure 6.8B & C**).

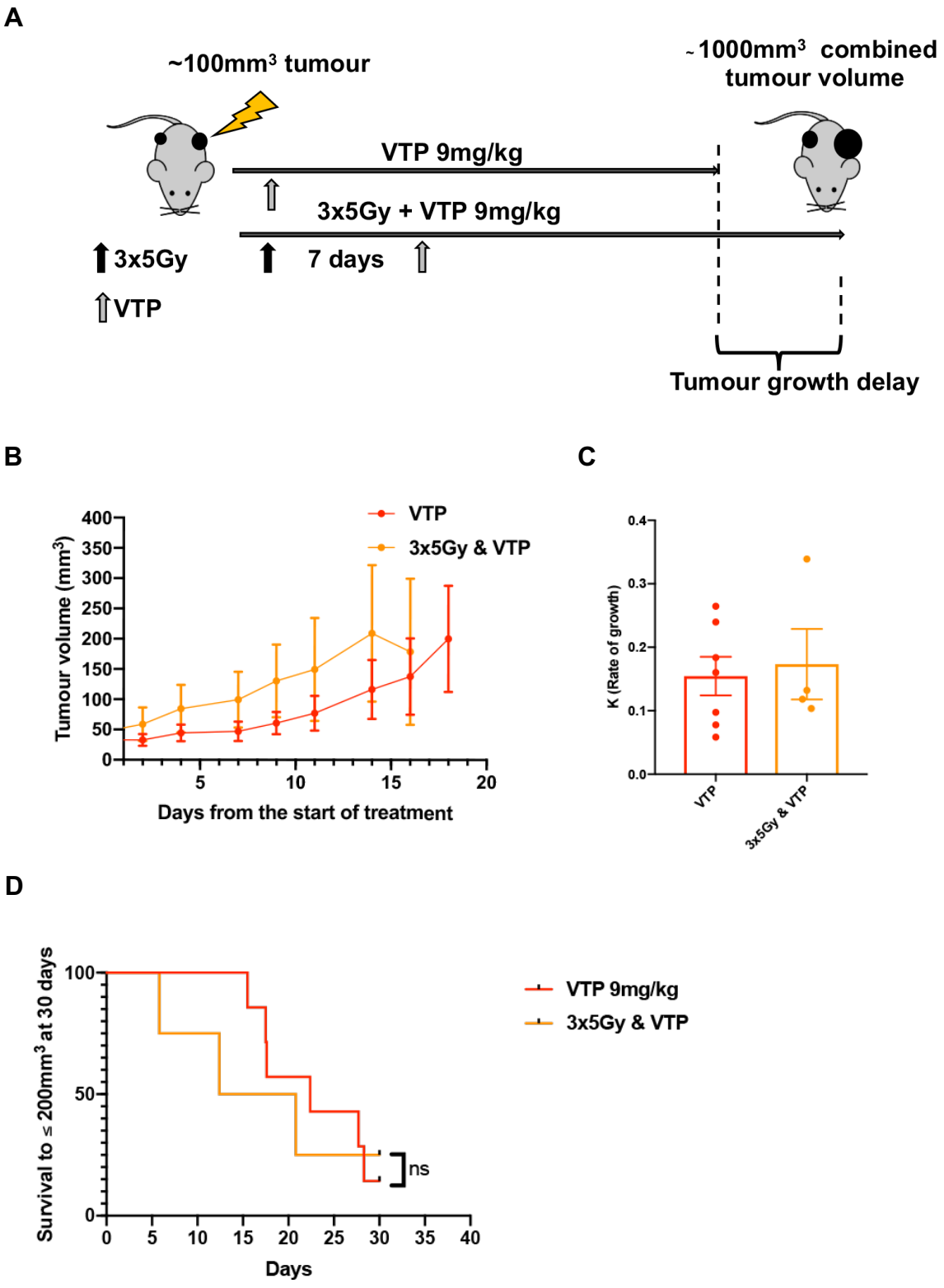


Figure 6.8. **Combination therapy with 3 x 5 Gy RT and VTP in a bilateral tumour model does not cause tumour growth delay in the contralateral untreated tumour**. **(A)** Outline schematic of treatment of TRAMP-C1 tumours in a bilateral flank tumour model with VTP or its combination with 3 x 5 Gy RT. **(B&C)** Growth kinetics of TRAMP-C1 tumours following the indicated treatments (n=7, VTP; n=4, 3 x 5 Gy RT & VTP). Data are presented as **(B)** mean tumour volume ± SEM over time from the start of treatment and as **(C)** rate of growth (K constant) of the untreated contralateral tumours. **(D)** Days from start of treatment to growth of contralateral untreated tumour to 200 mm^3 presented as a survival curve between the two different treatments.

FACS analysis of the contralateral tumours following 3 x 5 Gy RT & VTP, or VTP alone, was performed once the combined total volume of both tumours reached just below 1000 mm^3. Analysis showed an overall increased $CD45^+$ immune infiltrate in the 3 x 5 Gy RT and VTP arm, compared to the VTP monotherapy group. Overall, there was a non-significant trend towards an increased proportion of immune cells across all different myeloid and lymphoid immune subtypes studied apart from $CD45^+CD3^+CD4^+$ T-cells (**figure 6.9A & B**).

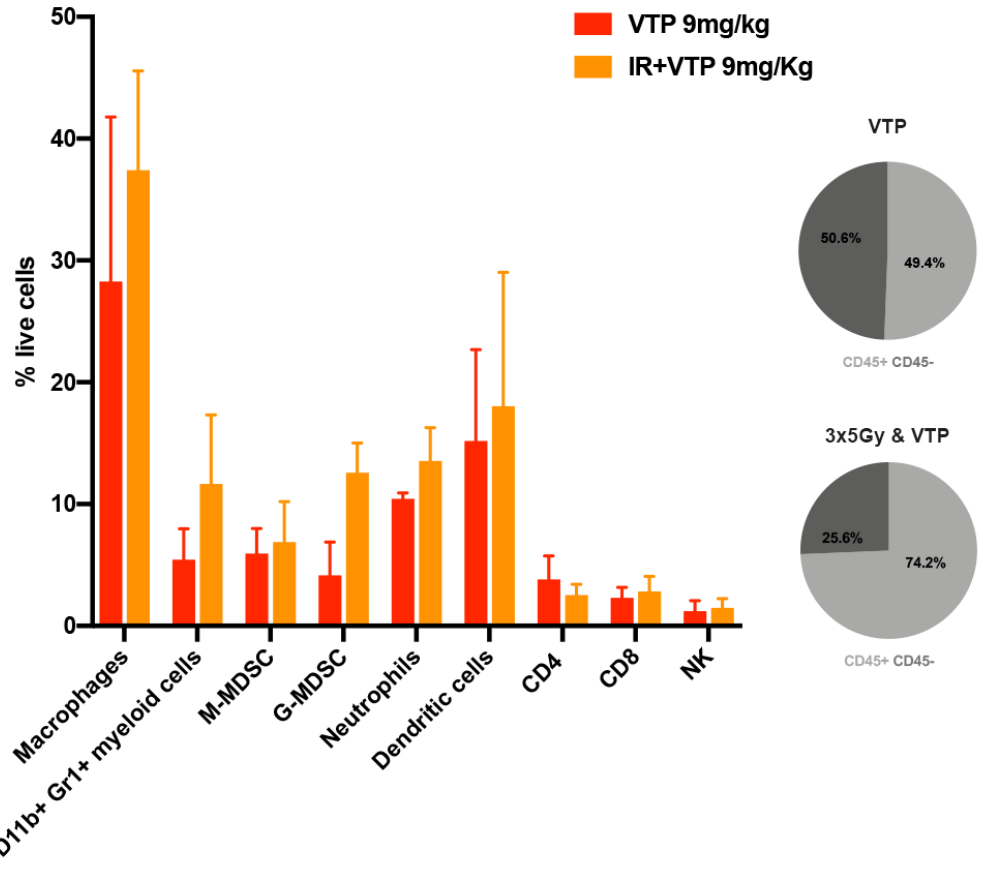


Figure 6.9. FACS analysis of contralateral untreated tumours following 3 x 5 Gy RT and VTP, or VTP alone. FACS analysis of the contralateral untreated tumours showed a trend towards an increased proportion of immune cell infiltrate across most myeloid and lymphoid immune cells of interest in the 3 x 5 Gy RT and VTP treatment arm. FACS data are presented as mean percentage of total live cells ± SEM and analysed by the unpaired t-test (n= 3 independent tumour samples analysed in both groups).

6.3 Discussion

The experimental data described herein provides evidence that initial 3 x 5 Gy RT ahead of VTP, with VTP being delivered during a window of time when the irradiated TRAMP-C1 flank PCa tumour allograft displays improved vascular perfusion, leads to enhanced tumour growth delay, with a resultant survival benefit in this animal model, and the possibility of complete tumour cure. It may be possible, and indeed it is attractive, to combine fractionated RT with VTP in the treatment of men with PCa. This may obviate the need for neo-adjuvant and/or concomitant ADT, and may allow a reduction in the dose of conventional RT administered. This new multimodality therapy approach will require formal clinical evaluation, and in particular will require determination of the optimal dose and fractionation schedule of fractionated RT in patients, combined with the feasibility of performing VTP during the window of tumour vascular changes observed following RT. To date, no such studies using imaging modalities such as MRI have been performed in human PCa to determine the early effects of fractionated RT on the tumour vasculature, ahead of multi-modality therapy.

The observation that VTP delivered shortly after fractionated RT increases delay in tumour growth is intriguing, and suggests that fractionated RT delivered in the correct fraction size and dose ahead of subsequent VTP improves the efficacy of this FT. One possible explanation is that transient vascular changes induced by fractionated RT transiently increases tumour vessel perfusion, thereby enhancing WST-11 delivery and subsequent tumour ablation by VTP. Subsequent experiments performed by the group have shown that when VTP is delivered during concomitant fractionated RT there was no benefit from combination, whereas a benefit was seen with VTP delivered 7 days following initiation of fractionated RT, suggesting that the fractionated RT-induced

increased tumour perfusion may be important in the efficacy of sequential combination treatment (data not shown).

To explore the concept of improved tumour perfusion leading to an enhanced anti-tumour effect of VTP when administered 7 days after fractionated RT, further experiments were performed by collaborators using post fractionated RT (3 x 5 Gy) treated tumour samples. In particular, TRAMP-C1 tumour tissue samples were stained with anti-CD31 and anti-αSMA antibodies to stain for endothelial cells and pericytes (endothelial supporting cells) respectively. αSMA is often used to identify pericytes, as these are relatively poorly defined heterogeneous perivascular cell types without highly specific markers available for their identification [Skalli et al., 1989; Yamazaki and Mukouyama, 2018]. These CD-31 and αSMA stained tumour samples were digitally annotated using the Annotation of Image Data by Assignments (AIDA) web application platform (*https://github.com/alanaberdeen/AIDA.*, *last accessed 9th May 2021)* developed 'in-house' for the annotation of large microscopy files. Here, relevant regions of interest in the tumour were selected, and four independent annotators (including myself) marked αSMA-positive cells and CD-31 positive blood vessels in these regions. Areas in the αSMA channel selected by at least 3 of 4 independent annotators were accepted as αSMA-positive pericytes. In order to investigate the extent of αSMA-positive pericyte coverage of CD-31 positive blood vessels, the fraction of blood vessels in each region with a spatially adjacent αSMA-positive cells was computed, and control untreated samples were compared against fractionated RT-treated samples. The data from this analysis suggested that TRAMP-C1 flank tumour allografts 7-days post fractionated RT demonstrated CD31-positive tumour vessels that were larger in size, fewer in number, further apart, with enhanced αSMA-positive pericyte coverage. These RT-treated tumours had enhanced vascular perfusion on DCE-MRI. Taken together, this data indicates that fractionated RT at a dose of 3 x 5 Gy had induced 'vascular normalisation' changes by 7-days post-fractionated RT in the TRAMP-C1 flank tumours (**Appendix 9.3**).

The observed improved tumour perfusion on DCE-MRI following fractionated RT at 7 days post treatment is consistent with other studies using similar fractions and doses of RT [Kleibeuker et al., 2016]. The dose and fraction size of fractionated RT, along with the window of time in which to look for 'vascular normalisation' changes, are key issues. It is known that large irradiation doses rapidly destroys the tumour vasculature, rather than transiently enhancing vascular function and perfusion [Barker et al., 2015; Clément-Colmou et al., 2020; Park et al., 2012; Supiot et al., 2019]. The results of *in vivo* xenograft pre-clinical model experiments show that the size and number of irradiation fractions determines whether transient induction of enhanced tumour vascularity occurs. In general: 5-10 Gy fractions cause transient blood flow increase, which returns to normal; 10-15 Gy fractions cause tumour blood flow decrease, which then recovers; and 15-20 Gy fractions cause blood flow to rapidly decrease, and vessels deteriorate (49,52). It is important for future clinical translation to consider these aspects of fractionated RT delivery.

It was observed that 7 mg/kg WST-11 resulted in a more pronounced reduction in tumour growth following fractionated RT than 9 mg/kg WST-11. One might speculate that near-infrared illumination of 7 mg/kg WST-11 might ablate fewer tumour vessels than 9 mg/kg WST-11, leaving sufficient tumour vessels available for immune cells to infiltrate the tumour and elicit an anti-tumour immune response, thereby enhancing the observed anti-tumour effects. This intriguing hypothesis warrants investigation in future research. Preliminary FACS studies have hinted towards an anti-tumour immune response following combination treatment, however these experiments have few numbers of mice, and had to terminate prematurely due to the Covid-19 pandemic in March 2020. However, whatever anti-tumour immune responses are generated by the combination treatment, these were not strong enough to cause an abscopal shrinkage of the contralateral untreated tumour, as demonstrated in a bilateral tumour model. Addition of

immunotherapy to fractionated RT and VTP may be necessary to achieve such a response, and this warrants investigation in future experiments.

This study has several limitations. Firstly, it has not adequately investigated the immune response to sequential treatment with fractionated RT and VTP, and this will be a focus of future research. Fractionated RT [Philippou et al., 2020c] and VTP [Preise et al., 2009, 2011] each induce immunological changes within tumours including PCa, and the effects of sequential fractionated RT and VTP on the TIME are important future aims of this research. Secondly, this work was performed on the TRAMP-C1 flank tumour allograft model of PCa in C57BL/6 mice, which is the most commonly used *in vivo* pre-clinical PCa model. It would be helpful to validate the benefit of combined sequential fractionated RT and VTP in an alternative model of PCa (such as the MyC-CaP flank tumour allograft model in FVB mice) – indeed, there were plans to perform such experiments in early 2020, however this was affected by the Covid-19 pandemic. The feasibility of performing combined RT and VTP experiments in an orthotopic mouse model of PCa would be challenging due to concerns over rectal and urethral toxicity of combined treatment. Thirdly, it is an important relative limitation of the reported experiments that they have not incorporated ADT, which is conventionally used in the neo-adjuvant clinical setting prior to fractionated. ADT could modulate the effect of sequentially combined fractionated RT and VTP, as it is recognised that ADT can affect the tumour vasculature [Røe et al., 2012]. Further experiments should therefore incorporate ADT with combined fractionated RT and VTP, and will be an important next step to evaluate this multimodality treatment approach. Fourthly, although we demonstrate the growth kinetics of TRAMP-C1 allograft tumours are slower post-VTP following prior fractionated RT, compared to VTP monotherapy, it will be important to investigate the microenvironment of recurrent tumours, as recurrence following combination therapy may promote aggressive disease. Fifthly, we administered a single VTP treatment following fractionated RT, whereas VTP can be repeatedly administered.

Taken together, these pre-clinical findings demonstrate that combined sequential fractionated RT and VTP may be a promising clinical strategy to treat PCa, paving the way for the development of future early phase clinical trials. This approach may also be a useful strategy for other solid organ cancers such as pancreatic cancers where improved therapy is desirable.

Chapter 7. Discussion

7.1 The prostate cancer research landscape

PCa is a heterogeneous cancer with respect to underlying causative mechanism, initial presentation, and prognosis, and has widely varying levels of morbidity and mortality depending upon grade and stage of disease. Over the last decade there has been an expansion in the PCa research landscape due to the need to improve outcomes for patients with PCa. The PCa research spectrum extends from screening and early diagnosis, to implementation of effective diagnostic biomarkers, better characterisation of disease biology including genomics to better stratify patients more at risk of clinical progression, and treatment optimisation by implementing more of a 'precision medicine' approach. In addition, research has focused on discovering more effective therapeutic strategies for PCa patients with localised, locally advanced, oligometastatic, and advanced metastatic disease, aiming for improved oncological outcomes whilst also reducing treatment-associated morbidity.

There is an important clinical need to improve the treatment efficacy of high-risk localised, and locally advanced, PCa. Patients with localised PCa may be offered radical surgery, radical fractionated RT (the latter with neoadjuvant and concomitant ADT for up to three years), or BT. Carefully selected cases of low-volume, low- or intermediate-risk disease may be offered FT (within the context of clinical trials) in the form of HIFU, cryotherapy, or VTP. However, the current treatments for PCa still cause significant harm from side effects, reducing the quality of life in long-term survivors, and they are not always effective at curing the disease. Approximately a third of patients with high-risk PCa treated with radical surgery or fractionated RT develop disease recurrence at long-term follow-up. An

unmet clinical need exists to transform the treatment for localised PCa in a way that reduces the risk of harm from side effects, and maximises the chance of cure. This may be achieved by developing new effective treatments for PCa, or enhancing the therapeutic effect of existing treatments such as fractionated RT, perhaps through combination therapy approaches. The Prostate Cancer UK research strategy published in 2020 has identified a need for improved treatments for localised PCa, and their new strategy focuses on funding large scale studies and clinical trials to transform treatment for localised PCa in a way that reduces the risk of harm from side effects and maximises chance of cure [*PCUK strategy*, last accessed 28th May 2021].

The aim of this DPhil project was to investigate whether a multi-modality treatment approach using fractionated RT in combination with either immunotherapy in the form of ICB or a novel precision surgery focal ablation technique (VTP), can enhance local tumour control in a pre-clinical model of PCa. There is increasing interest in adopting immunotherapy in the treatment of advanced and metastatic PCa, as evident by the multiple clinical trials ongoing in this area, either as monotherapy, or combination immunotherapy, or a combination of immunotherapy with other treatment modalities such as fractionated RT (table 1.5). An aim of this thesis was therefore to generate robust pre-clinical data in a PCa model combining immunotherapy with fractionated RT, due to the paucity of such pre-clinical studies in PCa. The results of pre-clinical work could help inform the design of clinical trials, providing insight as to why clinical trials to date using immunotherapy in PCa have largely been disappointing in terms of significantly extending survival of patients with advanced and metastatic disease [Antonarakis et al., 2020; Philippou et al., 2020a].

The concept of organ-sparing PCa treatment strategies, directed towards a focal lesion or using a hemi- gland approach to deliver effective tumour control and/or cure with reduced toxicity versus whole gland treatment, is an increasing focus of PCa research. This

approach may have less detrimental effects on quality of life versus current SOC whole gland therapy (39,42,43). VTP has advantages as a FT, for example it has been evaluated in a phase-III randomised clinical trial (19), and can anatomise treatment to conform to the malignant lesion along with a margin of normal tissue within the prostate gland, preserving urinary and sexual function. However, VTP has not been investigated as part of multimodality therapy in close sequential combination with fractionated RT, in either pre-clinical or clinical studies. Salvage VTP has been demonstrated to be safe and effective in early phase clinical trials in a small number of patients with recurrent PCa following RT, however there was an interval of several years between RT and delivery of VTP. Given that the treatment parameters for VTP have been established for optimal targeted tumour ablation, whilst fractionated RT for PCa is well established, it could be feasible, based on pre-clinical data, to combine these treatments in first-in-man early phase clinical trials. Pre-clinical data could provide proof-of-concept that such an approach may be beneficial in achieving local tumour control, and provide insight regarding the sequential timing of these treatments, and the mechanisms of action of any potential synergistic or additive effects of combination treatment, compared against monotherapy with fractionated RT or VTP.

7. 2 Combination of RT and anti-PD-L1 does not enhance tumour growth delay in the TRAMP-C1 prostate cancer flank tumour model

Initial experiments characterising the immunogenicity of the TRAMP-C1 and MyC-CaP murine PCa cell lines showed that TRAMP-C1 was the more immunogenic cell line, based on MHCI and PD-L1 expression at baseline and following stimulation with γIFN. TRAMP-C1 was therefore chosen as the model to investigate iRT. 3 x 5 Gy hypofractionated RT resulted in tumour growth delay in both TRAMP-C1 and MyC-CaP

PCa models. However, experiments treating the TRAMP-C1 PCa flank tumour model with iRT showed that combination of fractionated RT and anti-PD-L1 ICB did not significantly delay tumour growth compared to fractionated RT alone. Although there was evidence of an early anti-tumour immune response following hypofractioned RT, with increased tumour infiltration of APCs and $CD4^+$ T-helper cells in addition to an increased expression of cytotoxic $CD8^+$ T-cell immune function genes, the $CD8^+$ T-cells that play important roles in the anti-tumour effects of ablative RT remained at low levels following 3 x 5 Gy fractionated RT and following iRT with anti-PD-L1. This observation from analysis of the TIME may be partly due to the low somatic mutational burden exhibited in PCa, and the relatively low expression of neoantigens compared to other tumours such as lung cancer or melanoma, together with the infiltration of pro-tumourigenic monocyte populations in PCa [Alexandrov et al., 2013; Lawrence et al., 2013]. Although mutational burden and neoantigen expression were not investigated in this pre-clinical PCa tumour model, a monocyte infiltrate was demonstrated in analysis of the TIME of these flank tumours in both untreated control tumours and following fractionated RT. The experimental findings suggest that therapeutic strategies combining fractionated RT with T-cell-based therapies such as ICB may not be clinically effective without first finding strategies to enhance T-cell immunosurveillance. Monocytes in particular play important roles in the immune evasion/tolerance of PCa, and it may be that immunotherapy directed at inhibiting recruitment of TAMs or MDSCs to the TIME, in combination with fractionated RT, may be needed to improve PCa disease control. This may partly explain why clinical trials using ICB have failed to significantly prolong overall survival in patients with metastatic PCa [Antonarakis et al., 2020]. Further iRT strategies targeting the high monocyte immune infiltrate seen in human PCa are necessary at a pre-clinical level to determine the optimal timing, sequence of delivery, and type of immunomodulation to be used in iRT. In addition, the results suggest that combination therapies incorporating hypofractionated RT may require adjuncts beyond immunomodulation to improve the anti-tumour response from RT fraction sizes used in the clinic.

7.3 Hypofractionated RT causes vascular normalisation in pre-clinical models of prostate cancer

The reported experiments demonstrated that moderate hypofractionated RT (at the dose of 3 x 5 Gy) caused ‘vascular normalisation’ changes, as evidenced by improved tumour vessel perfusion on DCE-MRI 7 days following fractionated RT, increased pericyte coverage of endothelial cells, and a reduced proportion of small-diameter CD-31 positive vessels. The dose and fraction size of fractionated RT, along with the window of time in which to look for ‘vascular normalisation’ changes, are important issues to determine, and this was a key objective of this DPhil thesis ahead of combination experiments investigating fractionated RT and VTP. Hypofractionated RT is increasingly used clinically [Philippou et al., 2020b], and it could be feasible to use fractionated RT schedules that are likely to induce ‘vascular normalisation’ changes ahead of VTP in a multimodality approach.

7.4 Combination therapy using fractionated RT followed by VTP suppressed tumour growth to a greater extent than either treatment alone

Results of experiments described in this thesis provide evidence that initial moderate hypofractionated RT ahead of VTP, with VTP being delivered during a window of time when the irradiated PCa tumour displays ‘vascular normalisation’ changes, leads to enhanced tumour growth delay, with a resultant survival benefit in mice, and the possibility of complete tumour cure in some cases. This suggests that combining hypofractionated RT with other treatment strategies beyond immunomodulation may be more effective, though in this thesis direct comparison of the different combination strategies of iRT and RT & VTP was not performed. The data generated from this research provides pre-clinical evidence that hypofractionated RT in sequential

combination with VTP may be effective in men with localised PCa, if taken forwards to first-in-man early phase clinical trials. The mechanisms by which this combination improves anti-tumour effects are unclear and require further evaluation. One might speculate that the sequential combination of fractionated RT and VTP may stimulate an effective anti-tumour immune response, however this hypothesis requires formal investigation, and this will be an ongoing focus of this research. Preliminary FACS experiments of the TIME following combination therapy points towards the generation of an immunostimulatory TIME however this needs to be evaluated further. It is also possible that improved WST-11 VTP drug delivery via a 'normalised vasculature' enhances subsequent tumour ablation by VTP, and therefore initial hypofractionated RT may improve the effects of subsequent VTP.

7.5 Conclusion and future work

The aim of this research was to investigate in a pre-clinical PCa model the treatment strategy of combining hypofractionated RT with VTP, ahead of possible first-in-man early phase clinical trials. Whilst this research has generated evidence to support this treatment strategy, further research is needed before this can progress to an early clinical trial. Future experiments will focus on characterising the immune response to combination treatment, along with repeating some of these experiments in a second pre-clinical model for validation purposes. In addition, it will be important to incorporate ADT in this combination treatment protocol, to understand how the addition of ADT could modulate the anti-tumour effects of this combination treatment approach. Understanding the effects of hypofractionated RT on the tumour vasculature of human PCa is paramount to understand whether 'vascular normalisation' observed in pre-clinical model also occurs in human PCa. Finally, the start of the PART Trial: Partial prostate Ablation versus Radical prostatectomy, using VTP in Oxford [Hamdy et al., 2018] will facilitate experience of

treating patients with localised PCa with VTP, providing a stepping stone to subsequent combination with hypofractionated RT.

Chapter 8. References

Abiraj K, Mansi R, Tamma ML, Fani M, Forrer F, Nicolas G, Cescato R, Reubi JC, Maecke HR. 2011. Bombesin antagonist-based radioligands for translational nuclear imaging of gastrin-releasing peptide receptor-positive tumors. J Nucl Med. https://doi.org/10.2967/jnumed.111.094375.

Abuodeh Y, Venkat P, Kim S. 2016. Systematic review of case reports on the abscopal effect. Curr Probl Cancer. https://doi.org/10.1016/j.currproblcancer.2015.10.001.

Ager CR, Reilley MJ, Nicholas C, Bartkowiak T, Jaiswal AR, Curran MA. 2017. Intratumoral STING Activation with T-cell Checkpoint Modulation Generates Systemic Antitumor Immunity. Cancer Immunol Res 5(8):676–684.

Agrawal N, Bettegowda C, Cheong I, Geschwind JF, Drake CG, Hipkiss EL, Tatsumi M, Dang LH, Diaz LA, Pomper M, Abusedera M, Wahl RL, Kinzler KW, Zhou S, Huso DL, Vogelstein B. 2004. Bacteriolytic therapy can generate a potent immune response against experimental tumors. Proc Natl Acad Sci U S A. https://doi.org/10.1073/pnas.0406242101.

Ahmed HU, Dickinson L, Charman S, Weir S, McCartan N, Hindley RG, Freeman A, Kirkham AP, Sahu M, Scott R, Allen C, Meulen J Van Der, Emberton M. 2015. Focal Ablation Targeted to the Index Lesion in Multifocal Localised Prostate Cancer: A Prospective Development Study. Eur Urol. https://doi.org/10.1016/j.eururo.2015.01.030.

Ahmed HU, Moore C, Emberton M. 2009. Minimally-invasive technologies in uro-oncology: the role of cryotherapy, HIFU and photodynamic therapy in whole gland and focal therapy of localised prostate cancer. Surgical Oncology.

Ahn GO, Brown JM. 2008. Matrix Metalloproteinase-9 Is Required for Tumor Vasculogenesis but Not for Angiogenesis: Role of Bone Marrow-Derived Myelomonocytic Cells. Cancer Cell. https://doi.org/10.1016/j.ccr.2007.11.032.

Ahn GO, Tseng D, Liao CH, Dorie MJ, Czechowicz A, Brown JM. 2010. Inhibition of Mac-1 (CD11b/CD18) enhances tumor response to radiation by reducing myeloid cell recruitment. Proc Natl Acad Sci U S A. https://doi.org/10.1073/pnas.0911378107.

Alexandrov LB, Nik-Zainal S, Wedge DC, Aparicio SAJR, Behjati S, Biankin A V., Bignell GR, Bolli N, Borg A, Børresen-Dale AL, Boyault S, Burkhardt B, Butler AP, Caldas C, Davies HR, Desmedt C, Eils R, Eyfjörd JE, Foekens JA, Greaves M, Hosoda F, Hutter B, Ilicic T, Imbeaud S, Imielinsk M, Jäger N, Jones DTW, Jonas D, Knappskog S, Koo M, Lakhani SR, López-Otín C, Martin S, Munshi NC, Nakamura H, Northcott PA, Pajic M, Papaemmanuil E, Paradiso A, Pearson J V., Puente XS, Raine K, Ramakrishna M, Richardson AL, Richter J, Rosenstiel P, Schlesner M, Schumacher TN, Span PN, Teague JW, Totoki Y, Tutt ANJ, Valdés-Mas R, Buuren MM Van, 'T Veer L Van, Vincent-Salomon A, Waddell N, Yates LR, Zucman-Rossi J, Andrew Futreal P, McDermott U, Lichter P, Meyerson M, Grimmond SM, Siebert R, Campo E, Shibata T, Pfister SM, Campbell PJ, Stratton MR. 2013. Signatures of mutational processes in human cancer. Nature. https://doi.org/10.1038/nature12477.

Antonarakis ES, Piulats JM, Gross-Goupil M, Goh J, Ojamaa K, Hoimes CJ, Vaishampayan U, Berger R, Sezer A, Alanko T, Wit R de, Li C, Omlin A, Procopio G,

Fukasawa S, Tabata K ichi, Park SH, Feyerabend S, Drake CG, Wu H, Qiu P, Kim J, Poehlein C, Bono JS de. 2020. Pembrolizumab for treatment-refractory metastatic castration-resistant prostate cancer: Multicohort, open-label phase II KEYNOTE-199 study.

Apetoh L, Ghiringhelli F, Tesniere A, Obeid M, Ortiz C, Criollo A, Mignot G, Maiuri MC, Ullrich E, Saulnier P, Yang H, Amigorena S, Ryffel B, Barrat FJ, Saftig P, Levi F, Lidereau R, Nogues C, Mira JP, Chompret A, Joulin V, Clavel-Chapelon F, Bourhis J, André F, Delaloge S, Tursz T, Kroemer G, Zitvogel L. 2007. Toll-like receptor 4-dependent contribution of the immune system to anticancer chemotherapy and radiotherapy. Nat Med. https://doi.org/10.1038/nm1622.

Ashur I, Goldschmidt R, Pinkas I, Salomon Y, Szewczyk G, Sarna T, Scherz A. 2009. Photocatalytic generation of oxygen radicals by the water-soluble bacteriochlorophyll derivative WST1I, noncovalently bound to serum albumin. J Phys Chem A. https://doi.org/10.1021/jp900580e.

Avigdor Sherz, Alexander Brandis, Ohad Mazor, Yoram Solomon HS. 2011. Water-soluble anionic bacteriochlorophyll derivatives and their uses. Patent No:US8461142B2

Azad A, Yin Lim S, D'Costa Z, Jones K, Diana A, Sansom OJ, Kruger P, Liu S, McKenna WG, Dushek O, Muschel RJ, Fokas E. 2017. PD -L1 blockade enhances response of pancreatic ductal adenocarcinoma to radiotherapy . EMBO Mol Med. https://doi.org/10.15252/emmm.201606674.

Azzi S, Hebda JK, Gavard J. 2013. Vascular permeability and drug delivery in cancers. Front Oncol. https://doi.org/10.3389/fonc.2013.00211.

Azzouzi AR, Barret E, Bennet J, Moore C, Taneja S, Muir G, Villers A, Coleman J, Allen C, Scherz A, Emberton M. 2015a. TOOKAD® Soluble focal therapy: pooled analysis of three phase II studies assessing the minimally invasive ablation of localized prostate cancer. World J Urol. https://doi.org/10.1007/s00345-015-1505-8.

Azzouzi AR, Barret E, Moore CM, Villers A, Allen C, Scherz A, Muir G, Wildt M De, Barber NJ, Lebdai S, Emberton M. 2013. TOOKAD®Soluble vascular-targeted photodynamic (VTP) therapy: Determination of optimal treatment conditions and assessment of effects in patients with localised prostate cancer. BJU Int. https://doi.org/10.1111/bju.12265.

Azzouzi AR, Lebdai S, Benzaghou F, Stief C. 2015b. Vascular-targeted photodynamic therapy with TOOKAD® Soluble in localized prostate cancer: standardization of the procedure. World J Urol. https://doi.org/10.1007/s00345-015-1535-2.

Azzouzi AR, Vincendeau S, Barret E, Cicco A, Kleinclauss F, Poel HG van der, Stief CG, Rassweiler J, Salomon G, Solsona E, Alcaraz A, Tammela TT, Rosario DJ, Gomez-Veiga F, Ahlgren G, Benzaghou F, Gaillac B, Amzal B, Debruyne FM, Fromont G, Gratzke C, Emberton M, Group PCMS. 2017a. Padeliporfin vascular-targeted photodynamic therapy versus active surveillance in men with low-risk prostate cancer (CLIN1001 PCM301): an open-label, phase 3, randomised controlled trial. Lancet Oncol 18(2):181–191.

Baker DG, Krochak RJ. 1989. The response of the microvascular system to radiation: a review. Cancer Invest 7(3):287–94.

Banks TI, Eyben R von, Hristov D, Kidd EA. 2018. Pilot study of combined FDG-PET and dynamic contrast-enhanced CT of locally advanced cervical carcinoma before and during

concurrent chemoradiotherapy suggests association between changes in tumor blood volume and treatment response. Cancer Med. https://doi.org/10.1002/cam4.1632.

Barker HE, Paget JTE, Khan AA, Harrington KJ. 2015. The tumour microenvironment after radiotherapy: mechanisms of resitance and recurrence.Nature Reviews Cancer.

Baskar R, Lee KA, Yeo R, Yeoh K-W. 2012. Cancer and radiation therapy: current advances and future directions. Int J Med Sci 9(3):193–9.

Beckman JS, Beckman TW, Chen J, Marshall PA, Freeman BA. 1990. Apparent hydroxyl radical production by peroxynitrite: Implications for endothelial injury from nitric oxide and superoxide. Proc Natl Acad Sci U S A. https://doi.org/10.1073/pnas.87.4.1620.

Bernier J, Hall EJ, Giaccia A. 2004. Radiation oncology: a century of achievement. Nature Reviews Cancer.

Betrouni N, Lopes R, Puech P, Colin P, Mordon S. 2011. A model to estimate the outcome of prostate cancer photodynamic therapy with TOOKAD soluble WST11. Phys Med Biol. https://doi.org/10.1088/0031-9155/56/15/009.

Binder RJ, Blachere NE, Srivastava PK. 2001. Heat Shock Protein-chaperoned Peptides but not Free Peptides Introduced into the Cytosol are Presented Efficiently by Major Histocompatibility Complex I Molecules. J Biol Chem. https://doi.org/10.1074/jbc.M011547200.

Biopharmaceutics A, Pharmacokinetics E, Appleton, Lange, Stamford. 1984. PHAR 7633 Chapter 7 Routes of Drug Administration Routes of Drug Administration Student Objectives for this Chapter. Biopharm Clin Pharmacokinet.

Blankenstein T, Coulie PG, Gilboa E, Jaffee EM. 2012. The determinants of tumour immunogenicity. Nature Reviews Cancer.

Bodo S, Campagne C, Thin TH, Higginson DS, Vargas HA, Hua G, Fuller JD, Ackerstaff E, Russell J, Zhang Z, Klingler S, Cho HJ, Kaag MG, Mazaheri Y, Rimner A, Manova-Todorova K, Epel B, Zatcky J, Cleary CR, Rao SS, Yamada Y, Zelefsky MJ, Halpern HJ, Koutcher JA, Cordon-Cardo C, Greco C, Haimovitz-Friedman A, Sala E, Powell SN, Kolesnick R, Fuks Z. 2019. Single-dose radiotherapy disables tumor cell homologous recombination via ischemia/reperfusion injury. J Clin Invest. https://doi.org/10.1172/JCI97631.

Bolla M, Collette L, Blank L, Warde P, Dubois JB, Mirimanoff RO, Storme G, Bernier J, Kuten A, Sternberg C, Mattelaer J, Lopez Torecilla J, Pfeffer JR, Lino Cutajar C, Zurlo A, Pierart M. 2002. Long-term results with immediate androgen suppression and external irradiation in patients with locally advanced prostate cancer (an EORTC study): a phase III randomised trial. Lancet 360(9327):103–106.

Bolla M, Gonzalez D, Warde P, Dubois JB, Mirimanoff RO, Storme G, Bernier J, Kuten A, Sternberg C, Gil T, Collette L, Pierart M. 1997. Improved survival in patients with locally advanced prostate cancer treated with radiotherapy and goserelin. N Engl J Med 337(5):295–300.

Bolla M, Maingon P, Carrie C, Villa S, Kitsios P, Poortmans PMP, Sundar S, Steen-Banasik EM van der, Armstrong J, Bosset J-F, Herrera FG, Pieters B, Slot A, Bahl A, Ben-Yosef R, Boehmer D, Scrase C, Renard L, Shash E, Coens C, Bergh ACM van den, Collette L. 2016. Short Androgen Suppression and Radiation Dose Escalation for

Intermediate- and High-Risk Localized Prostate Cancer: Results of EORTC Trial 22991. J Clin Oncol 34(15):1748–56.

Bolla M, Reijke TM de, Tienhoven G Van, Bergh ACM Van den, Oddens J, Poortmans PMP, Gez E, Kil P, Akdas A, Soete G, Kariakine O, Steen-Banasik EM van der, Musat E, Piérart M, Mauer ME, Collette L, EORTC Radiation Oncology Group and Genito-Urinary Tract Cancer Group. 2009. Duration of androgen suppression in the treatment of prostate cancer. N Engl J Med 360(24):2516–27.

Brand DH, Tree AC, Ostler P, Voet H van der, Loblaw A, Chu W, Ford D, Tolan S, Jain S, Martin A, Staffurth J, Camilleri P, Kancherla K, Frew J, Chan A, Dayes IS, Henderson D, Brown S, Cruickshank C, Burnett S, Duffton A, Griffin C, Hinder V, Morrison K, Naismith O, Hall E, As N van, Dodds D, Lartigau E, Patton S, Thompson A, Winkler M, Wells P, Lymberiou T, Saunders D, Vilarino-Varela M, Vavassis P, Tsakiridis T, Carlson R, Rodrigues G, Tanguay J, Iqbal S, Morgan S, Mihai A, Li A, Din O, Panades M, Wade R, Rimmer Y, Armstrong J, Oommen N. 2019a. Intensity-modulated fractionated radiotherapy versus stereotactic body radiotherapy for prostate cancer (PACE-B): acute toxicity findings from an international, randomised, open-label, phase 3, non-inferiority trial. Lancet Oncol. https://doi.org/10.1016/S1470-2045(19)30569-8.

Breslow N, Chan CW, Dhom G, Drury RA, Franks LM, Gellei B, Lee YS, Lundberg S, Sparke B, Sternby NH, Tulinius H. 1977. Latent carcinoma of prostate at autopsy in seven areas. The International Agency for Research on Cancer, Lyons, France. Int J Cancer.

Brown JM. 2020. Radiation Damage to Tumor Vasculature Initiates a Program that Promotes Tumor Recurrences. Int J Radiat Oncol. https://doi.org/10.1016/j.ijrobp.2020.05.028.

Brown JM, Carlson DJ, Brenner DJ. 2014. The tumor radiobiology of SRS and SBRT: are more than the 5 Rs involved? Int J Radiat Oncol Biol Phys 88(2):254–62.

Brown JM, Wilson WR. 2004. Exploiting tumour hypoxia in cancer treatment. Nat Rev Cancer 4(6):437–447.

Bussink J, Kaanders JHAM, Rijken PFJW, Raleigh JA, Kogel AJ Van der. 2000. Changes in Blood Perfusion and Hypoxia after Irradiation of a Human Squamous Cell Carcinoma Xenograft Tumor Line. Radiat Res. https://doi.org/10.1667/0033-7587(2000)153[0398:cibpah]2.0.co;2.

Cahill DP, Kinzler KW, Vogelstein B, Lengauer C. 1999. Genetic instability and darwinian selection in tumours.Trends in Biochemical Sciences.

Callahan MK, Chaillot D, Jacquin C, Clark PR, Ménoret A. 2002. Differential acquisition of antigenic peptides by Hsp70 and Hsc70 under oxidative conditions. J Biol Chem. https://doi.org/10.1074/jbc.M202890200.

Carlson DJ, Stewart RD, Li XA, Jennings K, Wang JZ, Guerrero M. 2004. Comparison of in vitro and in vivo α/β ratios for prostate cancer. Phys Med Biol. https://doi.org/10.1088/0031-9155/49/19/003.

Chaudary N, Pintilie M, Jelveh S, Lindsay P, Hill RP, Milosevic M. 2017. Plerixafor improves primary tumor response and reduces metastases in cervical cancer treated with radio-chemotherapy. Clin Cancer Res. https://doi.org/10.1158/1078-0432.CCR-16-1730.

Chen FH, Chiang CS, Wang CC, Tsai CS, Jung SM, Lee CC, McBride WH, Hong JH.

2009. Radiotherapy decreases vascular density and causes hypoxia with macrophage aggregation in TRAMP-C1 prostate tumors. Clin Cancer Res. https://doi.org/10.1158/1078-0432.CCR-08-1471.

Chevalier S, Anidjar M, Scarlata E, Hamel L, Scherz A, Ficheux H, Borenstein N, Fiette L, Elhilali M. 2011. Preclinical study of the novel vascular occluding agent, WST11, for photodynamic therapy of the canine prostate. J Urol. https://doi.org/10.1016/j.juro.2011.03.039.

Chevalier S, Cury FL, Scarlata E, El-Zayat E, Hamel L, Rocha J, Zouanat FZ, Moussa S, Scherz A, Elhilali M, Anidjar M. 2013. Endoscopic vascular targeted photodynamic therapy with the photosensitizer WST11 for benign prostatic hyperplasia in the preclinical dog model. J Urol. https://doi.org/10.1016/j.juro.2013.05.014.

Chi N, Tan Z, Ma K, Bao L, Yun Z. 2014. Increased circulating myeloid-derived suppressor cells correlate with cancer stages, interleukin-8 and -6 in prostate cancer. Int J Clin Exp Med.

Chouaib S, Umansky V, Kieda C. 2017. The role of hypoxia in shaping the recruitment of proangiogenic and immunosuppressive cells in the tumor microenvironment. Wspolczesna Onkologia.

Clarke NW, Hart CA, Brown MD. 2009. Molecular mechanisms of metastasis in prostate cancer. Asian Journal of Andrology.

Clément-Colmou K, Potiron V, Pietri M, Guillonneau M, Jouglar E, Chiavassa S, Delpon G, Paris F, Supiot S. 2020. Influence of radiotherapy fractionation schedule on the tumor vascular microenvironment in prostate and lung cancer models. Cancers (Basel). https://doi.org/10.3390/cancers12010121.

Cooper BT, Sanfilippo NJ. 2015. Concurrent chemoradiation for high-risk prostate cancer. World Journal of Clinical Oncology.

Cornford P, Bellmunt J, Bolla M, Briers E, Santis M De, Gross T, Henry AM, Joniau S, Lam TB, Mason MD, Poel HG van der, Kwast TH van der, Rouvière O, Wiegel T, Mottet N. 2017. EAU-ESTRO-SIOG Guidelines on Prostate Cancer. Part II: Treatment of Relapsing, Metastatic, and Castration-Resistant Prostate Cancer. Eur Urol 71(4):630–642.

Corradi RB, LaRosa S, Jebiwott S, Murray KS, Rosenzweig B, Somma AJ, Gomez RS, Scherz A, Kim K, Coleman JA. 2019. Effectiveness of the combination of vascular targeted photodynamic therapy and anti-cytotoxic T-lymphocyte-associated antigen 4 in a preclinical mouse model of urothelial carcinoma. Int J Urol. https://doi.org/10.1111/iju.13878.

Crane CH, Ellis LM, Abbruzzese JL, Amos C, Xiong HQ, Ho L, Evans DB, Tamm EP, Ng C, Pisters PWT, Charnsangavej C, Delclos ME, O'Reilly M, Lee JE, Wolff RA. 2006. Phase I trial evaluating the safety of bevacizumab with concurrent radiotherapy and capecitabine in locally advanced pancreatic cancer. J Clin Oncol. https://doi.org/10.1200/JCO.2005.03.6780.

Crittenden MR, Zebertavage L, Kramer G, Bambina S, Friedman D, Troesch V, Blair T, Baird JR, Alice A, Gough MJ. 2018. Tumor cure by radiation therapy and checkpoint inhibitors depends on pre-existing immunity. Sci Rep 8(1):7012.

Crokart N, Jordan BF, Baudelet C, Ansiaux R, Sonveaux P, Grégoire V, Beghein N, DeWever J, Bouzin C, Feron O, Gallez B. 2005. Early reoxygenation in tumors after irradiation: Determining factors and consequences for radiotherapy regimens using daily multiple fractions. Int J Radiat Oncol Biol Phys.

CRUK. 2015. Cancer Research UK. https://www.cancerresearchuk.org/health-professional/cancer-statistics/statistics-by-cancer-type/prostate-cancer. Accessed 23/09/2021.

Czito BG, Bendell JC, Willett CG, Morse MA, Blobe GC, Tyler DS, Thomas J, Ludwig KA, Mantyh CR, Ashton J, Yu D, Hurwitz HI. 2007. Bevacizumab, Oxaliplatin, and Capecitabine With Radiation Therapy in Rectal Cancer: Phase I Trial Results. Int J Radiat Oncol Biol Phys. https://doi.org/10.1016/j.ijrobp.2007.02.001.

D'Amico A V., Whittington R, Bruce Malkowicz S, Schultz D, Blank K, Broderick GA, Tomaszewski JE, Renshaw AA, Kaplan I, Beard CJ, Wein A. 1998. Biochemical outcome after radical prostatectomy, external beam radiation therapy, or interstitial radiation therapy for clinically localized prostate cancer. J Am Med Assoc. https://doi.org/10.1001/jama.280.11.969.

D'Amico A V, Manola J, Loffredo M, Renshaw AA, DellaCroce A, Kantoff PW. 2004. 6-month androgen suppression plus radiation therapy vs radiation therapy alone for patients with clinically localized prostate cancer: a randomized controlled trial. JAMA 292(7):821–827.

Dearnaley DP, Jovic G, Syndikus I, Khoo V, Cowan RA, Graham JD, Aird EG, Bottomley D, Huddart RA, Jose CC, Matthews JHL, Millar JL, Murphy C, Russell JM, Scrase CD, Parmar MKB, Sydes MR. 2014. Escalated-dose versus control-dose conformal radiotherapy for prostate cancer: Long-term results from the MRC RT01 randomised controlled trial. Lancet Oncol 15(4):464–473.

Delaney G, Jacob S, Featherstone C, Barton M. 2005. The role of radiotherapy in cancer treatment. Cancer.

Demaria S, Ng B, Devitt ML, Babb JS, Kawashima N, Liebes L, Formenti SC. 2004. Ionizing radiation inhibition of distant untreated tumors (abscopal effect) is immune mediated. Int J Radiat Oncol Biol Phys. https://doi.org/10.1016/j.ijrobp.2003.09.012.

Deng L, Liang H, Xu M, Yang X, Burnette B, Arina A, Li XD, Mauceri H, Beckett M, Darga T, Huang X, Gajewski TF, Chen ZJ, Fu YX, Weichselbaum RR. 2014. STING-dependent cytosolic DNA sensing promotes radiation-induced type I interferon-dependent antitumor immunity in immunogenic tumors. Immunity.https://doi.org/10.1016/j.immuni.2014.10.019.

Dess RT, Soni PD, Jackson WC, Berlin A, Cox BW, Jolly S, Efstathiou JA, Feng FY, Kishan AU, Stish BJ, Pisansky TM, Spratt DE. 2019. The current state of randomized clinical trial evidence for prostate brachytherapy. Urol Oncol. https://doi.org/10.1016/j.urolonc.2019.04.009.

Devlin HL, Mudryj M. 2009. Progression of prostate cancer: Multiple pathways to androgen independence Cancer Letters.

Dewan MZ, Galloway AE, Kawashima N, Dewyngaert JK, Babb JS, Formenti SC, Demaria S. 2009. Fractionated but not single-dose radiotherapy induces an immune-mediated abscopal effect when combined with anti-CTLA-4 antibody. Clin Cancer Res 15(17):5379–5388.

Ding Z, Wu CJ, Jaskelioff M, Ivanova E, Kost-Alimova M, Protopopov A, Chu GC, Wang G, Lu X, Labrot ES, Hu J, Wang W, Xiao Y, Zhang H, Zhang J, Zhang J, Gan B, Perry SR, Jiang S, Li L, Horner JW, Wang YA, Chin L, Depinho RA. 2012. Telomerase reactivation following telomere dysfunction yields murine prostate tumors with bone metastases. Cell. https://doi.org/10.1016/j.cell.2012.01.039.

Dovedi SJ, Adlard AL, Lipowska-Bhalla G, McKenna C, Jones S, Cheadle EJ, Stratford IJ, Poon E, Morrow M, Stewart R, Jones H, Wilkinson RW, Honeychurch J, Illidge TM. 2014. Acquired resistance to fractionated radiotherapy can be overcome by concurrent PD-L1 blockade. Cancer Res 74(19):5458–68.

Dudzinski SO, Cameron BD, Wang J, Rathmell JC, Giorgio TD, Kirschner AN. 2019b. Combination immunotherapy and radiotherapy causes an abscopal treatment response in a mouse model of castration resistant prostate cancer. J Immunother Cancer. https://doi.org/10.1186/s40425-019-0704-z.

Dunst J, Ӧansgen G, LautenschӀager C, Ӫuchsel G, Becker A. 1999. Oxygenation of cervical cancers during radiotherapy and radiotherapy + cis-retinoic acid/interferon. Int J Radiat Oncol Biol Phys. https://doi.org/10.1016/S0360-3016(98)00361-7.

Duque JLF, Loughlin KR, Adam RM, Kantoff PW, Zurakowski D, Freeman MR. 1999. Plasma levels of vascular endothelial growth factor are increased in patients with metastatic prostate cancer. Urology. https://doi.org/10.1016/S0090-4295(99)00167-3.

Durante M, Loeffler JS. 2010. Charged particles in radiation oncology. Nat Rev Clin Oncol 7(1):37–43.

Egen JG, Kuhns MS, Allison JP. 2002. CTLA-4: new insights into its biological function and use in tumor immunotherapy. Nature Immunology.

Eggener SE, Coleman JA. 2008. Focal Treatment of Prostate Cancer with Vascular-Targeted Photodynamic Therapy. The Scientific World Journal.

Eidelman E, Twum-Ampofo J, Ansari J, Siddiqui MM. 2017. The metabolic phenotype of prostate cancer. Frontiers in Oncology.

Ellis L, Lehet K, Ramakrishnan S, Adelaiye R, Pili R. 2012. Development of a castrate resistant transplant tumor model of prostate cancer. Prostate. https://doi.org/10.1002/pros.21465.

Eriksson D, Stigbrand T. 2010. Radiation-induced cell death mechanisms. Tumour Biol 31(4):363–72.

Eymerit-Morin C, Zidane M, Lebdai S, Triau S, Azzouzi AR, Rousselet MC. 2013. Histopathology of prostate tissue after vascular-targeted photodynamic therapy for localized prostate cancer. Virchows Arch. https://doi.org/10.1007/s00428-013-1454-9.

Faure Walker NA, Norris JM, Shah TT, Yap T, Cathcart P, Moore CM, Ahmed HU, Emberton M, Minhas S. 2018. Urologic Oncology: Seminars and Original Investigations. Feldman BJ, Feldman D. 2001. The development of androgen-independent prostate cancer. Nat Rev Cancer. https://doi.org/10.1038/35094009.

Feng X, Tian L, Zhang Z, Yu Y, Cheng J, Gong Y, Li CY, Huang Q. 2015. Caspase 3 in

dying tumor cells mediates post-irradiation angiogenesis. Oncotarget. https://doi.org/10.18632/oncotarget.5898.

Fenton BM, Paoni SF, Ding I. 2004. Pathophysiological effects of vascular endothelial growth factor receptor-2-blocking antibody plus fractionated radiotherapy on murine mammary tumors. Cancer Res. https://doi.org/10.1158/0008-5472.CAN-04-0434.

Filatenkov A, Baker J, Mueller AMS, Kenkel J, Ahn G-O, Dutt S, Zhang N, Kohrt H, Jensen K, Dejbakhsh-Jones S, Shizuru JA, Negrin RN, Engleman EG, Strober S. 2015. Ablative Tumor Radiation Can Change the Tumor Immune Cell Microenvironment to Induce Durable Complete Remissions. Clin Cancer Res 21(16):3727–39.

Finkelstein SE, Rodriguez F, Dunn M, Farmello M-J, Smilee R, Janssen W, Kang L, Chuang T, Seigne J, Pow-Sang J, Torres-Roca JF, Heysek R, Biagoli M, Shankar R, Scott J, Antonia S, Gabrilovich D, Fishman M. 2012. Serial assessment of lymphocytes and apoptosis in the prostate during coordinated intraprostatic dendritic cell injection and radiotherapy. Immunotherapy 4(4):373–382.

Finkelstein SE, Salenius S, Mantz CA, Shore ND, Fernandez EB, Shulman J, Myslicki FA, Agassi AM, Rotterman Y, DeVries T, Sims R. 2015. Combining Immunotherapy and Radiation for Prostate Cancer. Clin Genitourin Cancer 13(1):1–9.

Fleshker S, Preise D, Kalchenko V, Scherz A, Salomon Y. 2008. Prompt assessment of WST11-VTP outcome using luciferase transfected tumors enables second treatment and increase in overall therapeutic rate. Photochem Photobiol. https://doi.org/10.1111/j.1751-1097.2008.00340.x.

Foster BA, Gingrich JR, Kwon ED, Madias C, Greenberg NM. 1997a. Characterization of prostatic epithelial cell lines derived from transgenic adenocarcinoma of the mouse prostate (TRAMP) model. Cancer Res.

Foster BA, Gingrich JR, Kwon ED, Madias C, Greenberg NM. 1997b. Characterization of prostatic epithelial cell lines derived from transgenic adenocarcinoma of the mouse prostate (TRAMP) model. Cancer Res.

Frei E. 2011. Albumin binding ligands and albumin conjugate uptake by cancer cells. Diabetology and Metabolic Syndrome.

Gage AA. 1998. History of cryosurgery. Semin Surg Oncol. https://doi.org/10.1002/(SICI)1098-2388(199803)14:2<99::AID-SSU2>3.0.CO;2-1.

Gaipl US, Multhoff G, Scheithauer H, Lauber K, Hehlgans S, Frey B, Rödel F. 2014. Kill and spread the word: Stimulation of antitumor immune responses in the context of radiotherapy Immunotherapy.

Gaither TW, Awad MA, Osterberg EC, Murphy GP, Allen IE, Chang A, Rosen RC, Breyer BN. 2017. The Natural History of Erectile Dysfunction After Prostatic Radiotherapy: A Systematic Review and Meta-Analysis Journal of Sexual Medicine.

Galluzzi L, Buqué A, Kepp O, Zitvogel L, Kroemer G. 2017. Immunogenic cell death in cancer and infectious disease. Nat Rev Immunol 17(2):97–111.

Ganss R, Ryschich E, Klar E, Arnold B, Hämmerling GJ. 2002. Combination of T-cell therapy and trigger of inflammation induces remodeling of the vasculature and tumor eradication. Cancer Res. https://doi.org/10.1078/0171-2985-00078.

Garg AD, Krysko D V., Vandenabeele P, Agostinis P. 2011. DAMPs and PDT-mediated photo-oxidative stress: Exploring the unknown Photochemical and Photobiological Sciences.

Garnett CT, Palena C, Chakarborty M, Tsang KY, Schlom J, Hodge JW. 2004. Sublethal irradiation of human tumor cells modulates phenotype resulting in enhanced killing by cytotoxic T lymphocytes. Cancer Res. https://doi.org/10.1158/0008-5472.CAN-04-1525.

Geiss GK, Bumgarner RE, Birditt B, Dahl T, Dowidar N, Dunaway DL, Fell HP, Ferree S, George RD, Grogan T, James JJ, Maysuria M, Mitton JD, Oliveri P, Osborn JL, Peng T, Ratcliffe AL, Webster PJ, Davidson EH, Hood L. 2008. Direct multiplexed measurement of gene expression with color-coded probe pairs. Nat Biotechnol. https://doi.org/10.1038/nbt1385.

Gevensleben H, Dietrich D, Golletz C, Steiner S, Jung M, Thiesler T, Majores M, Stein J, Uhl B, Müller S, Ellinger J, Stephan C, Jung K, Brossart P, Kristiansen G. 2016. The immune checkpoint regulator PD-L1 is highly expressed in aggressive primary prostate cancer. Clin Cancer Res. https://doi.org/10.1158/1078-0432.CCR-15-2042.

Gilchrist S, Gomes AL, Kinchesh P, Kersemans V, Allen PD, Smart SC. 2016. An MRI-compatible high frequency AC resistive heating system for homeothermic maintenance in small animals. PLoS One. https://doi.org/10.1371/journal.pone.0164920.

Gill IS, Azzouzi AR, Emberton M, Coleman JA, Coeytaux E, Scherz A, Scardino PT. 2018. Randomized Trial of Partial Gland Ablation with Vascular Targeted Phototherapy versus Active Surveillance for Low Risk Prostate Cancer: Extended Followup and Analyses of Effectiveness. J Urol. https://doi.org/10.1016/j.juro.2018.05.121.

Goedegebuure RSA, Klerk LK De, Bass AJ, Derks S, Thijssen VLJL. 2019. Combining radiotherapy with anti-angiogenic therapy and immunotherapy; A therapeutic triad for cancer? Frontiers in Immunology.

Goel S, Duda DG, Xu L, Munn LL, Boucher Y, Fukumura D, Jain RK. 2011. Normalization of the vasculature for treatment of cancer and other diseases Physiological Reviews.

Golden EB, Apetoh L. 2015. Radiotherapy and Immunogenic Cell Death. Semin Radiat Oncol 25(1):11–17.

Golden EB, Pellicciotta I, Demaria S, Barcellos-Hoff MH, Formenti SC. 2012. The convergence of radiation and immunogenic cell death signaling pathways. Front Oncol 2:88.

Gomer CJ, Ryter SW, Ferrario A, Rucker N, Wong S, Fisher AMR. 1996. Photodynamic therapy-mediated oxidative stress can induce expression of heat shock proteins. Cancer Res.

Grassberger C, Ellsworth SG, Wilks MQ, Keane FK, Loeffler JS. 2019. Assessing the interactions between radiotherapy and antitumour immunity Nature Reviews Clinical Oncology.

Gravis G, Fizazi K, Joly F, Oudard S, Priou F, Esterni B, Latorzeff I, Delva R, Krakowski I, Laguerre B, Rolland F, Théodore C, Deplanque G, Ferrero JM, Pouessel D, Mourey L, Beuzeboc P, Zanetta S, Habibian M, Berdah JF, Dauba J, Baciuchka M, Platini C, Linassier C, Labourey JL, Machiels JP, Kouri C El, Ravaud A, Suc E, Eymard JC, Hasbini

A, Bousquet G, Soulie M. 2013. Androgen-deprivation therapy alone or with docetaxel in non-castrate metastatic prostate cancer (GETUG-AFU 15): a randomised, open-label, phase 3 trial. Lancet Oncol 14(2):149–158.

Green MML, Hiley CT, Shanks JH, Bottomley IC, West CML, Cowan RA, Stratford IJ. 2007. Expression of vascular endothelial growth factor (VEGF) in locally invasive prostate cancer is prognostic for radiotherapy outcome. Int J Radiat Oncol Biol Phys. https://doi.org/10.1016/j.ijrobp.2006.08.077.

Greenberg NM, Demayo F, Finegold MJ, Medina D, Tilley WD, Aspinall JO, Cunha GR, Donjacour AA, Matusik RJ, Rosen JM. 1995. Prostate cancer in a transgenic mouse. Proc Natl Acad Sci U S A. https://doi.org/10.1073/pnas.92.8.3439.

Grenga I, Donahue RN, Lepone L, Bame J, Schlom J, Farsaci B. 2014. PD-L1 and MHC-I expression in 19 human tumor cell lines and modulation by interferon-gamma treatment. J Immunother Cancer 2(Suppl 3):P102.

Gross S, Gilead A, Scherz A, Neeman M, Salomon Y. 2003. Monitoring photodynamic therapy of solid tumors online by BOLD-contrast MRI. Nat Med. https://doi.org/10.1038/nm940.

Guillaumier S, Peters M, Arya M, Afzal N, Charman S, Dudderidge T, Hosking-Jervis F, Hindley RG, Lewi H, McCartan N, Moore CM, Nigam R, Ogden C, Persad R, Shah K, Meulen J van der, Virdi J, Winkler M, Emberton M, Ahmed HU. 2018. A Multicentre Study of 5-year Outcomes Following Focal Therapy in Treating Clinically Significant Nonmetastatic Prostate Cancer. Eur Urol. https://doi.org/10.1016/j.eururo.2018.06.006.

Hamdy FC, Elliott D, Conte S Le, Davies LC, Burns RM, Thomson C, Gray R, Wolstenholme J, Donovan JL, Fitzpatrick R, Verrill C, Gleeson F, Singh S, Rosario D, Catto JWF, Brewster S, Dudderidge T, Hindley R, Emara A, Sooriakumaran P, Ahmed HU, Leslie TA. 2018. Partial ablation versus radical prostatectomy in intermediate-risk prostate cancer: The PART feasibility RCT. Health Technol Assess (Rockv). https://doi.org/10.3310/hta22520.

Hamming LC, Slotman BJ, Verheul HMW, Thijssen VL. 2017. The clinical application of angiostatic therapy in combination with radiotherapy: past, present, future Angiogenesis.

Hanahan D, Weinberg RA. 2000. The hallmarks of cancer.Cell.

Hanahan D, Weinberg RA. 2011. Hallmarks of cancer: the next generation. Cell 144(5):646–74.

Handy CE, Antonarakis ES. 2018. Sipuleucel-T for the treatment of prostate cancer: Novel insights and future directions. Futur Oncol. https://doi.org/10.2217/fon-2017-0531.

Harris AL. 2002. Hypoxia — a key regulatory factor in tumour growth. Nat Rev Cancer 2(1):38–47.

Harris TJ, Hipkiss EL, Borzillary S, Wada S, Grosso JF, Yen HR, Getnet D, Bruno TC, Goldberg M V., Pardoll DM, DeWeese TL, Drake CG. 2008. Radiotherapy augments the immune response to prostate cancer in a time-dependent manner. Prostate. https://doi.org/10.1002/pros.20794.

Heckmann M, Douwes K, Peter R, Degitz K. 1998. Vascular activation of adhesion molecule mRNA and cell surface expression by ionizing radiation. Exp Cell Res

238(1):148–154.

Hegemann NS, Guckenberger M, Belka C, Ganswindt U, Manapov F, Li M. 2014. Hypofractionated radiotherapy for prostate cancer. Radiation Oncology.

Heidenreich A, Bastian PJ, Bellmunt J, Bolla M, Joniau S, Kwast T van der, Mason M, Matveev V, Wiegel T, Zattoni F, Mottet N, European Association of Urology. 2014a. EAU guidelines on prostate cancer. part 1: screening, diagnosis, and local treatment with curative intent-update 2013. Eur Urol 65(1):124–37.

Heidenreich A, Bastian PJ, Bellmunt J, Bolla M, Joniau S, Kwast T van der, Mason M, Matveev V, Wiegel T, Zattoni F, Mottet N, European Association of Urology. 2014b. EAU guidelines on prostate cancer. Part II: Treatment of advanced, relapsing, and castration-resistant prostate cancer. Eur Urol 65(2):467–79.

Heidenreich A, Bellmunt J, Bolla M, Joniau S, Mason M, Matveev V, Mottet N, Schmid HP, Kwast T Van Der, Wiegel T, Zattoni F. 2011. European Urology.
Hemminki K. 2012. World Journal of Urology.

Hohlweg-Majert B, Ristow O, Gust K, Kehl V, Wolff KD, Pigorsch S. 2012. Impact of radiotherapy on microsurgical reconstruction of the head and neck. J Cancer Res Clin Oncol. https://doi.org/10.1007/s00432-012-1263-6.

Horsman MR, Overgaard J. 2016. The impact of hypoxia and its modification of the outcome of radiotherapy. J Radiat Res 57 Suppl 1:i90–i98.

Hoskin PJ, Rojas AM, Bownes PJ, Lowe GJ, Ostler PJ, Bryant L. 2012. Randomised trial of external beam radiotherapy alone or combined with high-dose-rate brachytherapy boost for localised prostate cancer. Radiother Oncol 103(2):217–222.

Hoskin PJ, Rojas AM, Ostler PJ, Hughes R, Bryant L, Lowe GJ. 2014. Dosimetric predictors of biochemical control of prostate cancer in patients randomised to external beam radiotherapy with a boost of high dose rate brachytherapy. Radiother Oncol 110(1):110–113.

https://github.com/alanaberdeen/AIDA. https://github.com/alanaberdeen/AIDA. Accessed May 9, 2021.

https://humanhealth.iaea.org/HHW/RadiationOncology/Treatingpatients/Treatment_planning_and_techniques/Training_Course/03_Altered_fractionation.pdf. https://humanhealth.iaea.org/HHW/RadiationOncology/Treatingpatients/Treatment_planning_and_techniques/Training_Course/03_Altered_fractionation.pdf. Accessed July 26, 2021.

https://www.lgcstandards-atcc.org/en.aspx. Accessed December 16, 2020.

Huang Z, Chen Q, Dole KC, Barqawi AB, Chen YK, Blanc D, Wilson BC, Hetzel FW. 2007. The effect of Tookad-mediated photodynamic ablation of the prostate gland on adjacent tissues - In vivo study in a canine model.

Idorn M, Køllgaard T, Kongsted P, Sengeløv L, thor Straten P. 2014. Correlation between frequencies of blood monocytic myeloid-derived suppressor cells, regulatory T cells and negative prognostic markers in patients with castration-resistant metastatic prostate cancer. Cancer Immunol Immunother. https://doi.org/10.1007/s00262-014-1591-2.

Isaacs W, Kainu T. 2001. Oncogenes and tumor suppressor genes in prostate cancer. Epidemiologic Reviews.

Ittmann M, Huang J, Radaelli E, Martin P, Signoretti S, Sullivan R, Simons BW, Ward JM, Robinson BD, Chu GC, Loda M, Thomas G, Borowsky A, Cardiff RD. 2013. Cancer Research.

Jaakkola P, Mole DR, Tian YM, Wilson MI, Gielbert J, Gaskell SJ, Kriegsheim A Von, Hebestreit HF, Mukherji M, Schofield CJ, Maxwell PH, Pugh CW, Ratcliffe PJ. 2001. Targeting of HIF-α to the von Hippel-Lindau ubiquitylation complex by O2-regulated prolyl hydroxylation. Science (80-). https://doi.org/10.1126/science.1059796.

Jain RK. 2001. Normalizing tumor vasculature with anti-angiogenic therapy: A new paradigm for combination therapy. Nat Med 7(9):987–989.

Jain RK. 2005. Normalization of tumor vasculature: An emerging concept in antiangiogenic therapy Science.

James ND, Sydes MR, Clarke NW, Mason MD, Dearnaley DP, Spears MR, Ritchie AWS, Parker CC, Russell JM, Attard G, Bono J De, Cross W, Jones RJ, Thalmann G, Amos C, Matheson D, Millman R, Alzouebi M, Beesley S, Birtle AJ, Brock S, Cathomas R, Chakraborti P, Chowdhury S, Cook A, Elliott T, Gale J, Gibbs S, Graham JD, Hetherington J, Hughes R, Laing R, McKinna F, McLaren DB, O'Sullivan JM, Parikh O, Peedell C, Protheroe A, Robinson AJ, Srihari N, Srinivasan R, Staffurth J, Sundar S, Tolan S, Tsang D, Wagstaff J, Parmar MKB. 2016. Addition of docetaxel, zoledronic acid, or both to first-line long-term hormone therapy in prostate cancer (STAMPEDE): Survival results from an adaptive, multiarm, multistage, platform randomised controlled trial. Lancet. https://doi.org/10.1016/S0140-6736(15)01037-5.

Janiak MK, Wincenciak M, Cheda A, Nowosielska EM, Calabrese EJ. 2017. Cancer immunotherapy: how low-level ionizing radiation can play a key role. Cancer Immunol Immunother 66(7):819–832.

Janssen MHM, Aerts HJWL, Kierkels RGJ, Backes WH, Öllers MC, Buijsen J, Lambin P, Lammering G. 2010. Tumor perfusion increases during hypofractionated short-course radiotherapy in rectal cancer: Sequential perfusion-CT findings. Radiother Oncol. https://doi.org/10.1016/j.radonc.2009.12.013.

Jeong H, Bok S, Hong B-J, Choi H-S, Ahn G-O. 2016. Radiation-induced immune responses: mechanisms and therapeutic perspectives. Blood Res 51(3):157–163.

Jones KI, Tiersma J, Yuzhalin AE, Gordon-Weeks AN, Buzzelli J, Im JH, Muschel RJ. 2018. Radiation combined with macrophage depletion promotes adaptive immunity and potentiates checkpoint blockade. EMBO Mol Med. https://doi.org/10.15252/emmm.201809342.

Jung JH, Risk MC, Goldfarb R, Reddy B, Coles B, Dahm P. 2018. Primary cryotherapy for localised or locally advanced prostate cancer. Cochrane Database of Systematic Reviews.

Kachikwu EL, Iwamoto KS, Liao YP, Demarco JJ, Agazaryan N, Economou JS, McBride WH, Schaue D. 2011. Radiation enhances regulatory T cell representation. Int J Radiat Oncol Biol Phys 81(4):1128–1135.

Kalbasi A, Komar C, Tooker GM, Liu M, Lee JW, Gladney WL, Ben-Josef E, Beatty GL.

2017. Tumor-derived CCL2 mediates resistance to radiotherapy in pancreatic ductal adenocarcinoma. Clin Cancer Res. https://doi.org/10.1158/1078-0432.CCR-16-0870.

Kane JL, Krueger SA, Hanna A, Raffel TR, Wilson GD, Madlambayan GJ, Marples B. 2016. Effect of Irradiation on Tumor Microenvironment and Bone Marrow Cell Migration in a Preclinical Tumor Model. Int J Radiat Oncol Biol Phys. https://doi.org/10.1016/j.ijrobp.2016.04.028.

Kanthou C, Tozer G. 2018. Targeting the vasculature of tumours: combining VEGF pathway inhibitors with radiotherapy. Br J Radiol 20180405.

Kantoff PW, Higano CS, Shore ND, Berger ER, Small EJ, Penson DF, Redfern CH, Ferrari AC, Dreicer R, Sims RB, Xu Y, Frohlich MW, Schellhammer PF. 2010. Sipuleucel-T Immunotherapy for Castration-Resistant Prostate Cancer. N Engl J Med 363(5):411–422.

Karan D, Dubey S. 2016. From inflammation to prostate cancer: The role of inflammasomes Advances in Urology.

Karan D, Lin MF, Johansson SL, Batra SK. 2003. Current status of the molecular genetics of human prostatic adenocarcinomas International Journal of Cancer.

Karantanos T, Corn PG, Thompson TC. 2013. Prostate cancer progression after androgen deprivation therapy: Mechanisms of castrate resistance and novel therapeutic approaches Oncogene.

Katsogiannou M, Ziouziou H, Karaki S, Andrieu C, Henry de Villeneuve M, Rocchi P. 2015. The hallmarks of castration-resistant prostate cancers Cancer Treatment Reviews.

Kawczyk-Krupka A, Wawrzyniec K, Musiol SK, Potempa M, Bugaj AM, Sieroń A. 2015. Treatment of localized prostate cancer using WST-09 and WST-11 mediated vascular targeted photodynamic therapy-A review Photodiagnosis and Photodynamic Therapy.

Kersemans V, Gilchrist S, Allen PD, Beech JS, Kinchesh P, Vojnovic B, Smart SC. 2015. A resistive heating system for homeothermic maintenance in small animals. Magn Reson Imaging. https://doi.org/10.1016/j.mri.2015.03.011.

Keyzer F De, Vandecaveye V, Thoeny H, Chen F, Ni Y, Marchal G, Hermans R, Nuyts S, Landuyt W, Bosmans H. 2009. Dynamic contrast-enhanced and diffusion-weighted MRI for early detection of tumoral changes in single-dose and fractionated radiotherapy: Evaluation in a rat rhabdomyosarcoma model. Eur Radiol. https://doi.org/10.1007/s00330-009-1451-1.

Kilkenny C, Browne WJ, Cuthill IC, Emerson M, Altman DG. 2010. Improving bioscience research reporting: The arrive guidelines for reporting animal research. PLoS Biol. https://doi.org/10.1371/journal.pbio.1000412.

Kim K, Watson PA, Lebdai S, Jebiwott S, Somma AJ, Rosa S La, Mehta D, Murray KS, Lilja H, Ulmert D, Monette S, Scherz A, Coleman JA. 2018. Androgen deprivation therapy potentiates the efficacy of vascular targeted photodynamic therapy of prostate cancer xenografts. Clin Cancer Res. https://doi.org/10.1158/1078-0432.CCR-17-3474.

Kim K, Zhang H, Rosa S La, Jebiwott S, Desai P, Kimm S, Scherz A, O'Donoghue JA, Weber WA, Coleman JA. 2017. Bombesin antagonist-based radiotherapy of prostate cancer combined with WST-11 vascular targeted photodynamic therapy. Clin Cancer Res.

https://doi.org/10.1158/1078-0432.CCR-16-2745.

King CR, Collins S, Fuller D, Wang P-C, Kupelian P, Steinberg M, Katz A. 2013. Health-related quality of life after stereotactic body radiation therapy for localized prostate cancer: results from a multi-institutional consortium of prospective trials. Int J Radiat Oncol Biol Phys 87(5):939–45.

Kioi M, Vogel H, Schultz G, Hoffman RM, Harsh GR, Brown JM. 2010. Inhibition of vasculogenesis, but not angiogenesis, prevents the recurrence of glioblastoma after irradiation in mice. J Clin Invest. https://doi.org/10.1172/JCI40283.

Kleibeuker EA, Fokas E, Allen PD, Kersemans V, Griffioen AW, Beech J, Im JH, Smart SC, Castricum KC, Berg J van den, Schulkens IA, Hill SA, Harris AL, Slotman BJ, Verheul HM, Muschel RJ, Thijssen VL. 2016. Low dose angiostatic treatment counteracts radiotherapy-induced tumor perfusion and enhances the anti-tumor effect. Oncotarget. https://doi.org/10.18632/oncotarget.12814.

Kleibeuker EA, Hooven MA ten, Verheul HM, Slotman BJ, Thijssen VL. 2015. Combining radiotherapy with sunitinib: lessons (to be) learned. Angiogenesis.

Klotz L, Vesprini D, Sethukavalan P, Jethava V, Zhang L, Jain S, Yamamoto T, Mamedov A, Loblaw A. 2015. Long-term follow-up of a large active surveillance cohort of patients with prostate cancer. J Clin Oncol. https://doi.org/10.1200/JCO.2014.55.1192.

Ko EC, Formenti SC. 2018. Radiotherapy and checkpoint inhibitors: a winning new combination? Ther Adv Med Oncol 10:1758835918768240.

Koh CM, Bieberich CJ, Dang C V., Nelson WG, Yegnasubramanian S, Marzo AM De. 2010. MYC and prostate cancer. Genes and Cancer. https://doi.org/10.1177/1947601910379132.

Korbelik M, Sun J, Cecic I. 2005. Photodynamic therapy-induced cell surface expression and release of heat shock proteins: Relevance for tumor response. Cancer Res.

Kotecha R, Djemil T, Tendulkar RD, Reddy CA, Thousand RA, Vassil A, Stovsky M, Berglund RK, Klein EA, Stephans KL. 2016. Dose-Escalated Stereotactic Body Radiation Therapy for Patients With Intermediate- and High-Risk Prostate Cancer: Initial Dosimetry Analysis and Patient Outcomes. Int J Radiat Oncol Biol Phys 95(3):960–964.

Kothari G, Loblaw A, Tree AC, As NJ van, Moghanaki D, Lo SS, Ost P, Siva S. 2018. Stereotactic Body Radiotherapy for Primary Prostate Cancer. Technol Cancer Res Treat 17:1533033818789633.

Koudinova N V., Pinthus JH, Brandis A, Brenner O, Bendel P, Ramon J, Eshhar Z, Scherz A, Salomon Y. 2003. Photodynamic therapy with Pd-Bacteriopheophorbide (TOOKAD): Successful in vivo treatment of human prostatic small cell carcinoma xenografts. Int J Cancer. https://doi.org/10.1002/ijc.11002.

Koukourakis MI, Giatromanolaki A, Skarlatos J, Corti L, Blandamura S, Piazza M, Gatter KC, Harris AL. 2001. Hypoxia inducible factor (HIF-1a and HIF-2a) expression in early esophageal cancer and response to photodynamic therapy and radiotherapy. Cancer Res.

Kozin S V., Kamoun WS, Huang Y, Dawson MR, Jain RK, Duda DG. 2010. Recruitment of myeloid but not endothelial precursor cells facilitates tumor regrowth after local

irradiation. Cancer Res. https://doi.org/10.1158/0008-5472.CAN-09-4446.

Kozin S V, Boucher Y, Hicklin DJ, Bohlen P, Jain RK, Suit HD. 2001. Vascular endothelial growth factor receptor-2-blocking antibody potentiates radiation-induced long-term control of human tumor xenografts. Cancer Res 61(1):39–44.

Kulkarni MM. 2011. Digital multiplexed gene expression analysis using the nanostring ncounter system. Curr Protoc Mol Biol. https://doi.org/10.1002/0471142727.mb25b10s94.

Kupelian PA, Buchsbaum JC, Patel C, Elshaikh M, Reddy CA, Zippe C, Klein EA. 2002. Impact of biochemical failure on overall survival after radiation therapy for localized prostate cancer in the PSA era. Int J Radiat Oncol Biol Phys. https://doi.org/10.1016/S0360-3016(01)02778-X.

Kurien BT, Hensley K, Bachmann M, Scofield RH. 2006. Oxidatively modified autoantigens in autoimmune diseases. Free Radical Biology and Medicine.

Kwon EDED., Drake CGCG., Scher HIHI., Fizazi KK., Bossi AA., Eertwegh AJM. den, Krainer M. M, Houede NN. i, Santos R. R, Mahammedi H, Ng SS., Maio MM., Franke FAFA., Sundar SS., Agarwal N. N, Bergman AMAM., Ciuleanu TETE., Korbenfeld E. E, Sengeløv LL., Hansen S. S, Logothetis CC., Beer TMTM., McHenry MB. B, Gagnier P. P, Liu DD., Gerritsen WRWR., Eertwegh AJM Van den, Krainer M. M, Houede NN. i, Santos R. R, Mahammedi H, Ng SS., Maio MM., Franke FAFA., Sundar SS., Agarwal N. N, Bergman AMAM., Ciuleanu TETE., Korbenfeld E. E, Sengeløv LL., Hansen S. S, Logothetis CC., Beer TMTM., McHenry MB. B, Gagnier P. P, Liu DD., Gerritsen WRWR. 2014. Ipilimumab versus placebo after radiotherapy in patients with metastatic castration-resistant prostate cancer that had progressed after docetaxel chemotherapy (CA184-043): A multicentre, randomised, double-blind, phase 3 trial. Lancet Oncol 15(7):700–712.

Lancet Oncology T. 2014. Proton therapy for prostate cancer: time for evidence. Lancet Oncol 15(103):775.

Lardas M, Liew M, Bergh RC van den, Santis M De, Bellmunt J, Broeck T Van den, Cornford P, Cumberbatch MG, Fossati N, Gross T, Henry AM, Bolla M, Briers E, Joniau S, Lam TB, Mason MD, Mottet N, Poel HG van der, Rouvière O, Schoots IG, Wiegel T, Willemse P-PM, Yuan CY, Bourke L. 2017a. Quality of Life Outcomes after Primary Treatment for Clinically Localised Prostate Cancer: A Systematic Review. Eur Urol 72(6):869–885.

Lawrence MS, Stojanov P, Polak P, Kryukov G V., Cibulskis K, Sivachenko A, Carter SL, Stewart C, Mermel CH, Roberts SA, Kiezun A, Hammerman PS, McKenna A, Drier Y, Zou L, Ramos AH, Pugh TJ, Stransky N, Helman E, Kim J, Sougnez C, Ambrogio L, Nickerson E, Shefler E, Cortés ML, Auclair D, Saksena G, Voet D, Noble M, Dicara D, Lin P, Lichtenstein L, Heiman DI, Fennell T, Imielinski M, Hernandez B, Hodis E, Baca S, Dulak AM, Lohr J, Landau DA, Wu CJ, Melendez-Zajgla J, Hidalgo-Miranda A, Koren A, McCarroll SA, Mora J, Lee RS, Crompton B, Onofrio R, Parkin M, Winckler W, Ardlie K, Gabriel SB, Roberts CWM, Biegel JA, Stegmaier K, Bass AJ, Garraway LA, Meyerson M, Golub TR, Gordenin DA, Sunyaev S, Lander ES, Getz G. 2013. Mutational heterogeneity in cancer and the search for new cancer-associated genes. Nature. https://doi.org/10.1038/nature12213.

Leal F, Figueiredo MAN de, Sasse AD. 2015. International Braz J Urol.
Lebdai S, Gigoux M, Alvim R, Somma A, Nagar K, Azzouzi AR, Cussenot O, Merghoub T, Wolchok JD, Scherz A, Kim K, Coleman J. 2019. Potentiating vascular-targeted photodynamic therapy through CSF-1R modulation of myeloid cells in a preclinical model

of prostate cancer. Oncoimmunology. https://doi.org/10.1080/2162402X.2019.1581528.

Lechner MG, Karimi SS, Barry-Holson K, Angell TE, Murphy KA, Church CH, Ohlfest JR, Hu P, Epstein AL. 2013. Immunogenicity of murine solid tumor models as a defining feature of in vivo behavior and response to immunotherapy. J Immunother. https://doi.org/10.1097/01.cji.0000436722.46675.4a.

Lee CG, Heijn M, Tomaso E di, Griffon-Etienne G, Ancukiewicz M, Koike C, Park KR, Ferrara N, Jain RK, Suit HD, Boucher Y. 2000. Anti-Vascular endothelial growth factor treatment augments tumor radiation response under normoxic or hypoxic conditions. Cancer Res 60(19):5565–70.

Lee JT, Lehmann BD, Terrian DM, Chappell WH, Stivala F, Libra M, Martelli AM, Steelman LS, McCubrey JA. 2008. Targeting prostate cancer based on signal transduction and cell cycle pathways. Cell Cycle. https://doi.org/10.4161/cc.7.12.6166. Leitzmann MF, Rohrmann S. 2012. Clinical Epidemiology.

Liauw SL, Connell PP, Weichselbaum RR. 2013. New paradigms and future challenges in radiation oncology: An update of biological targets and technology. Science Translational Medicine.

Lin BK, Clyne M, Walsh M, Gomez O, Yu W, Gwinn M, Khoury MJ. 2006. Tracking the epidemiology of human genes in the literature: The HuGE published literature database. American Journal of Epidemiology.

Liu SC, Alomran R, Chernikova SB, Lartey F, Stafford J, Jang T, Merchant M, Zboralski D, Zöllner S, Kruschinski A, Klussmann S, Recht L, Brown JM. 2014. Blockade of SDF-1 after irradiation inhibits tumor recurrences of autochthonous brain tumors in rats. Neuro Oncol. https://doi.org/10.1093/neuonc/not149.

Lomax ME, Folkes LK, O'Neill P. 2013. Biological consequences of radiation-induced DNA damage: relevance to radiotherapy. Clin Oncol (R Coll Radiol) 25(10):578–85. Lopez-Bujanda Z, Drake CG. 2017. Myeloid-derived cells in prostate cancer progression: phenotype and prospective therapies. J Leukoc Biol. https://doi.org/10.1189/jlb.5vmr1116-491rr.

Lugade AA, Moran JP, Gerber SA, Rose RC, Frelinger JG, Lord EM. 2005. Local Radiation Therapy of B16 Melanoma Tumors Increases the Generation of Tumor Antigen-Specific Effector Cells That Traffic to the Tumor. J Immunol 174(12):7516–7523.

Madar-Balakirski N, Tempel-Brami C, Kalchenko V, Brenner O, Varon D, Scherz A, Salomon Y. 2010a. Permanent occlusion of feeding arteries and draining veins in solid mouse tumors by vascular Targeted Photodynamic Therapy (VTP) with tookad. PLoS One. https://doi.org/10.1371/journal.pone.0010282.

Maeda A, Chen Y, Bu J, Mujcic H, Wouters BG, DaCosta RS. 2017. In Vivo Imaging Reveals Significant Tumor Vascular Dysfunction and Increased Tumor Hypoxia-Inducible Factor-1α Expression Induced by High Single-Dose Irradiation in a Pancreatic Tumor Model. Int J Radiat Oncol Biol Phys. https://doi.org/10.1016/j.ijrobp.2016.09.005.

Magali Lecavalier-Barsoum, Naz Chaudary , Kathy Han, Melania Pintilie RPHMM. 2019. Targeting CXCL12/CXCR4 and Myeloid Cells to Improve the Therapeutic Ratio in Patient-Derived Cervical Cancer Models Treated With Radio-Chemotherapy. Br J Cancer 121(3):249–256.

Makkouk A, Weiner GJ. 2015. Cancer immunotherapy and breaking immune tolerance: new approaches to an old challenge. Cancer Res 75(1):5–10.

Marberger M, Carroll PR, Zelefsky MJ, Coleman JA, Hricak H, Scardino PT, Abenhaim LL. 2008. New Treatments for Localized Prostate Cancer. Urology. https://doi.org/10.1016/j.urology.2008.08.506.

Marzo AM De, Platz EA, Sutcliffe S, Xu J, Grönberg H, Drake CG, Nakai Y, Isaacs WB, Nelson WG. 2007. nflammation in prostate carcinogenesis. Nature Reviews Cancer.

Matta R, Chapple CR, Fisch M, Heidenreich A, Herschorn S, Kodama RT, Koontz BF, Murphy DG, Nguyen PL, Nam RK. 2019b. Pelvic Complications After Prostate Cancer Radiation Therapy and Their Management: An International Collaborative Narrative Review. Eur Urol 75(3):464–476.

Mauceri HJ, Hanna NN, Beckett MA, Gorski DH, Staba MJ, Stellato KA, Bigelow K, Heimann R, Gately S, Dhanabal M, Soff GA, Sukhatme VP, Kufe DW, Weichselbaum RR. 1998. Combined effects of angiostatin and ionizing radiation in antitumour therapy. Nature 394(6690):287–91.

Mazor O, Brandis A, Plaks V, Neumark E, Rosenbach-Belkin V, Salomon Y, Scherz A. 2004. WST11, A Novel Water-Soluble Bacteriochlorophyll Derivative; Cellular uptake, Pharmacokinetics, Biodistribution, and Vascular Targeted Photodynamic Activity Against Melanoma tumors. Photochem Photobiol. https://doi.org/10.1562/2004-06-14-ra-199.

Mccurdy TR, Gataiance S, Eltringham-Smith LJ, Sheffield WP. 2004. A covalently linked recombinant albumin dimer is more rapidly cleared in vivo than are wild-type and mutant C34A albumin. J Lab Clin Med. https://doi.org/10.1016/j.lab.2003.10.008.

McKenzie S, Kyprianou N. 2006. Apoptosis evasion: The role of survival pathways in prostate cancer progression and therapeutic resistance. Journal of Cellular Biochemistry.

Melegh Z, Oltean S. 2019. International Journal of Molecular Sciences.
Mendez MH, Passoni NM, Pow-Sang J, Jones JS, Polascik TJ. 2015. Comparison of outcomes between preoperatively potent men treated with focal versus whole gland cryotherapy in a matched population. J Endourol. https://doi.org/10.1089/end.2014.0881.

Meng Y, Beckett MA, Liang H, Mauceri HJ, Rooijen N Van, Cohen KS, Weichselbaum RR. 2010. Blockade of tumor necrosis factor α signaling in tumor-associated macrophages as a radiosensitizing strategy. Cancer Res. https://doi.org/10.1158/0008-5472.CAN-09-2995.

Mimeault M, Batra SK. 2011. Biochimica et Biophysica Acta - Reviews on Cancer.
Miralbell R, Roberts SA, Zubizarreta E, Hendry JH. 2012a. Dose-fractionation sensitivity of prostate cancer deduced from radiotherapy outcomes of 5,969 patients in seven international institutional datasets: α/β = 1.4 (0.9-2.2) Gy. Int J Radiat Oncol Biol Phys 82(1).

Miralbell R, Roberts SA, Zubizarreta E, Hendry JH. 2012b. Dose-fractionation sensitivity of prostate cancer deduced from radiotherapy outcomes of 5,969 patients in seven international institutional datasets: α/β = 1.4 (0.9-2.2) Gy. Int J Radiat Oncol Biol Phys. https://doi.org/10.1016/j.ijrobp.2010.10.075.

Mitra S, Cassar SE, Niles DJ, Puskas JA, Frelinger JG, Foster TH. 2006. Photodynamic therapy mediates the oxygen-independent activation of hypoxia-inducible factor 1α. Mol

Cancer Ther. https://doi.org/10.1158/1535-7163.MCT-06-0421.

Moore CM, Azzouzi AR, Barret E, Villers A, Muir GH, Barber NJ, Bott S, Trachtenberg J, Arumainayagam N, Gaillac B, Allen C, Schertz A, Emberton M. 2015. Determination of optimal drug dose and light dose index to achieve minimally invasive focal ablation of localised prostate cancer using WST11-vascular-targeted photodynamic (VTP) therapy. BJU Int. https://doi.org/10.1111/bju.12816.

Moore CM, Hoh IM, Bown SG, Emberton M. 2005. Does photodynamic therapy have the necessary attributes to become a future treatment for organ-confined prostate cancer? BJU International.

Morris WJ, Tyldesley S, Rodda S, Halperin R, Pai H, McKenzie M, Duncan G, Morton G, Hamm J, Murray N. 2017. Androgen Suppression Combined with Elective Nodal and Dose Escalated Radiation Therapy (the ASCENDE-RT Trial): An Analysis of Survival Endpoints for a Randomized Trial Comparing a Low-Dose-Rate Brachytherapy Boost to a Dose-Escalated External Beam Boost f. Int J Radiat Oncol Biol Phys 98(2):275–285.

Mottet N, Bellmunt J, Bolla M, Briers E, Cumberbatch MG, Santis M De, Fossati N, Gross T, Henry AM, Joniau S, Lam TB, Mason MD, Matveev VB, Moldovan PC, Bergh RCN van den, Broeck T Van den, Poel HG van der, Kwast TH van der, Rouviere O, Schoots IG, Wiegel T, Cornford P. 2017. EAU-ESTRO-SIOG Guidelines on Prostate Cancer. Part 1: Screening, Diagnosis, and Local Treatment with Curative Intent. Eur Urol 71(4):618–629.

Natsagdorj A, Izumi K, Hiratsuka K, Machioka K, Iwamoto H, Naito R, Makino T, Kadomoto S, Shigehara K, Kadono Y, Lin W-J, Maolake A, Mizokami A. 2019. CCL2 induces resistance to the antiproliferative effect of cabazitaxel in prostate cancer cells. Cancer Sci 110(1):279–288.

Neefjes JJ, Hammerling GJ, Momburg F. 1993. Folding and Assembly of Major Histocompatibility Complex Class I Heterodimers in the Endoplasmic Reticulum of Intact Cells Precedes the Binding of Peptide. J Exp Med. https://doi.org/10.1084/jem.178.6.1971.

Neuschmelting V, Kim K, Malekzadeh-Najafabadi J, Jebiwott S, Prakash J, Scherz A, Coleman JA, Kircher MF, Ntziachristos V. 2018. WST11 vascular targeted photodynamic therapy effect monitoring by multispectral optoacoustic tomography (MSOT) in mice. Theranostics. https://doi.org/10.7150/thno.20386.

Nogueira L, Tracey AT, Alvim R, Reisz P, Scherz A, Coleman JA, Kim K. 2020. Developments in Vascular-Targeted Photodynamic Therapy for Urologic Malignancies. Molecules (Basel, Switzerland).

Nora Ness, Sigve Andersen, Mehrdad Rakaee Khanehkenari C V., Nordbakken, Andrej Valkov, Erna-Elise Paulsen, Yngve Nordby RM, Bremnes,Tom Donnem, Lill-Tove Busund ER. 2017. The prognostic role of immune checkpoint markers programmed cell death protein 1 (PD-1) and programmed death ligand 1 (PD-L1) in a large, multicenter prostate cancer cohort. Oncotarget 8(16):26789–26801.

Noy D, Fiedor L, Hartwich G, Scheer H, Scherz A. 1998. Metal-substituted bacteriochlorophylls. 2. Changes in redox potentials and electronic transition energies are dominated by intramolecular electrostatic interactions. J Am Chem Soc. https://doi.org/10.1021/ja970875m.

O'Shaughnessy MJ, Murray KS, Rosa SP La, Budhu S, Merghoub T, Somma A, Monette

S, Kim K, Corradi RB, Scherz A, Coleman JA. 2018. Systemic antitumor immunity by PD-1/PD-L1 inhibition is potentiated by vascular-targeted photodynamic therapy of primary tumors. Clin Cancer Res. https://doi.org/10.1158/1078-0432.CCR-17-0186.

Oh YT, Chen DWC, Dougherty GJ, McBride WH. 2004. Adenoviral interleukin-3 gene-radiation therapy for prostate cancer in mouse model. Int J Radiat Oncol Biol Phys. https://doi.org/10.1016/j.ijrobp.2004.01.030.

Olama AA Al, Dadaev T, Hazelett DJ, Li Q, Leongamornlert D, Saunders EJ, Stephens S, Cieza-Borrella C, Whitmore I, Garcia SB, Giles GG, Southey MC, Fitzgerald L, Gronberg H, Wiklund F, Aly M, Henderson BE, Schumacher F, Haiman CA, Schleutker J, Wahlfors T, Tammela TL, Nordestgaard BG, Key TJ, Travis RC, Neal DE, Donovan JL, Hamdy FC, Pharoah P, Pashayan N, Khaw KT, Stanford JL, Thibodeau SN, Mcdonnell SK, Schaid DJ, Maier C, Vogel W, Luedeke M, Herkommer K, Kibel AS, Cybulski C, Wokolorczyk D, Kluzniak W, Cannon-Albright L, Brenner H, Butterbach K, Arndt V, Park JY, Sellers T, Lin HY, Slavov C, Kaneva R, Mitev V, Batra J, Clements JA, Spurdle A, Teixeira MR, Paulo P, Maia S, Pandha H, Michael A, Kierzek A, Govindasami K, Guy M, Lophatonanon A, Muir K, Viñuela A, Brown AA, Freedman M, Conti D V., Easton D, Coetzee GA, Eeles RA, Kote-Jarai Z. 2015. Multiple novel prostate cancer susceptibility signals identified by fine-mapping of known risk loci among Europeans. Hum Mol Genet. https://doi.org/10.1093/hmg/ddv203.

Ost P. 2018. It Ain't Over Till the Fat Lady Sings: The POPSTAR Trial. Eur Urol 74(4):463–464.

Ost P, Reynders D, Decaestecker K, Fonteyne V, Lumen N, Bruycker A De, Lambert B, Delrue L, Bultijnck R, Claeys T, Goetghebeur E, Villeirs G, Man K De, Ameye F, Billiet I, Joniau S, Vanhaverbeke F, Meerleer G De. 2017. Surveillance or Metastasis-Directed Therapy for Oligometastatic Prostate Cancer Recurrence: A Prospective, Randomized, Multicenter Phase II Trial. J Clin Oncol JCO.2017.75.485.

Ostrand-Rosenberg S, Sinha P. 2009. Myeloid-Derived Suppressor Cells: Linking Inflammation and Cancer. J Immunol. https://doi.org/10.4049/jimmunol.0802740. Overgaard J. 2007. Journal of Clinical Oncology.

Packer JR, Maitland NJ. 2016. The molecular and cellular origin of human prostate cancer. Biochimica et Biophysica Acta - Molecular Cell Research.

Palma DA, Olson RA, Harrow S, Gaede S, Louie AV, Haasbeek C, Mulroy LA, Lock MI, Rodrigues G, Yaremko BP, Schellenberg D, Ahmad B, Griffioen G, Senthi S, Liu MC, Moore K, Currie S, Bauman GS, Warner A, Senan S. 2018. Stereotactic Ablative Radiation Therapy for the Comprehensive Treatment of Oligometastatic Tumors (SABR-COMET): Results of a Randomized Trial. Int J Radiat Oncol 102(3):S3–S4.

Park HJ, Griffin RJ, Hui S, Levitt SH, Song CW. 2012. Radiation-Induced Vascular Damage in Tumors: Implications of Vascular Damage in Ablative Hypofractionated Radiotherapy (SBRT and SRS). Radiat Res. https://doi.org/10.1667/rr2773.1.

Parker CC, James ND, Brawley CD, Clarke NW, Hoyle AP, Ali A, Ritchie AWS, Attard G, Chowdhury S, Cross W, Dearnaley DP, Gillessen S, Gilson C, Jones RJ, Langley RE, Malik ZI, Mason MD, Matheson D, Millman R, Russell JM, Thalmann GN, Amos CL, Alonzi R, Bahl A, Birtle A, Din O, Douis H, Eswar C, Gale J, Gannon MR, Jonnada S, Khaksar S, Lester JF, O'Sullivan JM, Parikh OA, Pedley ID, Pudney DM, Sheehan DJ, Srihari NN, Tran ATH, Parmar MKB, Sydes MR, Systemic Therapy for Advanced or Metastatic Prostate cancer: Evaluation of Drug Efficacy (STAMPEDE) investigators. 2018.

Radiotherapy to the primary tumour for newly diagnosed, metastatic prostate cancer (STAMPEDE): a randomised controlled phase 3 trial. Lancet 392(10162):2353–2366.

Payne H, Mason M. 2011. Androgen deprivation therapy as adjuvant/neoadjuvant to radiotherapy for high-risk localised and locally advanced prostate cancer: recent developments. Br J Cancer 105(11):1628–34.

PCUK strategy. https://prostatecanceruk.org/research/our-research-strategy. Accessed 28/05/21.

Philippou Y, Protheroe AS, Bryant RJ. 2020a. Re: Pembrolizumab for Treatment-refractory Metastatic Castration-resistant Prostate Cancer: Multicohort, Open-label Phase II KEYNOTE-199 Study. European Urology.

Philippou Y, Sjoberg H, Lamb AD, Camilleri P, Bryant RJ. 2020b. Harnessing the potential of multimodal radiotherapy in prostate cancer. Nature Reviews Urology.

Philippou Y, Sjoberg HT, Murphy E, Alyacoubi S, Jones KI, Gordon-Weeks AN, Phyu S, Parkes EE, Gillies McKenna W, Lamb AD, Gileadi U, Cerundolo V, Scheiblin DA, Lockett SJ, Wink DA, Mills IG, Hamdy FC, Muschel RJ, Bryant RJ. 2020c. Impacts of combining anti-PD-L1 immunotherapy and radiotherapy on the tumour immune microenvironment in a murine prostate cancer model. Br J Cancer. https://doi.org/10.1038/s41416-020-0956-x.

Plaks V, Koudinova N, Nevo U, Pinthus JH, Kanety H, Eshhar Z, Ramon J, Scherz A, Neeman M, Salomon Y. 2004. Photodynamic Therapy of Established Prostatic Adenocarcinoma with TOOKAD: A Biphasic Apparent Diffusion Coefficient Change as Potential Early MRI Response Marker. Neoplasia. https://doi.org/10.1593/neo.03352.

Poel HG van der, Bergh RCN van den, Briers E, Cornford P, Govorov A, Henry AM, Lam TB, Mason MD, Rouvière O, Santis M De, Willemse PPM, Poppel H van, Mottet N. 2018. Focal Therapy in Primary Localised Prostate Cancer: The European Association of Urology Position in 2018. Eur Urol. https://doi.org/10.1016/j.eururo.2018.01.001.

Postow MA, Callahan MK, Barker CA, Yamada Y, Yuan J, Kitano S, Mu Z, Rasalan T, Adamow M, Ritter E, Sedrak C, Jungbluth AA, Chua R, Yang AS, Roman R-A, Rosner S, Benson B, Allison JP, Lesokhin AM, Gnjatic S, Wolchok JD. 2012. Immunologic Correlates of the Abscopal Effect in a Patient with Melanoma. N Engl J Med. https://doi.org/10.1056/nejmoa1112824.

Potiron VA, Abderrahmani R, Cleḿent-Colmou K, Marionneau-Lambot S, Oullier T, Paris F, Supiot S. 2013. Improved functionality of the vasculature during conventionally fractionated radiation therapy of prostate cancer. PLoS One. https://doi.org/10.1371/journal.pone.0084076.

Preise D, Mazor O, Koudinova N, Liscovitch M, Scherz A, Salomon Y. 2003. Bypass of Tumor Drug Resistance by Antivascular Therapy. Neoplasia. https://doi.org/10.1016/s1476-5586(03)80031-3.

Preise D, Oren R, Glinert I, Kalchenko V, Jung S, Scherz A, Salomon Y. 2009. Systemic antitumor protection by vascular-targeted photodynamic therapy involves cellular and humoral immunity. Cancer Immunol Immunother. https://doi.org/10.1007/s00262-008-0527-0.

Preise D, Scherz A, Salomon Y. 2011. Antitumor immunity promoted by vascular occluding therapy: Lessons from vascular-targeted photodynamic therapy

(VTP)Photochemical and Photobiological Sciences.

Ramsay CR, Adewuyi TE, Gray J, Hislop J, Shirley MD, Jayakody S, Maclennan G, Fraser C, Maclennan S, Brazzelli M, N'dow J, Pickard R, Robertson C, Rothnie K, Rushton SP, Vale L, Lam TB. 2015. Ablative therapy for people with localised prostate cancer: A systematic review and economic evaluation. Health Technol Assess (Rockv). https://doi.org/10.3310/hta19490.

Reginato E. 2014. Immune response after photodynamic therapy increases anti-cancer and anti-bacterial effects. World J Immunol. https://doi.org/10.5411/wji.v4.i1.1.

Reits EA, Hodge JW, Herberts CA, Groothuis TA, Chakraborty M, K.Wansley E, Camphausen K, Luiten RM, Ru AH de, Neijssen J, Griekspoor A, Mesman E, Verreck FA, Spits H, Schlom J, Veelen P van, Neefjes JJ. 2006. Radiation modulates the peptide repertoire, enhances MHC class I expression, and induces successful antitumor immunotherapy. J Exp Med 203(5):1259–1271.

Røe K, Mikalsen LTG, Kogel AJ van der, Bussink J, Lyng H, Ree AH, Marignol L, Olsen DR. 2012. Vascular responses to radiotherapy and androgen-deprivation therapy in experimental prostate cancer. Radiat Oncol. https://doi.org/10.1186/1748-717X-7-75.

Royce TJ, Efstathiou JA. 2018. Proton therapy for prostate cancer: A review of the rationale, evidence, and current state. Urol Oncol. https://doi.org/10.1016/j.urolonc.2018.11.012.

Rudqvist NP, Pilones KA, Lhuillier C, Wennerberg E, Sidhom JW, Emerson RO, Robins HS, Schneck J, Formenti SC, Demaria S. 2018. Radiotherapy and CTLA-4 blockade shape the tcr repertoire of tumor-infiltrating t cells. Cancer Immunol Res. https://doi.org/10.1158/2326-6066.CIR-17-0134.

Samir S. Taneja, James Bennett, Jonathan Coleman, Robert Grubb, Gerald Andriole, Robert E. Reiter, Leonard Marks, Abdel-Rahmene Azzouzi ME. 2016. Final Results of a Phase I/II Multicenter Trial of WST11 (TOOKAD® Soluble) Vascular-Targeted Photodynamic Therapy (VTP) for Hemiablation of the Prostate in Men with Unilateral Low Risk Prostate Cancer Conducted in the United States. J Urol 196(4):1096–1104.

Sanda MG, Cadeddu JA, Kirkby E, Chen RC, Crispino T, Fontanarosa J, Freedland SJ, Greene K, Klotz LH, Makarov D V., Nelson JB, Rodrigues G, Sandler HM, Taplin ME, Treadwell JR. 2018. Clinically Localized Prostate Cancer: AUA/ASTRO/SUO Guideline. Part I: Risk Stratification, Shared Decision Making, and Care Options. J Urol. https://doi.org/10.1016/j.juro.2017.11.095.

Santin AD, Hermonat PL, Hiserodt JC, Chiriva-Internati M, Woodliff J, Theus JW, Barclay D, Pecorelli S, Parham GP. 1997. Effects of irradiation on the expression of major histocompatibility complex class I antigen and adhesion costimulation molecules ICAM-1 in human cervical cancer. Int J Radiat Oncol Biol Phys. https://doi.org/10.1016/S0360-3016(97)00372-6.

Santos AF Dos, Almeida DRQ De, Terra LF, Baptista MS, Labriola L. 2019. Photodynamic therapy in cancer treatment - an update review. J Cancer Metastasis Treat. https://doi.org/10.20517/2394-4722.2018.83.

Sathianathen NJ, Omer A, Harriss E, Davies L, Kasivisvanathan V, Punwani S, Moore CM, Kastner C, Barrett T, Bergh RC Van Den, Eddy BA, Gleeson F, Macpherson R, Bryant RJ, Catto JW, Murphy DG, Hamdy FC, Ahmed HU, Lamb AD. 2020. Negative

Predictive Value of Multiparametric Magnetic Resonance Imaging in the Detection of Clinically Significant Prostate Cancer in the Prostate Imaging Reporting and Data System Era: A Systematic Review and Meta-analysis. Eur Urol.

Schabel MC, Parker DL. 2008. Uncertainty and bias in contrast concentration measurements using spoiled gradient echo pulse sequences. Phys Med Biol. https://doi.org/10.1088/0031-9155/53/9/010.

Schaue D, Ratikan JA, Iwamoto KS, McBride WH. 2012. Maximizing tumor immunity with fractionated radiation. Int J Radiat Oncol Biol Phys. https://doi.org/10.1016/j.ijrobp.2011.09.049.

Schnitzer JE, Oh P. 1994. Albondin-mediated capillary permeability to albumin. Differential role of receptors in endothelial transcytosis and endocytosis of native and modified albumins. J Biol Chem.

Schreiber S, Gross S, Brandis A, Harmelin A, Rosenbach-Belkin V, Scherz A, Salomon Y. 2002. Local photodynamic therapy (PDT) of rat C6 glioma xenografts with Pd-bacteriopheophorbide leads to decreased metastases and increase of animal cure compared with surgery. Int J Cancer. https://doi.org/10.1002/ijc.10299.

Schwartz DL, Bankson JA, Lemos R, Lai SY, Thittai AK, He Y, Hostetter G, Demeure MJ, Hoff DD Von, Powis G. 2010. Radiosensitization and stromal imaging response correlates for the HIF-1 inhibitor PX-478 given with or without chemotherapy in pancreatic cancer. Mol Cancer Ther. https://doi.org/10.1158/1535-7163.MCT-09-0768.

Senapati S, Chakraborty S, Nath I, K Panda S, C Patra R, K Batra S. 2012. Non-human prostate cancer cell lines | Oncology, Gastroenterology and Hepatology Reports. Oncol Gastroenterol Hepatol Reports.

Shah TT, Peters M, Eldred-Evans D, Miah S, Yap T, Faure-Walker NA, Hosking-Jervis F, Thomas B, Dudderidge T, Hindley RG, McCracken S, Greene D, Nigam R, Valerio M, Minhas S, Winkler M, Arya M, Ahmed HU. 2019. Early-Medium-Term Outcomes of Primary Focal Cryotherapy to Treat Nonmetastatic Clinically Significant Prostate Cancer from a Prospective Multicentre Registry. Eur Urol. https://doi.org/10.1016/j.eururo.2018.12.030.

Sharabi AB, Lim M, DeWeese TL, Drake CG. 2015a. Radiation and checkpoint blockade immunotherapy: Radiosensitisation and potential mechanisms of synergy. The Lancet Oncology.

Sharabi AB, Nirschl CJ, Kochel CM, Nirschl TR, Francica BJ, Velarde E, Deweese TL, Drake CG. 2015b. Stereotactic radiation therapy augments antigen-specific PD-1-mediated antitumor immune responses via cross-presentation of tumor antigen. Cancer Immunol Res. https://doi.org/10.1158/2326-6066.CIR-14-0196.

Sheer Hug, Brandis Alexander; Salomon Yoram; Scherz Avigdor. 1999. Palladium-substituted bacteriochlorophyll derivaties and use thereof. Patent No:US6569846B1

Shen MM, Abate-Shen C. 2010. Molecular genetics of prostate cancer: New prospects for old challenges. Genes and Development.

SHIBUYA K, TSUSHIMA Y, HORISOKO E, NODA S, TAKETOMI-TAKAHASHI A, OHNO T, AMANUMA M, ENDO K, NAKANO T. 2011. Blood Flow Change Quantification in

Cervical Cancer before and during Radiation Therapy Using Perfusion CT. J Radiat Res. https://doi.org/10.1269/jrr.11079.

Shipley WU, Thames HD, Sandler HM, Hanks GE, Zietman AL, Perez CA, Kuban DA, Hancock SL, Smith CD. 1999. Radiation therapy for clinically localized prostate cancer: A multi- institutional pooled analysis. J Am Med Assoc. https://doi.org/10.1001/jama.281.17.1598.

Siva S, Bressel M, Murphy DG, Shaw M, Chander S, Violet J, Tai KH, Udovicich C, Lim A, Selbie L, Hofman MS, Kron T, Moon D, Goad J, Lawrentschuk N, Foroudi F. 2018. Stereotactic Abative Body Radiotherapy (SABR) for Oligometastatic Prostate Cancer: A Prospective Clinical Trial. Eur Urol 74(4):455–462.

Skalli O, Pelte MF, Peclet MC, Gabbiani G, Gugliotta P, Bussolati G, Ravazzola M, Orci L. 1989. α-Smooth muscle actin, a differentiation marker of smooth muscle cells, is present in microfilamentous bundles of pericytes. J Histochem Cytochem. https://doi.org/10.1177/37.3.2918221.

Slone HB, Peters LJ, Milas L. 1979. Effect of host immune capability on radiocurability and subsequent transplantability of a murine fibrosarcoma. J Natl Cancer Inst. https://doi.org/10.1093/jnci/63.5.1229.

Slovin SF, Higano CS, Hamid O, Tejwani S, Harzstark A, Alumkal JJ, Scher HI, Chin K, Gagnier P, McHenry MB, Beer TM. 2013. Ipilimumab alone or in combination with radiotherapy in metastatic castration-resistant prostate cancer: Results from an open-label, multicenter phase i/ii study. Ann Oncol 24(7):1813–1821.

Sofia Vala I, Martins LR, Imaizumi N, Nunes RJ, Rino J, Kuonen F, Carvalho LM, Rüegg C, Grillo IM, Barata JT, Mareel M, Santos SCR. 2010. Low doses of ionizing radiation promote tumor growth and metastasis by enhancing angiogenesis. PLoS One. https://doi.org/10.1371/journal.pone.0011222.

Solberg TD, Balter JM, Benedict SH, Fraass BA, Kavanagh B, Miyamoto C, Pawlicki T, Potters L, Yamada Y. 2012. Quality and safety considerations in stereotactic radiosurgery and stereotactic body radiation therapy: Executive summary. Pract Radiat Oncol 2(1):2–9.

Song C, Hong BJ, Bok S, Lee CJ, Kim YE, Jeon SR, Wu HG, Lee YS, Cheon GJ, Paeng JC, Carlson DJ, Kim HJ, Ahn GO. 2016. Real-time Tumor Oxygenation Changes After Single High-dose Radiation Therapy in Orthotopic and Subcutaneous Lung Cancer in Mice: Clinical Implication for Stereotactic Ablative Radiation Therapy Schedule Optimization. Int J Radiat Oncol Biol Phys. https://doi.org/10.1016/j.ijrobp.2016.01.064.

Song CW, Sung JH, Clement JJ, Levitt SH. 1974. Vascular Changes In Neuroblastoma Of Mice Following X-Irradiation 1. Cancer Res.

Steel GG, Mcmillan TJ, Peacock JH. 1989. International Journal of Radiation Biology. Stephens TC, Currie GA, Peacock JH. 1978. Repopulation of γ-irradiated lewis lung carcinoma by malignant cells and host macrophage progenitors. Br J Cancer. https://doi.org/10.1038/bjc.1978.252.

Strohmeyer D, Rössing C, Bauerfeind A, Kaufmann O, Schlechte H, Bartsch G, Loening S. 2000. VEGF and its correlation with angiogenesis and p53 expression in prostate cancer. Prostate.

Supiot S, Rousseau C, Dore M, Chèze-Le-Rest C, Kandel-Aznar C, Potiron V, Guerif S, Paris F, Ferrer L, Campion L, Meingan P, Delpon G, Hatt M, Visvikis D. 2019. Reoxygenation during radiotherapy in intermediate-risk prostate cancer. Radiother Oncol. https://doi.org/10.1016/j.radonc.2018.12.022.

Sweeney CJ, Chen Y-H, Carducci M, Liu G, Jarrard DF, Eisenberger M, Wong Y-N, Hahn N, Kohli M, Cooney MM, Dreicer R, Vogelzang NJ, Picus J, Shevrin D, Hussain M, Garcia J a., DiPaola RS. 2015. Chemohormonal Therapy in Metastatic Hormone-Sensitive Prostate Cancer. N Engl J Med 150805140037008.

Tan DSW, Mok TSK, Rebbeck TR. 2016. Cancer genomics: Diversity and disparity across ethnicity and geography. J Clin Oncol. https://doi.org/10.1200/JCO.2015.62.0096.

Tay KJ, Polascik TJ, Elshafei A, Tsivian E, Jones JS. 2017. Propensity Score-Matched Comparison of Partial to Whole-Gland Cryotherapy for Intermediate-Risk Prostate Cancer: An Analysis of the Cryo On-Line Data Registry Data. J Endourol. https://doi.org/10.1089/end.2016.0830.

Taylor BS, Schultz N, Hieronymus H, Gopalan A, Xiao Y, Carver BS, Arora VK, Kaushik P, Cerami E, Reva B, Antipin Y, Mitsiades N, Landers T, Dolgalev I, Major JE, Wilson M, Socci ND, Lash AE, Heguy A, Eastham JA, Scher HI, Reuter VE, Scardino PT, Sander C, Sawyers CL, Gerald WL. 2010. Integrative Genomic Profiling of Human Prostate Cancer. Cancer Cell. https://doi.org/10.1016/j.ccr.2010.05.026.

Tosoian JJ, Carter HB, Lepor A, Loeb S. 2016. Active surveillance for prostate cancer: Current evidence and contemporary state of practice. Nature Reviews Urology.

Trachtenberg J, Bogaards A, Weersink RA, Haider MA, Evans A, McCluskey SA, Scherz A, Gertner MR, Yue C, Appu S, Aprikian A, Savard J, Wilson BC, Elhilali M. 2007. Vascular Targeted Photodynamic Therapy With Palladium-Bacteriopheophorbide Photosensitizer for Recurrent Prostate Cancer Following Definitive Radiation Therapy: Assessment of Safety and Treatment Response. J Urol. https://doi.org/10.1016/j.juro.2007.07.036.

Trachtenberg J, Weersink RA, Davidson SRH, Haider MA, Bogaards A, Gertner MR, Evans A, Scherz A, Savard J, Chin JL, Wilson BC, Elhilali M. 2008b. Vascular-targeted photodynamic therapy (padoporfin, WST09) for recurrent prostate cancer after failure of external beam radiotherapy: A study of escalating light doses. BJU Int. https://doi.org/10.1111/j.1464-410X.2008.07753.x.

Tsai C-S, Chen F-H, Wang C-C, Huang H-L, Jung S-M, Wu C-J, Lee C-C, McBride WH, Chiang C-S, Hong J-H. 2007. Macrophages from irradiated tumors express higher levels of iNOS, arginase-I and COX-2, and promote tumor growth. Int J Radiat Oncol Biol Phys 68(2):499–507.

Tsai CH, Hong JH, Hsieh KF, Hsiao HW, Chuang WL, Lee CC, McBride WH, Chiang CS. 2006. Tetracycline-regulated intratumoral expression of interleukin-3 enhances the efficacy of radiation therapy for murine prostate cancer. Cancer Gene Ther. https://doi.org/10.1038/sj.cgt.7700977.

Tu H, Jacobs SC, Borkowski A, Kyprianou N. 1996. Incidence of apoptosis and cell proliferation in prostate cancer: Relationship with TGF-β1 and bcl-2 expression. Int J Cancer. https://doi.org/10.1002/(SICI)1097-0215(19961021)69:5<357::AID-IJC1>3.0.CO;2-4.

Vakifahmetoglu H, Olsson M, Zhivotovsky B. 2008. Death through a tragedy: mitotic catastrophe. Cell Death Differ 15(7):1153–1162.

Valerio M, Ahmed HU, Emberton M, Lawrentschuk N, Lazzeri M, Montironi R, Nguyen PL, Trachtenberg J, Polascik TJ. 2014. The role of focal therapy in the management of localised prostate cancer: A systematic review. European Urology.

Valerio M, Cerantola Y, Eggener SE, Lepor H, Polascik TJ, Villers A, Emberton M. 2017a. New and Established Technology in Focal Ablation of the Prostate: A Systematic Review. European Urology.

Valerio M, Shah TT, Shah P, Mccartan N, Emberton M, Arya M, Ahmed HU. 2017b. Magnetic resonance imaging-transrectal ultrasound fusion focal cryotherapy of the prostate: A prospective development study. Urol Oncol Semin Orig Investig. https://doi.org/10.1016/j.urolonc.2016.11.008.

Vanneste BGL, Limbergen EJ Van, Lin EN van, Roermund JGH van, Lambin P. 2016. Prostate Cancer Radiation Therapy: What Do Clinicians Have to Know? Biomed Res Int 2016:6829875.

Vanpouille-Box C, Pilones KA, Wennerberg E, Formenti SC, Demaria S. 2015. In situ vaccination by radiotherapy to improve responses to anti-CTLA-4 treatment. Vaccine. https://doi.org/10.1016/j.vaccine.2015.05.105.

Vilensky J, Koudinova N V., Harmelin A, Scherz A, Salomon Y. 2005. Vascular-targeted photodynamic therapy (VTP) of a canine-transmissible venereal tumour in a murine model with Pd-bacteriopheophorbide (WST09). Vet Comp Oncol. https://doi.org/10.1111/j.1476-5810.2005.00078.x.

Vitkin N, Nersesian S, Siemens DR, Koti M. 2019. The tumor immune contexture of prostate cancer. Frontiers in Immunology.

Vral A, Magri V, Montanari E, Gazzano G, Gourvas V, Marras E, Perletti G. 2012. Topographic and quantitative relationship between prostate inflammation, proliferative inflammatory atrophy and low-grade prostate intraepithelial neoplasia: A biopsy study in chronic prostatitis patients. Int J Oncol. https://doi.org/10.3892/ijo.2012.1646.

Wachsberger PR, Burd R, Cardi C, Thakur M, Daskalakis C, Holash J, Yancopoulos GD, Dicker AP. 2007. VEGF Trap in Combination With Radiotherapy Improves Tumor Control in U87 Glioblastoma. Int J Radiat Oncol Biol Phys. https://doi.org/10.1016/j.ijrobp.2006.11.011.

Wan S, Pestka S, Jubin RG, Lyu YL, Tsai YC, Liu LF. 2012. Chemotherapeutics and radiation stimulate MHC class i expression through elevated interferon-beta signaling in breast cancer cells. PLoS One. https://doi.org/10.1371/journal.pone.0032542.

Wang G, König R, Ansari GAS, Khan MF. 2008. Lipid peroxidation-derived aldehyde-protein adducts contribute to trichloroethene-mediated autoimmunity via activation of CD4+ T cells. Free Radic Biol Med. https://doi.org/10.1016/j.freeradbiomed.2008.01.012.

Wang Y, Deng W, Li N, Neri S, Sharma A, Jiang W, Lin SH. 2018. Combining Immunotherapy and Radiotherapy for Cancer Treatment: Current Challenges and Future Directions. Front Pharmacol 9:185.

Watson PA, Ellwood-Yen K, King JC, Wongvipat J, LeBeau MM, Sawyers CL. 2005.

Context-dependent hormone-refractory progression revealed through characterization of a novel murine prostate cancer cell line. Cancer Res. https://doi.org/10.1158/0008-5472.CAN-05-3441.

Winkler F, Kozin S V., Tong RT, Chae S-S, Booth MF, Garkavtsev I, Xu L, Hicklin DJ, Fukumura D, Tomaso E di, Munn LL, Jain RK. 2004. Kinetics of vascular normalization by VEGFR2 blockade governs brain tumor response to radiation. Cancer Cell 6(6):553–563.

Wisenbaugh ES, Andrews PE, Ferrigni RG, Schild SE, Keole SR, Wong WW, Vora SA. 2014. Proton beam therapy for localized prostate cancer 101: basics, controversies, and facts. Rev Urol 16(2):67–75.

Wong CP, Bray TM, Ho E. 2009. Induction of proinflammatory response in prostate cancer epithelial cells by activated macrophages. Cancer Lett. https://doi.org/10.1016/j.canlet.2008.10.025.

Wong SY, Haack H, Crowley D, Barry M, Bronson RT, Hynes RO. 2005. Tumor-secreted vascular endothelial growth factor-C is necessary for prostate cancer lymphangiogenesis, but lymphangiogenesis is unnecessary for lymph node metastasis. Cancer Res. https://doi.org/10.1158/0008-5472.CAN-05-0901.

Wu S-Q, Su H, Wang Y-H, Zhao X-K. 2019. Role of tumor-associated immune cells in prostate cancer: angel or devil? Asian J Androl 21(5):433–437.

Wuttge DM, Bruzelius M, Stemme S. 1999. T-cell recognition of lipid peroxidation products breaks tolerance to self proteins. Immunology. https://doi.org/10.1046/j.1365-2567.1999.00872.x.

Wysocki PJ, Kwiatkowska EP, Kazimierczak U, Suchorska W, Kowalczyk DW, Mackiewicz A. 2006. Captopril, an angiotensin-converting enzyme inhibitor, promotes growth of immunogenic tumors in mice. Clin Cancer Res. https://doi.org/10.1158/1078-0432.CCR-05-2489.

Xu J, Escamilla J, Mok S, David J, Priceman S, West B, Bollag G, McBride W, Wu L. 2013. CSF1R signaling blockade stanches tumor-infiltrating myeloid cells and improves the efficacy of radiotherapy in prostate cancer. Cancer Res. https://doi.org/10.1158/0008-5472.CAN-12-3981.

Yamazaki T, Mukouyama YS. 2018. Frontiers in Cardiovascular Medicine.
Yla-Herttuala S, Palinski W, Butler SW, Picard S, Steinberg D, Witztum JL. 1994. Rabbit and human atherosclerotic lesions contain IgG that recognizes epitopes of oxidized LDL. Arterioscler Thromb. https://doi.org/10.1161/01.atv.14.1.32.

Yoshimura M, Itasaka S, Harada H, Hiraoka M. 2013. Microenvironment and radiation therapy. BioMed Research International.

Young KH, Baird JR, Savage T, Cottam B, Friedman D, Bambina S, Messenheimer DJ, Fox B, Newell P, Bahjat KS, Gough MJ, Crittenden MR. 2016. Optimizing Timing of Immunotherapy Improves Control of Tumors by Hypofractionated Radiation Therapy. PLoS One 11(6):e0157164.

Yu JW, Bhattacharya S, Yanamandra N, Kilian D, Shi H, Yadavilli S, Katlinskaya Y, Kaczynski H, Conner M, Benson W, Hahn A, Seestaller-Wehr L, Bi M, Vitali NJ, Tsvetkov L, Halsey W, Hughes A, Traini C, Zhou H, Jing J, Lee T, Figueroa DJ, Brett S, Hopson CB, Smothers JF, Hoos A, Srinivasan R. 2018. Tumor-immune profiling of murine

syngeneic tumor models as a framework to guide mechanistic studies and predict therapy response in distinct tumor microenvironments. PLoS One. https://doi.org/10.1371/journal.pone.0206223.

Yushkevich PA, Pashchinskiy A, Oguz I, Mohan S, Schmitt JE, Stein JM, Zukić D, Vicory J, McCormick M, Yushkevich N, Schwartz N, Gao Y, Gerig G. 2019. User-Guided Segmentation of Multi-modality Medical Imaging Datasets with ITK-SNAP. Neuroinformatics. https://doi.org/10.1007/s12021-018-9385-x.

Zaorsky NG, Davis BJ, Nguyen PL, Showalter TN, Hoskin PJ, Yoshioka Y, Morton GC, Horwitz EM. 2017. The evolution of brachytherapy for prostate cancer. Nat Rev Urol 14(7):415–439.

Zaretsky JM, Garcia-Diaz A, Shin DS, Escuin-Ordinas H, Hugo W, Hu-Lieskovan S, Torrejon DY, Abril-Rodriguez G, Sandoval S, Barthly L, Saco J, Homet Moreno B, Mezzadra R, Chmielowski B, Ruchalski K, Shintaku IP, Sanchez PJ, Puig-Saus C, Cherry G, Seja E, Kong X, Pang J, Berent-Maoz B, Comin-Anduix B, Graeber TG, Tumeh PC, Schumacher TNM, Lo RS, Ribas A. 2016. Mutations Associated with Acquired Resistance to PD-1 Blockade in Melanoma. N Engl J Med. https://doi.org/10.1056/nejmoa1604958.

Zelefsky MJ, Fuks Z, Hunt M, Lee HJ, Lombardi D, Ling CC, Reuter VE, Venkatraman ES, Leibel SA. 2001. High dose radiation delivered by intensity modulated conformal radiotherapy improves the outcome of localized prostate cancer. J Urol. https://doi.org/10.1016/S0022-5347(05)65855-7.

Zhang J, Patel L, Pienta KJ. 2010. CC chemokine ligand 2 (CCL2) promotes prostate cancer tumorigenesis and metastasis. Cytokine Growth Factor Rev 21(1):41–8.
Zywietz F, Hahn LS, Lierse W. 1994. Ultrastructural studies on tumor capillaries of a rat rhabdomyosarcoma during fractionated radiotherapy. Acta Anat (Basel). https://doi.org/10.1159/000147605.

Chapter 9. Appendix

9.1 Plasmid transfection of TRAMP-C1 cells

TRAMP-C1 cells were transfected with lentivirus harbouring an OVA-Green Fluorescent Protein (OVA-GFP) construct. Lentiviral vectors were a kind donation from the Cerundolo Lab (Weatherall Institute of Molecular Medicine, University of Oxford). In brief, on day 1, $1x10^5$ TRAMP-C1 cells were co-incubated with lentiviral particles in the presence of 8 μl/mL polybrene in 0.5 mL medium. Cells together with lentiviral particles were centrifuged at 3500 rpm at 4ºC for 30 minutes. Cells were then seeded in a 12-well plate in 0.5 mL medium and placed at 4ºC for 2 hours. Cells were then transferred to 37ºC and 5% CO_2. The medium was changed on day 2 and on day 3 cells were washed with PBS for x6 times to remove all lentivirus particles. Selection was performed using GFP cell sorting using a flow cytometer (**figure 9.1**). The OVA-GFP TRAMP-C1 cell line was designed to extend the analysis of immunological effects of fractionated RT, VTP by providing a model to study antigen specific T-cell responses generated by these treatments.

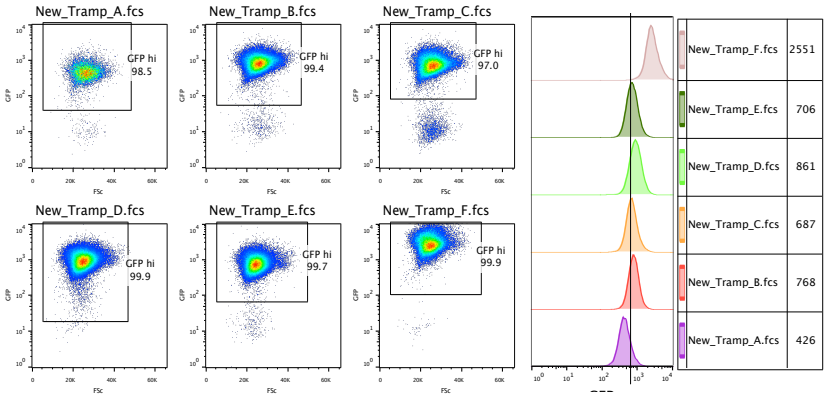


Figure 9.1. Generation of OVA-GFP TRAMP-C1 cells. Selection of six OVA-GFP TRAMP-C1 clones during flow-cytometry sorting according to GFP levels (low – high). *Experiments performed in collaboration with Uzi Gileadi.*

9.2 OVA-GFP TRAMP-C1 as a model to study antigen specific T-cell responses

To determine whether OVA-GFP TRAMP-C1 cells were capable of inducing an antigen-specific T-cell response to the SIINFEKL 8 peptide degradation product of OVA recognised by the MHC-I receptors of OT-I T-cells, OVA-GFP TRAMP-C1 cells were co-incubated with $CD8^+$ T-cells derived from the OT-I transgenic mouse. Spleens from OT-I mice were a generous donation from the Gerrard lab (Kennedy Research Institute, University of Oxford). Spleens were dissociated using PBS and gentle pressure. Cells were passed through a $50\ \mu m$ cell strainer and RBC lysis performed. $CD8^+$ T-cells were isolated from the splenocyte cell suspension using a mouse $CD8a^+$ T cell isolation kit (Miltenyi Biotec) according to the manufacturers' protocol, and co-incubated in RPMI (supplemented with 10% FBS) in 96 well plates with OVA-GFP TRAMP-C1 cells at a ratio of 1:5. After 24 hours of co-incubation with OVA-GFP TRAMP-C1 cells, CD8 T-cells were stained with the following antibodies: Pe-Cy7 CD8a (Biolegend – 53-6.7), APC TCR $V\alpha 2$ (Biolegend – B20.1) and PE-Cy7 $CD69^+$ (eBioscience – H1.2F3). OT-1 T-cells were co-incubated with wild-type (untransfected) TRAMP-C1 cells as a control experiment or alone as a negative control. All experiments were performed in triplicate and repeated three times. The results showed that the OVA-GFP TRAMP-C1 cells were able to activate CD8+ T-cells isolated from the spleen of the OT-I mouse in the *in vitro* setting in the presence or absence of increasing (0.1-10 ng/mL) concentrations of IFN-γ (**figure 9.2**). However despite multiple attempts at injecting then OVA-GFP TRAMP-C1 transfected cell line into the flank of TRAMP-C1 cells, we were unsuccessful in establishing an *in vivo* model and therefore we abandoned this model. We suspect, following Ellispot assays (data not shown), that the transfected cell line had become more immunogenic due to the introduction of proteins such as GFP and OVA and therefore

could not be established as a tumour in the syngeneic C57BL/6 mouse due to enhanced immune rejection compared to its 'wild-type' TRAMP-C1 cell counterpart.

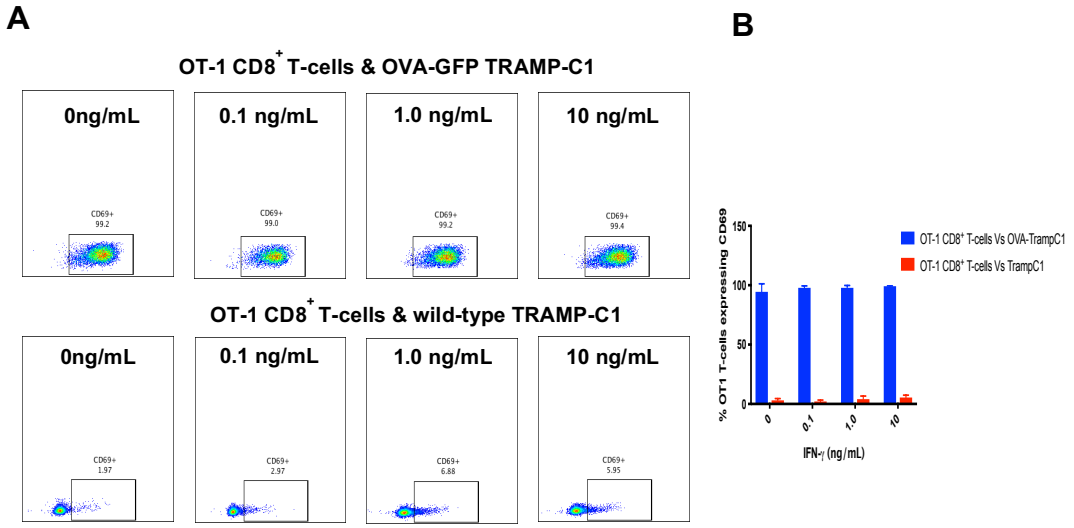


Figure 9.2. **CD69 expression (an early T-cell activation marker) on OT-1 CD8⁺ T-cells after co-incubation with OVA-GFP TRAMP-C1 cells or wilt-type (untransfected) TRAMP-C1 controls with 0 ng/mL – 10 ng/mL IFN-γ**. (**A**) Percentage positive OT-1 CD8⁺ T- cells expressing CD69 following co-incubation with target tumour cells. (**B**) Data shown as mean with SEM; n=3 independent experiments. *Experiments performed in collaboration with Uzi Gileadi.*

9.3 Radiotherapy induces 'vascular normalisation' changes in prostate cancer flank tumour allografts

CD31 and αSMA expression was analysed in tissue sections from control untreated and fractionated RT treated TRAMP-C1 tumours (**figure 9.3A**). Image segmentation analysis revealed a reduced proportion of smaller-diameter CD31-positive vessels at 7 days post-initiation of fractionated RT versus untreated control tumours (**figure 9.3B**), whilst no difference was observed at ≥400 mm^3 tumour recurrence post fractionated RT. The density of CD31-positive tumour vessels (or number of vessels/cm^2) was lower for fractionated RT-treated tumours than for untreated control tumours at 7 days post-initiation of fractionated RT (**figure 9.3C**). Two-dimensional Euclidian distance transformation analysis of the distance between any tissue image pixel and the closest

CD31-positive vessel segment revealed a reduced frequency of short distances between any pixel and the closest CD31-positive vessel at 7 days post-initiation of fractionated RT versus untreated control tumours (**figure 9.3D**). This demonstrates that there were longer distances between CD31-positive vessels at 7 days post-initiation of fractionated RT compared to control untreated tumours. No difference was observed at ≥400 mm^3 tumour recurrence post fractionated RT.

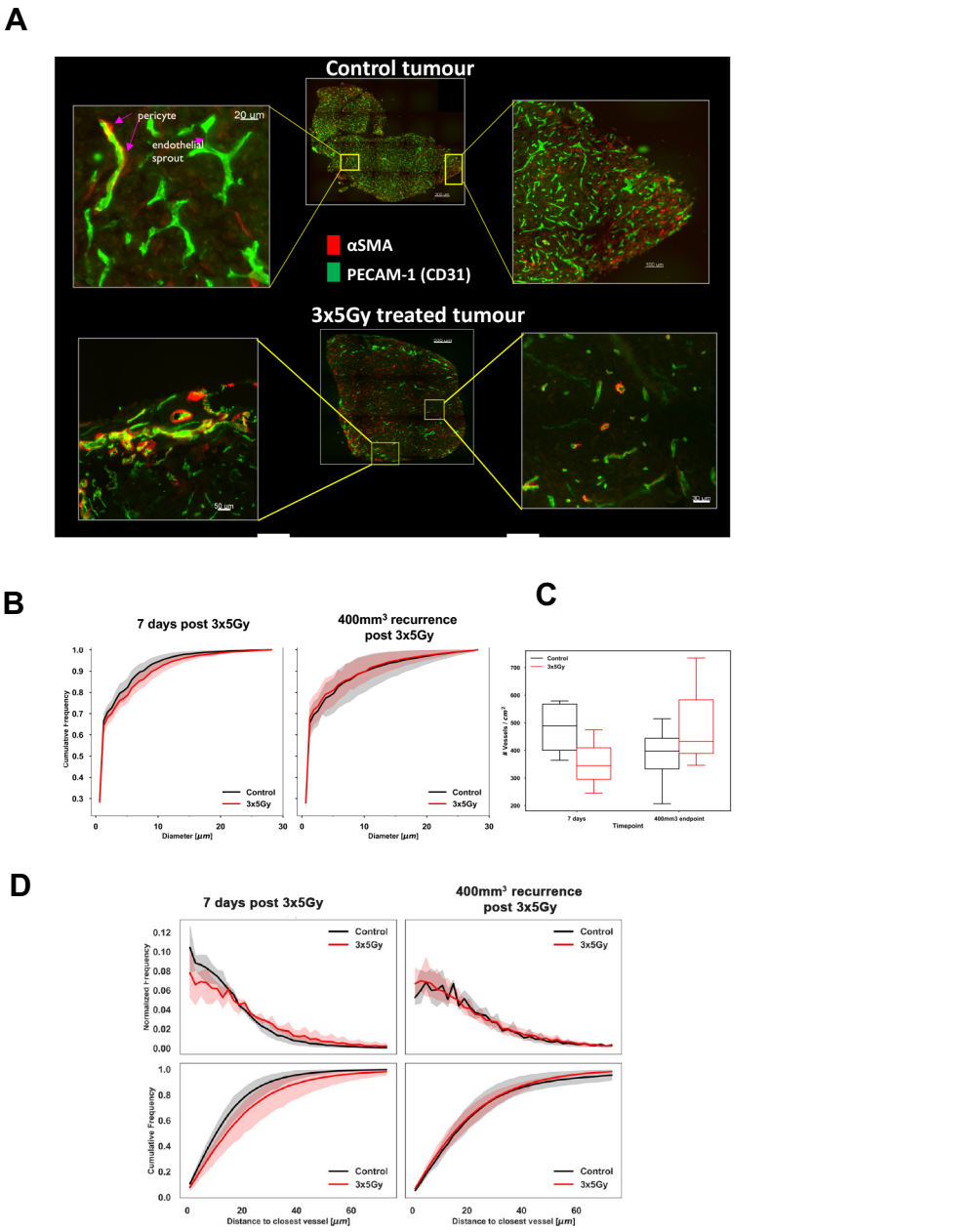


Figure 9.3. Fractionated radiotherapy induces vascular normalisation in flank TRAMP-C1 prostate cancer tumour allografts. (A) Immunofluorescence images from 3x5Gy and control treated tumours stained for anti-CD31 (green) and anti-αSMA (red) showing endothelial cells (green) with supporting pericyte cells (red). (**B-C**) Image segmentation analysis of immunofluorescence images from untreated control (n=3) and 3x5Gy treated (n=5) TRAMP-C1 flank tumours revealed a trend towards a reduced proportion of smaller-diameter blood vessels at 7 days post-initiation of 3x5Gy compared to control (not statistically significant as n=4 control and n=4 3x5Gy; overlapping shaded 95% confidence intervals). (**D**) There was a non-significant (p = 0.28) trend towards a lower density (number of vessels/cm^2) of CD31-positive tumor vessels for 3x5Gy treated tumours (n=4) than for control tumours (n=4) at 7 days post 3x5Gy. (**E**) 2D Euclidian distance transformation analysis of the distance between any tissue section pixel and the closest CD31-positive tumour vessel segment in 3x5Gy treated and control TRAMP-C1 tumours. This analysis revealed a trend towards a reduced frequency of short distances between any tissue pixel and the closest CD31-positive tumor vessel at 7 days post-initiation of 3x5Gy, indicating that there were longer distances between tumour vessels at this time point (not statistically significant as n=4 control and n=4 3x5Gy; overlapping shaded 95% confidence intervals). *Experiments performed in collaboration with Jens Rittscher, Andrea Chatrian, Joel Lefebvre, Ka Ho Tam and Annette Magnussen.*

The association of digitally annotated αSMA-positive pericyte cells with CD31-positive vessels (figure 9.4A) was analysed in TRAMP-C1 flank tumour allografts following fractionated RT. An increased fraction of CD31-positive tumour vessels with ≥1 adjacent αSMA-positive pericyte was observed in TRAMP-C1 flank tumour allografts at 7 days post-initiation of fractionated RT compared to untreated control tumours (**figure 9.4A**). This effect was not seen at ≥400 mm^3 tumour regrowth end-point post-fractionated RT. An increased mean fraction of CD31-positive vessels with an adjacent αSMA-positive pericyte was observed in TRAMPC1 flank tumour allografts at 7 days post-initiation of fractionated RT compared to untreated control tumours (**figure 9.4B**). No difference was observed between fractionated RT-treated tumours and untreated control tumours at ≥400 mm^3 tumour regrowth end-point post-RT.

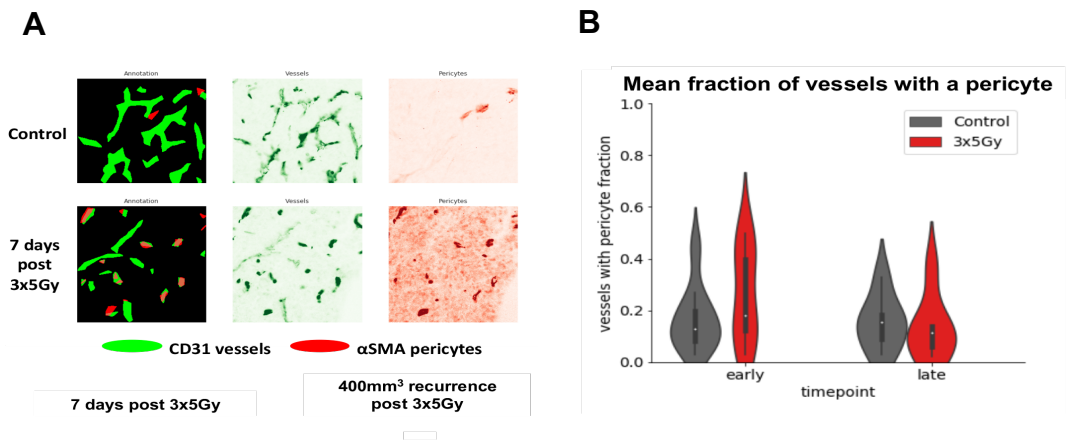


Figure 9.4. Fractionated RT induces 'vascular normalisation' changes in flank TRAMP-C1 PCa tumour allografts. **(A)** Image annotation analysis of immunofluorescence images from control and fractionated RT-treated TRAMP-C1 flank tumours (green – anti-CD31; red – anti-αSMA) revealed a trend towards an increased fraction of vessels with ≥1 adjacent αSMA-positive pericyte at 7 days post fractionated RT. **(B)** A trend towards an increased mean fraction of CD31-positive tumour vessels with an adjacent αSMA-positive pericyte was observed 7 days post-fractionated RT compared to control tumours (not statistically significant; overlapping 95% confidence intervals in violin plot). *Experiments performed in collaboration with Jens Rittscher, Andrea Chatrian, Joel Lefebvre, Ka Ho Tam and Annette Magnussen.*

9.4 Myeloid immune population gating strategy

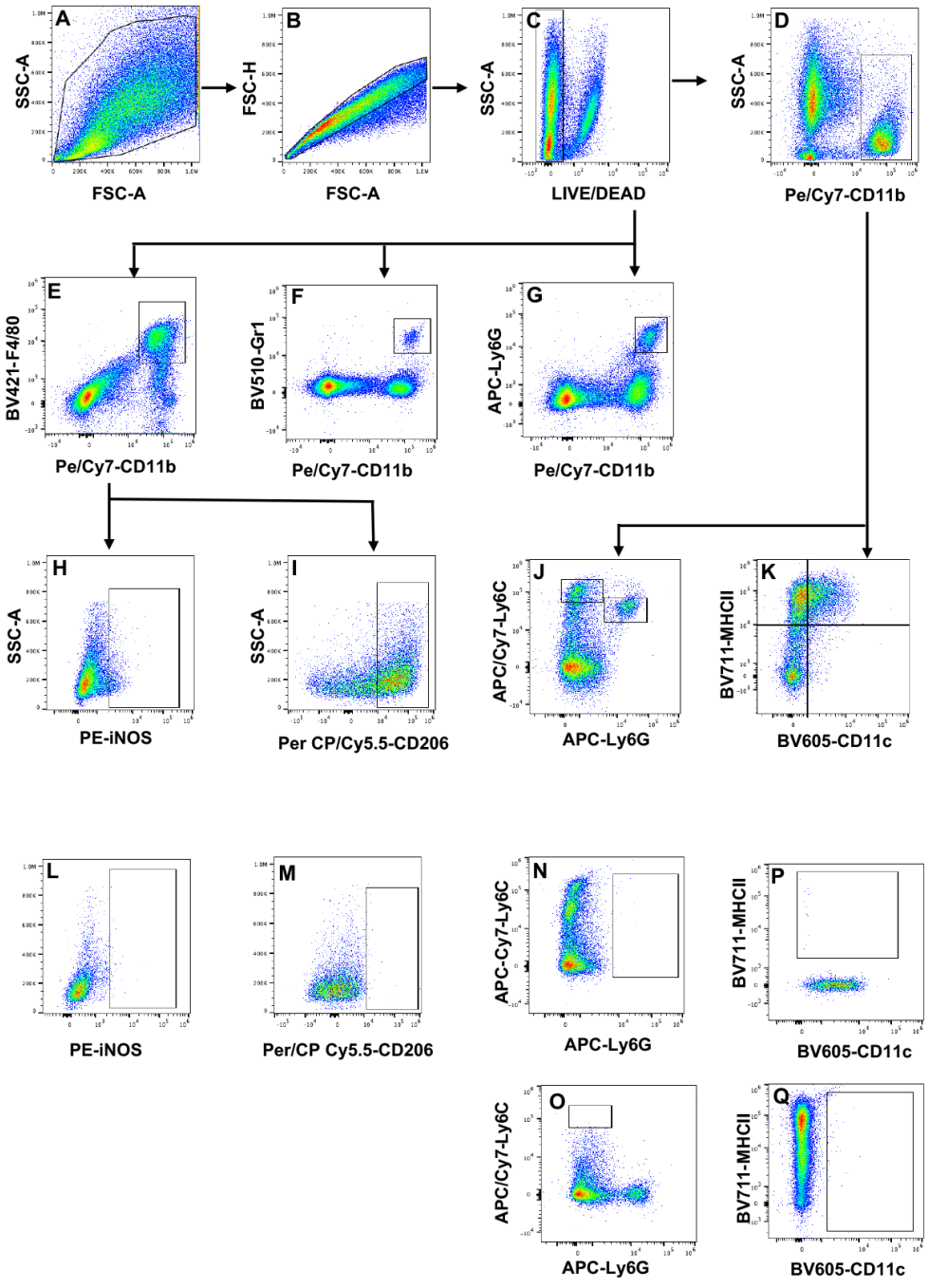


Figure 9.4. Representative flow cytometry dot plots indicating the gating strategy for identification of myeloid populations. Gates were used to exclude (**A**) debris, **(B)** doublets and **(C)** dead cells. **(E)** Live cells were gated for subsequent analysis of macrophages, **(F)** MDSCs and **(G)** neutrophils. **(D)** CD11b+ cells were gated for subsequent analysis of **(J)** Ly6C+ (monocytic MDSCs) versus Ly6G+ (granulocytic MDSCs) (K) and CD11c+ and MHCII+ expression. (**E**) CD11b+F4/80+ macrophages were gated and **(H)** iNOS+ and **(I)** CD206+ expression measured. (**L-Q**) iNOS+ and CD206+ isotype controls and fluorescence minus one (FMO) controls for Ly6G+, Ly6C+, MHCII+ and CD11c+ are shown.

9.5 Lymphoid immune population gating strategy

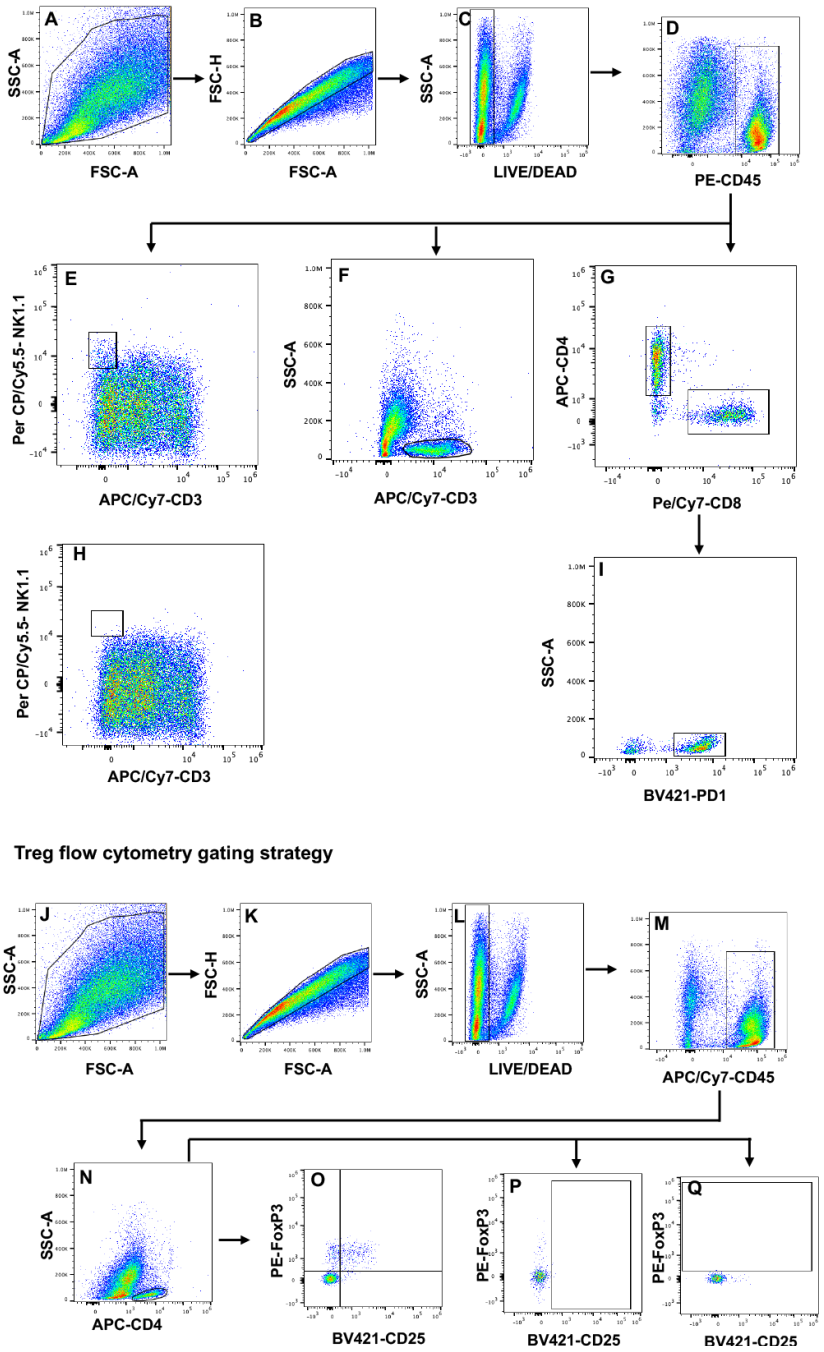


Figure 9.5. Representative flow cytometry dot plots indicating the gating strategy for identification of lymphoid populations. Representative flow cytometry dot plots indicating the gating strategy for identification of lymphoid and Treg populations. Gates were used to exclude (**A**) debris, (**B**) doublets and (**C**) dead cells. (**D**) CD45+cells were subsequently analysed for (**E**) NK1.1+ (**F**) CD3+ and **(G)** CD4+ or CD8+. CD45+CD3+CD8+ cells were gated for (**I**) PD1+ expression. FMO for NK1.1 is shown in panel **H**. For Treg cells, (**M**) CD45+ cells were gated for **(N)** CD4+ expression followed by **(O)** CD25+ and FoxP3+ expression. (**P&Q**). FMO controls for CD25+ and FoxP3+.

9.6 Antibodies used for all FACS experiments

Panel	Antibodies
Tumour infiltrating myeloid cells	PE-Cy7 CD11b (eBioscience – M1/70), PerCP/Cy5.5 CD206 (BioLegend – C068C2), BV510 Gr-1 (BioLegend – RB6-8C5), BV421 F4/80 (BioLegend – BM8), APC Ly6G (BioLegend – 1A8), APC-Cy7 Ly6C, (BioLegend – HK1.4), BV605 CD11c (BioLegend – N418), BV711 I-A/I-E (BioLegend – M5/114.15.2), PE iNOS2 (Invitrogen – CXNFT), LIVE/DEAD™ Fixable Green Dead Cell Stain Kit (ThermoFisher Scientific - L23101)
Tumour infiltrating lymphoid cells	PE CD45 (invitrogen – 30-F11), APC-Cy7 CD3 (BioLegend – 17A2), APC CD4 (BioLegend – RM4-5), PECy7 CD8 (BioLegend – 53-6.7), PerCP/Cy5.5 NK1.1 (BioLegend - PK136), LIVE/DEAD™ Fixable Green Dead Cell Stain Kit (ThermoFisher Scientific - L23101)
$CD8^+/CD4^+$ T-cell PD1	PE CD45 (Invitrogen – 30-F11), CD8a BioLegend – 53-6.7), APC CD4 (BioLegend – RM4-5), BV421 PD1 (BioLegend – 29F.1A12), LIVE/DEAD™ Fixable Green Dead Cell Stain Kit (ThermoFisher Scientific - L23101)
$CD4^+$ regulatory T-cells	APC-Cy7 CD45 (BioLegend – 30-F11), APC CD4 (BioLegend – RM4-5), BV421 CD25 (BioLegend 29F.1A12), PE Anti-Mo FoxP3 (invitrogen – NRRF–30), LIVE/DEAD™ Fixable Green Dead Cell Stain Kit (ThermoFisher Scientific - L23101)

Table 9.1 Antibodies used for flow cytometry analysis